EXPERIMENTAL STUDY OF THE INTERACTION OF NATURAL AND MAN-MADE EXPLOITATION SYSTEMS WITH THE ENVIRONMENT IN THE ATMOSPHERIC SURFACE BOUNDARY LAYER

Application to olive fields and wind farms

Doctoral Thesis

MARÍA JIMÉNEZ PORTAZ

UNIVERSIDAD
DE GRANADA

UNIVERSIDAD
DE GRANADA

DOCTORAL THESIS

Experimental study of the interaction of natural and man-made exploitation systems with the environment in the atmospheric surface boundary layer: application to olive fields and wind farms

Author:
María Jiménez Portaz

Supervisor:
María Clavero Gilabert

Tutor:
Miguel Ángel Losada Rodriguez

A thesis submitted in fulfillment of the requirements for the Doctoral degree

in the

Doctoral Program in Biogeochemical Fluid Dynamics and their Applications
University of Granada, Spain

June 18, 2021

Editor: Universidad de Granada. Tesis Doctorales
Autor: María Jiménez Portaz
ISBN: 978-84-1306-964-7
URI: http://hdl.handle.net/10481/69861

Acknowledgements

I want to express my deep gratitude to my supervisor, María Clavero, for your help and support. For our long conversations with a smile on your face and creating a small family in the laboratory. And as could not be otherwise, to Miguel Losada, for his time, his ideas, and for showing infinite patience. Thank you very much, Miguel, for so many productive and enriching conversations.

Special gratitude goes out to all the members (past and present) of the Environmental Fluid Dynamics Research Group of the University of Granada. It was fantastic to have the opportunity to meet you and work with you. I want to thank Pedro Magaña for diligently attending to the thousand "Pedro, do you have a minute?". Without your help, this manuscript would not have reached its form. Especially to Marivi, for making every day more enjoyable. These years would certainly not have been the same without you on the other side of the six screens of our desk.

My sincere appreciation to Maria José Polo for allowing me to start working at the Andalusian Institute for Earth System Research (IISTA), culminating in this thesis. And my sincere thanks to the Department of Engineering and Architecture of the University of Parma for their collaboration and contribution of scientific knowledge to the research lines of our group. In particular, to Sandro Longo and to Luca Chiapponi, for helping me with the "more turbulent" part of the thesis, making accessible the difficult and possible what seemed impossible.

I would like to thank all the Institute of Theoretical and Applied Mechanics (ITAM), Czech Republic, and the colleagues of the Centre of Excellence, Telc. In memory of Sergei Kuznetsov for his willingness and warm welcome during my research stay. *Sit tibi terra levis.*

This thesis would not have been possible without the funding provided by the research group TEP-209 and the project *ODISEA* of the program ”Proyectos de Investigación Precompetitivos para Jóvenes Investigadores” from the University of Granada. In addition, I would like to acknowledge the Vice-rectorate for research and knowledge transfer from the University of Granada for funding my research stay in the ITAM.

And finally, last but by no means least, I am forever grateful to my family and friends for being there for me. To my parents, for their support and understanding, and for knowing how to deal with a PhD student. To my sister, always by my side.

And to you, for everything and forever.

To my grandma María,
all we are is dust in the wind

"*Toda sabiduría humana estaba contenida en estas dos palabras:* ***espera*** *y* ***confía****"*

Le Comte de Monte-Cristo, 1844

Alexandre Dumas

Abstract

When we refer to exploitation systems, we talk about obtaining resources through natural or man-made management systems. Resources exploitation in Mediterranean countries covers energy extraction to agricultural or forestry production. In some cases, inadequate management methods promote environmental degradation, aggravated by climate, desertification, and climate change, among others.

Global change represents an inflection point in the management of ecosystems and the way we obtain energy. For this reason, two representative Mediterranean systems (one natural and one other artificial) have been selected in this work to be studied in an integrated way: i) olive groves and ii) onshore wind farms. A new management model requires a global understanding of the system, analyzing its elements, how they interact, and modify the surrounding environment. This model must include, in turn, how dynamic phenomena are affected through exchanges and processes on the Earth's surface, in particular the surface boundary layer of the atmosphere. These processes become more critical in high ecological value and high environmental sensitivity areas, as the Southern Mediterranean areas, and specifically, the region of Andalusia.

One of the best methods to study these systems is through experimental wind tunnel tests due to their large scale and spatio–temporal variability. For this reason, in Chapter 2, a study of the quality, homogeneity, and turbulent characteristics of the flow in the IISTA boundary layer wind tunnel has been carried out to guarantee and optimize its correct operation. A behavioral overview of the flow inside the tunnel has been obtained, and at the same time, it has been compared with a closed-circuit climatic wind tunnel with similar characteristics. With all the information obtained, it is enough to carry out environmental studies and improve the facility that is necessary for this purpose.

Secondly, the Andalusian olive grove is selected as representative of natural exploitation due to its historical importance, an emblematic ecosystem of the Mediterranean countries, and its importance at economic, health, and environmental levels. Sustainable ecosystem management is one of the most significant challenges for managers. Climate change, together with the increase in allergies associated with olive pollen and the ecosystem's long-term improvement and preservation, has generated a social problem that needs to be analyzed in-depth to obtain a satisfactory solution covering all areas: environmental, social, and economic. As a first approach to the problem, in Chapter 3 three olive grove configurations representative of Andalusia have been studied, based on experimental tests, analyzing their influence

on the atmosphere dynamics. Moreover, the relationship between exploitation and plantation characteristics has been obtained, such as the tree height and its spatial distribution, with fundamental aerodynamic variables, such as the aerodynamic diameter and the Reynolds number.

As an artificial production system, wind farms have been selected because of their relevance and their fast and unstoppable expansion worldwide, where they play a leading role in sustainability and climate change actions. Despite being clean energy, it can generate alterations associated with the wind fields, directly affecting the energy potential to be extracted by the wind turbines around it. Based on this behavior, it has been proven the importance of properly selecting the location of a wind farm due to the direct influence of topography, vegetation cover, and the position of other turbines previously installed. The different spatial configurations studied in Chapter 4 show the amplitude of the turbulent wake generated behind the wind turbine, both in height and flow direction, and its impact on the surface atmospheric boundary layer.

On the other hand, the new exchange system after installing the wind turbine, directly and indirectly, affects environmental components related to the atmosphere dynamics. Therefore, there is a wide range of environmental impacts related to wind energy associated with each other and must be studied comprehensively. However, current methodologies applied to the study of environmental impacts are lacking in specificity and adaptability to the particularities of this type of energy system. For this reason, based on scientific knowledge, guidelines and recommendations for the study of the environmental impact of wind farms in Andalusia are presented in Chapter 5. Furthermore, the methodology proposed is based on the experimental studies described in Chapter 4 and an exhaustive literature review, resulting in an example of how to apply part of this methodology.

In a nutshell, this work analyzes, from experimental tests, the relationship between the atmospheric boundary layer and two relevant exploitation systems in the Southern Mediterranean. It concludes in Chapter 6 that the study of this interaction is significant to understand the system behavior as a whole, foreseeing possible environmental alterations, optimizing their exploitation from a sustainable, social, and sanitary point of view, and at the same time, optimizing their profitability.

Resumen

Cuando hablamos de sistemas de explotación, nos referimos a aquellos sistemas naturales o artificiales de los cuales obtenemos recursos, limitados o ilimitados, a través de la gestión y aprovechamiento de cada uno de ellos. La explotación de recursos en los países mediterráneos abarca desde la obtención de energía, hasta los aprovechamientos agrícolas o forestales. Sin embargo, los inadecuados métodos de gestión fomentan la degradación del entorno, agravados por el clima, la desertificación, y el cambio climático, entre otros.

El cambio global supone un punto de inflexión a la hora de gestionar los ecosistemas, así como la forma en la que obtenemos energía. Por ello, en este trabajo se han seleccionado dos sistemas representativos del Mediterráneo (uno natural y otro artificial), para ser estudiados de forma integral: i) el olivar, y ii) los parques eólicos terrestres. Un nuevo modelo de gestión requiere entender el sistema de forma global e integrada, analizando los elementos que lo componen, cómo interactúan y cómo modifican el medio, que ha de incluir, a su vez, las afecciones sobre los fenómenos dinámicos en la superficie terrestre, especialmente en la capa límite superficial de la atmósfera. Esto cobra mayor importancia en áreas de alto valor ecológico y altamente sensibles, como es el caso del sur del Mediterráneo, y más concretamente, la región de Andalucía.

Una de las mejores formas de estudiar estos sistemas, debido a su la escala de trabajo y la variabilidad espacio temporal, es a través de ensayos experimentales en túnel de viento. Por este motivo, en el Capítulo 2 se ha realizado un estudio de la calidad, homogeneidad y características turbulentas del flujo en el túnel de viento de capa límite del IISTA, con el objetivo de garantizar y optimizar su correcto funcionamiento. De este modo, se ha conseguido una visión global del comportamiento del flujo en su interior, y a su vez se ha comparado con un túnel de viento climático de circuito cerrado de similares características. Con toda la información obtenida, tenemos información suficiente para llevar a cabo estudios de carácter ambiental y realizar las adaptaciones y mejoras que sean necesarias para ello.

En segundo lugar, se selecciona el olivar andaluz como explotación natural, por su importancia a nivel histórico, al ser un ecosistema emblemático de los países mediterráneos, pero también a nivel económico, sanitario y medioambiental. La gestión de ecosistemas de forma sostenible es uno de los mayores retos a los que se enfrentan los gestores. El cambio climático, unido al aumento de las alergias asociadas al polen del olivo y la necesidad de mejorar y conservar los ecosistemas a largo plazo, ha generado un problema a nivel social, económico y ambiental. Esta

problemática ha de ser analizada en profundidad, a fin de obtener una solución intermedia y satisfactoria en todos los ámbitos: ambientales, sociales y económicos. Como una primera aproximación al problema, en el Capítulo 3 se han estudiado, a través de ensayos experimentales, tres configuraciones de olivar representativas de Andalucía, analizando su influencia sobre la dinámica de la atmósfera. Además, se ha obteniendo la relación entre el tipo aprovechamiento y las características de la plantación, como la altura del árbol y su disposición espacial, con variables aerodinámicas fundamentales, como el diámetro aerodinámico y el número de Reynolds.

Como sistema de producción artificial se han seleccionado las explotaciones de energía eólica, por su relevancia, pero también por su rápida e imparable expansión a nivel mundial, donde juegan un papel fundamental en la sostenibilidad y las medidas contra el cambio climático. A pesar de ser una energía limpia, puede generar alteraciones asociadas al campo de vientos, traducidas en la generación de una estela turbulenta tras cada aerogenerador, que afectará de forma directa al potencial energético a extraer por parte de las turbinas cercanas. Con base en este comportamiento, se ha comprobado la importancia de seleccionar adecuadamente el emplazamiento de un parque eólico, por la influencia directa de la topografía, la cobertura vegetal y la posición espacial de otras turbinas instaladas previamente. Las diferentes configuraciones espaciales estudiadas en el Capítulo 4 muestran el alcance de dicha estela turbulenta, tanto en altura como en la dirección del flujo, y su impacto sobre la estructura de la capa límite de la atmósfera.

El nuevo sistema de intercambios tras la instalación del aerogenerador, afecta directa e indirectamente a las componentes ambientales relacionadas con la dinámica de la atmósfera. Existen entorno a la energía eólica una serie de impactos ambientales que pueden relacionarse entre sí y que deben ser estudiados desde un punto de vista integral e integrado. Sin embargo, las actuales metodologías aplicadas al estudio del impacto ambiental carecen de especificidad y adaptabilidad a las particularidades de este tipo de sistemas. Por este motivo, en el Capítulo 5 se presentan unas directrices y recomendaciones para el estudio del impacto ambiental de parques eólicos en Andalucía. La metodología propuesta está fundamentada en los estudios experimentales recogidos en el Capítulo 4 y una revisión bibliográfica completa, culminando en un ejemplo de aplicación con base en el conocimiento científico.

En definitiva, este trabajo analiza de forma experimental, la relación entre la capa límite de la atmósfera y dos de los sistemas de explotación más relevantes en el sur del Mediterráneo. Se concluye en el Capítulo 6 la relevancia del estudio la interacción descrita anteriormente, con el objetivo de comprender el funcionamiento de estos sistemas, prever posibles alteraciones ambientales, optimizar su explotación desde un punto de vista sostenible, y a su vez, optimizar su rentabilidad.

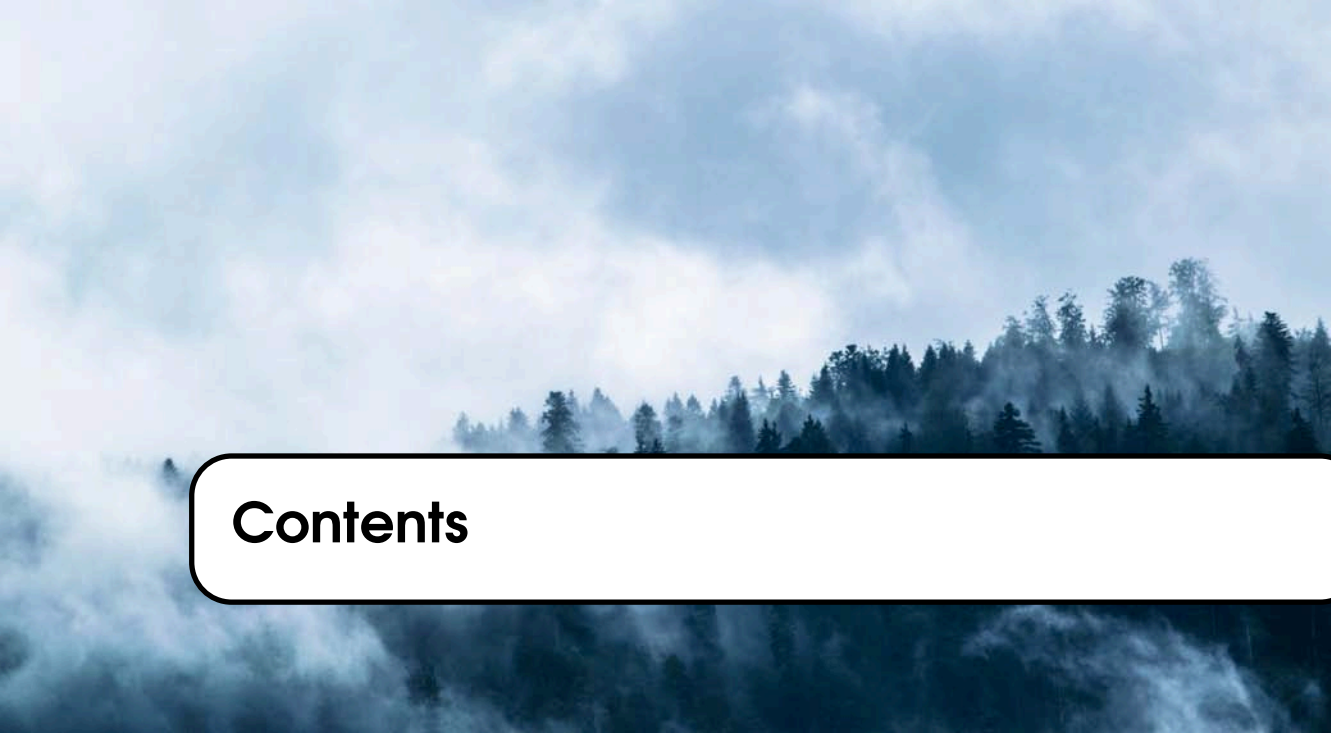

Contents

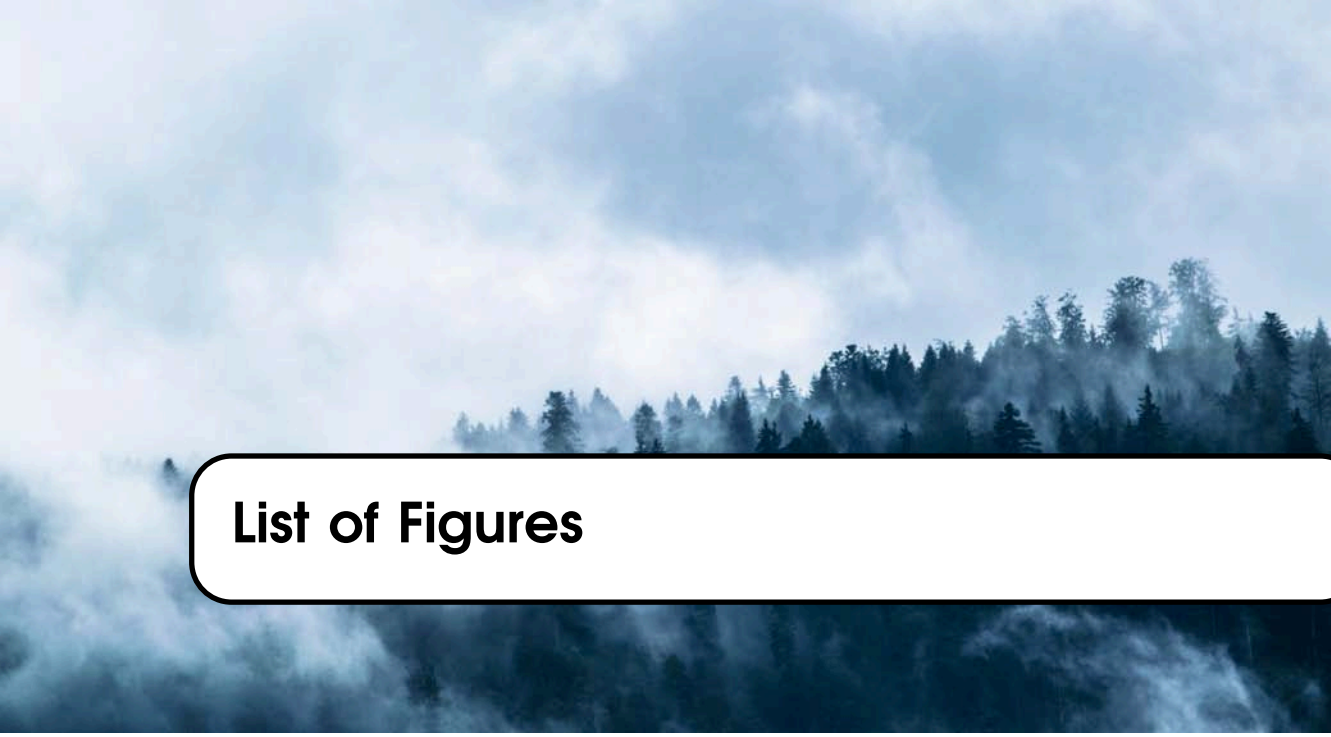

List of Figures

Chapter 1

Chapter 2

Chapter 3

Chapter 4

Chapter 5

List of Tables

Chapter 2

Chapter 3

Chapter 4

Chapter 5

Part I

1. Introduction

1.1 Context

1.1.1 Mediterranean ecosystems and their particular attributes

When we refer to the Mediterranean region, we mean mountainous formations, coastal areas, deserts, wetlands, and forests, which comprise a territory beyond comparison characteristics and rich ecosystem biodiversity. This region is associated with an extreme climate and erratic weather, of droughts and floods, shaped by the rhythm of the years and the winter-summer pulses and their daily cycles. The climate, different from one location to another, is the average weather of a region for a long time (Whiteman, 2000). The Mediterranean climate is generated from the interaction of different atmospheric patterns dominated by the topography and the influence of the Mediterranean Sea and the Atlantic Ocean (Lionello et al., 2017), resulting in an extreme exhibition of the atmospheric agents: strong winds, extreme temperature, and high-intensity rainfall. According to environmental elements and weather patterns, the climate of Andalusia can be divided into coastal, inland, highland, mid-mountain, and southeastern climates (Gómez-Zotano et al., 2015).

Andalusian areas are partially degraded due, among other reasons, to the exploitation of their natural resources, historically carried out under inadequate management methods. Also, there exists a perturbation regime associated with climate, forest fires, unequal distribution of water resources, desertification, and mismanage-

ment of natural and fossil resources (Iglesias et al., 2007). These ecosystems and their capacity for adaptation, evolution, and, in extreme cases, extinction can be used as a reference for monitoring the effects of climate change, land-use changes, biogeochemical cycles, and the habitat distribution of flora and fauna populations.

1.1.2 Natural and man-made exploitation systems

Throughout history, society has exploited natural resources for human development. These resources could be divided into renewable resources, regenerated in a time interval equal to or less than their consumption, and non-renewable resources, whose regeneration is much slower and their quantity are limited. The latter include fossil fuels or mineral extractions.

Concerning natural resources, we can include resources of different nature, from agriculture, fishing, stock farming, or energy resources exploitations, such as wind or solar energy. When we refer to natural exploitation systems, we mean those from which we obtain the product of interest without large constructions or mechanization, but rather the natural system itself, or part of it, is the resource to be obtained. However, when referring to man-made exploitation systems, we refer to those requiring artificial systems to extract and transform the resource until its utilization.

In Mediterranean areas, especially in Andalusia, one of the essential natural resources is the olive grove, which depends on a great industry and tradition, is part of the agroforestry landscape, and plays a role in environmental sustainability. On the other hand, about the most important man-made exploitations, renewable energies stand out, mainly wind energy, with more than 160 wind farms throughout Andalusia. The development and growth of wind farms are exponential due to their ability to extract a large amount of GW by taking advantage of the wind's kinetic energy.

1.1.3 Atmospheric Boundary Layer fundamentals

The atmosphere, a complex fluid system composed of gases in different proportions, suspended particles, dust, is in constant movement due to the irregular radiation balance along the Earth's surface. Therefore, it is necessary to study the exchange processes and the interaction between the biosphere-cryosphere-atmosphere-hydrosphere systems. All these processes are complex and consequently have to be studied in detail to understand the system behavior as a whole. The thermal structure of the atmosphere allows it to be divided into several layers, each one defined by differentiated characteristics and influenced by layers below and above it. Once the vertical thermal scale of the atmosphere is known, the dynamic state of the atmosphere can be defined as the relationship between forces

on the air parcels (that vary in space and time), driven by the conservation laws (conservation of air mass, energy, and momentum). All these interrelationships and balances are summarized in Figure 1.1.

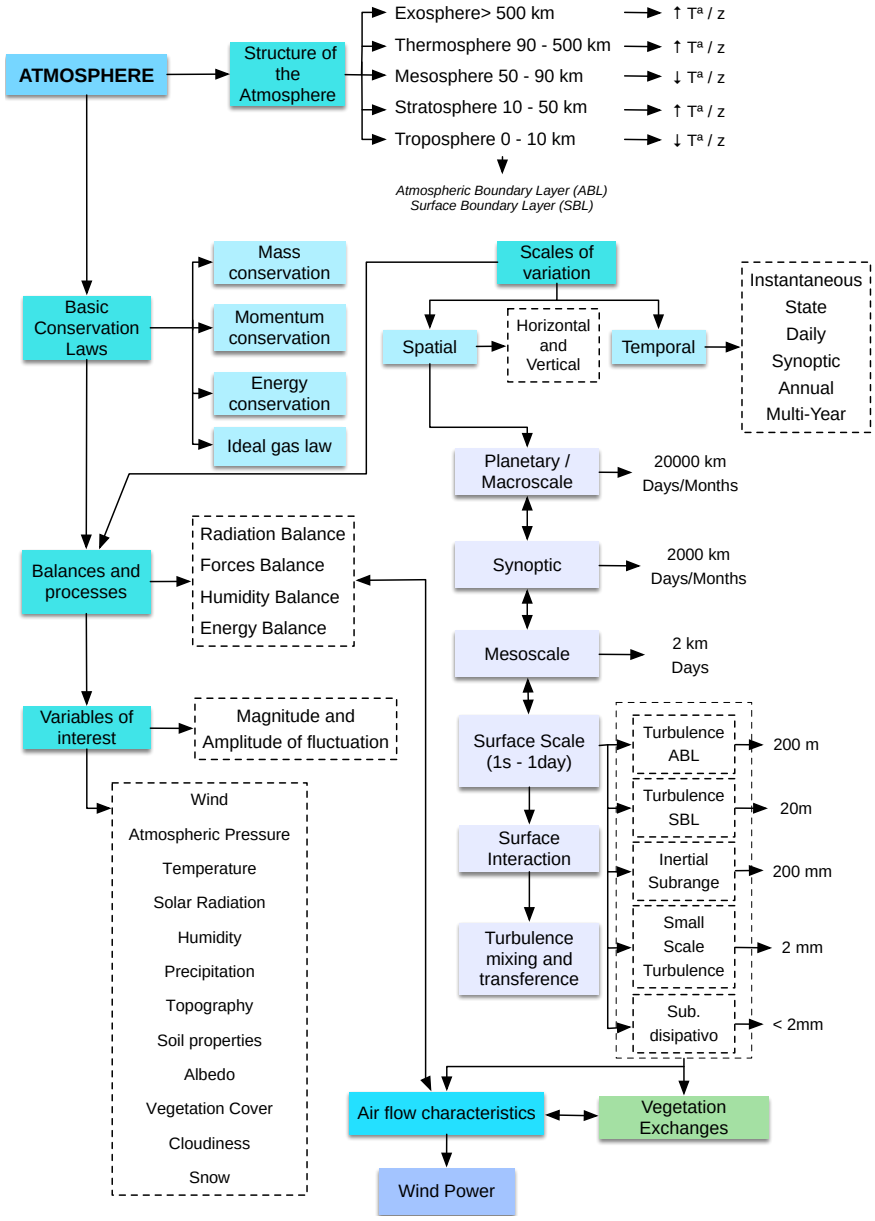

Figure 1.1: Structure, characteristics and processes in the Atmosphere.

This work is focused on the Atmospheric Surface Boundary Layer (from now on

SBL), which encompasses the bottom 5% (first 50-100 meters) of the Atmospheric Boundary Layer (ABL) –the lowest part of the atmosphere–, where all human activities are carried out, ecosystems are established, and the meteorological phenomena take place. In effect, the SBL is relevant to all phenomena observed at the Earth's surface level. The cycles of radiation, temperature, humidity, wind, turbulence and exchanges with the soil and ecosystems are developed. These are defined by gradients and balances with variation at different scales (Stull, 2016), which, in turn, determine the scope of wind energy projects and ecosystems management. To better understand all the agents involved, Figure 1.2 shows a schematic representation of the different components and their relationships to each other.

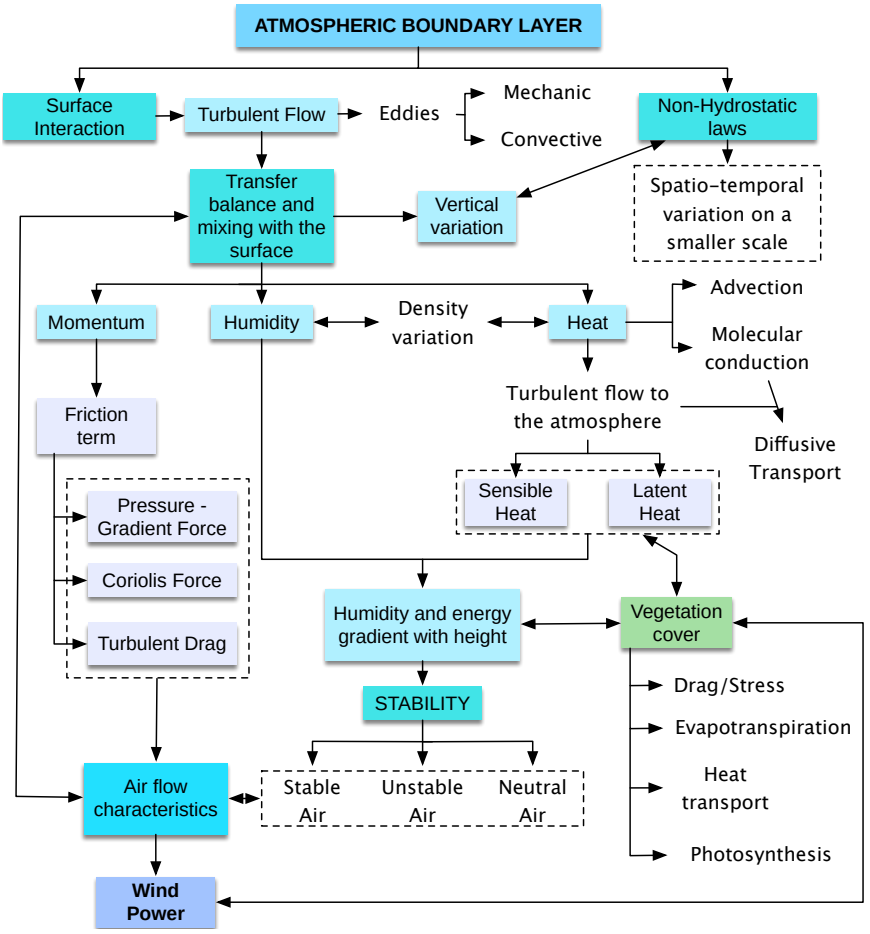

Figure 1.2: Structure, characteristics and processes in the Atmospheric Boundary Layer.

1.2 Justification and baseline hypothesis

Global change is a new context for ecosystems, including climate change, land-use changes, biogeochemical changes, and biodiversity loss. This leading the need to adapt the way we study, manage and maintain natural and artificial systems. Modifying the current management way is necessary, understanding the system in a global, comprehensive, and integrated way.

As summarized above and is shown in Figure 1.3, exchange processes between the Earth's surface and its constituent elements occur at different spatial and temporal scales. The main processes include: i) energy balances through radiation, convection, conduction, and advection, ii) mass balances through humidity flow, precipitation, water vapor, and evapotranspiration, and iii) forces balance, defined by wind velocity and turbulence phenomena (Haghighi and Kirchner, 2016).

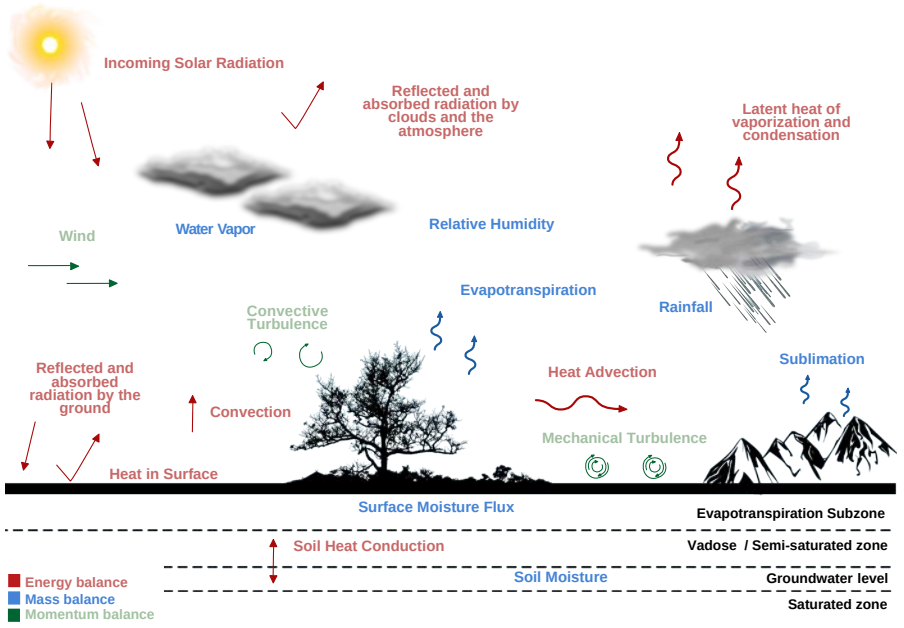

Figure 1.3: Processes and exchanges between the SBL and the Earth's surface.

This interface of trade-offs is even more critical in water-scarce environments (Baudena et al., 2008), where slight meteorological variations can affect the global ecosystem. From an ecosystemic approach, natural changes occur gradually, and to which natural adaptation is possible, as occurs with droughts in Mediterranean climates. On the other hand, there are artificial changes to which ecosystems may be adapted only under specific conditions. The second case is related to human interventions, such as constructing a wind farm or transforming a forest into an

agricultural system.

When we decide to exploit an ecosystem, such as an olive grove, a pasture, a timber extraction, or, on the contrary, we build infrastructures –in some cases in motion–, such as wind farms, buildings or bridges, the entire exchange system will be modified. Thus, we are in a dynamic system, driven by different exchanges, in which any minor natural or artificial modification will have a direct influence, leading in the most extreme cases to the disappearance of the initial ecosystem or its total or partial modification, which, in turn, will have an impact on our activities. Because of this, it is necessary to change the study/management models of resources based on the system's behavior in its baseline state, its evolution as time goes by, and the interventions planned in a given project are carried out. Thus, the first step to achieve comprehensive and integrated project management is the detailed study of these systems and their interaction with the environment to adopt a methodology based on scientific knowledge.

Therefore, depending on the environment and the project aims, it must therefore be studied according to the characteristics and particularities that define it. In this thesis, representative exploitations of the Andalusian community, based on environmental, cultural, technical, socio-economic, and health issues, are the olive grove ecosystems and the onshore wind farms. The aim is to bring together a comprehensive study of sustainability and management using traditional systems of exploitation with current scientific-technical knowledge.

1.3 Objectives

The main objective of this thesis is to study the interaction of natural and man-made production/exploitation systems with the environment, according to the system behavior, based on experimental tests carried out in the laboratory. According to the identified knowledge gaps, the following research questions were raised:

Q1. How does the airflow behave inside the wind tunnel? Can a boundary layer wind tunnel, conventionally used in aerodynamics and structural testing, be used in environmental studies?

Q2. What are the characteristics of wind flow and turbulence in the different sections of an empty wind tunnel?

Q3. Can an ecosystem itself affect the flow around it and other environmental components? Can it even affect the development of the ecosystem itself?

Q4. How to study and manage an agroforest system according to its land-use management or farming system?

Q5. How do wind farms interact with the atmospheric boundary layer? What

does this interaction depend on?

Q6. How can we study the disturbances generated by a wind farm and minimize their impact?

Q7. Can the management strategies of the systems studied be adapted to sustainability criteria?

Following the above questions, the following objectives were set for this thesis:

1. Test the homogeneity and quality of airflow in the IISTA boundary layer wind tunnel for its use in environmental studies.
2. Analyze the interaction between different olive groves with the atmospheric surface boundary layer.
3. Analyze the current methodologies of the olive grove and propose some recommendations for sustainable management.
4. Analyze the interaction between wind power generation systems and the atmospheric boundary layer, including the influence of the topography and the spatial layout under different scenarios.
5. Analyze the current methodologies and regulations applied to the environmental impact assessment of wind farms and propose a methodology and recommendations for a comprehensive analysis based on its interaction with the environment.

1.4 Thesis outline

This thesis presents the research divided into five chapters:

- **Chapter 1** provides an introduction to the study of the interaction between the Atmospheric Boundary Layer and the Earth System and an approach to the exploitation systems studied in the document and their importance within the Mediterranean area. It includes the justification, objectives, and starting hypothesis of this thesis.
- **Chapter 2** presents and details the analysis of the airflow characteristics in the IISTA boundary layer wind tunnel and its potential as a tool for environmental studies. Moreover, results are compared with respect to a closed-circuit wind tunnel.
- **Chapter 3** analyzes the interaction between different olive grove configurations with the SBL and its relationship with other variables of interest.
- **Chapter 4** describes the experimental study of the interaction between different wind turbine spatial configurations and the SBL through experimental wind tunnel tests.
- **Chapter 5** highlights a new methodology and a series of recommendations for the study of the environmental impact of an onshore wind farm, based on

the system dynamics and incorporating environmental components.
- **Chapter 6** compiles the main conclusions of the thesis and some future research lines of work.

1.5 Publications and activities derived from the thesis

The work done throughout this thesis has resulted in the following publications:

Journal Papers

- **Jiménez-Portaz, M.**, Clavero, M., & Losada, M. A. (2021). A new methodology for assessing the interaction between the Mediterranean olive agro-forest and the Atmospheric Surface Boundary Layer. Atmosphere 12, no. 6:658.
- **Jiménez-Portaz, M.**, Chiapponi, L., Clavero, M., & Losada, M. A. (2020). Air flow quality analysis of an open-circuit boundary layer wind tunnel and comparison with a closed-circuit wind tunnel. Physics of Fluids, 32(12), 125120.

International Conferences

- **Jiménez-Portaz, M.**, Del-Rosal-Salido, J., Pospísil S., Clavero M., & Ortega M. (2020). Hot Wire Anemometry and Particle Image Velocimetry techniques comparison for wind tunnel measurements. 6^{th} IAHR Europe Congress.
- **Jiménez-Portaz, M.**, Clavero M., Pospísil S. & Losada M.A. (2020). Wind tunnel tests applied to wind energy management: Comparison of measurements in closed-circuit and open-circuit wind tunnels. Renewable Energy and Power Quality Journal 18, 272-275. doi: 10.24084/repqj18.296
- **Jiménez-Portaz, M.**, Clavero, M., & Losada, M. (2019). Experimental analysis of wind interaction with olive grove and the atmospheric surface boundary layer. European Journal of Sustainable Development, 8(5), 180-180.
- **Jiménez-Portaz, M.**, Bello-Millán, F. J., Folgueras, P., Clavero, M., & Losada, M. A. (2016). Wind flow around a wind turbine system over hilly terrain and its environmental effects: Wind tunnel tests. Renewable Energy and Power Quality Journal, 1(14), 318-321. doi:10.24084/repqj14.307

National Conferences

- **Jiménez-Portaz, M.**, Clavero, M., & Losada, M. (2019). Estudio a escala global de ecosistemas mediterráneos en túnel de viento. El caso del olivar andaluz. II Congreso Nacional de Investigadores en Formación: Fomentando la Interdisciplinariedad (JIFFI).
- **Jiménez-Portaz, M.** (2019). Ponente Invitado. Técnicas láser de velocimetría

para medidas en túnel de viento y canal de oleaje. IMPhocus19. II Congreso de Tecnologías Fotónicas e Imagen. Madrid.

- **Jiménez-Portaz, M.**, & Clavero, M. (2018). Interacción e integración: energías renovables y medio ambiente. I Congreso Nacional de Investigadores en Formación: Fomentando la Interdisciplinariedad (JIFFI).
- **Jiménez-Portaz, M.**. (2017). Túnel de viento de capa límite: el gran aliado de los parques eólicos. II Jornadas de Investigadores en Formación: Fomentando la Interdisciplinariedad (JIFFI).
- **Jiménez-Portaz, M.** (2017). Ponente Invitado. Aplicaciones de la técnica PIV and V3V en ensayos aerodinámicos e hidrodinámicos. IMPhocus17. I Congreso de Tecnologías Fotónicas e Imagen. Madrid.

Part II

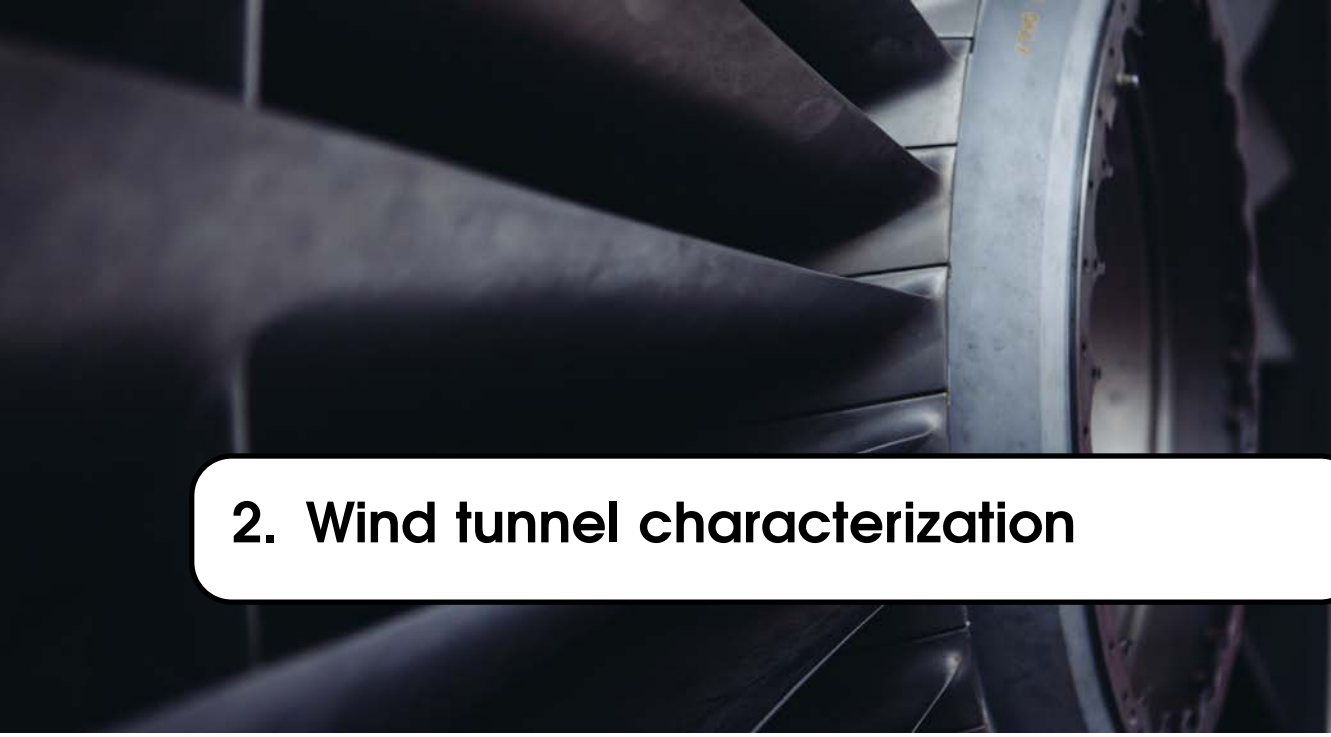

2. Wind tunnel characterization

The wide use of wind tunnels as a tool to measure the flow properties and the flow effects on different structures/ecosystems makes it necessary to guarantee the facility's correct functioning and carry out continuous monitoring. The main objectives of this chapter are: (i) to provide an overview of the use of wind tunnels and their operation, (ii) to provide an objective comparison of some of the most commonly used air flow measurement instruments, the Hot Wire Anemometry and the Particle Velocimetry Image system, for their proper use and selection, (iii) to check the homogeneity and quality of the airflow in an open-circuit boundary layer wind tunnel, and (iv) to compare some of the results with the behavior of a classic closed-circuit wind tunnel. The results concern the mean and turbulent flow characteristics, including the analysis of the turbulence production, the Reynolds stresses, the vertical velocity skewness, the vorticity, and the spectral properties. It is concluded that in terms of mean velocity, both instruments compared show similar results. However, in terms of turbulence, hot wire anemometry systems provide higher values. Finally, comparing the results concerning a closed-circuit wind tunnel shows that the turbulence intensity is generally higher, and the mean flow is more homogeneous in the open-circuit wind tunnel.

The information included in this chapter has been published in:

Jiménez-Portaz, M., Chiapponi, L., Clavero, M., & Losada, M. A. (2020). Air flow quality analysis of an open-circuit boundary layer wind tunnel and comparison with a closed-circuit wind tunnel. Physics of Fluids, 32(12), 125120.

Jiménez-Portaz, M., Del-Rosal-Salido, J., Pospísil S., Clavero M., & Ortega M. (2020). Hot Wire Anemometry and Particle Image Velocimetry techniques comparison for wind tunnel measurements. 6^{th} IAHR Europe Congress.

2.1 Fundamentals of wind tunnel operation

2.1.1 Wind engineering and wind tunnels

The interest and increase in the use of wind tunnels express the need to study the flow field and the effects of turbulence in a wide variety of practical cases. Classic examples are the study of model aerodynamics or the characterization of the Atmospheric Boundary Layer (ABL), whose kinematic properties are fundamental to quantify the impact of wind on infrastructures (Simiu and Yeo, 2019). Also, in recent years there has been an increasing interest in the study of the flow around renewable energy systems (Coudou et al., 2017), around forests or different ecosystems. Furthermore, in a wind tunnel, it is also possible to study (i) the dispersion processes of pollutants, dust, and pollen, and (ii) the evolution of parameters such as the Reynolds number in the presence of obstacles like a group of trees and/or buildings (Gromke, 2018; Hao et al., 2020).

There are two main types of wind tunnels: open-circuit wind tunnel and closed-circuit wind tunnel. In an open-circuit tunnel, the airflow follows a straight path from the entrance through a contraction zone to the test section, followed by a diffuser, a fan section, and an outlet. Such a tunnel may have a test section with no solid boundaries (Eiffel type) or solid boundaries (NPL type, which stands for National Physical Laboratory type). On the contrary, in a closed-circuit wind tunnel, the air recirculates continuously with little or no exchanges with the outside. A closed-circuit tunnel with no solid boundaries at the test section is called the Prandtl tunnel, whereas it is defined as a Göttingen tunnel if solid boundaries are present at that section. Nevertheless, it should be remembered that almost endless variations on the specific features of the various tunnels are possible (Barlow et al., 1999).

Open-circuit wind tunnels have the advantage of being more economical and more accessible to build than closed-circuit tunnels. However, the open-circuit

type is influenced by atmospheric conditions, with a strong dependence on (i) the architecture of the room in which the tunnel is located, (ii) the size and shape of the different parts of the tunnel, and (iii) the type of material used to construct the tunnel, mainly wood, so the structure could expand or contract with the weather and be affected by humidity (Barlow et al., 1999). In addition, continuous monitoring is necessary to ensure the homogeneity and quality of the flow, and a strict testing protocol must be followed to prevent any exchange with adjacent rooms, even avoiding the occasional entry of air through doors and windows. Closed-circuit tunnels allow better control of the flow, independent of the external conditions, and they are usually less noisy than open-circuit tunnels; however, the initial cost of construction and maintenance is higher.

A boundary layer wind tunnel offers the possibility to measure both the flow properties and the flow effects on different structures. The wind is initially characterized by parallel current lines and by a constant mean velocity set through a control system, and then it evolves depending on the surface roughness elements that are strategically arranged for the generation of the desired ABL (Barlow et al., 1999). In general, an experimental study in a wind tunnel aims to obtain the mean and instantaneous values of the kinematic variables of the airflow, and in some cases, the forces, pressures, and moments that wind exerts on the scaled structures.

For the characterization and analysis of the ABL evolution in a wind tunnel, a sufficiently large and homogeneous section is needed, with a tunnel length approximately 8-10 times the height of the section (Varshney and Poddar, 2011). Such a length guarantees the homogeneity of the flow at the test section, and it is necessary to have enough space for placing the energy dissipating devices designed to model the target ABL. The precise definition of all the geophysical variables that affect the ABL over complex topographies is a non-trivial matter, and it is essential to reproduce the physical characteristics of wind flow and its interaction with the scaled models. The control of all these variables and the fulfillment of the similarity conditions allow extrapolating the results to reality (Mattuella et al., 2016).

Wind tunnel tests provide large amounts of information and data, which represent fundamental support to decisions making for the management and planning of projects (Azzawi and Hasan, 2018), due to the multidisciplinary nature and versatility of this facility, applicable to different areas of knowledge, levels of detail in the study, and the extrapolation of data to reality. Currently, to obtain more accurate and reliable results, data are frequently validated and compared with in-situ measurements (Cheng et al., 2017) and numerical simulations. For example, Computational Fluid Dynamics (CFD) methodologies were used to improve the ABL generation and to design an optimized set-up for an open-jet facility, as the work of Aly and Gol-Zaroudi, 2017 shows. Comparative studies between tunnels and numerical simulations were also helpful for a proper and optimal design of new

tunnels (Azzawi and Hasan, 2018).

2.1.2 Characterization of the Atmospheric Boundary Layer

The different studies carried out within the framework of wind engineering require the analysis of the spectral characteristics of turbulence in boundary layer winds. Atmospheric spectra are usually represented by curves obtained by fitting to experimental results. The spectral representation associated with each scale of motion of kinetic energy, variance, or turbulent flow, provides a new perspective on the ABL structure. According to the ESDU manual (ESDU, 2001), it is recommended the use of the Von Karman spectral equation to study the turbulence properties for the management of dynamic-wind response, although it may underestimate the values in the higher frequency ranges.

Field experiments carried out in the past decades confirm that the spectral representations in the frequency or wavelength domain have similarities with some time-averaged statistics. Thus, in this work, the spectrum proposed by Kaimal has been taken as a reference to calibrate the desired atmospheric boundary layers (Kaimal and Finnigan, 1994).

$$\frac{f \cdot Su}{u_*^2} = \frac{102 \cdot n}{(1+33n)^{5/3}} \tag{2.1}$$

where u_* is the air friction velocity, S_u is the spectral density function of u, n is the dimensionless frequency, calculated as follow: $n = f \cdot z/U$, being f the frequency, z the height and U the mean wind velocity.

When considering neutral atmosphere conditions, the effects of thermal turbulence are neglected; therefore, the use of the Von Karman expression for the calculation of the mean vertical velocity profile is approximated by the expression:

$$U(z) = \frac{u_*}{k} ln\left(\frac{z}{z_0}\right) \tag{2.2}$$

where $k \approx 0.4$ is the Von Karman constant, and z_o is the aerodynamic roughness length. The aerodynamic roughness length depends on the characteristics of the surface over which the wind flows, and it is defined as the height at which the wind speed obtains a value equal to zero.

In general, due to its reliability, good results, and validity, the classic Davenport-Wieringa classification is used to obtain the value of the aerodynamic roughness height (Wieringa, Jon, 1992). Many of the investigations focused on the achievement of new roughness classifications are based on it and try to improve it, such as the use of LiDAR technology to obtain high-quality results and the use of remote

sensing to get this parameter, through direct and indirect methods (Ramli et al., 2009).

The second variable of interest is the turbulence intensity, a dimensionless measure that helps to correctly simulate the temporal variation of the velocity at every single point. From the expression of the spectrum, it is possible to calculate the vertical profile for this variable:

$$IT(z) = \frac{\sigma_u(z)}{U(z)} = \frac{1}{U(z)} \left[\int_0^\infty S_u(z,n) dn \right]^{1/2} \tag{2.3}$$

where σ_u is the temporal wind velocity standard deviation and $U(z)$ is the reference mean wind velocity.

2.1.3 Instruments selection and comparison

Hot-Wire Anemometry (HWA) and Particle Image Velocimetry (PIV) are two of the most widely used instruments for fluid flow quantification, especially for wind tunnels, where wind fields and turbulent movements are studied to understand the spatial and temporal evolution of the phenomena and the interaction with infrastructures and the ecosystems. Although hot-wire anemometry systems are the most used instrument for wind fluctuation measurements in aerodynamic wind tunnels (Martín Rodríguez et al., 2014), PIV has become one of the most valuable and powerful methods for velocimetry, allowing a better understanding of turbulent flows (Westerweel et al., 2013). This section aims to analyze the differences between measurement systems to select the most suitable to carry out the experiments in this thesis. This comparison is significant to improve the study of the interaction between wind flow and infrastructures, for example, for wind farm design, management, and optimization.

Experimental tests were performed in the Climatic Boundary Layer Wind Tunnel (CWT) of the Institute of Theoretical and Applied Mechanics (ITAM), Prague (Czech Republic), described in more detail in Section 2.5. The HWA was a Dantec Dynamics cross hot-wire, taking measurements with a sampling frequency of $1kHz$ and recording data during 120 seconds for each point. The data acquisition and analysis were performed using StreamWare Pro Software. The PIV was a Dantec Dynamics system with 532 nm green Dual Power Nano L 200-15 PIV laser from Litron Lasers and laser sheet optics with 80X91 Focus Module from Dantec Dynamics. For each test, 200 images were taken at a frequency of $8.15Hz$. And the analysis was performed with Dynamic Studio Software. Both instruments, set-ups, and methodology are described mode extensively in Chapter 4.

The main variables used for comparison are the mean wind velocity and the turbulence intensity, measured on the leeward side of a wind turbine and represented in non-dimensional form. Figure 2.1 shows vertical wind velocity and turbulence intensity profiles and the differences between HWA and PIV measurements for the same section. For both U and IT, comparing HWA data with PIV data, the values are 2% and 11% higher, respectively. Analyzing PIV data (Figure 2.2), it is noticed that, as the number of images increases during the processing, results improve. It is necessary to increase the number of images used to analyze turbulence and avoid fluctuations, allowing us to obtain more homogeneous, accurate, and physically meaningful profiles for U and IT.

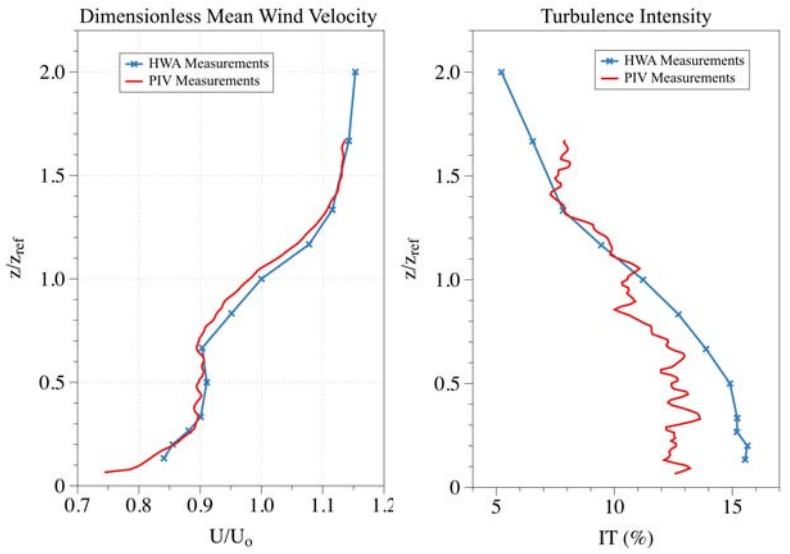

Figure 2.1: Instruments comparison. Mean wind profiles and turbulence intensity profiles from the results obtained for each instrument. The comparison shown in this figure was performed using 200 images for PIV data analysis, in order to obtain the most accurate results.

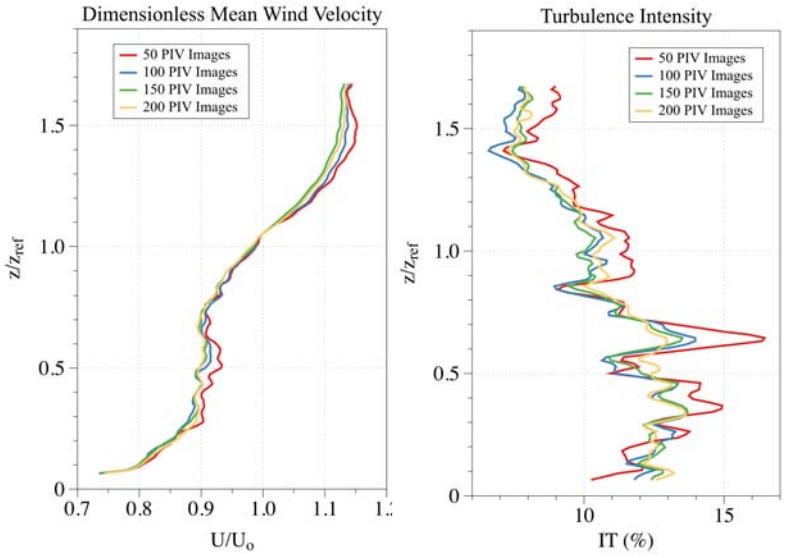

Figure 2.2: Comparison of the results obtained as we increase the number of images used in data processing.

It is concluded that the type of instrument can affect the results and should be taken into account, especially for turbulence intensity quantification. The differences between data from both instruments are almost negligible for mean wind velocity results, although, for turbulence intensity, values are higher for HWA data than PIV data. Nevertheless, it should be noted that the number of images is considered insufficient to obtain a statistically significant analysis of turbulence intensity. The faster installation and calibration of hot-wire sensors, their high sampling rate, high accuracy, and reliability, as well as the ease of taking measurements at different spatial points obtaining a three-dimensional grid of measurements, have led to the selection of this type of instrument for data collection in this Chapter and generally in the rest of the thesis.

2.2 Objectives

The main objectives of this chapter are:

- Provide an overview of the use of wind tunnels, applications, and their operation, as well as their potential use for environmental studies.
- Provide an objective comparison of some of the most commonly used air flow measurement instruments for their proper use and selection.
- Check the homogeneity and quality of the airflow in an open-circuit boundary layer wind tunnel.

- Compare the performances with those of a closed-circuit wind tunnel with similar geometry to the test section and analyze the differences between them.
- Highlight critical issues that may be common to tunnels of the same type, providing data and ideas useful for the management and the improvement of these facilities

2.3 Facilites and methodology

2.3.1 Open-Circuit Boundary Layer Wind Tunnel

In 2003, a boundary layer wind tunnel was built in the Laboratory of Environmental Hydraulics at the Andalusian Institute for Earth System Research (IISTA, University of Granada), shown in Figure 2.3. The IISTA wind tunnel is an open-circuit facility, and its total length is equal to $22m$. The closed test section is $13.6m$ long, with a $2.15m$ wide and $1.80m$ high cross-section, constant in the longitudinal direction. Therefore, the tunnel layout is of the NPL type. The choice of an open-circuit design was due, among other reasons, to space limitations. Figure 2.4(a) shows the arrangement of the tunnel inside the laboratory. The schematic view and more technical details can be found in Figure 2.4b-c). The flow velocity can be regulated from $1m/s$ to $20m/s$. In the past years, this tunnel has been used for many research activities, including the interaction between the wind field and ecosystems, the study of marine systems, dunes, and port areas, the aerodynamic and pressure effects of wind fields on infrastructures, and its interaction with the environment (Cuesta Cañas et al., 2008; Jiménez-Portaz et al., 2016; Jiménez-Portaz et al., 2019; Rodríguez Folgueras et al., 2012).

Figure 2.3: Open Circuit Wind Tunnel (IISTA). Photo taken in 2018.

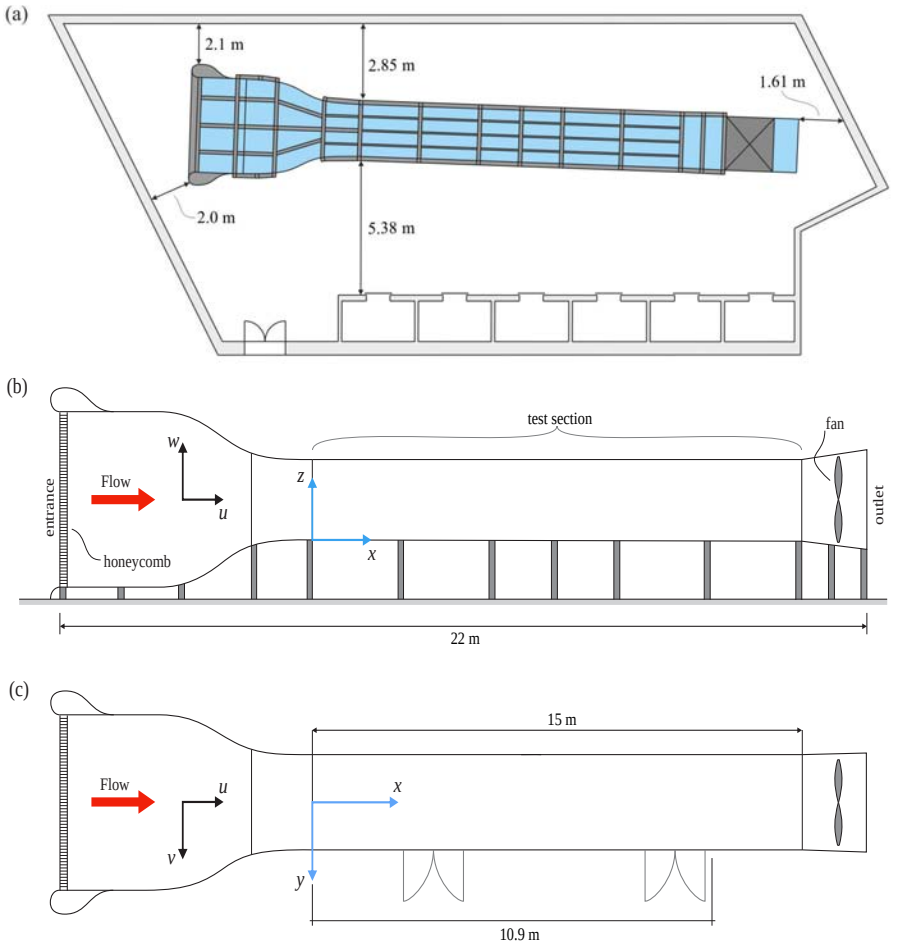

Figure 2.4: Open Circuit Wind Tunnel (IISTA). (a) Sketch of the wind tunnel inside the IISTA laboratory. (b) Front view. (c) Top view with the detail of the section where the measurements have been taken.

2.3.2 Instrumentation selected

A TSI constant temperature anemometer was used to obtain high-resolution and instantaneous measurements of the streamwise and vertical velocity components, u and w, respectively. The IFA-300 board controlled a cross-wire X-probe (model $1241-20$). The hot wire is held by a TSI Standard Probe Support, which is connected to a 3D positioning system. This positioning system is rigid, and it is fixed with screws onto the surface of the tunnel, avoiding any possible vibration. The probe has a total length of $47.5mm$ including the hot wire, and the sensor diameter is equal to $3.2mm$. The probe was placed perpendicular to the airflow, with

the wires oriented to obtain the longitudinal component and the vertical component of the wind speed vector. Calibration of the cross-wire anemometer was performed at the beginning of each experimental run.

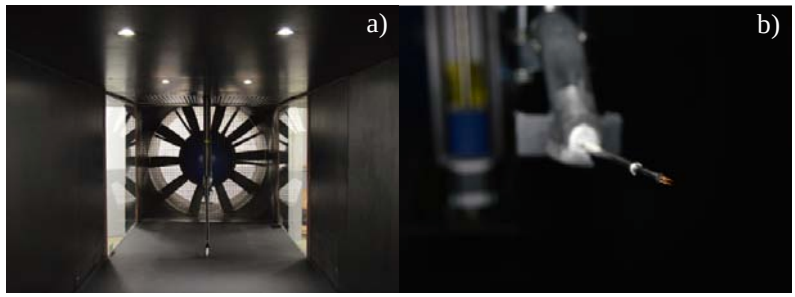

Figure 2.5: Instruments and devices: (a) 3D positioning system of instruments inside the BLWT; (b) cross hot wire anemometry system.

The principle of operation of this instrument is based on the heat transfer from the sensor to the surrounding fluid medium. The relation between the sensor voltage output and the flow velocity is established through a calibration transfer function. The IFA 300 system is characterized by a frequency response up to $300kHz$, depending on the sensor used. The high-pass filter was disabled, and the low-pass filter was set to $1kHz$. During the calibration process, a thermocouple system is used to reduce uncertainty and incorporate temperature variations. The average absolute difference between the instrument readings and the actual values (i.e., the velocities imposed during calibration) is of the order of $2mm/s$; this gives an estimate of the instrumental accuracy. The measurements in some points were also repeated on different days to check the reproducibility of the experiment. Data acquisition and processing were conducted using the software *ThermalPro*®, and statistical analysis of the variables was subsequently performed with the same software.

2.3.3 Experimental set-up

Systematic measurements of the wind velocity were taken, working with a constant reference velocity, which was obtained setting the rotation rate of the turbine. In the IISTA tunnel, the rotation generates a suction effect responsible for the air entering the inlet and flowing through the test sections towards the turbine and the outlet. The operation of the device induces an unavoidable air recirculation inside the room housing the tunnel (Figure 2.4(a)).

Eight different cross-sections were selected for the data acquisition, four at the entrance of the test section (group No 1, starting at $x = 0m$) and four at its end

(group No 2, starting at $x = 10.9m$ of the test section; see Figure 2.6). Considering one group at a time, the cross-sections are $0.20m$ apart from each other for group No 1, and $0.175m$ for the group No 2, and 11 equally spaced vertical profiles were acquired in each of them. The vertical resolution in group No 2 is finer to give a better description of the flow field in the testing region, where physical models are located for research activities, and the boundary layer is more developed.

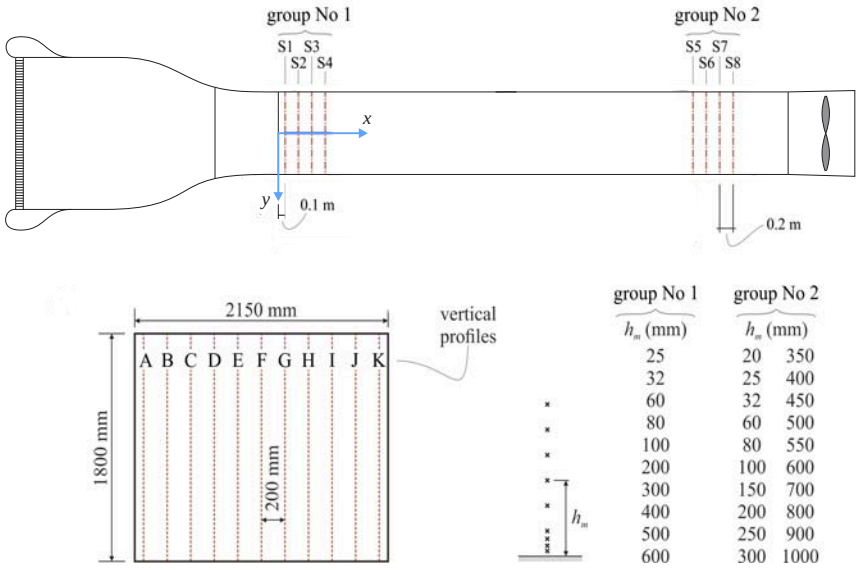

Figure 2.6: Experimental setup. Layout of the vertical profiles (A-K) in the cross-section; h_m is the distance from the bottom of the points where the speed has been measured.

Figure 2.6 shows the position of the profiles within a section. The velocity was measured in several points along with each vertical profile; 10 points in the case of profiles belonging to group No 1 and 20 points for the group No 2. In sum, 1320 wind speed time series were acquired for a given wind reference velocity. All these data are summarized in Table 2.1. The spacing of the points on the vertical increases from the bottom to the top as the influence of the tunnel surface decreases. The 3D positioning system allows the probe to be accurately placed in the desired position.

Since spectral and turbulence analysis requires a high sampling rate, data were acquired at each point with a sampling frequency of $1kHz$ for at least 130 seconds, under ergodicity assumption. A first statistical elaboration of the temporal series is necessary to perform real-time monitoring of the acquisitions. An example of the time series obtained is shown in Figure 2.7, for the two sections and three

representative heights. At the height of $0.025m$ there is a strong influence of the wind tunnel surface. The low-frequency content is related to the presence of coherent structures that are generated close to the bottom. Hairpin-like vortices Theodorsen, 1952 may follow each other, growing outwards from the wall and being responsible for this experimental evidence.

This analysis and data recording were performed using Thermal Pro software®. Measurements were repeated with three different reference wind velocities (see Table 2.1), which fall in the range most commonly used in the study of environmental systems.

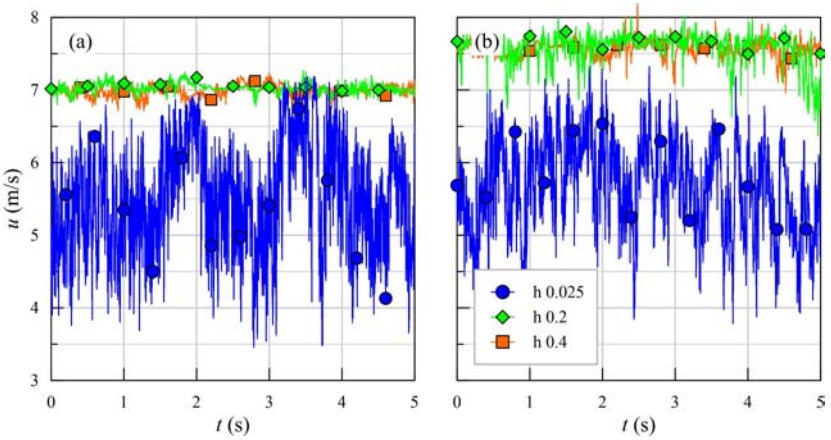

Figure 2.7: Time series recorded for: (a) entrance section (S1) and (b) tests section (S5), for three representative heights.

	Entrance Section	Tests Section
Number of vertical profiles	44	44
Number of points per profile	10	20
Number of total wind time series	440	880
Wind reference velocity (m/s)	3, 7.5, 10	3, 7.5, 10
Sample frequency (Hz)	1000	1000
Duration of the test (s)	130	130

Table 2.1: Tests carried out for each section, characteristics of data measuring and reference values.

2.3.4 Physical quantities and scales

Experimental results from this work are reported as mean and turbulent characteristics of the flow in the tunnel entrance and test sections. $\langle u(z) \rangle$ is the mean

streamwise velocity at a height equal to z. As a velocity scale we adopted the reference velocity ($7.5m/s$).

The Reynolds number is defined as

$$Re = \frac{\rho \langle u \rangle D_{ref}}{\mu}, \tag{2.4}$$

where μ is the dynamic viscosity of the air, ρ the air density, and $D_{ref} = 1.96m$ is the hydraulic diameter of the wind tunnel, defined as:

$$D_{ref} = \frac{2ab}{a+b}, \tag{2.5}$$

where $a = 1.8m$ and $b = 2.15m$ are the height and the width of the tunnel section, respectively.

Notice that the velocity range of the present experiments ensures the flow is fully turbulent ($Re = 1.05 \cdot 10^6$), and the viscosity effects on a local scale are minimal. This condition (i) is satisfied when the Reynolds number is greater than 2300 (critical Re for the pipe flow), and (ii) must be guaranteed in the case of tests performed on a reduced scale model in order to have a mechanically similar flow around the model, and the prototype (Chamorro et al., 2012; Schlichting and Gersten, 2016).

Turbulence is the most common, the most important, and the most complicated kind of fluid motion. The turbulent part, or wind fluctuations u', is defined as the instantaneous value of the wind speed minus the mean value; such a definition can be applied to all the other variables of interest (Stull, 2016). Therefore, the variance σ^2 is defined as:

$$\sigma_u^2 = \overline{u'^2} \qquad \sigma_w^2 = \overline{w'^2} \tag{2.6}$$

The turbulence intensity, as the simplest descriptor of the atmospheric turbulence for the x direction, is defined as IT and derived from the variance:

$$IT(z) = \frac{\sigma_u(z)}{U(z)} \tag{2.7}$$

Moreover, to obtain the kinematic momentum flux it was used the expression Stull, 2016:

$$u_*^2 = \mid \tau/\rho \mid = \mid \overline{u'w'} \mid \tag{2.8}$$

where u_* is the friction velocity and τ is the Reynolds stress.

The velocity fluctuations of the wind are caused by the superposition of eddies, which are transported by the mean flow. Vorticity and energy transfer processes characterize turbulence, and it can be analyzed and represented through its energy spectrum, among others variables.

The energy spectrum can be obtained using the Fourier transform of its auto-correlation function. From the energy spectral density function, it is also possible to represent how the Turbulent Kinetic Energy (TKE) is distributed with respect to the frequency (Uruba, 2012).

There is a relationship between the generation of turbulent Reynolds stresses and the interaction between vorticity and velocity. The vorticity, which is twice the rate of rotation of the fluid (Nieuwstadt et al., 2016), is also defined as the curl angular velocity (CAV).

$$\mathrm{CAV} = \nabla \times \mathrm{u}. \tag{2.9}$$

A positive angular velocity indicates a counter-clockwise rotation. In the present work, the vorticity has been calculated only in longitudinal planes since just two wind velocity components are available (longitudinal, x, and vertical, z).

2.4 Results

The present section describes measurements and data processing results, intending to characterize the flow field in the entrance and test regions. The cross-section area where the flow can be tested without being affected by the blockage effect is defined, which will be helpful for planning future research activities.

2.4.1 Mean flow characterization

To check the characteristics of the flow field and validate the wind tunnel in the present configuration, the average values of the velocity are analyzed first. Figure 2.8 shows the contour of the dimensionless wind velocity, U/U_o, for all the investigated sections (both in the entrance and in the test regions), with the effect of the solid boundaries: flow retardation and turbulence enhancement in the areas adjacent to the walls. However, it is possible to observe that, outside the boundary layer and at a sufficiently large distance from the sidewalls, the homogeneity of the wind field is pretty good. Few vertical patterns are visible, and they may be due to an asymmetry in the flow resistances outside and/or inside the tunnel. The different spacing of the walls surrounding the tunnel could prevent a constant air supply at the entrance. Moreover, some imperfections on the side walls (e.g., minimal

steps between the covering panels) may arise as a consequence of the thermal deformations of the structure, and they could be responsible for local variations in roughness.

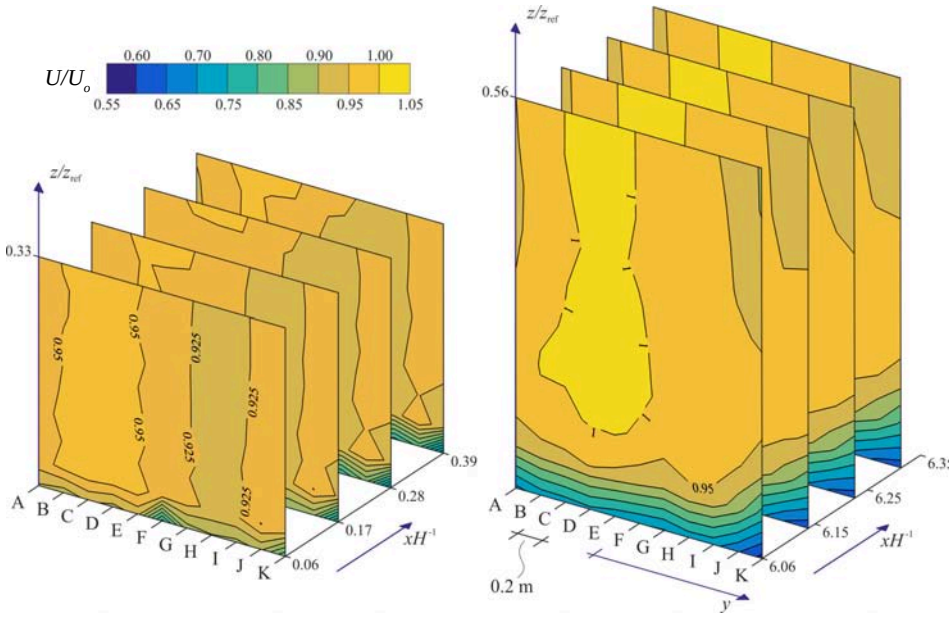

Figure 2.8: Mean streamwise velocity of the wind, U/U_o, in the entrance region (a) and in the test region (b). The color bar is the same for both panels.

The logarithmic profile can express the mean velocity profiles in the near-wall region of a turbulent boundary layer over rough walls. This gives the velocity at a height above the surface, $u(z)$, defined by the equation 2.2. In the present study, a logarithmic profile is evident in the test region, where the data fitting allows to obtain both the values of z_0 and u_*. On the contrary, the wind profile at the entrance is not sufficiently developed, and there are not enough measurements near the bottom to carry out any quantitative evaluation. The roughness length is almost constant in the test region, and it is of the order of $1 \times 10^{-4} m$, with minimal variations except near the right wall (for $y = 1m$). Figure 2.9(a) shows some of the measured profiles in the test region and the thickness, z_b, of the boundary layer. The value $z_b = 0.18m$, obtained by means of the classical 99% method, is in accordance with the values 0.181 and 0.188 calculated using the well known expression (Xie et al., 2018).

$$z_b = 0.37 \frac{x}{\mathrm{Re}_x^{1/5}}, \tag{2.10}$$

for sections S5 and S8, respectively. $\mathrm{Re}_x = ux/\nu$ is the Reynolds number in the x direction, and ν is the kinematic viscosity of the air.

The friction velocity map in the test region is represented in Figure 2.9(b), and it is possible to observe that u_* is almost constant, with most of the values in the range $0.38 - 0.40 m/s$. Again, near the right wall, an anomaly is present with the friction velocity decreasing to $0.2 m/s$. This behavior can be due to the asymmetry of the hosting room or to a local disturbance (e.g., a discontinuity in the bottom coating).

A comparison of some velocity profiles with the classical law of the wall is shown in Figure 2.10(a). In the logarithmic region,

$$u^+ = \frac{1}{k}\ln\left(y^+\right) + C - \Delta u^+, \tag{2.11}$$

where $u^+ = u/\ u_*$ and $y^+ = zu_*/\nu$ are dimensionless velocity, C is assumed to be a constant for smooth-walled flows ($C = 5.1$ according to Schlichting and Gersten, 2016) and Δu^+ is defined as the roughness function and it represents a roughness-caused shift. As expected for a rough surface, the experimental profiles are located below the smooth wall profile, with $\Delta u^+ \approx 8.5$.

Near a rough wall, the characteristic scale, instead of being controlled by a frictional scale may be controlled by roughness length z_0; if $z_0 > z_f \equiv \nu/\ u_*$, a better scaling is $z^+ = z/z_0$, as shown in Figure 2.10(b).

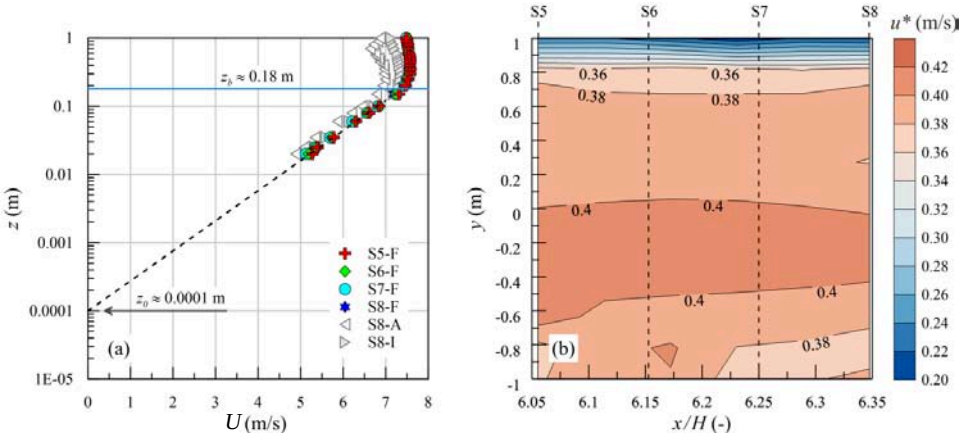

Figure 2.9: Vertical profiles of the mean wind velocity (a) and friction velocity map (b), in the test region. z_0 is the roughness length and z_b is the boundary layer length. For clarity, only a limited number of profiles are shown listed in panel (a).

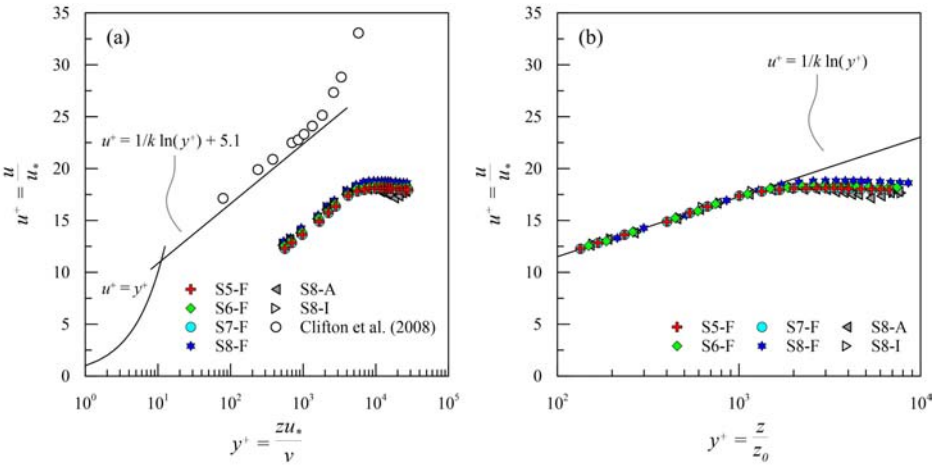

Figure 2.10: Vertical profiles of wind speed and turbulence intensity measured in the tunnel entrance section (a) and in the tunnel test section (b)

A summary of the main parameters and variables that define the boundary layer obtained for the tests section is shown in the Table 2.2:

Section	z_b	z_0(m)	u_*(m/s)
S5	0.181	$0.99 \cdot 10^{-4}$	0.382
S6	0.183	$1.09 \cdot 10^{-4}$	0.382
S7	0.186	$1.02 \cdot 10^{-4}$	0.373
S8	0.188	$0.96 \cdot 10^{-4}$	0.371

Table 2.2: Boundary layer characteristics: average value in section S5-S8.

2.4.2 Spectral analysis

The energy distribution in the frequency domain is described by the power spectrum, which has a significant influence (i) on the wind-structure interaction and (ii) on the aerodynamic loads (Kozmar and Laschka, 2019).

In particular, turbulence has a wide range of length (time) scales. As is known, fluctuation energy is produced at the large eddies (with low frequencies). The vortex stretching mechanism generates smaller and smaller eddies, and energy flows down the spectrum to the high-frequency region. Finally, the energy is mainly dissipated into heat at the smallest eddies (of the order of the Kolmogorov scales). Larger eddies significantly contribute to aerodynamic loads; however, smaller eddies can affect bluff bodies more (Kozmar and Laschka, 2019). Inside the boundary layer, the turbulent eddies transfer momentum deficit away from the surface, meaning that low momentum fluid is transported away from the surface and replaced by fluid

with more momentum that came from above the surface.

The power spectra of the streamwise velocities are calculated via FFT (Fast Fourier Transform) and compared with the classical VonKarman formula (Tian et al., 2011) for the dimensionless spectrum of the longitudinal component of atmospheric turbulence:

$$\frac{nS_u(n)}{\sigma_u^2} = \frac{4n_u}{(1+70.8n_u^2)^{5/6}} \tag{2.12}$$

where $n_u = nL_u/U$, n is the frequency, U the longitudinal mean wind speed, σ_u the standard deviation and L_u the longitudinal length scale. It is proved (for large n) that if a VonKarman spectrum is plotted on log-log axes, the high-frequency part of the spectrum will approximate a straight line of gradient $-5/3$. The position of this line is determined by U, σ_u, and L_u.

Figure 2.11 shows two spectra obtained at height $z = 0.08$ and $1.00m$ in the test region (section S8, profile F). Values of the spectral function decrease as the distance from the tunnel floor z are increased. It is also possible to see a good definition of the inertial sub-range ($-5/3$ slope) starting at a frequency $\approx 10Hz$.

The comparison with Equation 2.12 was obtained for the spectra measured at different heights and in different sections, but it is only shown for the spectra represented in Figure 2.11. The agreement is fairly good both in and out of the boundary layer.

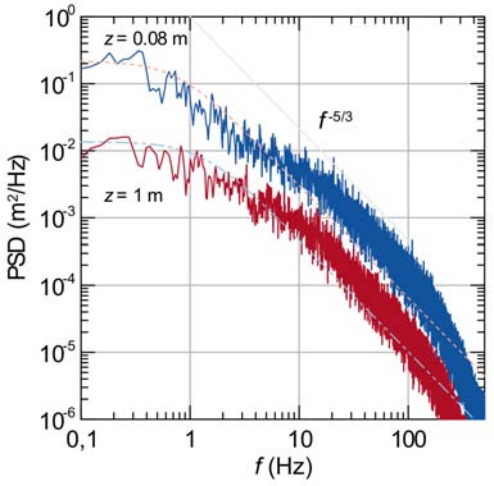

Figure 2.11: Power Spectral Density of the streamwise velocity in section S8 (test region) at different heights. Dashed and dot-dashed lines are the Von Karman spectra.

2.4.3 Turbulence characterization

Turbulence and Reynolds stresses

In order to study the air-flow turbulence and provide a better characterization of the flow in both sections, the turbulence intensity (IT) in the cross-sections has been analyzed.

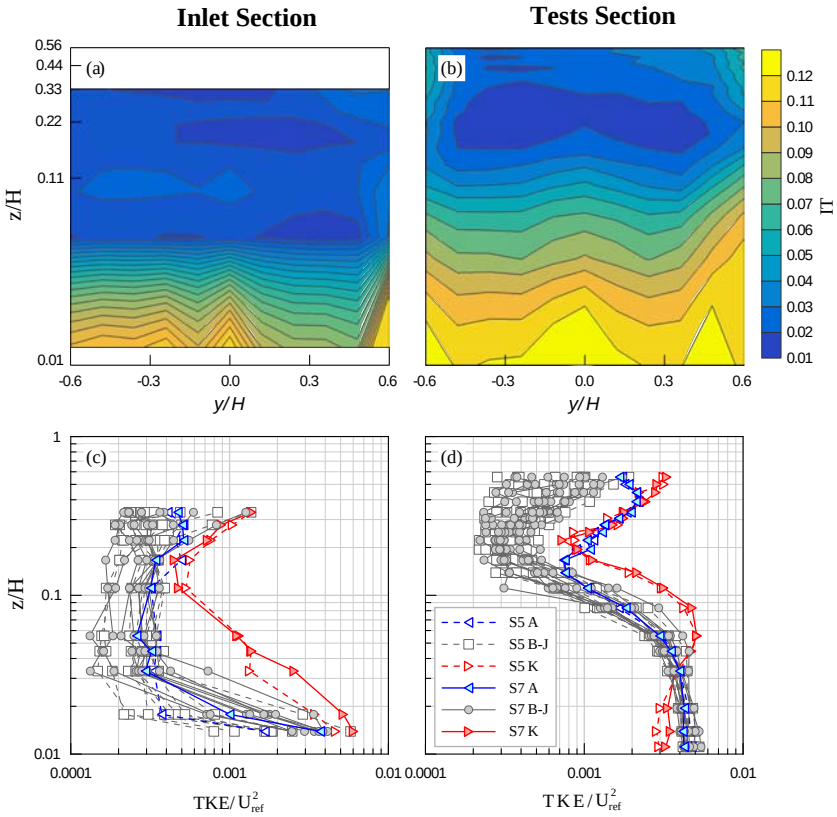

Figure 2.12: Turbulence Intensity. (a) section S3; (b) section S7; (c) vertical profiles of the turbulent kinetic energy in section S1 (empty symbols) and S3 (filled symbols); (d) vertical profiles of the turbulent kinetic energy in section S5 (empty symbols) and S7 (filled symbols).

Figures 2.12(a) and 2.12(b) show the contour map of the turbulent intensity in section S3 and section S7, respectively. It is possible to observe the influence exerted by the surface of the bottom and the lateral walls, with the turbulent intensity presenting the maximum values inside the bottom boundary layer. The variation along the x axis is practically nil within both group 1 and group 2. Most of the variables related to the turbulence are represented with a logarithmic vertical scale

to evaluate the details in the area near the tunnel bottom because the turbulence itself is higher right there.

Figures 2.12(c) and 2.12(d) show the vertical profiles of the turbulent kinetic energy in two sections of group 1 (S1 and S3) and two sections of group 2 (S5 and S7), respectively. Also, it is possible to observe the effect of the lateral walls, with a particular asymmetry between profile A and profile K, especially in the inlet region (group 1). This behavior can be once again addressed to the positioning of the tunnel in the hosting room, with an external recirculation of the air that can not be symmetrical.

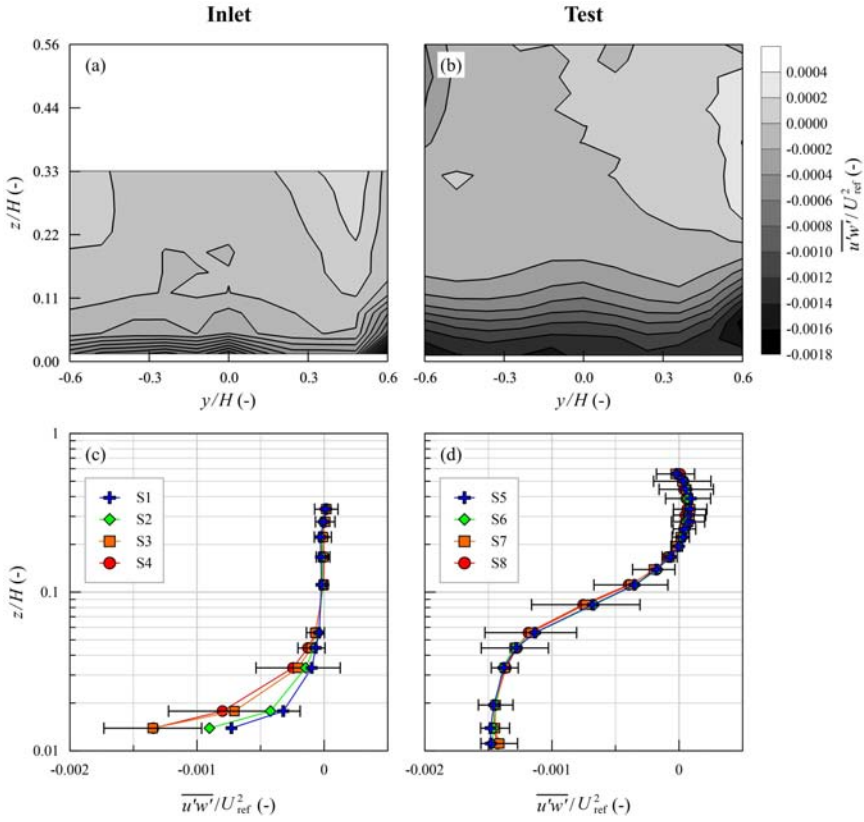

Figure 2.13: Reynolds Shear stress. (a) Section S3; (b) Section S7; (c) vertical profiles averaged in the spanwise y direction in the inlet region; (d) vertical profiles averaged in the spanwise y direction in the test region. Error bars refer to one standard deviation.

The Reynolds shear stresses, non-dimensional with respect to the reference velocity, are shown in Figure 2.13. In the inlet region, as the x coordinate increases, it is possible to observe an evolution of the shear stress profile within the boundary

layer. On the contrary, in the test region, there is no appreciable variation between the different sections. A layer of constant shear stress $\overline{u'w'}$ was observed, in the range of $z/H = 0$ to ≈ 0.06. Error bars refer to one standard deviation, and it is possible to observe that their maximum amplitude is reached near the bottom at the entrance and the upper limit of the boundary layer in the test region. This may be attributable to the following reasons: (i) the thickness of the boundary layer itself undergoes modest variations along the transverse direction; (ii) the side walls locally modify the entity and the distribution of shear stresses.

Reynolds stress tensor's principal axes

The interaction between the mean flow and the fluctuating velocity can also be analyzed by observing the Reynolds stress tensor. In the case of the action of a constant, pure plane strain on an initially isotropic turbulence Takahashi, 2018, the principal axes of the Reynolds stress tensor are those of the mean rate of strain, and the turbulent motion appears as oriented by the strain field. When the strain field changes, the axes of the Reynolds stress tensor tend to be reoriented along the axes of the new strain, with a delay that depends on the time scale of the imposed strain. If the strain tensor reduces to pure shear stress, for isotropic turbulence, the principal axes of the Reynolds stress tensor are not aligned with those of the strain, which is a consequence of the mean rotation.

The two principal stresses in the xz-plane, according to Champagne et al. (1970), are defined as

$$\sigma_{a,b} = \frac{\overline{u'u'} + \overline{w'w'}}{2} \pm \sqrt{\left(\frac{\overline{u'u'} - \overline{w'w'}}{2}\right)^2 + \left(\overline{u'w'}\right)^2}, \tag{2.13}$$

and their orientation is

$$\alpha_\sigma = \frac{1}{2}\arctan\left(\frac{2\overline{u'w'}}{\overline{u'u'} - \overline{w'w'}}\right). \tag{2.14}$$

The present experiments result in $\sigma_a/\sigma_b = 2$ to 8 in the boundary layer, with the highest value close to the bottom. The ratio tends towards unity in the outer region, especially in section S5 to S8, while its value is a bit higher in the inlet region, see Figures 2.14(a) and (b).

For comparison, the ranges of values in three traditional flows are:

$$\sigma_a/\sigma_b = 3 \text{ to } 4 \qquad \text{(boundary layer)} \tag{2.15a}$$

$$\sigma_a/\sigma_b = 3 \text{ to } 5 \qquad \text{(channel)} \tag{2.15b}$$

$$\sigma_a/\sigma_b = 2 \text{ to } 6 \qquad \text{(plane wake)} \tag{2.15c}$$

The orientation angle found in the boundary layer and channel flow is $\alpha_\sigma \approx -20^\circ$ to -25° and $\alpha_\sigma \approx 70^\circ$ to 65°, while that in the wake is $\alpha_\sigma \approx 40^\circ$ to 50° and $\alpha_\sigma \approx -50^\circ$ to -40°, as reported by Champagne et al.Champagne et al., 1970.

Figures 2.14(c) and (d) show the principal axis angle of turbulence in sections S3 and S7, respectively. In the present experiments, the Reynolds stress tensor has a principal axis at $\approx -15^\circ$ close to the bottom, with values that progressively grow up to $\approx -35^\circ$ near the upper limit of the boundary layer. In section S7, it is also possible to observe the influence of the right wall where the orientation is mainly in the range $\approx 15^\circ$ to $\approx 35^\circ$. In the upper part of the outer region, the pattern is not homogeneous, but we bear in mind that the values of the shear stresses are almost nil in that area, resulting in more significant uncertainty in the estimation of α_σ.

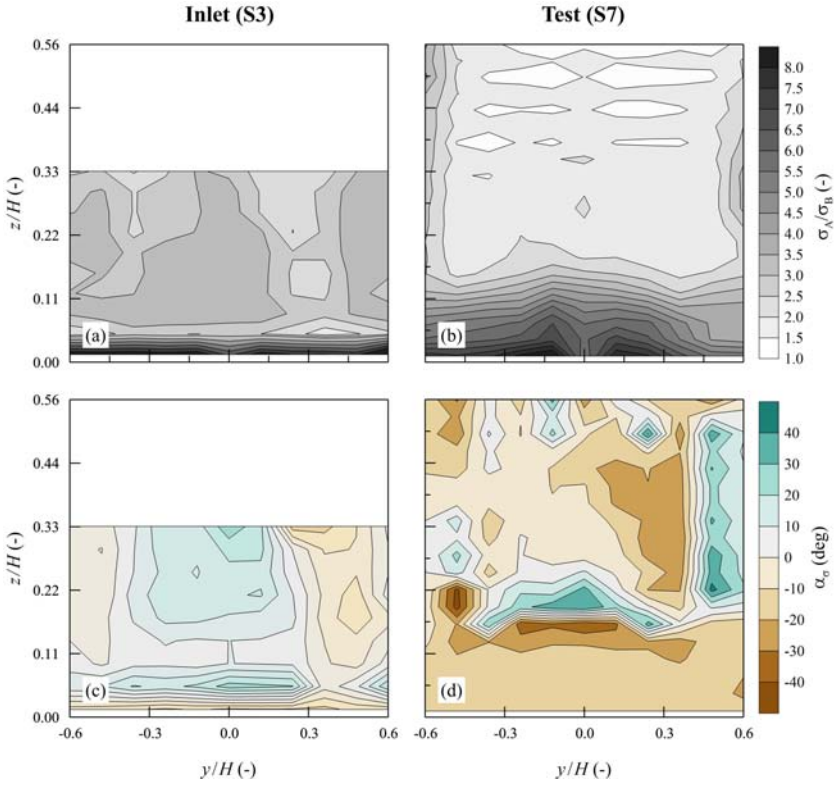

Figure 2.14: Ratio of the maximum–minimum stresses: (a) section S3, in the inlet region; (b) section S7, in the test region. Time-averaged principal axes angle of the Reynolds stress tensor: (c) section S3; (d) section S7.

Skewness

The statistics of turbulence can also be characterized by the vertical velocity skewness, that is given by

$$S_w = \overline{w'^3} / \overline{w'^2}^{3/2}, \tag{2.16}$$

and it is indicative of the structure of the motion (Hogan et al., 2009), since the triple correlation $\overline{w'^3}$ represents the vertical transport of $\overline{w'w'}$ by the turbulence itself. Skewness plays the same role in the equation for the evolution of turbulent kinetic energy (TKE). Hence when $\overline{w'w'}$ (and therefore skewness) is positive, both $\overline{w'w'}$ and TKE are being transported upwards. That, as expected, is what happens inside the boundary layers for the present experiments. Figure 2.15 shows the contour map of the skewness in two different sections.

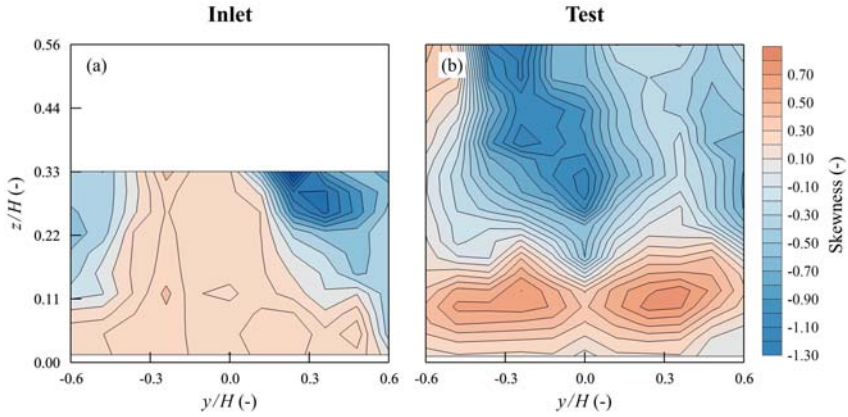

Figure 2.15: Skewness map: (a) section S3, in the inlet region; (b) section S7 in the test region.

Vorticity

The vorticity describes the local spinning motion of a continuum (e.g., the tendency of the fluid to rotate), and it is twice the local rotation rate. The curl angular velocity (*CAV*) is shown in Figure 2.16 for two longitudinal sections in the inlet region (panels a, b), and for two longitudinal sections in the test region (panels c, d). It is possible to observe that the CAV is almost nil out of the boundary layers, while it increases towards the bottom up to $-201/s$ in the test region, and up to $-601/s$ in the entrance region. The minus sign indicates a clockwise rotation direction. The generation of vorticity in the inlet region can be attributed to some minor irregularities between section S1 and the tunnel entrance. No appreciable variation

is present between plane F and K, which are in the tunnel center and close to the wall, respectively.

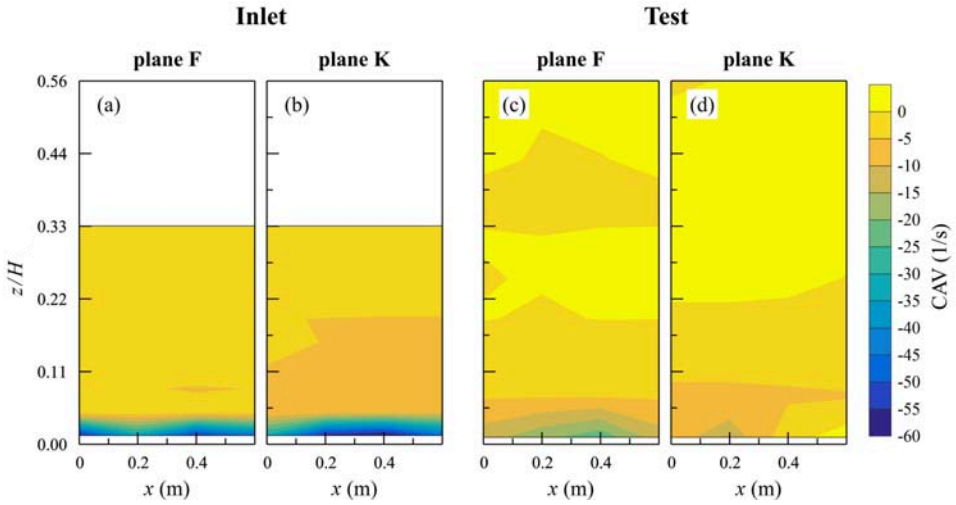

Figure 2.16: Curl angular velocity map. Inlet region: (a) plane F, (b) plane K. Test region: (c) plane F, (d) plane K.

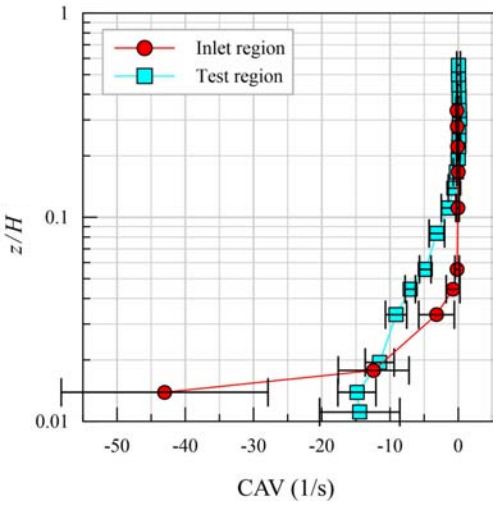

Figure 2.17: Profiles of the CAV (averaged in the x and y direction) for both the inlet and the test region. Error bars refer to one standard deviation.

Figure 2.17 shows the profiles of the CAV (averaged in the x and y direction);

error bars refer to one standard deviation. The variability is very low, except for the points close to the bottom, where horseshoe vortexes are generated. Their origin is related to the instability of the instantaneous velocity profile evolving into transverse vortices Theodorsen, 1952, whose structure is described in the literature Carlier and Stanislas, 2005.

2.5 Comparison with a Closed-Circuit Wind Tunnel

2.5.1 Closed-Circuit Wind Tunnel

The Climatic Boundary Layer Wind Tunnel from the Centre of Excellence Telč (CET), of the Institute of Theoretical and Applied Mechanics (ITAM), Prague (Czech Republic), is a Göttingen closed-circuit type wind tunnel, and its layout is shown in Figure 2.18. The tunnel consists of two distinct test sections, a climactic section, in which it is possible to simulate a wind flow of between 0.1 and 20 m/s, to modify the air temperature between $-10°C$ and $+40°C$, as well as to reproduce rain and snow on a small scale, and an aerodynamic section, which has a $11m$ long and a $1.9m$ wide $\times$ $1.8m$ high cross-section. In this section, the Atmospheric Boundary Layer and wind speeds between 0.1 m/s and 50 m/s can be simulated, and it is the section where the tests of interest for this thesis will be carried out.

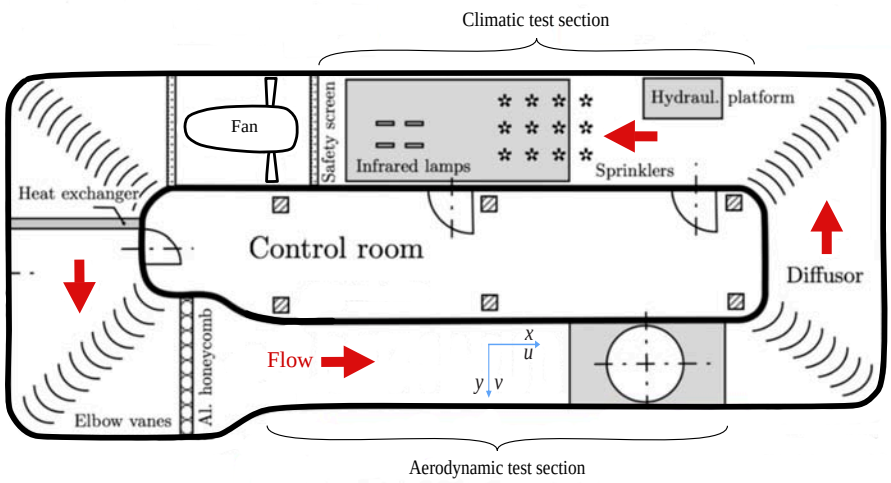

Figure 2.18: Closed-Circuit Wind Tunnel (CET). Sketch of the wind tunnel inside the CET laboratory.

2.5.2 Comparison set-up

The data are available in the literature and were acquired by the authors through a Dantec Dynamics cross hot-wire anemometer, with a sampling rate of $1kHz$ for a period equal to $20s$ at each point. The reference velocity was $U_o = 13.5m/s$. The test program and the complete description of the tests are detailed in the original manuscript Kuznetsov et al., 2017.

The Reynolds number has similar values in both tunnels: $Re = 1.05 \cdot 10^6$ for the OCWT and $Re = 1.6 \cdot 10^6$ for the CCWT, with D_{ref} equal to $1.96m$ and $1.85m$, respectively. This suggests that the tunnels are similar, and the comparison between scaled quantities can be performed even if the reference velocities are different.

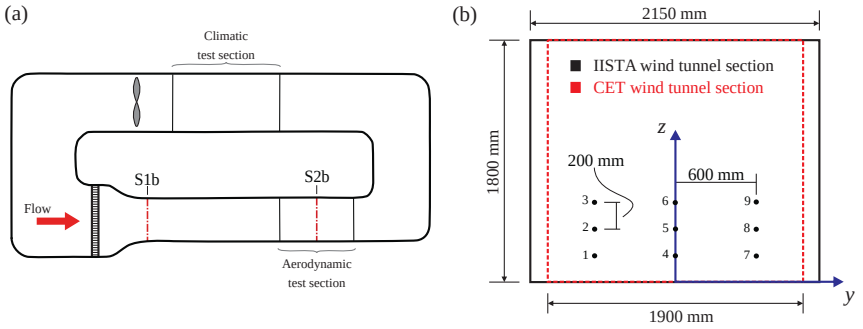

Figure 2.19: Climatic Boundary Layer Wind Tunnel at CET. (a) Layout of the tunnel showing (i) the two test sections (i.e., aerodynamic and climatic), (ii) the turbine, (iii) the mouthpiece and (iv) the section for the placement of roughness elements. A more complete sketch is shown in the work of Kuznetsov et al., 2017. (b) Cross section S2 compared with the section of the IISTA wind tunnel (OCWT is represented in black and CCWT in red). The points selected for the comparison are shown (1-9).

2.5.3 Results

Two pairs of cross-sections have been selected to perform the comparison. We will refer to sections S1 ($x/H = 0.06$) and S1b ($x/H = 0.33$) for the inlet region, belonging to IISTA and CET tunnel, respectively. For the test region, we will refer to section S5 ($x/H = 6.06$) and section S2b ($x/H = 5.26$). Data are available at 9 points within the area where models are usually located, and measurements are taken. The points are in the lower-central area of the section, avoiding (i) excessive proximity to the walls, (ii) possible distortions due to the different width of the tunnels, and (iii) the blockage effect exerted by the lateral and upper contours of the section; see Figure 2.19(b). The coordinates of the points are measured in a coordinate system with origin on the bottom, at the center of the section (Tables

2.3-2.4 report the coordinates in millimeters).

The comparison concerns the non-dimensional mean velocity, $Uc = u/u_{ref}$, and the turbulent intensity, $ITc(\%)$. Table 2.3 contains the values measured at the inlet cross-section in both the tunnels; Table 2.4 contains the same for the test cross-section. A comparison parameter for the turbulence intensity is also reported: $r_I = I_{IISTA}/I_{CET}$, which is the ratio between the turbulence intensities in the two tunnels. Values of r_I lower than unity mean that the turbulence intensity is lower in the IISTA tunnel than in the CET tunnel.

Point (#)	y (mm)	z (mm)	Uc (-)		ITc (%)		
			IISTA	CET	IISTA	CET	r_I
1	-600	200	0.96	0.91	1.4	1.8	0.8
2	-600	400	0.96	0.91	1.3	1	1.3
3	-600	600	0.95	0.92	1.4	1.1	1.3
4	0	200	0.93	0.90	1.2	1.3	0.9
5	0	400	0.93	0.91	1.2	1	1.2
6	0	600	0.93	0.90	1.4	1.2	1.2
7	600	200	0.92	0.86	1.1	1.4	0.8
8	600	400	0.91	0.87	1.4	1.5	0.9
9	600	600	0.90	0.86	2.4	1.8	1.3
mean value			0.93	0.89	1.42	1.34	1.08
standard deviation			0.02	0.02	0.38	0.31	0.22

Table 2.3: Data in the inlet cross-sections S1 and S1b (IISTA and CET tunnel, respectively).

Point (#)	y (mm)	z (mm)	Uc (-)		ITc (%)		
			IISTA	CET	IISTA	CET	r_I
1	-600	200	0.98	0.99	3.0	2.5	1.2
2	-600	400	0.98	1.01	1.3	1.3	1.0
3	-600	600	0.97	1.02	1.5	1.0	1.5
4	0	200	0.99	0.99	4.3	1.5	2.9
5	0	400	1.00	0.99	1.9	1.2	1.6
6	0	600	1.00	0.98	1.8	0.9	2.0
7	600	200	0.99	0.96	3.2	1.5	2.1
8	600	400	1.00	0.96	1.6	1.4	1.1
9	600	600	0.99	0.95	2.4	1.8	1.3
mean value			0.99	0.98	2.09	1.54	1.64
standard deviation			0.01	0.02	0.83	0.46	0.60

Table 2.4: Data in the test cross-sections S5 and S2b (IISTA and CET tunnel, respectively).

The non-dimensional velocity data are represented in Figure 2.20. A comparison can be made between panels (a) and (c) considering the inlet regions; both the tunnels present (i) a negative gradient from the left to the right side, and (ii) velocities slightly lower with respect to the reference one. In the case of the CET tunnel, the gradient can be an expression of the flow field non-homogeneity induced by the curves of the closed circuit. In the IISTA tunnel, it is probably due to the lack of symmetry in the positioning of the tunnel in the hosting room. Panels (b) and (d) allow comparing the velocity distribution in the test regions. The flow is more homogeneous in the IISTA tunnel with respect to the CET one, with values very close to the reference velocity and minimal gradients. We infer that the open circuit geometry allows the flow to recover uniformity, while that does not happen in the other facility. Also, a quantitative analysis is performed by considering the local flow velocity deviation from the average velocity:

$$Dev = \frac{U - \overline{U}}{\overline{U}}. \tag{2.17}$$

where U is the local velocity and $\overline{U}$ is the average velocity over the section. A zero deviation means that the local velocity magnitude is the same as that of average velocity. The average deviation index explains the overall behavior of flow uniformity, and it can be calculated as:

$$DI = \left(\int_{A_0} \frac{U - \overline{U}}{\overline{U}} dA \right) A_0^{-1}. \tag{2.18}$$

where dA is the differential element of the area and A_0 is the total area of the section. The deviation index represents local distribution very well in cases where the flow uniformity is high Om Ariara Guhan et al., 2016. In the IISTA tunnel, DI is equal to 1.7% and 0.8% for the inlet and test section, respectively. In the CET tunnel, the deviation index is higher, with values equal to 2.2% (inlet section) and 1.9% (test section).

The turbulence intensity is generally higher in the IISTA tunnel, except for the lower part of the inlet cross-section, where the ratio r_I presents values between 0.8 and 1. The main differences can be found in the test cross-section, with values of r_I up to 2.9, especially in the lower region. Figure 2.21 shows the contour maps of the parameter r_I. In any case, the maximum value of the turbulent intensity is equal to 4.3%.

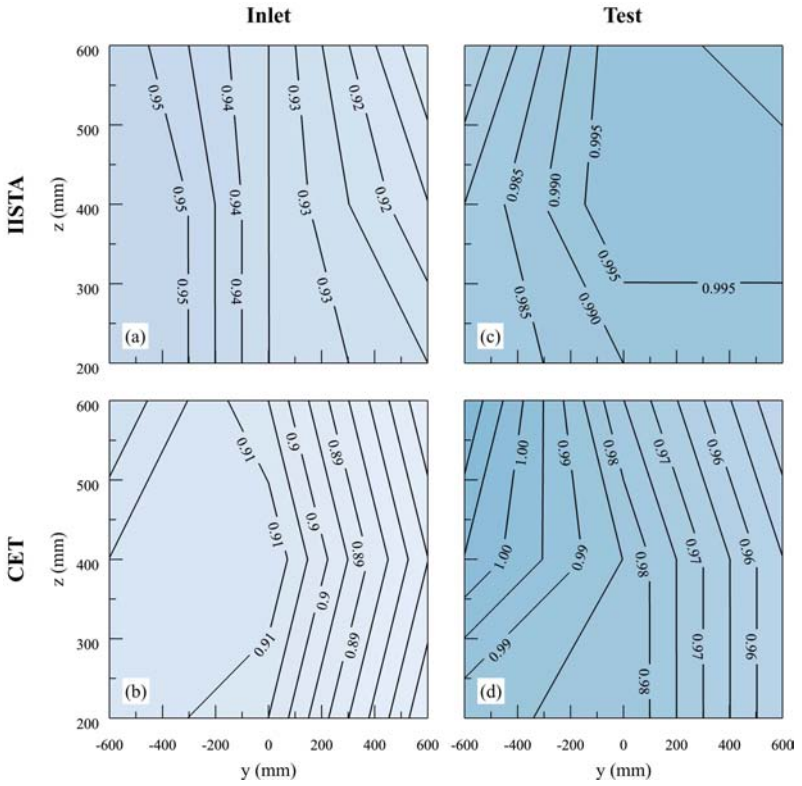

Figure 2.20: Non dimensional wind velocity, U/U_o. Panel (a) and panel (b) refer to IISTA inlet and test region, respectively. Panel (c) and panel (d) refer to CET inlet and test region, respectively.

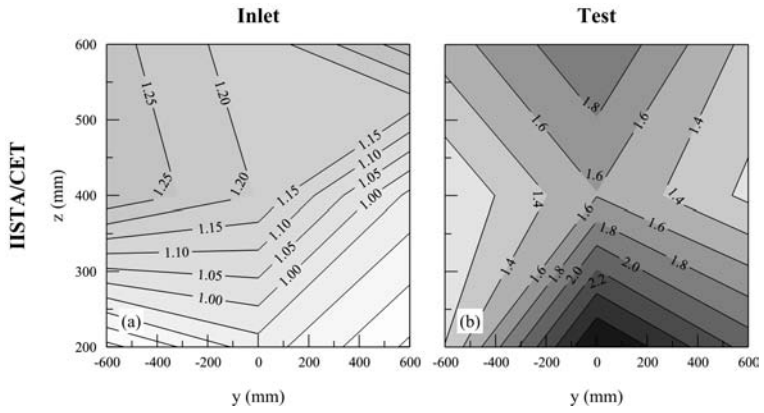

Figure 2.21: Ratio of the turbulent intensity in the OCWT tunnel with respect to the same quantity in the CCWT tunnel.

2.6 Conclusions and discussion

The multidisciplinary use of wind tunnels and their application to different systems and work scales makes it necessary to guarantee the facility's correct functioning and carry out continuous monitoring.

Experimental tests to study the airflow inside a Boundary Layer Wind Tunnel have been carried out in the open-circuit wind tunnel of the Andalusian Institute for Earth System Research from the University of Granada (Spain). The analysis regards the mean and turbulent characteristics of the flow, and it includes details about the turbulence production, the Reynolds stress, the vertical velocity skewness, the vorticity, and finally, the spectral properties. Data has been taken for the tunnel entrance and the test section to overview the tunnel performance.

There is flow retardation and turbulence enhancement in areas adjacent to the wall; however, the wind field is relatively homogeneous at a distance large enough from the sidewalls. The agreement between the power spectra of the streamwise velocities and the Von Karman spectrum is very good, in and out of the boundary layer, except for the highest frequencies. The curl angular velocity is almost nil out of the boundary layers for both sections but increases towards the bottom, higher for the tunnel entrance, with a clockwise rotation direction. To complete the turbulence analysis, according to the results for the vertical velocity skewness, it has been proven that there is a Turbulent Kinetic Energy transport upwards.

A lack of symmetry in the behavior of the tunnel has been observed. This behavior could be addressed to the positioning of the tunnel in the hosting room, with an external recirculation of the air that cannot be symmetrical.

The results obtained for the OCWT have been compared with similar data from the Climatic Boundary Layer Wind Tunnel from the Centre of Excellence Telč (Czech Republic), a closed-circuit wind tunnel. This comparison shows that, in both tunnels, velocities are slower than the reference one. The mean flow is more homogeneous in the OCWT, but the turbulence intensity is generally higher. Finally, similar values of Reynolds number suggest the tunnels are mechanically similar.

In conclusion, we have performed a flow characterization which (i) allows to estimate the behavior of an open circuit wind tunnel, and (ii) represents a fundamental knowledge to better schedule tests and better interpret results of future activity. Moreover, this chapter is a collection of valuable data for improving similar CCWTs or the design of new devices.

Based on the results obtained, a series of modifications are proposed, which may apply to all tunnels under similar conditions. For example, the open circuit tunnel should be isolated from the hosting room conditions by eliminating all possible elements that, being located in the room, could generate distortions. This should result in an improvement of the airflow generated in the external circuit around the tunnel. A first enhancement can be achieved by installing some deflectors in the room, especially in the area close to the turbine, to adjust the symmetry of the flow. Unfortunately, in the present case, it is impossible to install control sections (e.g., critical flow Venturi or sonic throat.), which are widely used to improve the behavior of similar devices. This limitation is common to all the cases with a lack of space around the tunnel and a limited length of the tunnel itself. Furthermore, the turbulent intensity could be reduced: (i) improving the flow-conditioner (honeycomb) at the entrance, placing screens in the settling duct Cattafesta et al., 2010, and (ii) modifying the roughness of the surfaces where the turbulence is generated (e.g., replacing the tunnel panels with new sheets of a smoother material). Some imperfections (small steps and gaps) can be present at the joints between the panels, they may be due to the deformation of the structure, and they should be removed to obtain a better behavior of the facility.

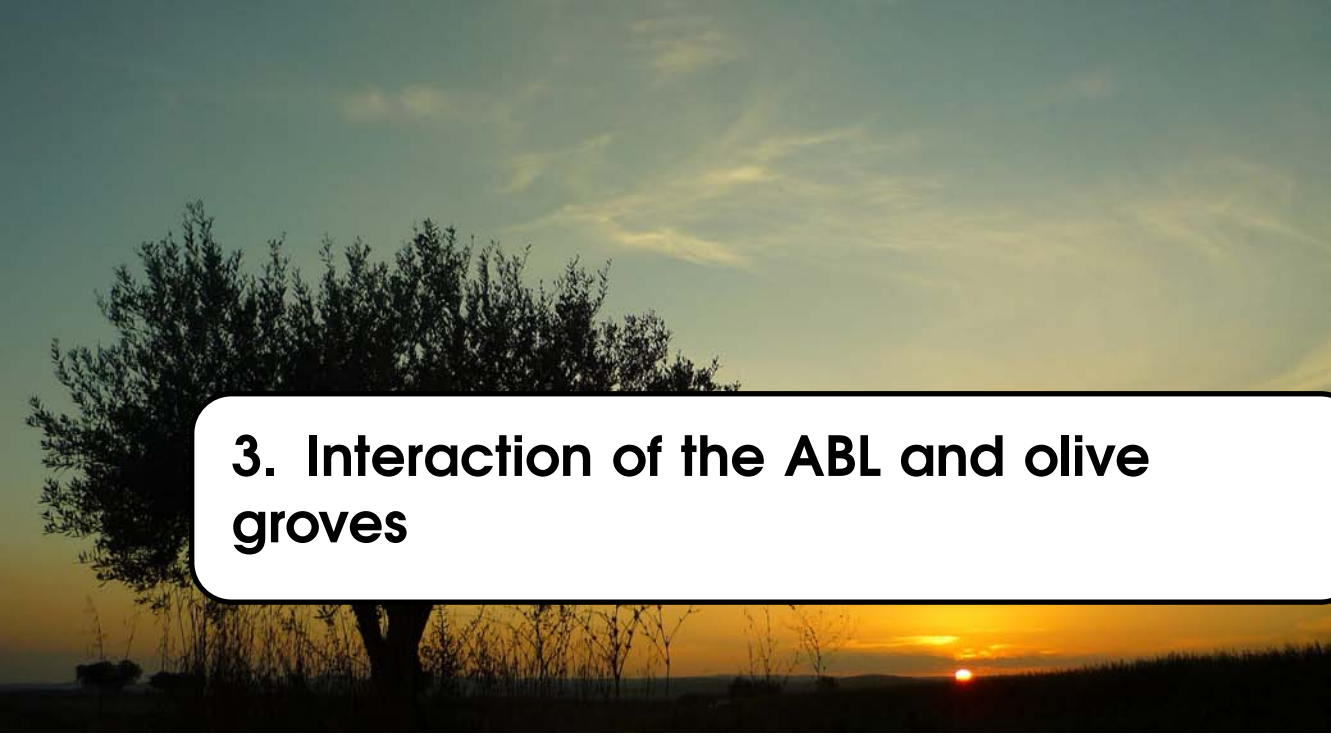

3. Interaction of the ABL and olive groves

Historically, the olive grove has been one of the most emblematic ecosystems in the Mediterranean countries. In Andalusia, Spain, the land under olive grove cultivation exceeds 1.5 million hectares, approximately 17% of the regional surface. Its exploitation has traditionally been based on the use of the available land and heterogeneous plantations, with different species adapted to southern Mediterranean climatic conditions, and the management of the traditional olive cultivation culture. In this chapter, three representative configurations of olive groves under neutral atmospheric conditions are tested. The wind flow time series are recorded at several distances and heights downwind the olive plantation models with a cross hot wire anemometry system. Herein, the spatial variability of mean flow and the turbulent characteristics depends on, among others, the size, the agro-forest length, the layout of the tree rows, the porosity, the tree height, the crown shape, and the surface vegetation cover. The aerodynamic diameter and Reynolds number for each agro-forest management unit are proposed as representative system response variables, as these could be related to olive grove management. The plantation, in turn, conforms to a windbreak, which affects the microclimate and benefits the elements of the ecosystem. Detailed knowledge of these variables and the interaction between the ecosystem and the atmosphere is relevant to optimize resource management, land use, and the sustainability of the overall crop.

The information included in this chapter has been published in:

Jiménez-Portaz, M., Clavero, M., & Losada, M. (2021). A new methodology for assessing the interaction between the Mediterranean olive agro-forest and the Atmospheric Surface Boundary Layer. Atmosphere 12, no. 6:658.

Jiménez-Portaz, M., Clavero, M., & Losada, M. (2019). Experimental analysis of wind interaction with olive grove and the atmospheric surface boundary layer. European Journal of Sustainable Development, 8(5), 180-180.

3.1 The Andalusian Olive Grove

Historically, the olive grove has been one of the most emblematic ecosystems in Andalusia (south of Spain), where there are more than 1.5 million hectares of olive orchard land, representing 17% of the regional surface (Guzmán-Álvarez et al., 2009). The livelihood of a high percentage of the population revolves around this ecosystem, emphasizing its relevance from social, environmental, and economic-financial points of view. However, last years, climate change is producing uncertainty about crop sustainability in the Mediterranean areas, risking the production of the olive groves (Orlandi et al., 2020).

The traditional olive grove is characterized by an irregular pattern, resulting from the use of wild olive trees, creating heterogeneous plantations with different species adapted to the topography and soil characteristics. In such cases, olive trees usually exhibit high arboreal bearing and natural or cultivated vegetation cover for cattle farm purposes (Gómez, 2009). Currently, changes in land use and intensive olive growth based on hedge-shaped crops have changed plantation systems. The olive grove type, its cover, and the silviculture treatments applied, regardless of the exchange processes, define the system dynamics and the interaction with the atmosphere (Chamizo et al., 2017).

3.1.1 Problem statement

The microclimate around the ecosystems varies depending on forest height and density, tree structure, ground cover, topography, among others (Brunet, 2020). The dynamic interaction between the SBL and the Earth's surface, forests, and agro-ecosystems includes the exchange processes and flows of energy, moisture, and gases. These are directly related to pollen concentration (Dupont et al., 2006), gases, and CO_2 exchanges (Belcher et al., 2012), pollutants dispersion (Poëtte et al., 2017), bushfires propagation (Quill et al., 2020), erosion and morphological

processes (Hesp et al., 2019), as well as the whole set of variables related to the mechanics of the system (Gardiner et al., 2019) and which are in coupling with atmospheric processes (Moon et al., 2020).

The studies of Gardiner et al. (2019) and Brunet (2020) discuss and summarize the most recent works on the interaction between wind and trees, including the mean flow and turbulent characteristics in grassland (Nemitz et al., 2009) and in forested canopies (Arnqvist et al., 2015). However, these studies do not provide a direct comparison between different layout configurations and plant species composition —with its morphological characteristics— for the same type of ecosystem. Advances in the study of vegetation-wind interaction and the near weak flow behind trees (Dellwik et al., 2019) are analyzed through statistical models or using on-site measurements to figure out how changes in tree density affect the wind speed and the turbulence. Other studies are focused on the impact of landscape fragmentation (Poëtte et al., 2017), the role of wind-trees interaction under wind storm conditions (Dupont et al., 2018) and also the consequent tree damage processes according to the work of Albrecht et al. (2019) and Kamimura et al. (2019).

In situ measurements can be used to analyze the dynamic response of trees to wind loads and possible damages to vegetation (Poëtte et al., 2017; Schindler and Mohr, 2019), and similarly, the influence of vegetation and trees structure on the flow in a particular location (Wei et al., 2016). Field data allow vertical wind profiles and direct measurements to be obtained at specific points, but this entails a high degree of difficulty because of its high temporal and spatial variability (Gromke, 2018). This is why the need arises to carry out laboratory experiments and wind tunnel tests to complement and obtain data in greater detail and under controlled conditions. Most of these studies are focused on the analysis of flow behavior around and above artificial or natural vegetation models, including variations in spatial layout, trees structure, spacing and density, (Hesp et al., 2019; Hong et al., 2016; Poëtte et al., 2017; Segalini et al., 2013), and the Reynolds number dependence regarding the forest canopy (Gromke, 2018). According to the work of Cheng et al. (2020), the plantation layout, the number of rows, and the arrangement affect the downwind airflow recovery and play a vital role in the protection against erosion (Jeong and Lee, 2020). In some cases, the results can be complemented with data from computational fluid dynamics analysis (CFD) (Liu et al., 2018) and other numerical simulations (Giometto et al., 2017).

A plantation works as windbreaks, allowing airflow through it according to porosity, tree structure, and spatial configuration, modifying and defining the streamwise flow, affecting nearby ecosystems (Cleugh, 1998). According to this behavior and the above information, it is assumed that the development of an olive agro-forest substantially modifies the kinematic airflow variables and the turbulence properties. However, it also changes the spatial and temporal gradients of

environmental variables and processes, such as erosion processes, surface moisture, air humidity flows, evapotranspiration, pollen, and seed dispersion. This work aims to characterize the mechanical behavior of the SBL (under neutral stability) interacting with different olive grove configurations. For this purpose, the spatial evolution of the wind dynamics has been calculated from temporal wind speed measurements, recorded in regularly spatially distributed points located behind the agro-forest system (in the x, y, and z directions) physical principles previously provided. Physical experiments have been carried out in the CCWT of the University of Granada (Jiménez-Portaz et al., 2020a), based on a dimensional analysis of the variables of interest and the particularities of the Andalusian olive grove.

3.2 Objectives

The main objectives of this chapter are:

- Provide an overview of the Andalusian olive grove problems, as well as the main factors that produce them.
- Characterize the mechanical behavior of the Atmospheric Surface Boundary Layer interacting with different olive groves.
- Analyze the spatial evolution of the wind dynamics streamwise the most common olive agroforest configurations from experimental tests.
- Relate the type of exploitation, and silvicultural treatment carried out on the olive grove with aerodynamic variables.

3.3 Study site

3.3.1 Description

For this work, a representative area of olive groves located in the province of Jaén was selected. The farm is composed of (1) an allotment of olive groves with vegetation cover and (2) an allotment of olive groves with bare soil, both arranged in a contiguous way. The site has a clayey terrain, mainly flat with tree species of $4-5m$ high in a $7 \times 7m$ layout. The layout and spatial distribution, and size of the individual trees have been taken as a reference for designing the models used in the experimental tests. In this way, the work scale, plantation porosity, and characteristic parameters have been adapted. For each allotment, field data are available from eddy covariance towers (Chamizo et al., 2017) that could be used for future comparison and verification of the results.

Figure 3.1: Othophoto of the selected area as reference, in the village of Úbeda (Jaén). Is shows an olive agroforest where two areas can be distinguished: one with vegetation cover and the other with bare soil.

3.4 Methodology

3.4.1 Physical principles

This section contains the physical principles of ABL regarding its airflow and turbulence characteristics. Only mechanical turbulence, generated by friction between the wind field and the olive grove, has been considered. Three main elements have been taken into account for the olive grove: tree unit, tree row, and plantation/agro-forest system. Hereafter, the methodology is described, including the dimensional analysis of the problem.

Wind flow velocity over the Earth's surface is reduced due to the turbulent motions caused by the interaction with the topography, ecosystems, among others. In this dynamic interface, it is recommended to perform a dimensional analysis of variables involved in the processes of interest, which allows the system to be analyzed when there is limited knowledge of the system physics (Sonin, 2001). This analysis allows the experimental measurements of a specific setup to be extrapolated to a global system. Dimensionally homogeneous equations are sought to ensure dynamic similarity, to reduce the number of variables, and to explain the mechanistic effects inside a given airflow (Longo, 2011).

When managing an olive plantation, the objective is to optimize resources, particularly water resources, and maximize production. Note that the layout depends

on the management and exploitation of the agro-forest and synthesize the rich experience acquired by the Mediterranean countries in the last 3000 years. To this end, plantations are made with trees distributed in different patterns, usually in rows with corridors, that facilitate tillage and harvesting, with production-focused silvicultural treatments (traditional or intensive). The type of soil, topography, vegetation, among others, are translated into different functional relationships. For this reason, in this paper, several cases of typical functional relationships in the olive grove will be analyzed.

The management problem has been divided into a 2DV, i.e., analysis in the streamwise direction (Figure 3.2(a)) and a 2DH, i.e., analysis in the crosswise direction (Figure 3.2(b)). Figure 3.2 is a 2D scheme of the interaction between agro-forest and wind dynamics. We aim to evaluate the physical quantities used to describe the transformation of wind dynamics leeward of the agro-forest, i.e., the instantaneous wind velocity at different distances from the forest edge.

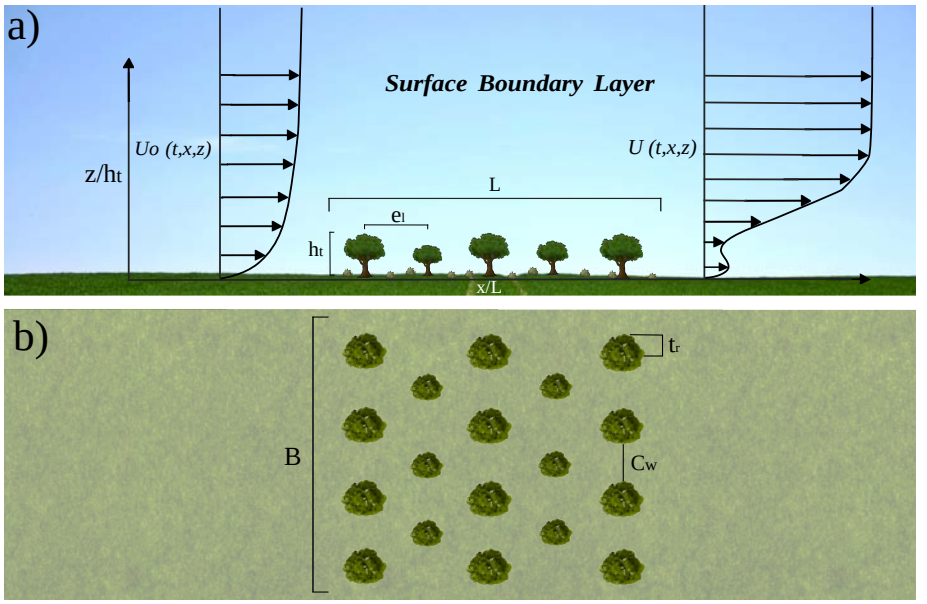

Figure 3.2: Scheme of wind profile transformation in the SBL streamwise and crosswise an agro-forest system (a) 2DV, Side view and (b) 2DH, Top view. Where h_t is the tree height, e_l is the streamwise distance between trees, t_r is the tree crown radius, C_w is the crosswise corridor width, L is the overall plantation length and B is the plantation width.

3.4.2 Dimensional analysis

First, dimensional analysis of the problem is performed, a 2D olive ecosystem is analyzed, assuming infinite width and no lateral variation. The first step of the dimensional analysis is to identify a complete set of independent quantities that determine the value of the wind speed over and behind the forest. For each height z, the set of independent variables related to wind velocity behind the agro-forest are summarized as follows:

1. Physical properties: air density ρ_a, air dynamic viscosity μ_a, and gravitational acceleration g.
2. Layout of the agro-forest (see Figure 3.2), including:
   - Tree properties: tree height h_t and tree crown radius t_r.
   - Trees row properties: the streamwise distance between trees e_l and the crosswise corridor width C_w.
   - Plantation properties: overall length L.
3. Input: instantaneous wind velocity profile upwind the forest, $U_o(x,y,z,t)$, used as reference velocity in this work, and friction velocity, $u_* = \tau/\rho_a = \overline{u'w'}$, related to each other through the Von Karman expression, considering neutral atmosphere:

$$U(z) = \frac{u_*}{k} ln\left(\frac{z}{z_0}\right) \tag{3.1}$$

   where $k \approx 0.4$ is the Von Karman constant, and z_o is the aerodynamic roughness length. In general, z_0 is assumed to be constant. However, for vegetation cover with discontinuities, this variable is markedly dynamic due to the natural flexibility of plants and its dependence on wind velocity and friction velocity (Zhang et al., 2012). In addition, this parameter affects the flow and modifies the vegetation itself and its surface characteristics. Performing a more formal analysis, u_* would be selected as a variable for the dimensional analysis; however, since it is directly related to U_o, for this specific case, U_o is selected as an input variable.
4. Output: measured instantaneous wind velocity time series downwind the agro-forest, $U_l(x,y,z,t)$.

On the other hand, by carrying on the experiment during a period long enough to record a statistically representative time series, but short enough to assume that the experiment is a stationary process, the input and output wind velocities can be split in two components,

$$U_i(x,y,z,t) = \overline{U_i}(x,y,z,t) + u_i'(x,y,z,t), \quad i = o,l \tag{3.2}$$

where $\overline{U_i}$ is the time average wind velocity and u_i' is the time wind velocity fluc-

tuation, and the subindex o and l indicates input and output respectively. Assuming stationarity of the process, the time variable is simplified.

A complete set of independent quantities is selected, which determine the time average wind speed value at any location behind the forest,

$$\overline{U_l}(x,y,z) = f\{\rho_a, \mu_a, g, L, t_r, C_w, h_t, e_l, \overline{U_o}\} \tag{3.3}$$

which comprises a total of $n = 9$ independent variables. It is convenient to separate the variables that hold for all the experiments to built a subset of n_f independent quantities, subset 1: $\rho_a, g, L, t_r, C_w, e_l$, and $n_f = 6$.

Choosing a base subset 1, $k_f = 3$ of independent quantities, ρ_a, g, L, then $n_f - k_f = 3$, three dimensionless monomial are obtained:

$$\frac{e_l}{L} \quad \frac{C_w}{L} \quad \frac{t_r}{L} \tag{3.4}$$

The remaining set of independent variables is a base subset 2 of $k = 3$: $\mu_a, h_t, \overline{U_o}$, then $n - n_f = 3$. Using the base subset 2, the base subset 1, and the output variable, the following non-dimensional quantities are obtained:

$$\frac{\overline{U_l}}{\overline{U_o}} = f\left\{ \underbrace{\frac{e_l}{L}}_{\text{I}}, \underbrace{\frac{2t_r}{L}}_{\text{II}}, \underbrace{\frac{C_w}{L}}_{\text{III}}, \underbrace{\frac{h_t}{L}}_{\text{IV}}, \underbrace{\frac{\overline{U}_o \cdot h_t}{\nu_a}}_{\text{V}}, \underbrace{\frac{\overline{U_o}^2}{g \cdot L}}_{\text{VI}} \right\} \tag{3.5}$$

where $\nu_a = \frac{\mu_a}{\rho_a}$, is the kinematic viscosity of the air, and the dimensionless quantities are: I) streamwise row length, II) tree crown length, III) crosswise corridor width, IV) plantation roughness length, V) relationship between viscosity and friction due to plantation height, and VI) relationship between plantation length and downwind system response. This last term (VI) approximates a Froude number, which relates inertial forces to gravitational forces. This allows relating the agro-forest length to the airflow characteristics streamwise.

3.4.3 Derived quantities

The analysis and results depend on the spatial position in which they are performed, being their coordinates:

$$x^* = \frac{x}{L}, \quad y^* = \frac{y}{L}, \quad z^* = \frac{z}{h_t} \tag{3.6}$$

In this case, the height z is made dimensionless with the tree height h_t. From measurements at each location, subtracting the measured instantaneous wind velocity and its time average over a given period, the wind speed fluctuation, or gust components, $u_l'(x,y,z,t)$, can be calculated. Theoretically, it is a Gaussian distributed variable with zero mean and non-zero variance. Thus, based on previous dimensional analysis, can be determined the dimensionless variance downwind of the agro-forest. The variance σ^2 should be considered as a first kind derived quantity. The local turbulence intensity IT and the local turbulence kinetic energy per unit mass downwind of the agro-forest TKE are defined in terms of the local variances (horizontal and vertical). Thus, those quantities can be considered as the second kind derived quantities, and their dimensionless forms are shown as:

1. First kind derived quantities: $\sigma_u^2 = \overline{u_o'^2}, \quad \sigma_w^2 = \overline{w_o'^2}$
2. Second kind derived quantities: $IT(z) = \frac{\sigma_u(z)}{\overline{U_o}(z)}, \quad TKE = \frac{0.5(\sigma_u^2+\sigma_w^2)}{\overline{U}_o^2}$

Furthermore, the velocity skewness S_w, which complement the statistics of turbulence and represent the vertical transport of $\overline{w'w'}$ by the turbulence (Hogan et al., 2009), is defined dimensionless as:

$$S_w = \frac{\overline{w'^3}}{\overline{w'^2}^{3/2}} \tag{3.7}$$

Approach to a 3D analysis and aerodynamic variables

In this work, the experiments are carried inside a wind tunnel. All the elements have dimensions quantifiable and correlated to the system's behavior through the aerodynamic diameter and the Reynolds number.

With the help of dimensional analysis, the following second-order quantities, which define the agroforest, can be calculated. Describing the agro-forest layout in terms of aerodynamic diameters of i) the tree row, D_r, ii) of the tree unit, D_t, iii) of the plantation, D_p, and iv) the aerodynamic diameter of the tunnel D_h, defined as follows:

$$D_h = \frac{2ab}{a+b} \quad D_t = \frac{4t_r h_t}{2t_r + h_t} \quad D_r = \frac{4r_r h_t}{r_r + h_t} \quad D_p = \frac{2Bh_t}{B+h_t} \tag{3.8}$$

where a and b are the height and the width of the tunnel section, respectively, B is the plantation width, and $r_r = 0.5C_w + t_r$ is the aerodynamic row radius.

The layout of the olive grove and the airflow along the tunnel allows the assumption that the experimental setup is repeated transversely. Thus, tests can be performed in 2D, being generated small cross-sectional variations between the tunnel walls. Consequently, the experiment is controlled by four Reynolds numbers,

defined by aerodynamic variables: (i) for the empty wind tunnel, Re_{ref}, (ii) for the tree unit, Re_t, (iii) for each trees row, Re_r, and (iv) for the plantation, Re_p, defined as:

$$Re_{ref} = \frac{\overline{U_o} D_h}{\nu_a} \quad Re_t = \frac{\overline{U_o} D_t}{\nu_a} \quad Re_r = \frac{\overline{U_o} D_r}{\nu_a} \quad Re_p = \frac{\overline{U_o} D_p}{\nu_a} \tag{3.9}$$

From the variables above, the behavior of the plantation as a whole is defined. It is responding to current exploitation techniques using aerodynamic variables. Thus, it must be determined whether the Reynolds number is high enough to ensure that the flow is fully turbulent and the viscosity effects at the local scale are minimal.

3.4.4 Experimental set-up

Experimental work in a wind tunnel involves satisfying the kinematic and dynamic similarity principle. The wind velocity at any point in the model must be proportional to the prototype scale velocity, and all forces must be scaled with a constant scale factor. A geometric scale E is obtained according to the SBL height, and the olive tree height to represent the agro-forest properly inside the wind tunnel (Figure 3.3), and the total area occupied by the forest is less than the total wind tunnel width. Thus, a working scale of $E = 1:50$ is defined to simulate an olive agro-forest surrounded by pasture with light vegetation cover.

Moreover, the Reynolds number must be high enough and similar to the Reynolds number in the olive agroforest. The aerodynamic diameters and Reynolds numbers for the input velocity and the agro-forest layout, obtained according to the analysis described in the previous section, are summarized in the following Tables 3.1 and 3.2.

$D_h(m)$	$D_t(m)$	$D_r(m)$	$D_p(m)$
1.96	0.085	0.11	0.16

Table 3.1: Aerodynamic diameters.

Re_{ref}	Re_t	Re_r	Re_p
$1.05 \cdot 10^6$	$1.73 \cdot 10^4$	$2.29 \cdot 10^4$	$3.34 \cdot 10^4$

Table 3.2: Reynolds numbers calculated for baseline conditions and $\overline{U_o} = 3\,m/s$.

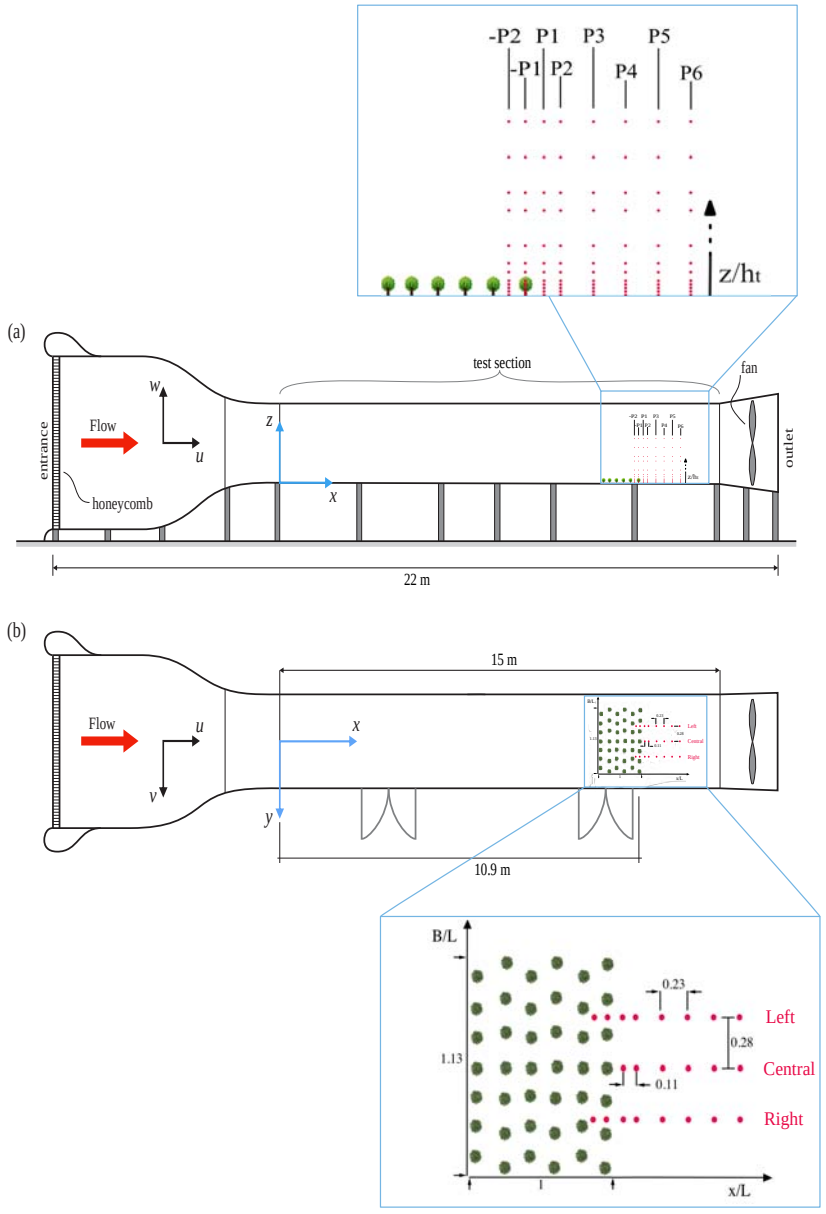

Figure 3.3: Sketch of the BLWT: (a) elevation view and (b) floor view, where profiles measured and scaled models position is shown. The blue squared enlargements show the olive tree model layout configuration, 22 measured profiles, and 12 points for each vertical profile with relative distances represented as a function of z/h_t, x/L, and B/L. The red arrow shows the wind flow direction.

Olive trees have complex structures; thus, rigid scale models are used to reproduce the trunk shape and irregularities of the crown accurately. There are two types of models, i.e., type 1 ($h_t = 0.07\,m$ and $r_r = 0.02\,m$) and type 2 ($h_t = 0.09\,m$ and $r_r = 0.04\,m$), which simulate medium-sized olive trees typical of agro-forest systems. To simulate intensive olive grove exploitations, models of equal sizes are used. In this work, and according to the aerodynamic porosity defined by Manickathan et al. (2018), a constant tree porosity value of approximately $\alpha = 0.22$ is assumed.

For traditional olive groves, models of both sizes are interleaved to reliably reproduce the controlled arrangement of olive trees. Six representative spatial configurations were designed in a spatial layout agro-forest with a length ($L = 0.8\,m$, a width $B = 0.9\,m$ and a tree separation distance of $e_l = 0.15\,m$ (Table 5.1). In this work, three configurations have been analyzed (see Figures 3.4, 3.5 and 3.6), whose characteristics are summarized in Table 5.1.

C	*Layout*	*Cover*	$h_t(m)$	$e_l(m)$	$r_r(m)$
1	G	No	0.09	0.15	0.04
2	S	No	0.07-0.09	0.15	0.02-0.04
3	S	Yes	0.07-0.09	0.15	0.02-0.04

Table 3.3: Characteristics of three configurations tested in the wind tunnel, including the number of configuration C, the layout type (Grid (G) of Staggered (S)), vegetation cover, tree height (h_t), streamwise distance between trees e_l and tree crown radius (r_r).

Figure 3.4: Images of grid olive grove configuration (intensive olive grove, C1).

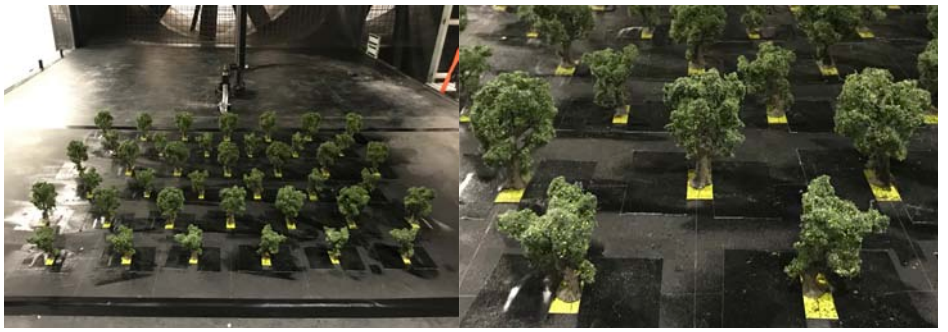

Figure 3.5: Images of staggered olive grove configuration (traditional olive grove without vegetation cover, C2).

Figure 3.6: Images of staggered olive grove configuration with cover (traditional olive grove with vegetation cover, C3).

Measurements were taken in 22 vertical profiles in the center and lateral sections, as shown in Figure 3.3. Data were recorded at 12 points in height per profile, and they were closer to each other in the area near the models, i.e., along the first $0.2m$ in the vertical direction, and progressively increasing the distance between points because the olive grove influence over the flow is predicted to be smaller as we move away from the surface.

For data acquisition, a cross-wire X-probe, controlled by the system *IFA 300*® by TSI Inc., was used to obtain measurements of the streamwise and vertical components of wind velocity $(u(x), w(z))$. Data acquisition and processing were conducted using the software *ThermalPro*®, and statistical analysis of the variables was subsequently performed with the same software. To ensure the data collected were representative, the sampling frequency for each point was $1kHz$ for 131 seconds, under ergodicity assumption. More details about the instruments and data acquisition are reported in Chapter 2.

3.5 Results

In this section, from the experimental measurements, first kind and second kind derived quantities are obtained, according to the expressions developed above. As a velocity scale, we adopted a constant reference velocity ($3m/s$). The results obtained are expected to be similar for different wind velocities, as it was shown in Cheng et al. (2020).

The results are presented as dimensionless variables for the mean wind speed $\overline{U}$, the turbulence intensity IT, the turbulent kinetic energy TKE, the vertical velocity skewness S_w, the aerodynamic surface roughness length z_o and the friction velocity u_*. As a reference length for measurements in the vertical direction, the height of the highest olive tree model (0.09 m) is used, designated h_t. The distance between measuring sections is $x/L = 0.28$, and it changes between profiles in the streamwise direction (Figure 3.3).

3.5.1 Neutral mean flow characteristics

As a preliminary step, the incoming flow homogeneity in the wind tunnel with an empty test section was performed for different velocities and elements for turbulence control (Section 2). Vertical profiles of the wind velocity ($\overline{U}$) and turbulence (IT and TKE), aerodynamic roughness length (z_o), friction velocity (u_*) and Reynolds number (Re) were obtained (Table 3.4), taken as reference values for the ABL. These results were used for comparison with later tests on scale models of olive groves.

$\overline{U}_o$	u_*	IT_o	z_o	D_h	Re
$3m/s$	$0.28m/s$	1.8%	$3 \cdot 10^{-4} m$	1.96 m	$1.05 * 10^6$

Table 3.4: Input values (ABL) obtained from wind tunnel flow calibration, where $D_h = 2ab/a+b$, $a = 1.8m$ and $b = 2.15m$.

As Figure 3.7 shows, the flow in the test section is uniform in the streamwise and crosswise sections, with a wind velocity decreasing of 30% and an increase of 13% in the turbulence intensity due to the wind profile generated by the wind tunnel floor roughness (Jiménez-Portaz et al., 2020a). The vertical profiles were measured for the same section, as shown in Figure 3.3(a), for later comparison with measurements downwind of the olive tree models. Only Profiles P1 and P4 are shown in Figure 3.7.

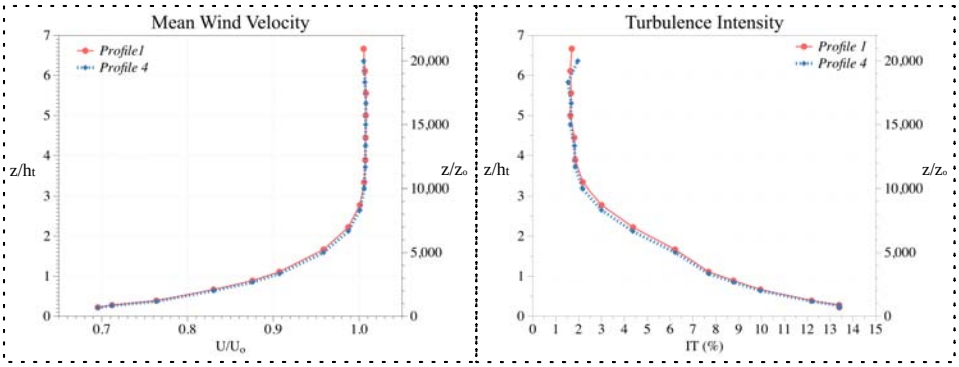

Figure 3.7: Profiles measured for the empty wind tunnel, corresponding to Profile 1 ($P1$) and Profile 4 ($P4$) in Figure 3.3(a). i) Vertical dimensionless wind velocity profiles (left), and ii) turbulence intensity (right) measured on the wind tunnel central axis with an empty section. In both cases, the dimensionless values in height are shown as a function of tree height (h_t) and aerodynamic roughness height z_o.

3.5.2 Mean flow and turbulence around olive groves

For the three configurations tested, vertical profiles are compared along the main axis, corresponding to the central trees line, and vertical profiles on the right and left sections include measurements between models. Two profiles are registered inside the olive grove from the coordinate origin, where the olive grove ends and the leeward side starts (-P1 and -P2 in Figure 3.3(a)). The models were distributed uniformly, so it has been proven that measurements in the central section represent the wind velocity distribution along the crosswise section.

Nine significant points were selected within the measured area, corresponding with profiles P1, P4, and P6, to compare the results for each configuration analyzed. Figure 3.8 shows the position of these points in which measurements have been taken (coordinates z and x), according to the spatial distribution shown in Figure 3.3.

Comparisons have been made between each configuration and the results obtained previously for the incoming flow (ABL) (Figure 3.7). For this purpose, the values of the dimensionless wind speed, turbulence intensity, and dimensionless TKE are shown. Some variation rates represented in percentages of variation are calculated and defined as:

$$\varphi_U(x,z) = ((\overline{U}_l - \overline{U}_o)/\overline{U}_o) \cdot 100 \tag{3.10}$$

$$\varphi_{IT}(x,z) = ((IT_l - IT_o)/IT_o) \cdot 100 \tag{3.11}$$

$$\varphi_{TKE}(x,z) = ((TKE_l - TKE_o)/TKE_o) \cdot 100 \tag{3.12}$$

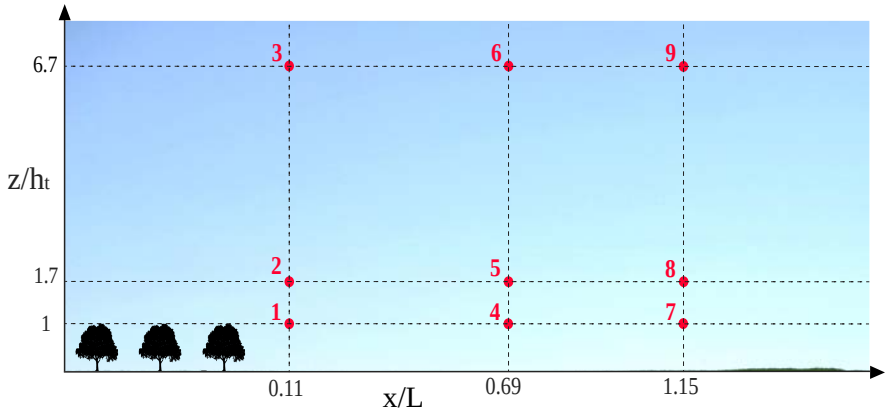

Figure 3.8: Points for comparison between the three configurations studied, and distance from the bottom (z/ht) and from the models (x/L) of the nine measuring points. Ratios of comparison for each point, calculated for all the analyzed configurations, are collected in Tables 3.5, 3.6 and 3.7.

Tables 3.5, 3.6 and 3.7 show the dimensionless mean velocity difference $\overline{U}/\overline{U_o}$, the dimensionless turbulence intensity IT and dimensionless turbulent kinematic energy TKE at the test section for the reference ABL (empty section) and the same variables for the three olive grove configurations (C1, C2 and C3). In all cases, the mean velocity $(\overline{U})$ is lower in the presence of olive trees (for this reason, the rate shows a negative value), and the turbulence parameters (IT and TKE) are higher.

Pt	$\overline{U}/\overline{U}_o$			IT			TKE		
	Grid	*ABL*	φ_U	*Grid*	*ABL*	φ_{IT}	*Grid*	*ABL*	φ_{TKE}
1	0.24	0.83	-71.35	44.87	9.95	350.92	$7.9 \cdot 10^{-3}$	$4.0 \cdot 10^{-3}$	97.5
2	0.88	0.96	-8.19	13.18	6.22	111.95	$1.0 \cdot 10^{-2}$	$2.0 \cdot 10^{-3}$	415.0
3	0.99	1.01	-1.24	2.20	1.70	29.38	$6.8 \cdot 10^{-4}$	$4.7 \cdot 10^{-4}$	44.7
4	0.48	0.83	-42.43	18.86	9.95	89.57	$7.1 \cdot 10^{-3}$	$4.0 \cdot 10^{-3}$	77.5
5	0.84	0.96	-12.44	12.78	6.22	105.48	$9.4 \cdot 10^{-3}$	$2.0 \cdot 10^{-3}$	370.0
6	0.99	1.01	-1.66	2.27	1.70	33.74	$6.7 \cdot 10^{-4}$	$4.7 \cdot 10^{-4}$	42.6
7	0.52	0.83	-37.94	16.81	9.95	68.97	$6.3 \cdot 10^{-3}$	$4.0 \cdot 10^{-3}$	57.5
8	0.81	0.96	-15.59	13.09	6.22	110.47	$9.2 \cdot 10^{-3}$	$2.0 \cdot 10^{-3}$	360.0
9	0.99	1.01	-1.47	1.89	1.70	11.18	$5.2 \cdot 10^{-4}$	$4.7 \cdot 10^{-4}$	10.6

Table 3.5: Mean values obtained for the grid configuration (C1) compared to the values obtained for the measured reference boundary layer. They are compared through ratios, represented as a percentage of the value of the reference conditions. The points of comparison are shown in Figure 3.8.

Pt	$\overline{U}/\overline{U}_o$			IT			TKE		
	Stag	*ABL*	φ_U	*Stag*	*ABL*	φ_{IT}	*Stag*	*ABL*	φ_{TKE}
1	0.14	0.83	-83.16	62.45	9.95	527.62	$4.7 \cdot 10^{-3}$	$4.0 \cdot 10^{-3}$	17.5
2	0.85	0.96	-11.62	14.33	6.22	130.43	$1.2 \cdot 10^{-2}$	$2.0 \cdot 10^{-3}$	490.0
3	0.99	1.01	-1.42	1.67	1.70	1.90	$4.0 \cdot 10^{-4}$	$4.7 \cdot 10^{-4}$	14.9
4	0.35	0.83	-58.34	25.68	9.95	158.06	$5.9 \cdot 10^{-3}$	$4.0 \cdot 10^{-3}$	47.5
5	0.74	0.96	-22.41	18.86	6.22	203.27	$1.5 \cdot 10^{-2}$	$2.0 \cdot 10^{-3}$	655.0
6	0.98	1.01	-2.22	1.92	1.70	13.18	$5.1 \cdot 10^{-4}$	$4.7 \cdot 10^{-4}$	8.5
7	0.41	0.83	-50.73	25.67	9.95	158.01	$7.8 \cdot 10^{-3}$	$4.0 \cdot 10^{-3}$	95.0
8	0.75	0.96	-21.24	17.39	6.22	179.52	$1.4 \cdot 10^{-2}$	$2.0 \cdot 10^{-3}$	575.0
9	0.99	1.01	-1.36	1.69	1.70	0.72	$4.0 \cdot 10^{-4}$	$4.7 \cdot 10^{-4}$	14.9

Table 3.6: Mean values obtained for the staggered configuration (C2) compared to the values obtained for the measured reference boundary layer. They are compared through ratios, represented as a percentage of the value of the reference conditions. The points of comparison are shown in Figure 3.8.

Pt	$\overline{U}/\overline{U}_o$			*IT*			*TKE*		
	Cover	*ABL*	φ_U	*Cover*	*ABL*	φ_{IT}	*Cover*	*ABL*	φ_{TKE}
1	0.16	0.83	-81.06	48.67	9.95	389.11	$4.8 \cdot 10^{-3}$	$4.0 \cdot 10^{-3}$	20.0
2	0.84	0.96	-12.76	15.10	6.22	142.78	$2.9 \cdot 10^{-3}$	$2.0 \cdot 10^{-3}$	45.0
3	0.99	1.01	-1.11	1.79	1.70	5.38	$4.3 \cdot 10^{-4}$	$4.7 \cdot 10^{-4}$	8.5
4	0.33	0.83	-60.48	31.44	9.95	215.98	$7.8 \cdot 10^{-3}$	$4.0 \cdot 10^{-3}$	95.0
5	0.74	0.96	-22.51	18.20	6.22	192.60	$1.5 \cdot 10^{-2}$	$2.0 \cdot 10^{-3}$	640.0
6	1.00	1.01	-0.96	1.98	1.70	16.54	$5.4 \cdot 10^{-4}$	$4.7 \cdot 10^{-4}$	14.9
7	0.41	0.83	-50.72	26.78	9.95	169.12	$9.2 \cdot 10^{-3}$	$4.0 \cdot 10^{-3}$	130.0
8	0.73	0.96	-23.48	18.02	6.22	189.76	$1.4 \cdot 10^{-2}$	$2.0 \cdot 10^{-3}$	600.0
9	0.99	1.01	-1.40	2.21	1.70	30.00	$6.5 \cdot 10^{-4}$	$4.7 \cdot 10^{-4}$	38.3

Table 3.7: Mean values obtained for the staggered with vegetation cover configuration (C3) compared to the values obtained for the measured reference boundary layer. They are compared through ratios, represented as a percentage of the value of the reference conditions. The points of comparison are shown in Figure 3.8.

Without an agro-forest system, the wind speed profile has a logarithmic shape (Figure 3.7). With an agro-forest system, the mean wind speed decreases between 80% and 50% in points 1 and 7 (P1 and P6 at the bottom), and around 1.5% at $z/h_t = 6.7$ (points 3, 6 and 9), where the effect produced by the ecosystem is very weak (Figures 3.9 and 3.10). The comparison values show that the traditional olive grove without cover (C2) is the configuration that most influences the mean flow in the area next to the models. Regarding φ_{IT} for the staggered configuration (C2), the percentages differ between 527% to 157% at the bottom and 1.90% to 0.72% at the top, for P1 and P6. However, the turbulent characteristics are maintained with a higher value for the case of the configuration with vegetation cover (C3), both in height and streamwise (Table 3.7).

Olive agro-forest presence is noticed up to an approximate height of $3.5 \leq z/h_t \leq 4$, where the vertical profile is not logarithmic. The logarithmic shape is not recovered until a distance of $x/L \leq 1.15$; however, a trend is still visible. At tree height, for the traditional configuration C2, the velocity is almost zero in Profile 1 and, from Profile 2, this velocity increases in the streamwise direction (Figures 3.9 and 3.10). Obstacle transmission is noticed from Profile 5, and it will be extended beyond a distance of $1.3 \leq x/L \leq 1.69$.

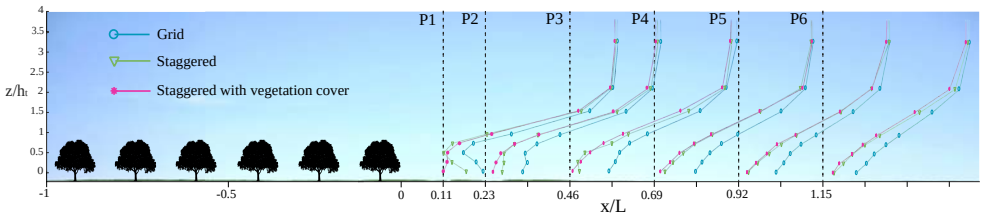

Figure 3.9: Mean wind velocity $\overline{U}/\overline{U}_o$ for the three configurations, measured leeward. In the abscissa, the distance is in the streamwise direction of wind flow normalized regarding x/L and in the ordinate is normalized respecting z/h_t. A greater velocity decrease is observed for the traditional olive grove (pink lines) when compared with the intensive olive grove (blue lines).

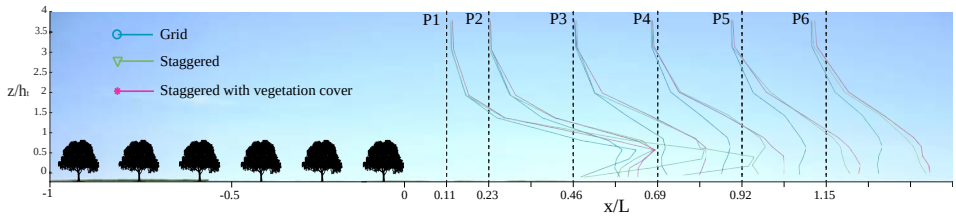

Figure 3.10: Turbulence intensity profiles IT for the three configurations, measured leeward. In the abscissa, the distance is in the streamwise direction of wind flow normalized regarding x/L and in the ordinate is normalized with z/h_t. The turbulence intensity decreases as the distance from the olive grove increases, especially for the intensive olive grove.

In a comparison of the traditional configurations with and without vegetation cover (C2 and C3), the profiles have a more uniform shape in the presence of vegetation cover, not only for the mean velocity $\overline{U}$ but also for the turbulence intensity IT (Figures 3.9 and 3.10). However, IT is similar for a vertical distance of $z/h_t \leq 2$, and at a height of $z/h_t \leq 4$, the flow is uniform, with a higher value for the case with vegetation cover.

In the following figures, the agro-forest length L is used as a reference length in the streamwise direction. In Figure 3.11 and Figure 3.13(a), the color gradient covers the range of $0.2 \leq U/U_o \leq 1$, with the lowest value corresponding to blue and the highest value to red. The intermediate values correspond to orange, yellow, and green shades. In the case of turbulence intensity (Figure 3.12 and 3.13(b)), the red range corresponds to the lowest values and the blue range to the highest

turbulence levels, ranging from $5 \leq IT(\%) \leq 50$. In the case of Figure 3.14, the color scale ranges from white and light yellow for lower values to dark red for higher values. Its range of values is $0 \leq TKE/U_o \leq 0.02$.

In Figures 3.11 and 3.12, the results for intensive farming without cover (C1) are compared with those for traditional farming with vegetation cover (C3). Darker blue colors indicate a greater distortion concerning the reference values. For a height of $z/h_t \leq 2$, the wind velocities are more uniform, up to 18% higher in the first case in areas close to the surface and 19% lower in terms of turbulence intensity. For a distance of $0.3 \leq x/L \leq 0.4$, the effects of intensive olive grove decrease; in contrast, these remain constant for the traditional configuration.

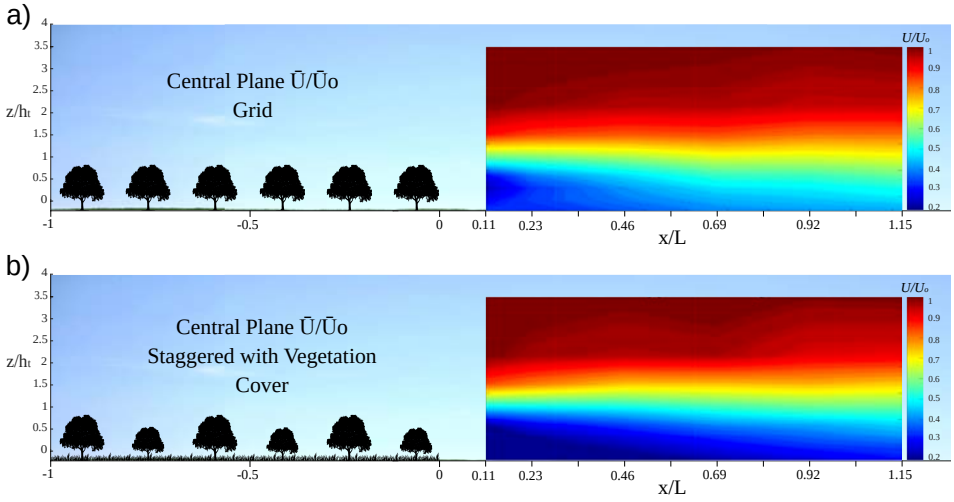

Figure 3.11: Dimensionless mean wind velocity for the intensive olive grove C1 and the traditional olive grove C3 measured along the central axis downwind: (a) streamwise distribution of $\overline{U}/\overline{U}_o$ for the intensive olive grove; (b) streamwise distribution of $\overline{U}/\overline{U}_o$ for the traditional olive grove with vegetation cover.

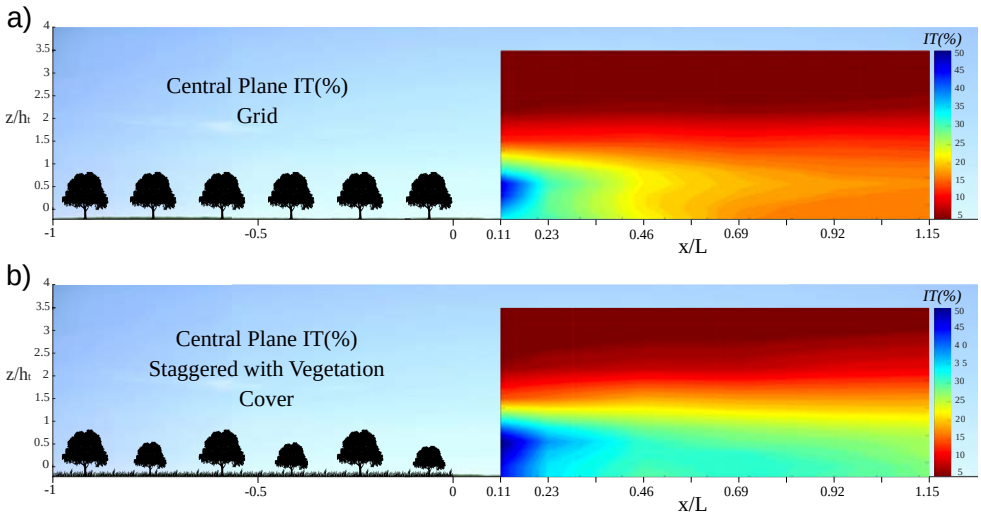

Figure 3.12: Dimensionless turbulence intensity for the intensive olive grove C1 and the traditional olive grove C3 measured along the central axis downwind: (a) streamwise distribution of IT for the intensive olive grove; (b) streamwise distribution of IT for the traditional olive grove with vegetation cover.

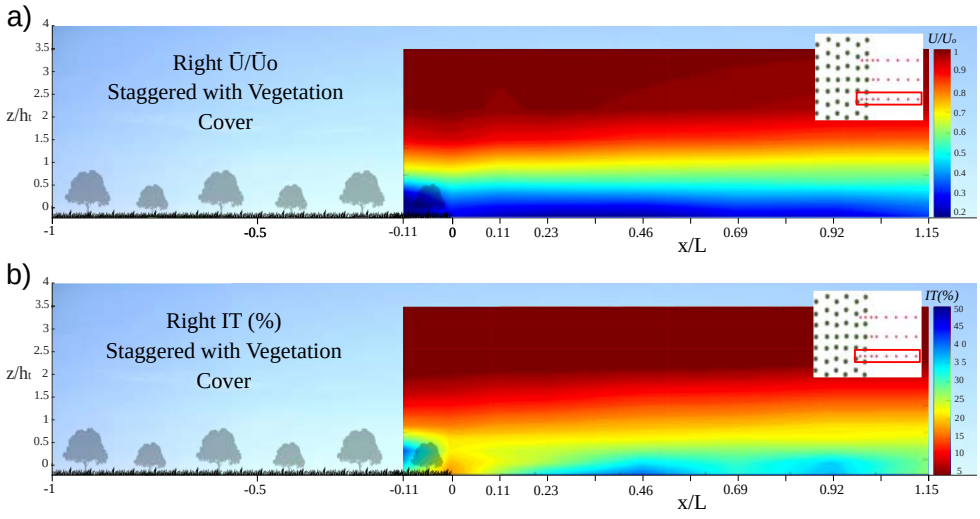

Figure 3.13: Lateral profile measurements for the traditional olive grove with vegetation cover C3. Measurements taken between the olive tree models and behind them reveal the (a) distribution of $\overline{U}$ and the (b) streamwise distribution of IT.

There are small differences between the lateral profiles and central profiles (Figure 3.13), due to some differences between the areas in which measurements were taken. Higher turbulence intensity is noticed for central section measurements at a distance between $0 \leq x/L \leq 0.3$ for measurements for the right section.

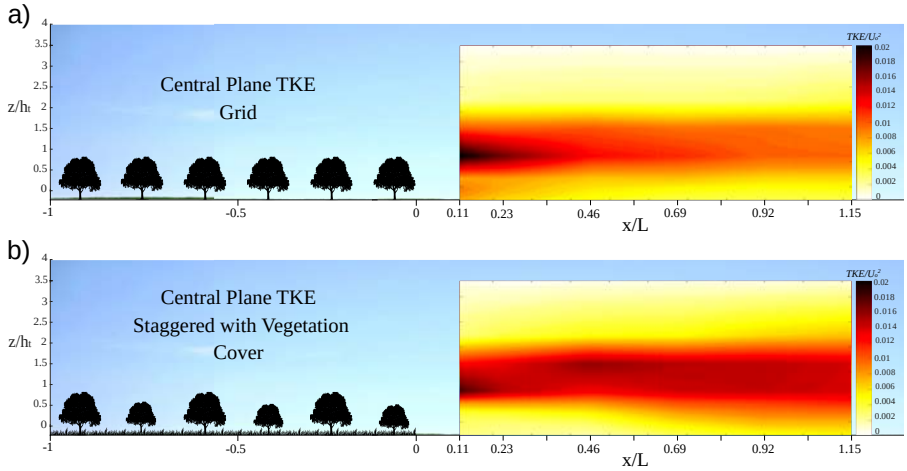

Figure 3.14: Streamwise distribution of the dimensionless TKE/U_o^2 for (a) the intensive olive grove without cover C1 and (b) the traditional olive grove with vegetation cover C3.

For the TKE, from a height of $z/h_t \leq 2$, the energy dissipation decreases and stabilizes vertically (Figure 3.14). In the case of the traditional olive grove, the turbulence generated at the surface is developed earlier than in other configurations. As Figure 3.14 shows, there is an increase and spatial dispersion of the TKE along with the flow downwind. In a comparison of the TKE values with and without the models (Figure 3.14), the flow around the olive groves has turbulence values between 300-600% higher than the free flow at the height of $z/h_t \leq 1.7$. By contrast, the TKE remains constant along with the streamwise distance, the most noticeable effect in the case of a staggered olive grove. In Figure 3.14, for intensive exploitation, a higher TKE is observed near the models up to a relative height of $0.7 \leq z/h_t \leq 2$. Moreover, the TKE increases and remains at a high level from that point and along the flow direction for the traditional olive grove, reaching a value of almost double that of the intensive olive grove.

Vertical velocity skewness has been analyzed, and the results for the grid and staggered with vegetation cover configurations are shown in Figure 3.15. These results are in agreement with those obtained by Segalini et al. (2013). S_w shows significant height (z) dependence, and its behavior can be divided into three areas: i) an area below the reference height (tree height h_t), in which the vertical skewness

values are negative, so $\overline{w'w'}$ is not transported vertically, ii) a second area from the height h_t to about $z/h_t \leq 4$, in which the values are positive, and vertical transport of $\overline{w'w'}$ is expected, and iii) a third area that covers from $z/h_t \leq 4$ to the end of the measurements taken, in which the values become negative again, although in the highest zone ($7 \leq z/h_t \leq 11$) a similar trend to that observed in the lower part is seen, towards values close to zero.

These values are intimately related to turbulent kinetic energy, so a logical behavior can be observed if we compare them. Results obtained are consistent with those shown in the work of Hogan et al. (2009), focused on the study of airflow over different types of the canopy and spatial distributions.

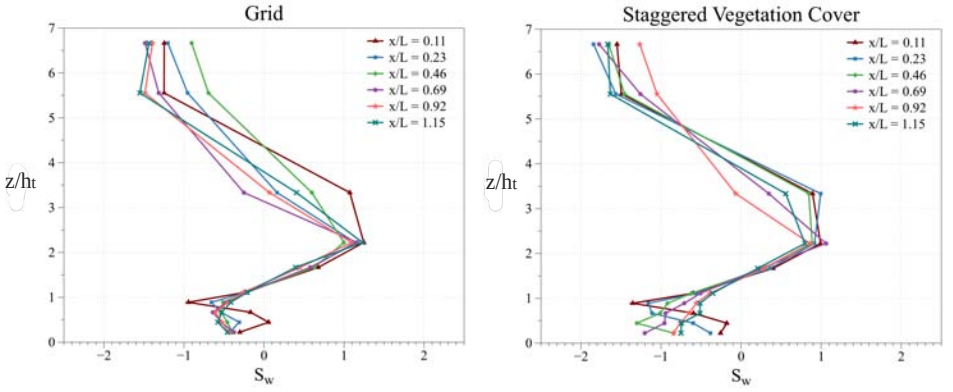

Figure 3.15: Dimensionless vertical velocity (w') skewness for grid and staggered with vegetation cover configuration.

3.6 Comprehensive analysis of the olive grove agro-forest

Maintenance and management of current and new olive grove allotments have become challenging for managers and decision-makers because of the new intensive farming models in the last decade. To do this, it is required to take into account all the elements shown in the Figure 3.16 so that the system is understood and analyzed based on all the processes, balances, agents involved, and scales.

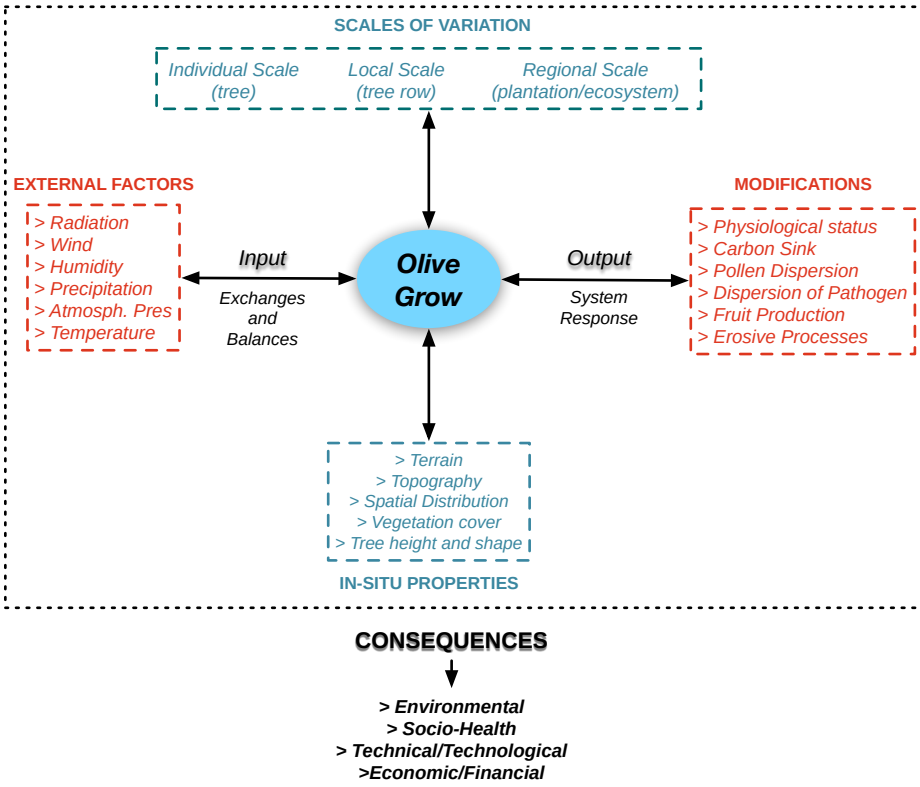

Figure 3.16: Elements involved in the study and comprehensive analysis of an olive grove.

Decreases in precipitation and temperature in Mediterranean regions are expected to diminish production and make the sustainability of olive groves difficult (Montaldo et al., 2020; Viola et al., 2013). In light of the results obtained, it is necessary to carry out surveys of the land topography, tree structure and density, vegetation cover, surface flow, and atmospheric conditions to optimize and manage the ecosystem sustainably and efficiently.

First of all, dimensional analysis of the variables involved in the problem has been carried out, from which it is possible to infer the direct relationship between the kinematic and environmental variables and the physical characteristics of the ecosystem. Some of the main physical characteristics are the tree height and tree crown radius (h_t and t_r), the streamwise distance between trees (e_l), the crosswise corridor width (C_w), and distribution of the plantation as a whole (B, L). From the dimensions and quantities detailed in this work, the Canopy Cover Fraction (FCC), which estimates the tree cover of an agroforestry stand, could be determined, which is common in studies of ecology and agroforestry management.

According to the work of Longo (2021), defining the Jensen number as $Je = \delta/z_o$ (where δ is the surface boundary layer thickness, which in this case is considered the wind tunnel total height, and z_o is the roughness height which in this case corresponds to the tree height h_t), and assuming its value constant in the model and the prototype, we obtain the geometrical scale. To ensure that the scale ratio of the roughness height is the same that the scale ratio of the boundary layer, where $\lambda_{z_o} = \lambda_\delta$, being $h_{t_{prototype}}/h_{t_{model}} = \delta_{prototype}/\delta_{model}$, equal to $4.5m/0.09m = 90m/1.8m$, a scale of $E = 1:50$ has been selected.

Because this experimental work employs rigid models, a minor deviation in the turbulence values is expected. In general, it is recommended to limit the use of dynamic models due to, among others, the difficulty of reproducing the Reynolds number (Solari, 2019). Based on the results of the measurements taken inside the agro-forest (Figure 3.13), the porosity of the plantation -due to the spacing between trees and the area around the trunks- allows the airflow, avoiding the reverse flow behind the ecosystem.

Neutral atmospheric stability was used due to the limitations of mechanical wind tunnel testing (Jiménez-Portaz et al. (2020a)). However, according to Moon et al. (2020) results, there is a small contribution from changes in atmospheric stability, so the main change is generated by the wind speed.

For each spatial position, global measurements defining the turbulent characteristics of the system are the turbulence intensity (IT), Turbulent Kinetic Energy TKE, the vertical velocity Skewness S_w, and Shear Velocity (u_*). Furthermore, the Reynolds number Re, which describes the degree of turbulence related to the viscous forces, is estimated for the empty wind tunnel, the tree unit, the tree row, and the plantation (Re_{ref},Re_t,Re_r,Re_p). As obtained for the initial flow conditions with the empty wind tunnel, the reference Reynolds number (Re_{ref}) is sufficiently high to neglect the influence of viscous forces. If we compare it with Re_r, Re_t and Re_p, as shown in the Figure 3.17(a) and (b), values are much lower, due to the influence and closeness of the models, increasing as we move away from these and the flow returns to its initial state. The value of Re is generally higher for the grid layout configuration, especially in the case of Re_r, due to the absence of obstacles, since in the staggered configuration there are trees between the rows (Figure **??**). However, the value of Re_p for the plantation is sufficiently high to be considered independent of the obstacle, in this case, the ecosystem.

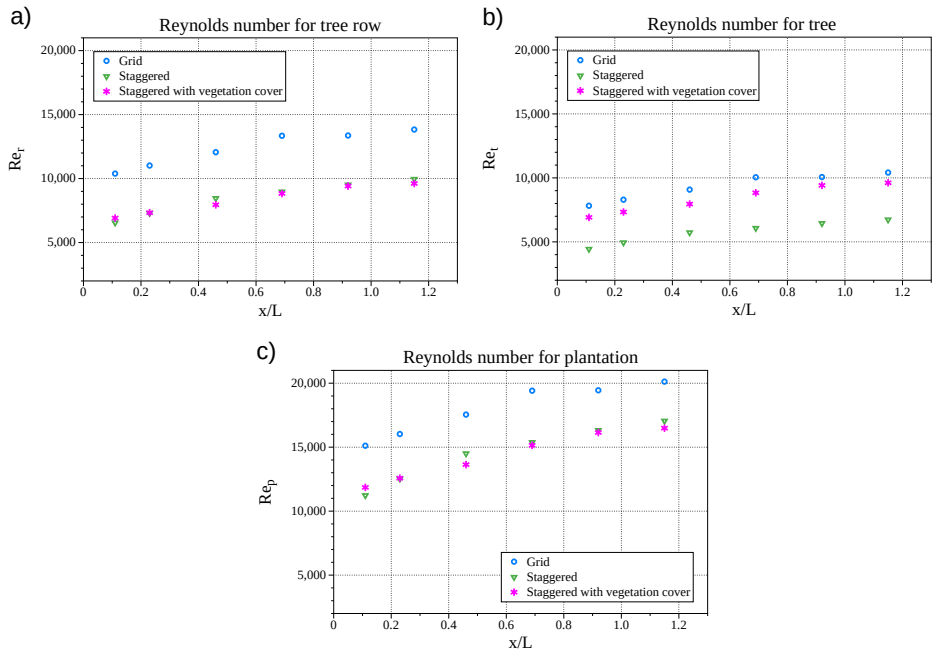

Figure 3.17: Reynolds number calculated for each profile position: a) Reynolds for tree row Re_r, b) Reynolds for tree Re_t (right) and c) Reynolds for plantation Re_p.

The experiments of this study were carried out for flat terrain, assuming that the experimental setup is repeated transversely and the tests are performed in 2D. Taking the staggered with cover vegetation configuration as reference, three profiles have been selected for comparison (right, center, and left), corresponding to Profiles 2, 4, and 6 (P2, P4, P6), from Figure 3.3. We compare how the results differ slightly from each other, so we can assume the hypothesis that the difference between the profiles is not relevant for the crosswise section, and the 2D results provide representative data of the plantation. Although the Reynolds number criteria are not fully met in the near field profiles, the system is ergodic. However, it is fulfilled in the medium-field and far-field profiles. Therefore, the ergodicity is confirmed in the tests performed, and it is assumed that the ensemble average coincides with the time average (stationary system). As shown in Figure 3.18, the variation in the profiles measured for the central, right, and left sections is small; in this way, the analysis performed and the results obtained could be extrapolated to the plantation as a whole.

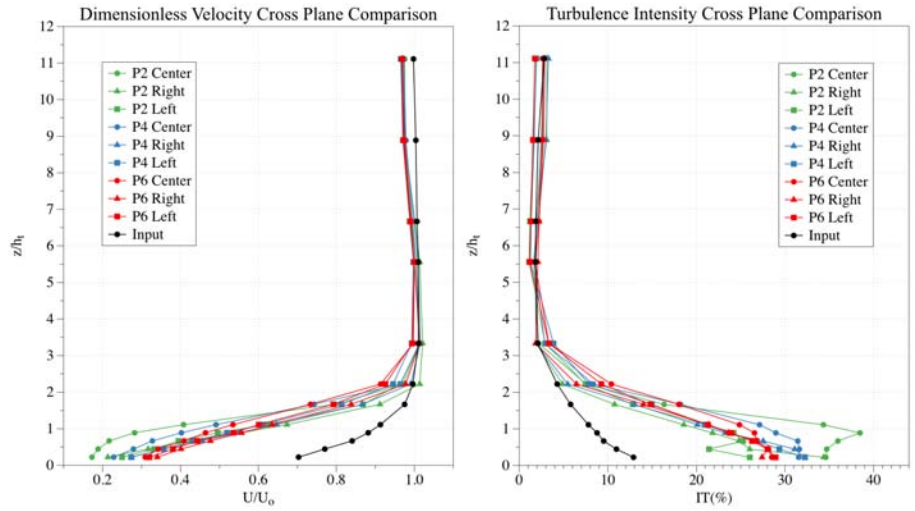

Figure 3.18: Comparison of (i) dimensionless mean wind velocity profiles (left) and (ii) dimensionless turbulence intensity profiles (right), obtained in profiles P2, P4 and P6 and the sections: right, central and left (Figure 3.3), for the staggered with vegetation cover configuration. The black dotted line represents the profiles obtained upwind the olive configuration.

According to the results shown in Figure 3.19, the airflow recovery occurs progressively, being recovered in its practical totality at the height of $z/h_t = 2$, that is, twice the height of the tree. The profiles measured inside the plantation (-P2) show a more significant reduction in velocity and increase in turbulence due to its location and surface vegetation. However, in position -P1, an acceleration of the flow and a decrease in turbulence can be observed. This acceleration phenomenon is related to the shape of the trees and the trunk height, but also it is associated with the porosity at that point.

The recovery effect shown in the Figure 3.19 demonstrates the function of the olive grove as a windbreak. On the other hand, Figures 3.9 and 3.10 show the differences between the studied configurations due to the plantation porosity and its spatial distribution, which is in agreement with the works of Podhrázská et al. (2021) and Pan et al. (2020).

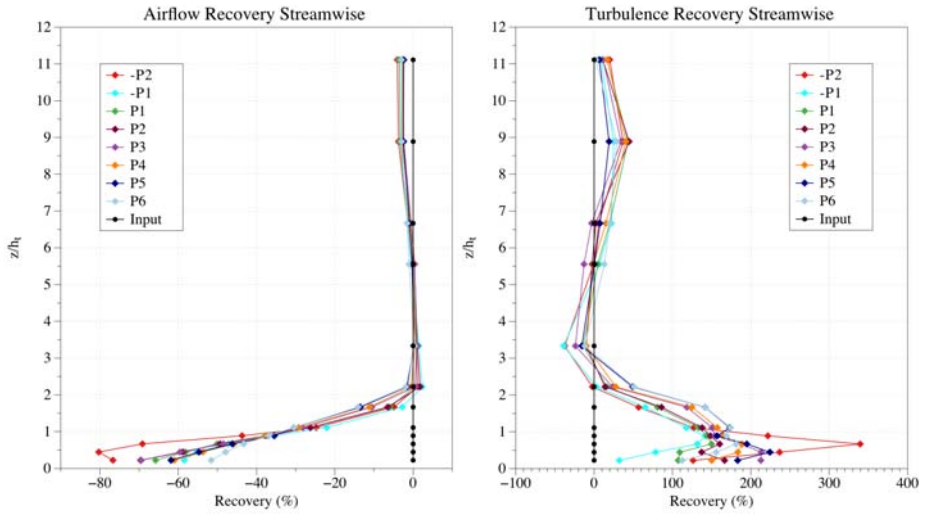

Figure 3.19: Comparison of the streamwise recovery (i) dimensionless mean wind velocity profiles (left) and (ii) dimensionless turbulence intensity profiles (right), obtained in the central section (Figure 3.3), for the staggered with vegetation cover configuration. This variation has been calculated according to the expressions 5.1, 3.11, and 3.12, and part of its values are shown in the Table 3.7.

Some variables analyzed in this work are involved in the dynamics of ecosystems and should be incorporated into a management model because of their direct relation to environmental variables such as pollen concentration, erosion processes, or water availability, among others (Dupont et al., 2006; Montaldo et al., 2020; Paço et al., 2014; Quill et al., 2020). The olive grove influences micrometeorology and is involved in the interaction between the surface and the atmosphere; then, turbulence parameters are fundamental in the surface transport of heat, humidity, and momentum.

3.7 Conclusions

This chapter analyzes the interaction of different olive agro-forests, representing Andalusia exploitations, with the airflow dynamics in the atmospheric surface boundary layer (SBL). Through wind tunnel tests, this interaction has been studied to obtain a comprehensive understanding of exchanges and variations in the system's mechanics and quantify kinematic variables that define the SBL. Whose spatial and temporal gradients have significant effects on many environmental processes, soil erosion processes, evapotranspiration, and water vapor fluxes, seeds and pollen dispersal distance, among others (Jiménez-Portaz et al., 2021).

These kinematic variables, for neutral atmosphere conditions, were measured in three different sections, inside and behind the forest, for a total of 22 vertical profiles for each configuration for a streamwise distance longer than the total length of the plantation.

Every configuration represents an Andalusian olive grove and has different layouts, tree composition, and vegetation covers. The extension of the interaction of the olive agro-forest and the wind dynamics depends on the overall length (L) and width (B) of the forest, the streamwise distance between trees (e_l), the crosswise corridor width (C_w), the tree height (h_t) and the tree crown radius (t_r), the characteristics of the soil cover, the incoming wind profile and the turbulence characteristics.

Windbreaks or plantation arrangements play a fundamental role in the ecosystem processes. They reduce velocity, modify the turbulence and affect the microclimate, but at the same time, it is essential to ensure the airflow through the agroecosystem, which depends on the spatial arrangement and characteristics of individual trees. This is in agreement with the results of several studies, such as the one presented by Podhrázská et al. (2021) and Pan et al. (2020).

In this work, sustainability and the traditional culture of the olive grove are combined with aerodynamic variables. The aerodynamic diameter of each agro-forest management unit studied is proposed as a representative variable of the system response and is directly related to the management and silvicultural treatment of the olive grove.

The results and conclusions obtained apply to the specific tree crown and trunk tested so that for other tree types, structures, and spatial configurations, the results will change. The following conclusions can be derived from this study:

1. Regarding wind velocity profiles, a decrease is observed just behind the plantation and an acceleration of the flow up to a height $z/h_t = 2$, from which the profiles tend to be recovered. On the other hand, acceleration is observed between trees (as it could be seen in profile -P1) at the base of the windbreak. These results are in agreement with the work of Cleugh (1998).
2. Analyzing streamwise flow, vertical profiles for the different variables studied are more homogeneous and similar to each other in the case of the traditional olive grove (staggered distribution), although the levels of turbulence are higher. Moreover, the traditional olive grove shows lower streamwise variations and longer airflow recovery than the intensive olive grove.
3. According to the leeward wind flow of the agro-forest, the wind velocity profile goes close to zero (but it is not zero on average) at a distance of $x/L \leq 0.11$ and height approximately equal to h_t. The vertical transition between the modified and incoming wind profiles is extended to $2.5 \leq z/h_t \leq 3$. One relevant characteristic of the vertical velocity wind profile for the traditional

olive grove is the inflection point around $z/h_t \leq 1.5$. At a distance of $x/L \leq 1.15$ (distance approximately equal to the total length of the plantation), the wind profile is still affected by the olive agroforest.

4. Regarding the turbulent characteristics, the turbulence intensity profiles grow significantly in the domain where the vertical wind profile transition occurs at $2.5 \leq z/h_t \leq 3$, showing maximum values at approximately $z/h_t = 1$. Furthermore, the maximum decreases and becomes smoother; at $x/L \leq 1.15$, the exponential shape seems to almost recover, except for near the surface, depending on the layout and the cover.
5. It is concluded that in the area next to the trees, the TKE is similar for all the configurations; however, it is significantly higher in the case of the traditional olive grove as we move in the streamwise direction.

4. Interaction of the ABL and wind farms

Wind energy is one of the most popular renewable energies, with more than 650GW installed worldwide. These systems operate by extracting kinetic energy from the airflow and modifying the dynamics of the atmosphere in the process. Therefore, it is crucial to predict the wind energy distribution, depending on the terrain and surrounding obstacles, to select the installation sites properly. It is also necessary to know how the wind field will be altered to avoid modifying the wind flow around other wind turbines and the impact on the environmental components related to the atmosphere. Thus, developing scientific-technical knowledge about the dynamic processes in the area adjacent to the wind farms is required to carry out a comprehensive exploitation analysis. In this chapter, wind tunnel tests were performed to study the wind flow field over hilly terrain and around wind turbine systems. Different study scenarios are proposed, changing the topography, terrain characteristics, surface roughness, and the wind turbine model location. Tests carried out show changes in the wake behind the turbine, decreasing the wind velocity and increasing the turbulence intensity, whose effects dissipate as we move away from the wind turbine. The main differences between the configurations studied are due to the disposition and type of topographic obstacle, making clear the importance of the proper emplacement, the wind turbine size, and the global effect it has on the atmosphere dynamics.

The information included in this chapter has been published in:

Jiménez-Portaz, M., Clavero M., Pospísil S. & Losada M.A. (2020). Wind tunnel tests applied to wind energy management: Comparison of measurements in closed-circuit and open-circuit wind tunnels. Renewable Energy and Power Quality Journal 18, 272-275.

Jiménez-Portaz, M., Bello-Millán, F. J., Folgueras, P., Clavero, M., & Losada, M. A. (2016). Wind flow around a wind turbine system over hilly terrain and its environmental effects: Wind tunnel tests. Renewable Energy and Power Quality Journal, 1(14), 318-321.

4.1 The wind energy in Andalusia

The peaks and mountainous areas, where the probability of strong winds is high and frequent, make it an ideal location for wind energy exploitation. The variation and distribution of wind speed estimate the generation of wind potential, so its study is essential in the design of wind farm projects. The meteorological variability in Spain, specifically in Andalusia, means that the wind resource is guaranteed in different areas, compensating the areas of greatest potential with those in which it is impossible to extract this resource.

In recent years, the sustainable use of energy sources has been enhanced to minimize the pressure on high ecological value systems and reduce fossil fuels' use to achieve decarbonization of the energy system by 2050. In this way, new energy extraction techniques, systems, site selection optimization, legislation, and regulations to control and support their use are being developed. Thus, in recent years there has been an exponential growth of these installations, especially for photovoltaic and wind farms.

In the case of wind energy (Florescu et al., 2019; Lindman and Söderholm, 2016), Andalusia currently has 160 wind farms, with a total of 3.5GW of installed power, of which a part corresponds to repowered wind farms (AEE, 2020). This high potential is due not only to the number of wind farms but also to the increasing size of wind turbines (Figure 4.1). In Andalusia, installations are mainly concentrated in the eastern part of the region (Figure 4.2), and in coastal areas near to the province of Cádiz (more than half of the wind farms are located in this province), as these areas have significant wind potential (Cuevas et al., 2018). The accelerated evolution and the need to use them to meet ever-increasing energy needs have focused attention on the potential environmental impacts they may generate.

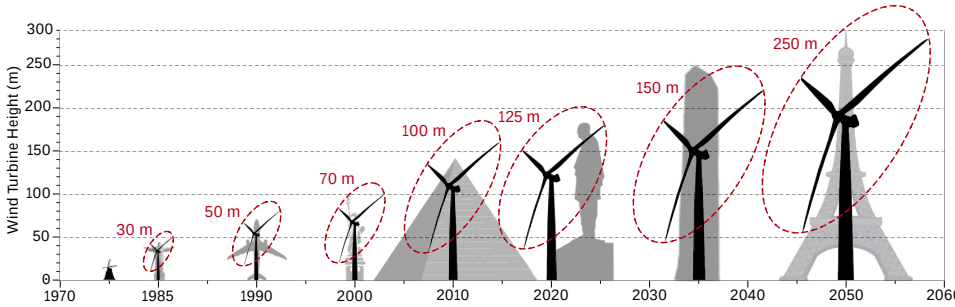

Figure 4.1: Evolution of wind turbine size and rotor diameter (numbers in red) in recent years and their future forecast. Data source: The European Wind Energy Association (EWEA).

Figure 4.2: Distribution of wind farms in the region of Andalusia. Data source: AEE (2020).

4.1.1 Wind farms classification

Wind farms are characterized by elements that compose them, their location, the characteristics of the environment, and the processes and changes that occur when interacting with the environment. A classification can be made that encompasses the types of parks according to their spatial location and the classification of the Andalusian landscape (Ghislanzoni et al., 2014):

- Offshore wind farm. Located offshore, more than 10 km away from the coastline. Being far from the land area and the obstacles of the area, the wind

resource is optimized.

- Coastal wind farm. This kind of wind farm includes all those located between 10 km offshore and 3 km inland. The wind potential in these areas is usually higher.
- Wind farms in high lands and sub-deserts. Areas with sub-desert climates, mostly depopulated by vegetation, reduce vegetation's influence on wind fields.
- Mountain wind farm. Mountainous regions with large wooded areas and protected areas. Due to the intrinsic characteristics of these areas, there will be a greater impact on the environmental components.
- Wind farm in the countryside. Plains characterized by their landscape and environmental heterogeneity.
- Wind farms in valleys, meadows, and marshes. They are usually less elevated areas, with herbaceous vegetation and scrub, and sporadic appearance of wooded areas of great size.
- Mini wind farms. Unattended installations for farms with less than 100 kW of power.
- Airborne. A wind power system consisting of an ungrounded device that is suspended in the air.

4.1.2 Principles of a wind turbine operation

Being an efficient and competitive technology at an economic and supply level comes from the advances in design and spatial distribution of infrastructures, increasing in number, size, and complexity. More aerodynamic and more powerful wind turbines have been achieved; when properly spatially arranged, they take full advantage of the area's wind potential.

However, efficient and high technical level technology to produce energy in a renewable way is not enough. It is necessary to have climatological knowledge and information of system behavior as a whole, to identify not only the maximum potential for wind energy production but also the interaction between the inflow and the wind farm infrastructure.

The operation of a wind turbine is based on the extraction of kinetic energy from the wind field, which means that a higher wind speed and a greater radius of the wind turbine will produce more energy (Figure 4.3). The theoretical power (P_w) availability depends on the wind velocity and is proportional to the velocity cubed. According to the Betz's Law, the energy (E) extracted by the turbine is the result of the difference between the incoming wind flow and the outgoing wind flow (Stull, 2016), defined both quantities as follow:

$$P_w = (\pi/2) \cdot \rho \cdot Ef \cdot R^2 \cdot U_{in}^3 \tag{4.1}$$

$$Ef = 0.5 \cdot m \cdot U_{in}^2 - 0.5 \cdot m \cdot U_{out}^2 \tag{4.2}$$

where ρ is the air density, Ef is the turbine efficiency, R is the turbine-blade radius, U_{in} is the incoming wind velocity, U_{out} is the outgoing wind velocity and m is the air mass.

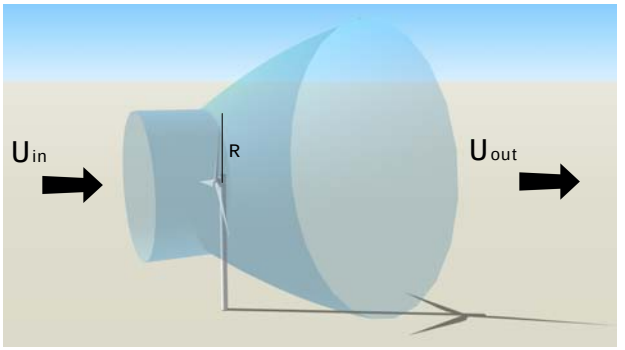

Figure 4.3: Air flow transfer through the wind turbine. Picture adapted from Stull (2016).

4.1.3 Problem statement

A direct effect of the integration of a wind turbine - or a set of wind turbines - in the environment is the generation of a turbulent wake derived from the movement of the blades and its structure (Porté-Agel et al., 2020), where three zones can be differentiated: near, medium and far wake. Some directly noticeable effects within or associated with the wake are (i) decrease in mean wind velocity and (ii) increase in turbulence intensity (Jiménez-Portaz et al., 2016; Yang et al., 2020). As turbulence is directly related to increased fatigue loads and environmental variables alterations, knowledge of the turbulence in the wake and its evolution is essential.

The scope and magnitude of the wake depend on the size of the wind turbine and the blades, the number of wind turbines, their spatial layout, and the superposition between wakes. The cumulative effect of having another wind farm nearby must also be taken into account. The larger the turbine, the more wind power is generated and, consequently, the greater the effect on the wind field (Stull, 2016). Moreover, the turbulent wake and the superposition can cause power loss and fatigue loads in wind turbines. There are different analytic, computational, and experimental works focused on this phenomenon, as stated in the study carried out by Porté-Agel et al. (2020). Besides, there may also be effects on the governing variables

or environmental descriptors, such as humidity, evapotranspiration, temperature, or precipitation, among others, on which ecosystems depend. These variables also control the phenomena that take place in the Surface Boundary Layer of the Atmosphere.

On the other hand, by not introducing the effects of the terrain and its modifications in the wind field, errors of more than 40% may be incurred; in other words, neglecting the effect of turbulence on the inflow can result in an overestimation of the outflow by 10% (Chamorro and Porté-Agel, 2009). Most of the studies carried out with and without wind turbines have incorporated roughness in their tests to avoid this effect. In work carried out by He et al. (2014), a detailed study of the topography was carried out to check the alterations in the wind flow, integrating experimental and in-situ data. However, as the Porté-Agel et al. (2020) paper explains, although there is extensive literature on ABL flows over topography, "the combination of wind turbines and topography still has much room for research."

4.2 Objectives

The main objectives of this chapter are:

- Provide an overview of the turbulent wake characteristics generated by a three blades wind turbine.
- Analyze the interaction between the ABL and different topographies to compare the differences between them and their potential as a wind farm site.
- Analyze the airflow behavior around a wind turbine system located over different hilly terrains and compare the results.

4.3 Study site

The first step in a wind energy project is the location selection. For this purpose, different factors must be studied: the wind potential, the environmental components susceptible to being affected, the exclusion zones, and the potential evacuation lines of the electrical grid. The use of wind maps facilitates the selection of areas with more significant wind potential, and therefore, candidates to host a wind energy exploitation. Within the maps, at least the wind speed and the main directions, as well as the temporary changes of both variables, must be collected (Cuevas et al., 2018).

Two areas of the Andalusian landscape and climate were selected as representative wind farms in Andalusia. First, a plain area near the coast in the province of Cádiz, located explicitly in La Janda, where the pressure generated by the implementation of wind farms is increasingly high. On the other hand, it was selected a

mountainous area inland of the province of Almería, where the pressure on ecosystems due to the semi-arid climate, limited water resources, and climate change make this area particularly sensitive to impacts.

Figure 4.4: Orthophoto of the selected area as reference, in La Janda (Cádiz). It shows the coverage type, topography and installed wind turbine type. Source: Google Earth.

Figure 4.5: Orthophoto of the selected area as reference, in the village of Hijate (Almería). It shows the coverage type, topography and installed wind turbine type. Source: Google Earth.

4.4 Methodology

A wide variety of computational, analytical, and experimental approaches have been used to study the interaction of the ABL with wind farms. Despite numerous scientific advances in this topic, the dynamic nature of the variables involved and the non-stationary boundary conditions, the existence of turbulence, or the fact of working at large scales, make it crucial to resort to experimental wind tunnel modeling. In this way, wind tunnel experiments provide high-quality information on the flow structure behind wind turbines, which exhibits essential differences for freestream flow (Porté-Agel et al., 2020).

Based on the type of surface and vegetation cover of the study site, a theoretical wind velocity profile and a turbulence intensity profile have been calculated for

each case, allowing to characterize the wind field where the study models were located. Thus, two-dimensional experimental tests were performed with different configurations, varying the simulated boundary layer and the topography, using the same wind turbine model. The tests were carried out in the two different wind tunnels described in Chapter 2.

4.4.1 Dimensional analysis

Airflow streamwise topographies and wind turbine models are studied in this chapter. This section contains the fundamentals of the airflow evolution through both obstacles, and Figures 4.6, 4.7, 4.8 and 4.9, are 2D schemes of the interaction described above. Across the board, the dimensional analysis described in this section will allow us to obtain the relationship of the kinematic variables with the wind turbine rotor diameter (D) and the height of a hill (h).

The first step of the dimensional analysis is to identify a complete set of independent quantities that determine the value of the wind speed behind a wind turbine or a topographic barrier. Then, for each height z, a set of independent variables related to wind velocity behind the system are defined for every case. Note that, assuming the stationarity of the process, the time variable is simplified throughout the analysis.

Hill over flat terrain

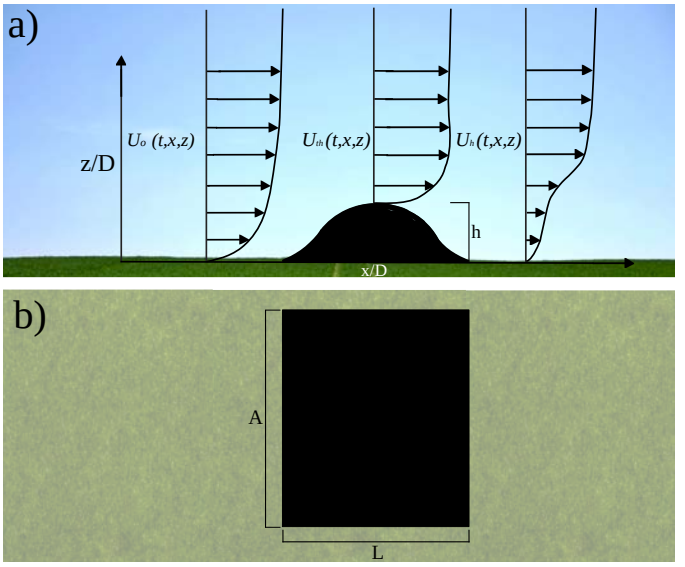

Figure 4.6: Sketch of a wind profile transformation in the SBL across a Hill. Where L is the hill length, A is the hill width, and h is the hill height.

According to Figure 4.6, the set of independent variables are defined as follows:

1. Physical properties: air density ρ_a, air dynamic viscosity μ_a, and gravitational acceleration g.
2. System components, including the topography properties: hill length L and hill height h.
3. Input: instantaneous wind velocity $U_o(x,y,z,t)$ profile upwind the hill.
4. Output: measured instantaneous wind velocity $U_{hill}(x,y,z,t)$ time series downwind the hill.

The input and output wind velocities can be splitted in two components:

$$U_i(x,y,z,t) = \overline{U_i}(x,y,z,t) + u_i'(x,y,z,t), i = o, hill \tag{4.3}$$

where $\overline{U_i}$ is the time average wind velocity and u_i' is the time wind velocity fluctuation, and the subindex o and $hill$ indicates input and output respectively. Next, a complete set of independent quantities is selected, which determine the time average wind speed value at any location behind the hill,

$$\overline{U_{hill}}(x,y,z) = f\{\rho_a, \mu_a, g, L, h, \overline{U_o}\} \tag{4.4}$$

which comprises a total of $n = 6$ independent variables. Choosing a base of 3 independent quantities, $\{\mu_a, h, \overline{U_o}\}$, $k_f = 3$, then $n - k_f = 3$, is the number of dimensionless monomials to obtain. Using the base subset, the following non-dimensional quantities are obtained:

$$\frac{\overline{U_{hill}}}{\overline{U_o}} = f\left\{ \underbrace{\frac{h}{L}}_{\text{I}}, \underbrace{\frac{\overline{U}_o \cdot h}{\nu_a}}_{\text{II}}, \underbrace{\frac{\overline{U}_o^2}{g \cdot L}}_{\text{III}} \right\} \tag{4.5}$$

where $\nu_a = \frac{\mu_a}{\rho_a}$, is the kinematic viscosity of the air, and the dimensionless quantities are: I) relative hill length, II) relationship between hill height and downwind system response, and III) relationship between hill length and downwind system response.

Wind turbine over flat terrain

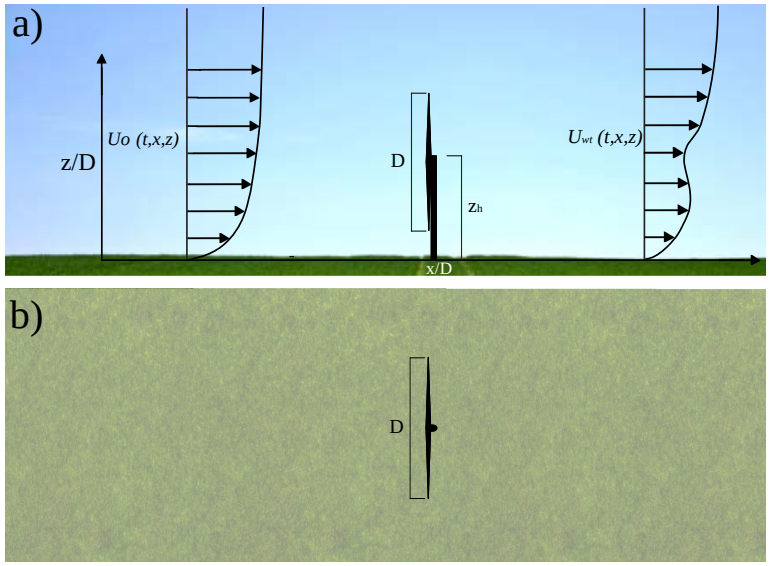

Figure 4.7: Sketch of a wind profile transformation in the SBL across a wind turbine over flat terrain. Where D is the rotor diameter and z_h is the wind turbine tower height.

According to Figure 4.7, the set of independent variables are defined as follows:

1. Physical properties: air density ρ_a, air dynamic viscosity μ_a, and gravitational acceleration g.
2. System components, including the wind turbine properties: rotor diameter D and wind turbine tower height z_h
3. Input: instantaneous wind velocity $U_o(x,y,z,t)$ profile upwind the wind turbine.
4. Output: measured instantaneous wind velocity $U_{wt}(x,y,z,t)$ time series downwind the wind turbine.

The input and output wind velocities can be splitted in two components, described above, and the subindex o and wt indicates input and output respectively. Then, a complete set of independent quantities is selected, which determine the time average wind speed value at any location behind the wind turbine,

$$\overline{U_{wt}}(x,y,z) = f\{\rho_a, \mu_a, g, D, z_h, \overline{U_o}\} \tag{4.6}$$

which comprises a total of $n = 6$ independent variables. Choosing a base of 3 independent quantities, $\{\mu_a, D, \overline{U_o}\}$, $k_f = 3$, then $n - k_f = 3$, the number of

dimensionless monomials to obtain. Using the base subset, the following non-dimensional quantities are obtained:

$$\frac{\overline{U_{wt}}}{\overline{U_o}} = f\left\{ \underbrace{\frac{z_h}{D}}_{\text{I}}, \underbrace{\frac{\overline{U}_o \cdot H_{wt}}{\nu_a}}_{\text{II}}, \underbrace{\frac{\overline{U}_o^2}{g \cdot D}}_{\text{III}} \right\} \tag{4.7}$$

where $\nu_a = \frac{\mu_a}{\rho_a}$ is the kinematic viscosity of the air, $H_{wt} = z_h + 0.5D$ is the wind turbine total height, and the dimensionless quantities are: I) relative wind turbine tower size, II) relationship between viscosity and friction due to the total wind turbine height, and III) relationship between rotor diameter and downwind system response.

Wind turbine behind a hill over flat terrain

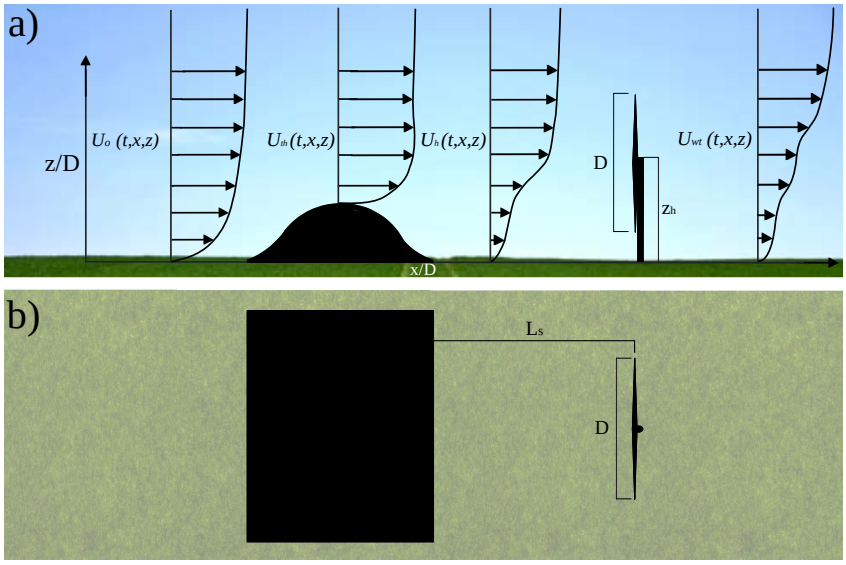

Figure 4.8: Sketch of a wind profile transformation in the SBL across a wind turbine located behind a hill. Where D is the rotor diameter, z_h is the wind turbine tower height, and L_s is the distance between hill and wind turbine.

According to Figure 4.8, the set of independent variables are defined as follows:

1. Physical properties: air density ρ_a, air dynamic viscosity μ_a, and gravitational acceleration g.
2. System components, including:

- Wind turbine properties: rotor diameter D and wind turbine tower height z_h.
- Topography: distance between hill and wind turbine L_s.

3. Input: instantaneous wind velocity $U_{hill}(x,y,z,t)$ profile downwind the hill.
4. Output: measured instantaneous wind velocity $U_{wt}(x,y,z,t)$ time series downwind the wind turbine.

The input and output wind velocities can be splitted in two components, described above, and the subindex *hill* and *wt* indicates input and output respectively. Then, a complete set of independent quantities is selected, which determine the time average wind speed value at any location behind the wind turbine,

$$\overline{U_{wt}}(x,y,z) = f\{\rho_a, \mu_a, g, D, z_h, L_s, \overline{U}_{hill}\} \tag{4.8}$$

which comprises a total of $n = 7$ independent variables. Choosing a base of 3 independent quantities, $\{\mu_a, h, \overline{U_{hill}}\}$, $k_f = 3$, then $n - k_f = 4$, the number of dimensionless monomials to obtain. Using the base subset, the following non-dimensional quantities are obtained:

$$\frac{\overline{U_{wt}}}{\overline{U_{hill}}} = f\left\{ \underbrace{\frac{z_h}{D}}_{\text{I}}, \underbrace{\frac{L_s}{D}}_{\text{II}}, \underbrace{\frac{\overline{U}_{hill} \cdot H_{wt}}{\nu_a}}_{\text{III}}, \underbrace{\frac{\overline{U}^2_{hill}}{g \cdot D}}_{\text{IV}} \right\} \tag{4.9}$$

where $\nu_a = \frac{\mu_a}{\rho_a}$ is the kinematic viscosity of the air, $H_{wt} = z_h + 0.5D$ is the wind turbine total height, and the dimensionless quantities are: I) relative wind tower size, II) relative distance from hill, III) relationship between viscosity and friction due to the total wind turbine height, and IV) relationship between rotor diameter and downwind system response.

Wind turbine on top of a hill

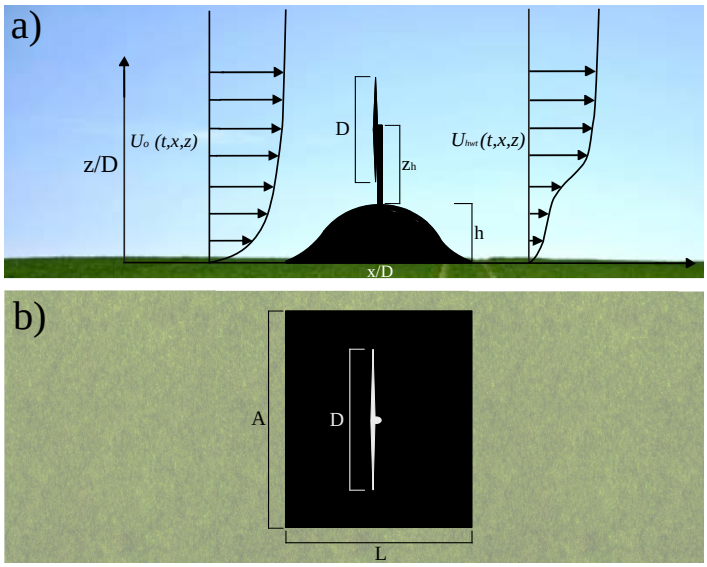

Figure 4.9: Sketch of a wind profile transformation in the SBL across a wind turbine located on top of a hill. Where A is the hill width, L is the hill length, h is the hill height, D is the rotor diameter, z_h is the wind turbine height.

According to Figure 4.9, the set of independent variables are defined as follows:

1. Physical properties: air density ρ_a, air dynamic viscosity μ_a, and gravitational acceleration g.
2. System components, including:
   - Wind turbine properties: rotor diameter D and wind turbine height z_h.
   - Topography: hill length L and hill height h.
3. Input: instantaneous wind velocity $U_o(x,y,z,t)$ profile downwind the hill.
4. Output: measured instantaneous wind velocity $U_{hwt}(x,y,z,t)$ time series downwind the wind turbine.

The input and output wind velocities can be split into two components, described above, and the subindex o and hwt indicates input and output respectively. Then, a complete set of independent quantities is selected, which determine the time average wind speed value at any location behind the obstacle,

$$\overline{U_{hwt}}(x,y,z) = f\{\rho_a, \mu_a, g, D, z_h, h, L, \overline{U_o}\} \tag{4.10}$$

which comprises a total of $n = 8$ independent variables. Choosing a base of 3 independent quantities, $\{\mu_a, g, D\}$, $k_f = 3$, then $n - k_f = 5$, the number of

dimensionless monomials to obtain. Using the base subset, the following non-dimensional quantities are obtained:

$$\frac{\overline{U_{hwt}}}{\overline{U_o}} = f\left\{ \underbrace{\frac{L}{D}}_{\text{I}}, \underbrace{\frac{h}{D}}_{\text{II}}, \underbrace{\frac{z_h}{D}}_{\text{III}}, \underbrace{\frac{U_o \cdot H_{obs}}{\nu_a}}_{\text{IV}}, \underbrace{\frac{\overline{U_o}^2}{g \cdot D}}_{\text{V}} \right\} \tag{4.11}$$

where $\nu_a = \frac{\mu_a}{\rho_a}$ is the kinematic viscosity of the air, $H_{obs} = z_h + h + 0.5D$ the obstacle total height, the dimensionless quantities are: I) relative hill length, II) relative hill height, III) relative wind turbine tower height, IV) relationship between viscosity and friction due to the total obstacle height, and V) relationship between rotor diameter and downwind system response.

4.4.2 Derived quantities and aerodynamic variables

The analysis and results depend on the spatial position in which they are performed, being their coordinates:

$$x^* = \frac{x}{D}, \quad y^* = \frac{y}{D}, \quad z^* = \frac{z}{D} \tag{4.12}$$

For this case, three spatial coordinates are dimensioned with D (rotor diameter) due to the direct dependence between the alterations in the wind field and the size of the wind turbine. This also facilitates comparing experimental results derived from each of the studied layout configurations, as detailed in the following section.

Considering the variance and the instantaneous variation of the wind speed for each of the velocity vectors, the local turbulence intensity (IT) and the Reynolds stress (u_*^2) downwind of the wind turbine are defined in terms of the local variances (horizontal and vertical) and instantaneous wind velocity values. Thus, these quantities can be considered as the second kind derived quantities, and thus dimensionless forms are described as:

1. First kind derived quantities: $\sigma_u^2 = \overline{u_o'^2}, \quad \sigma_w^2 = \overline{w_o'^2}$
2. Second kind derived quantities: $IT(z) = \frac{\sigma_u(z)}{\overline{U_o}(z)}, \quad u_*^2 = \frac{\tau}{\rho_a} = \frac{\overline{u'w'}}{\overline{U_o}^2}$

where u_*^2 is the kinematic stress against the Earth's surface, u_* is the friction velocity and τ is the stress. Based on the definitions of aerodynamic diameter and Reynolds number given in Chapters 2 and 3, these aerodynamic variables can be defined for all the cases considered. Being the variables that define the system behavior:

- Aerodynamic diameter for a hill over flat terrain: D_{hill}

- Aerodynamic diameter for a wind turbine over flat terrain: D_{wt}
- Aerodynamic diameter for a wind turbine on top of a hill : D_{hwt}

$$D_{hill} = \frac{2Ah}{A+h} \quad D_{wt} = \frac{2DH_{wt}}{D+H_{wt}} \quad D_{hwt} = \frac{2DH_{hwt}}{D+H_{hwt}} \tag{4.13}$$

- Reynolds number for a hill over flat terrain: Re_{hill}
- Reynolds number for a wind turbine over flat terrain: Re_{wt}
- Reynolds number for a wind turbine over flat terrain and behind a hill: Re_{wt2}
- Reynolds number for a wind turbine on top of a hill: Re_{hwt}

$$Re_{hill} = \frac{\overline{U_o} D_{hill}}{\nu_a} \quad Re_{wt} = \frac{\overline{U_o} D_{wt}}{\nu_a} \quad Re_{wt2} = \frac{\overline{U_{hill}} D_{wt}}{\nu_a} \quad Re_{hwt} = \frac{\overline{U_o} D_{hwt}}{\nu_a} \tag{4.14}$$

4.4.3 Experimental set-up

Once the theoretical boundary layer has been characterized as it was explained in Chapter 2, it is necessary to reproduce it in the wind tunnel at a small scale so that the behavior of the model is as close as possible to reality (Voutsinas et al., 1992). Not only the geometrical similarity between model and prototype must be fulfilled, but also certain relations of kinematic similarity, that is to say, that their velocity vectors are proportional and have the same orientation. Moreover, dynamic similarity, being their force vectors proportional and with the same orientation.

The same reduced-scaled model was used in both experiments, exhibited in Figure 4.10. It was a 3-blades free rotation wind turbine with a hub axis height of $z_h = 0.3\,m$ and a rotor diameter of $D = 0.35\,m$, and it was built with a scale factor of $E = 1:300$. This model was made based on the wind turbines currently located in Mediterranean wind farms. In both tunnels, neutral stability of the atmosphere has been considered, without any change in temperature or humidity. Two hills of different sizes have been used, the Hill1 has a size of $A = 0.80\,m$, $L = 0.80\,m$, and $h_1 = 0.15\,m$, and the Hill2 has a size of $A = 1\,m$, $L = 0.80\,m$, and $h_2 = 0.22\,m$.

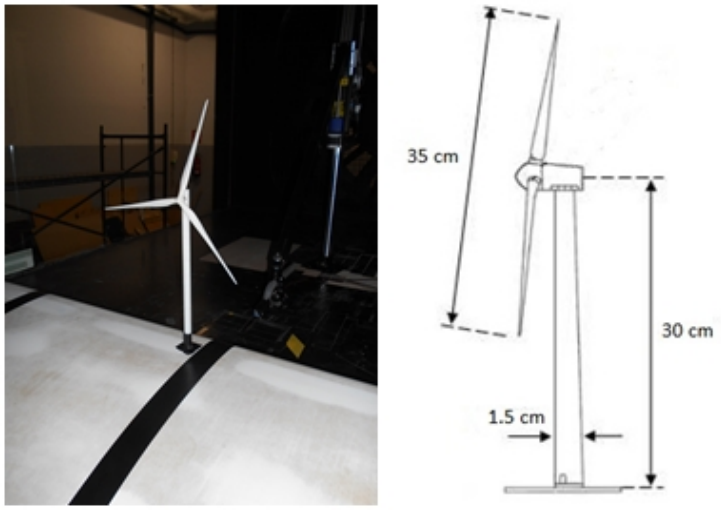

Figure 4.10: 3-blades wind turbine model.

Altogether, five configurations have been studied, with different obstacles, reference speeds, and characteristics of each test, which are summarized in Table 4.1. In addition, the aerodynamic diameters and Reynolds numbers for the input velocity and the topographies and wind turbine configurations obtained according to the analysis described in the previous section are also included in Table 4.1.

Config	Hill	WT	Terrain	$z_o(m)$	$U_o(m/s)$	$Dm(m)$	Re
C1	Hill1	No	Scrubland	0.1	7.5	0.26	$1.3 \cdot 10^5$
C2	Hill2	No	Grassland	0.07	3	0.36	$7.35 \cdot 10^4$
C3	No	Yes	Grassland	0.07	3	0.40	$8.22 \cdot 10^4$
C4	Hill2	Yes	Grassland	0.07	3	0.40	$7.01 \cdot 10^4$
C5	Hill1	Yes	Scrubland	0.1	7.5	0.45	$2.3 \cdot 10^5$

Table 4.1: Characteristics of the studied configurations. Including the number of Configuration, the presence or absence of hill and wind turbine (WT), the type of terrain, the aerodynamic roughness length (z_o), the input wind velocity (U_o), the aerodynamic diameter (Dm), and the Reynolds number (Re).

From wind tunnel tests performed by Chamorro et al. (2012) to quantify the Reynolds number dependence in the wake of a wind turbine model, starting from a $Re \geq 4.8 * 10^4$, mean flow statistics become independent of Re. Therefore, the Re values obtained for each test are high enough to neglect the effects generated by the viscosity and have a flow governed by the mechanical variables.

Experimental Tests in OCWT

In this case, models described for configurations C1 and C5 in Table 4.1 were used. To generate the required ABL model, reproducing a scrubland area, different roughness elements have been tested, modifying the elements' spatial distribution, height, and density. In this work, the final chosen configuration selected consists of a wooden barrier with height $WB = 0.15\,m$ located in the entrance of the tunnel, and two types of dissipation elements made by hexagonal nuts of sizes M10 and M16 arranged in a staggered layout, whose elements are arranged to each other at a distance of $0.15x0.15\,m$ along $2.7\,m$ in the wind tunnel surface, shown in Figures 4.11 and 4.12. Forty profiles distributed in a lattice of 8x5 were measured up to $1m$ in height. The distance between profiles was $D/2$, and each profile consisted of 12 measurement points.

The same TSI constant temperature anemometer, methodology, and analysis procedure described in Section 2.3.2 was used to obtain high-resolution and instantaneous measurements of the streamwise and vertical velocity components, u and w respectively. The inflow velocity in this case was $U_o = 7.5\,m/s$.

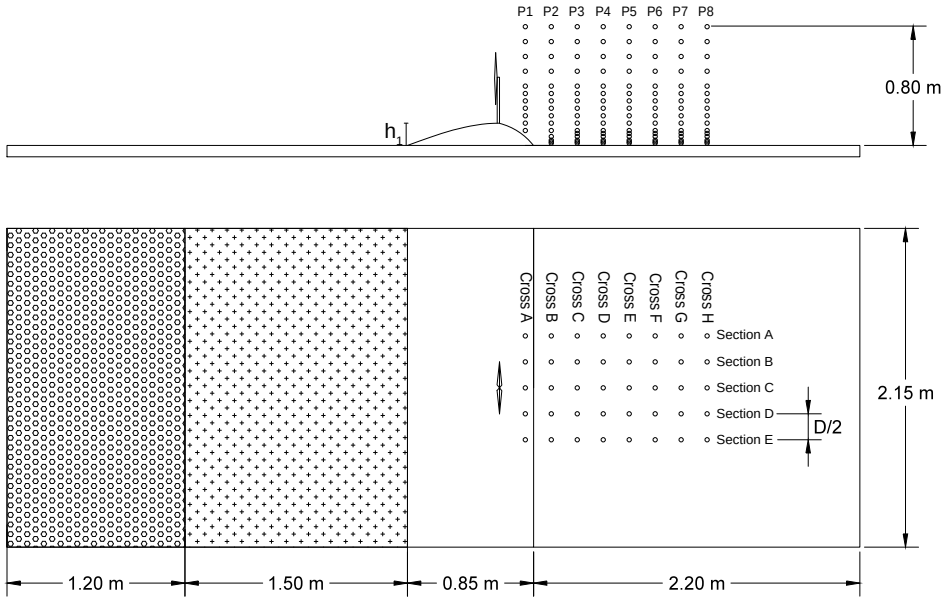

Figure 4.11: Experimental set-up in the OCWT. Simulation of a wind turbine on top of a hill over scrubland. For the configuration C1, only with the hill model, the set-up used was the same.

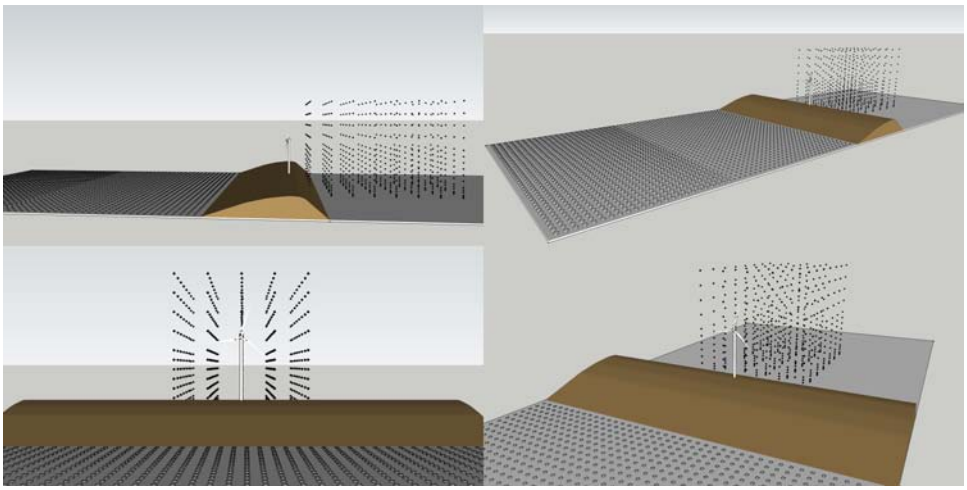

Figure 4.12: 3D sketch of the set-up of a wind turbine on top of a hill in a scrubland. This figure provides an illustrative example to show at which positions the measurements are taken, obtaining a cloud of points, for each of which a time series has been recorded.

Figure 4.13: Set up and wind turbine model used for tests in the Open Circuit Wind Tunnel. Simulation of a hill with a single wind turbine on top of it.

Experimental Tests in CCWT

For this case, the models described for configurations C2 and C4 in Table 4.1 were used. The final chosen configuration to reproduce an open grassland area consists of a wooden barrier with height $WB = 0.15\,m$ located in the entrance of the test section, and two sizes dissipation elements made of wood cylinders (two sizes: $15x10\,mm$ and $10x10\,mm$) and arranged in a staggered layout, whose elements are allotted to each other at a distance of $0.15x0.15\,m$ along $2.7\,m$ in the wind tunnel surface, shown in Figure 4.14.

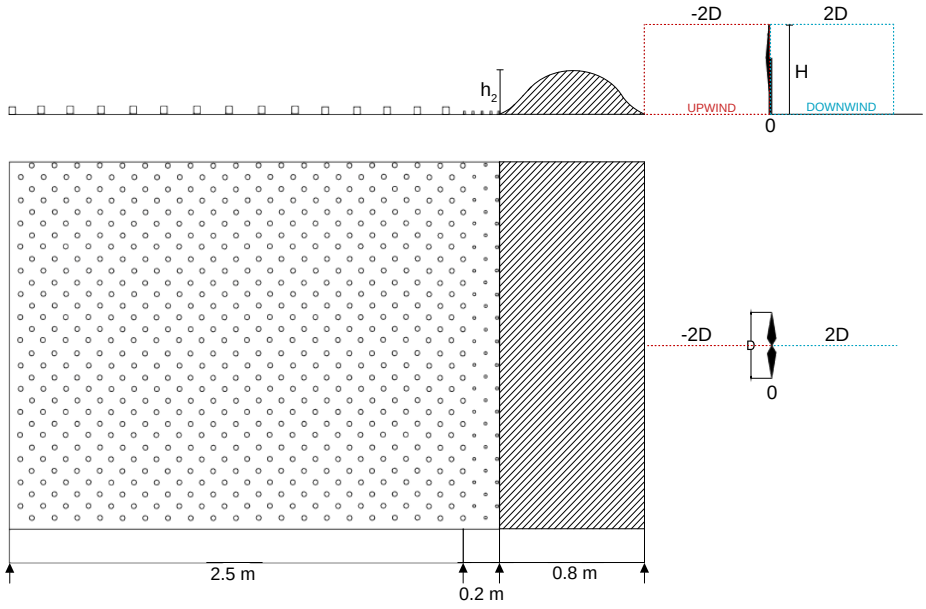

Figure 4.14: Experimental set-up in the CCWT. Simulation of a wind turbine over flat grassland and behind a hill.

A Dantec Dynamics Particle Image Velocimetry System instrument was used to take measurements, with 532 nm green Dual Power Nano L 200-15 PIV laser from Litron Lasers and laser sheet optics 80X91 Focus Module from Dantec Dynamics. Laser with optics was installed in the operator room so that the laser sheet passes through the ceiling window into the testing section. The seeding as tracer particles was Bi(2-Ethylhexyl) sebacate, dispersed using a fluid atomizer *Flow Tracker 700 CE*, located outside and connected to the inside of the tunnel, so that the dispersion was carried out efficiently without altering the flow due to the presence of extra instruments. The data were taken in two regions close to the model (Upwind and Downwind, Figure 4.14). For each test performed, 200 images were taken with HiSense 4M digital camera, at a frequency of 8.15 Hz and a variable pulse

time depending on the reference velocity, 1000 ms for the speed of $3\,m/s$ (inflow reference velocity). The analysis was performed with Dynamic Studio Software version 3.41 using the adaptive correlation algorithm.

Figure 4.15: Set up, hill, and wind turbine models used for tests the CCWT.

Experimental Tests in the OCWT and the CCWT

As a complement to the previous comparison, a series of tests were performed in both wind tunnels, using the same wind turbine model, boundary layer, and respecting the distances in the position of each element. On the other hand, the same type of instrument was also used to take measurements, and they were recorded in the same grid, previously fixed, so that the results were replicable and comparable. In both tunnels, a hot wire anemometry system was placed on a 3D positioning system, allowing it to take data at all points of the study section.

In this case, the models described for configuration C3 in Table 4.1 were used. The simulated ABL is the same as described in the previous section (4.4.3). Thirty profiles arranged in a lattice of 6x5 were measured up to 1 m high. The distance between profiles was $D/2$. Each profile consisted of 12 measurement points (Figure 4.16). A Dantec Dynamics cross hot-wire was used to take measurements with a sampling frequency of 1kHz and recording data during 120 seconds for each point for the CCWT, and the same TSI constant temperature anemometer and measurements procedure described in Section 4.4.3 was used for the OCWT. The inflow velocity in this case was $U_o = 3\,m/s$.

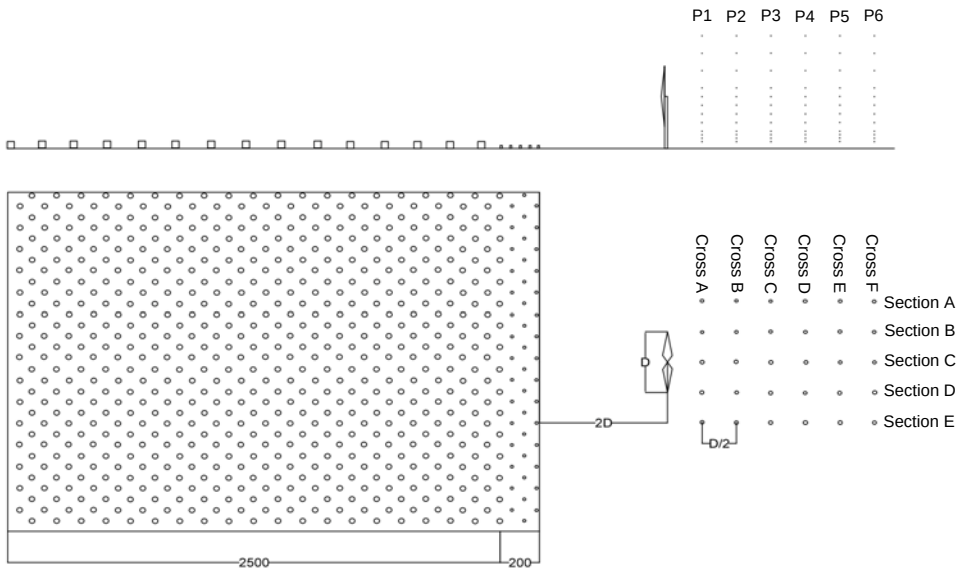

Figure 4.16: Experimental set-up in the CCWT. Simulation of a wind turbine over flat grassland.

Figure 4.17: ABL simulated with roughness elements inside the CCWT (left) and the OCWT (right).

Figure 4.18: Set up and wind turbine model used for tests in both wind tunnels.

4.5 Results

All data presented in this section have been dimensioned with the corresponding reference values specified for each case. In figures obtained from PIV data, no data are shown below a height of $z/D \leq 0.13$; due to the prevention of the reflection produced by the laser beam on the tunnel surface, so measurements were taken from that height.

4.5.1 Theoretical and experimental ABL

To obtain the theoretical profiles, and according to the expressions shown in Section 2.1.2, the corresponding roughness heights are selected for the calculation and profile fitting. In agreement with Davenport's classification (Wieringa, Jon, 1992), the aerodynamic roughness length takes the following values: i) for grassland with low mature crops, a value of the roughness length $z_o = 0.07$ can be adopted, which corresponds to the selected study area in the province of Cadiz, and ii) for high mature crops or discontinuous bushland, a value of $z_o = 0.1$ can be adopted, corresponding to the study area in the province of Almería.

Figures 4.20 and 4.19 show the theoretical and measured profiles for incident mean velocity and turbulence intensity over a hilly surface, and a smooth surface. The velocity is represented dimensionless, using the reference velocity (U_o), measured at the height of the wind turbine tower (z_h), and the axes are dimensioned with the rotor diameter D. Although the fit is not as good in the upper part of the graph, the characterization is valid since it satisfies the objective of the work, which is focused on the study around the wind turbine and the area near the surface.

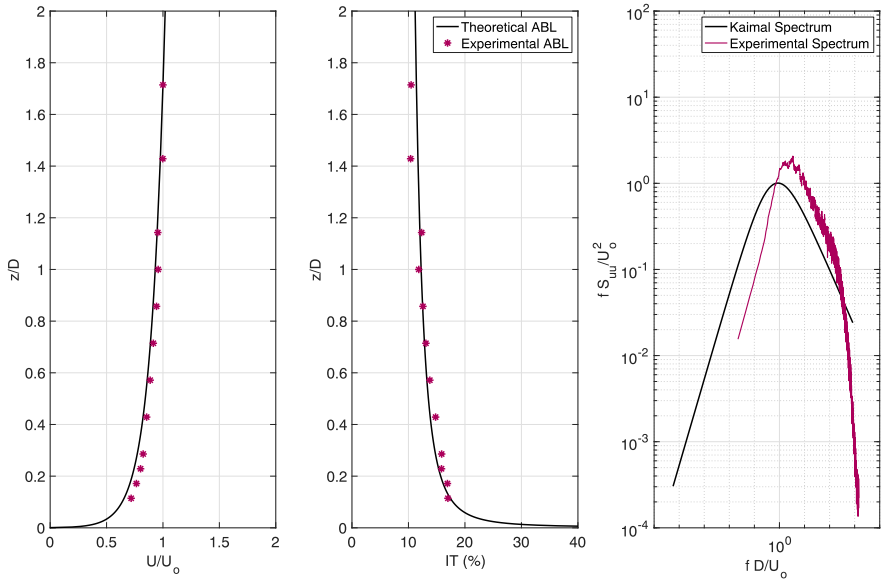

Figure 4.19: Vertical profile of mean wind speed, vertical profile of turbulence intensity, and Kaimal spectrum, respectively, for the simulated ABL in the case study of the province of Cádiz.

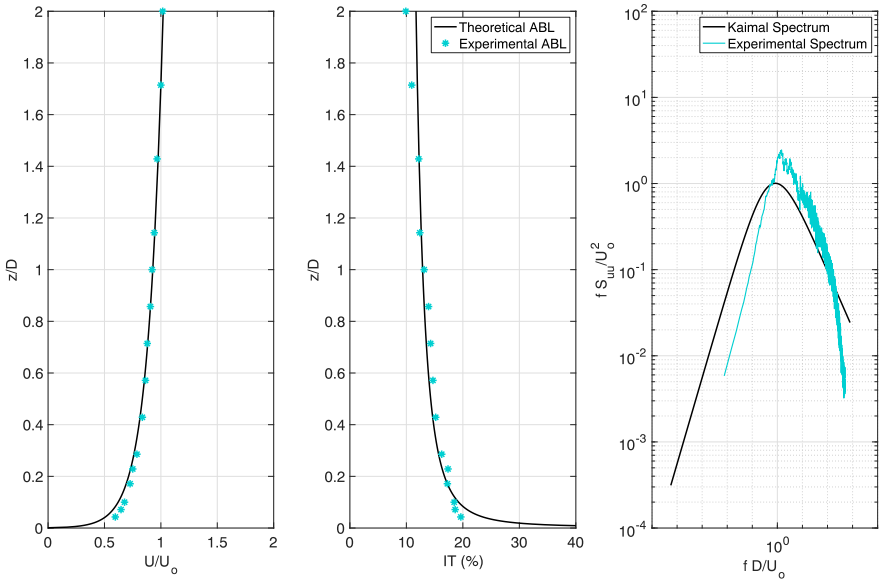

Figure 4.20: Vertical profile of mean wind speed, vertical profile of turbulence intensity, and Kaimal spectrum, respectively, for the simulated ABL in the case study of the province of Almería.

4.5.2 Hill over scrubland. Configuration 1.

In this section, measurements were taken behind a hill located on scrubland (Configuration C1). Figures 4.21 and 4.22 show central measurements in Section C behind the hill (Figure 4.11 ($y = 0$)). In Figure 4.21, the ABL inflow is represented by a continuous line with black triangles. These will be used for later comparison with the results obtained by integrating a wind turbine on top of it. Profile 1 has been measured over the hill, so the lowest point of measurement is $z/D = 0.28$. The greatest speed deceleration occurs at approximately $z/D = 0.4$, generating an inflection point, coinciding with the total height of the hill, from which the profiles increase in velocity. A greater asymmetry is observed in profiles closer to the model, recovering the inflow profile as we move away streamwise. Regarding turbulence, values are more homogeneous, and profiles are similar to each other from a height of $z/D = 0.6$, concentrating the highest level of turbulence below $z/D = 0.3$.

It can be seen how P1 and P2, closer to the hill, show higher disturbances, mainly up to a height $z/D = 0.4$. Under a height $z/D = 0.4$, the turbulence intensity is about 5% higher and the velocity $U/U_o = 0.2$, i.e., 20% lower when integrating the turbine over the hill.

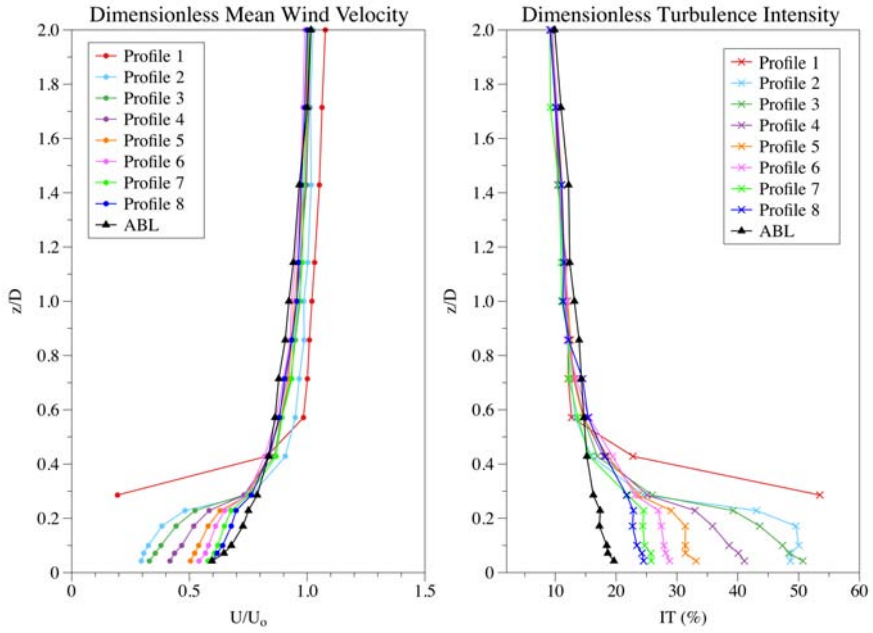

Figure 4.21: Vertical profiles of dimensionless velocity and turbulence intensity variables measured streamwise the hill.

In Figure 4.22, two x-axes are shown; the first one shows the distance non-

dimensionalized with the diameter of the rotor (D), considering as reference point (0,0) the position where the wind turbine will be located. The second axis shows the non-dimensionalized distances with the height of the hill h_1, considering the bottom of the hill as a reference point (0,0).

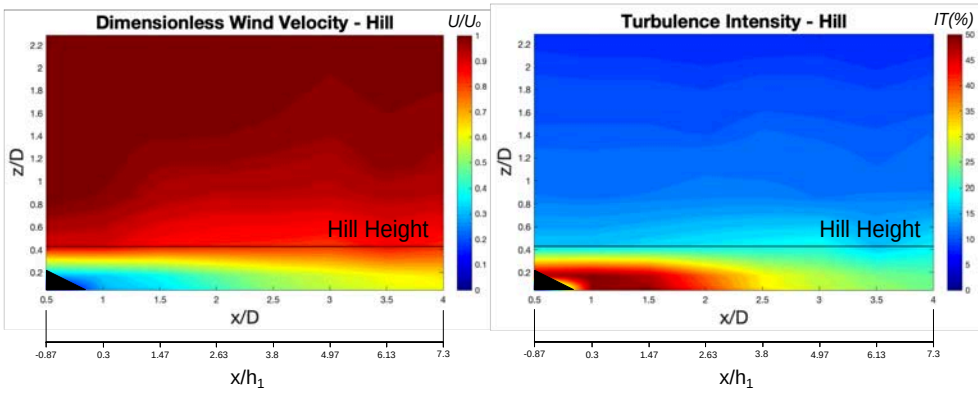

Figure 4.22: Dimensionless Wind velocity and Turbulence Intensity for Section C (Figure 4.11) from experimental measurements is shown. The black triangle shows the area where the hill is located, where there is no data, from which the measurements have been taken.

According to the results shown in this figure, from a distance of approximately $x/D = 3$, the influence of the hill starts to decrease, and the inflow is recovered. At profile P8 position($x/D = 4$), the shape of the inflow velocity profile has almost been recovered; however, there is a 10% difference in turbulence intensity with respect to the inflow values. Nevertheless, taking the hill's height as a reference, at a distance $x/h_1 = 7.3$ from the hill, alterations on wind flow are still noticeable.

4.5.3 Hill over flat grassland. Configuration 2.

In this section, measurements were taken behind a hill located on grassland (Configuration C2). The hill used in this tested configuration has a different shape than the one used in the tests described above. Its height is higher and shows different silhouettes and widths (Tabla 4.1). The measurements have been performed with the PIV system, as described in Section 4.4.3, so the measurement area is restricted to the upwind and downwind areas next to the wind turbine model. Both sections are located downwind the hill.

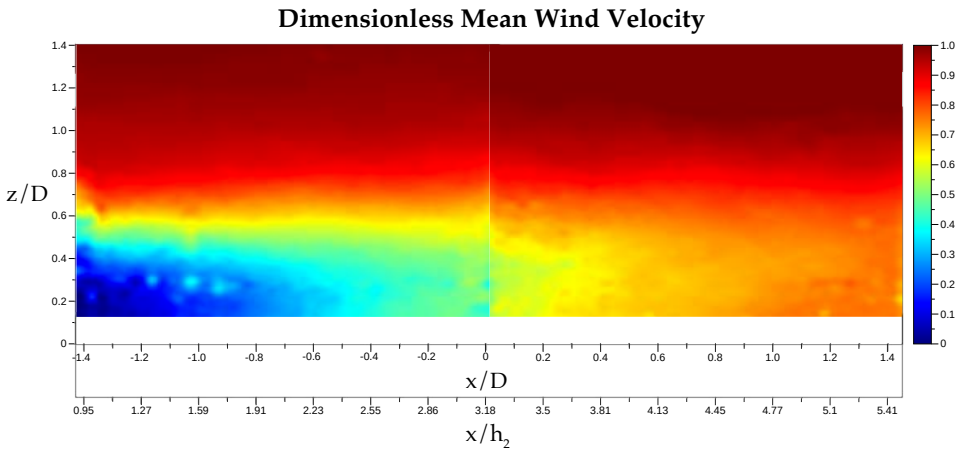

Figure 4.23: Dimensionless mean wind velocity upwind and downwind a wind turbine, located over flat grassland and behind a hill.

Figure 4.23 shows a flow behavior similar to the one obtained for a hill over scrubland (Figure 4.22). In this case, the influence of the topographic element is noticeable at a higher height because the hill height (h_2) is greater than the first hill analyzed (h_1). In this figure, two x-axes are shown. The first one shows the distance non-dimensionalized with the diameter of the rotor (D), considering as reference point $(0,0)$ the position where the wind turbine studied in Section 4.5.4 will be located. On the other hand, the second axis shows the non-dimensionalized distances with the hill height (h_2), considering the bottom of the hill as the reference point $(0,0)$. As expected, at a distance $x/h_2 = 5.41$ (Figure 4.23), the influence of the hill on the wind flow is still noticeable.

4.5.4 Wind turbine over flat grassland. Configuration 3.

In this particular case, we analyze in detail the alterations on the airflow exerted by the wind turbine itself since the simulated terrain is flat and there are no other topographic elements that could overlap its influence (Configuration C3). In Figure 4.24, the input ABL profile is represented by a continuous line marked with black triangles, so it can be seen how the first measured profiles, close to the wind turbine, are more disturbed concerning the inflow. The velocity and turbulence profiles are modified up to a height of $z/D = 1$, after which they begin to stabilize. The flow becomes more homogeneous as we move away from the wind turbine, especially in turbulence, which recovers its initial shape more quickly.

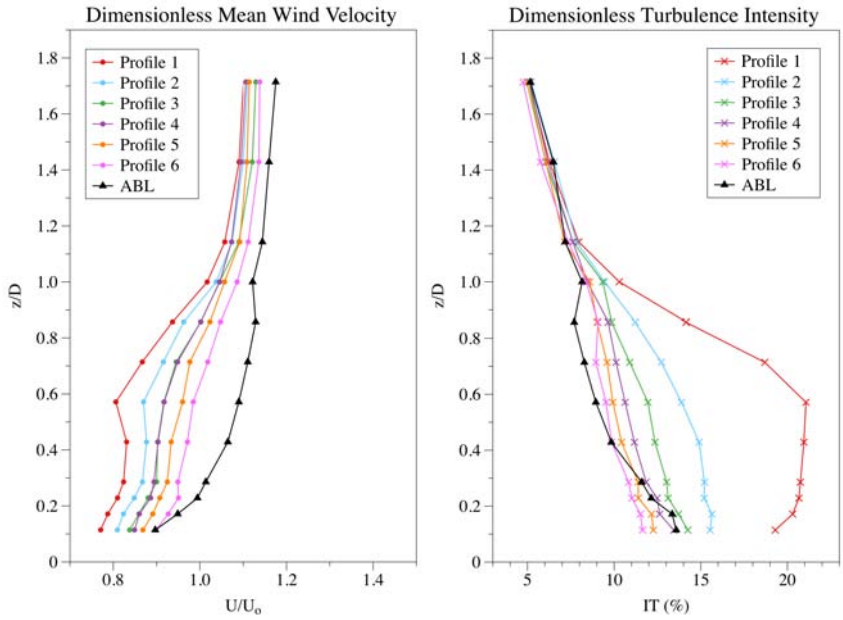

Figure 4.24: Vertical profiles of velocity and turbulence intensity measured streamwise the wind turbine located behind a hill over flat grassland.

Figure 4.25 has been obtained using PIV measurements, so the upwind and downwind data are shown. The left part of the plot $(-1.4 \leq x/D \leq 0)$ corresponds to measurements taken without a wind turbine, representing only the dimensionless mean velocity field of the simulated ABL. The right part of the graph $(0 \leq x/D \leq 1.4)$ shows the measurements taken streamwise the wind turbine, which allows the direct comparison with the inflow profiles. Just next to the turbine, at a distance of $0 \leq x/D \leq 0.3$, a significant velocity decreases, reaching values close to 0, due to the wind turbine tower reaching the rotor height in the area below $z/D = 1.1$. This figure shows values closer to the turbine than the other graphs shown in this work, which allows us to see the behavior of the flow just behind the wind turbine tower.

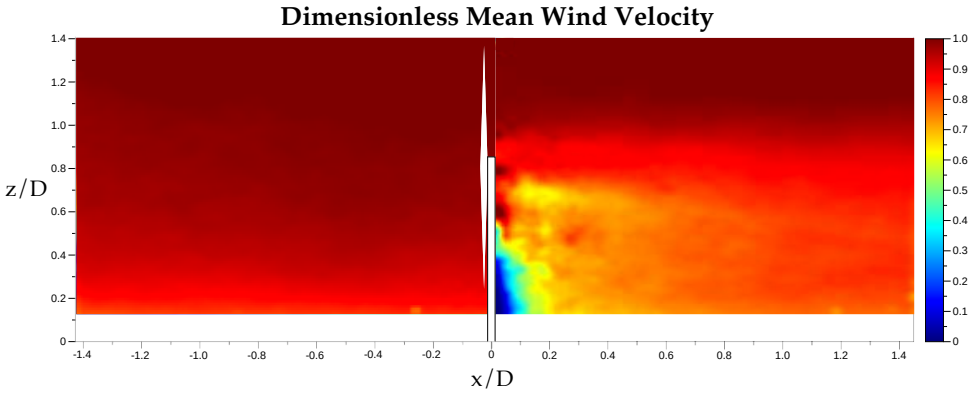

Figure 4.25: Dimensionless mean wind velocity upwind and downwind a wind turbine, located over flat grassland, from PIV measurements.

Figure 4.26 and the following have been obtained from data taken with cross hot wire anemometry, which data have been taken in other crosswise and streamwise sections. At rotor height, the dimensionless wind speed exhibits values $U/U_o = 0.83$ at the near wake. While at the wind turbine total height (height up to the blades), $z/D = 1.35$, the dimensionless wind speed reaches values of approximately $U/U_o = 0.93$ (Figure 4.26, dashed lines). In terms of turbulence, close to the wind turbine and at rotor height ($z/D = 0.85$), the IT reaches values of 18%, decreasing to 12% for the total height of the wind turbine.

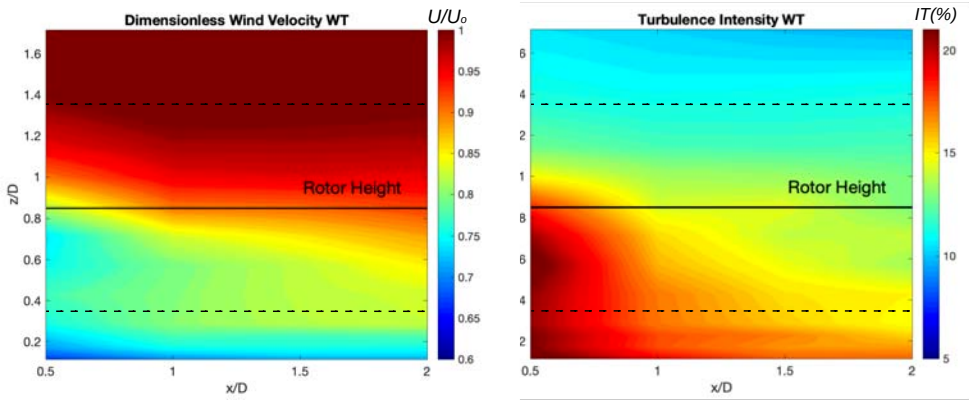

Figure 4.26: Dimensionless Wind velocity and Turbulence Intensity for Section C, using hot wire anemometry. The dashed line shows the height to which the wind turbine blades reach.

Although Figures 4.25 and 4.26 represent the dimensionless wind speed behind the wind turbine, the results may be different. These differences are because the measurement positions and color scales are not the same. On the one hand, the color scale in Figure 4.25 shows a dark blue color for values of $U/U_o = 0$, and deep red for $U/U_o = 1$; however, Figure 4.26 shows a dark blue color for $U/U_o = 0.6$ and deep red for $U/U_o = 1$.

To facilitate the comparison, four cross-sections are presented in the following Figures 4.27, 4.28 and 4.29. The evolution of the dimensionless mean wind velocity (U), Turbulence Intensity (IT), and the Reynolds stress ($\overline{u'w'}$) are shown as the distance from the model increases. For the mean wind speed, turbulence intensity, and Reynolds stress, the flow tends to stabilize towards the inflow conditions.

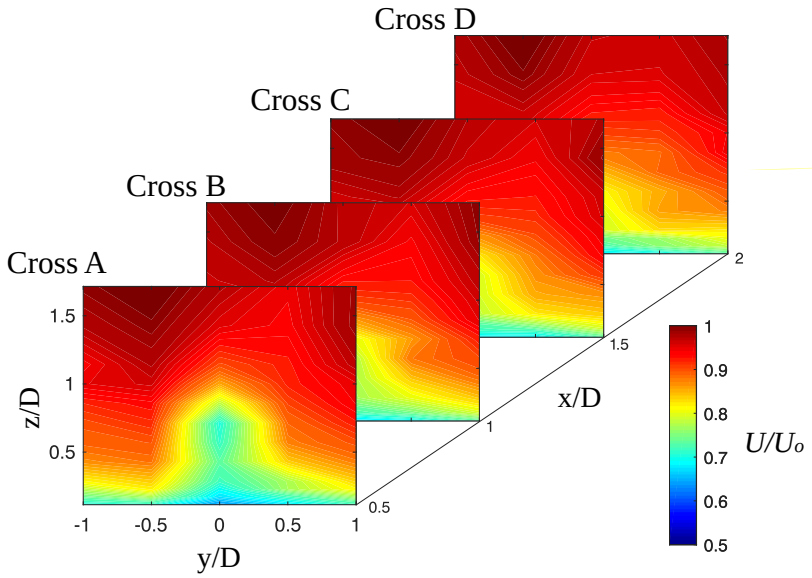

Figure 4.27: Dimensionless wind velocity for each cross section.

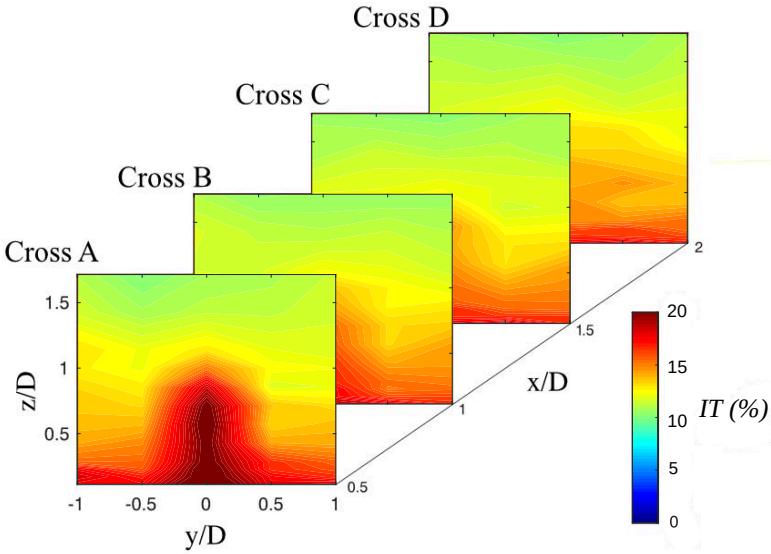

Figure 4.28: Dimensionless Turbulence Intensity for each cross section.

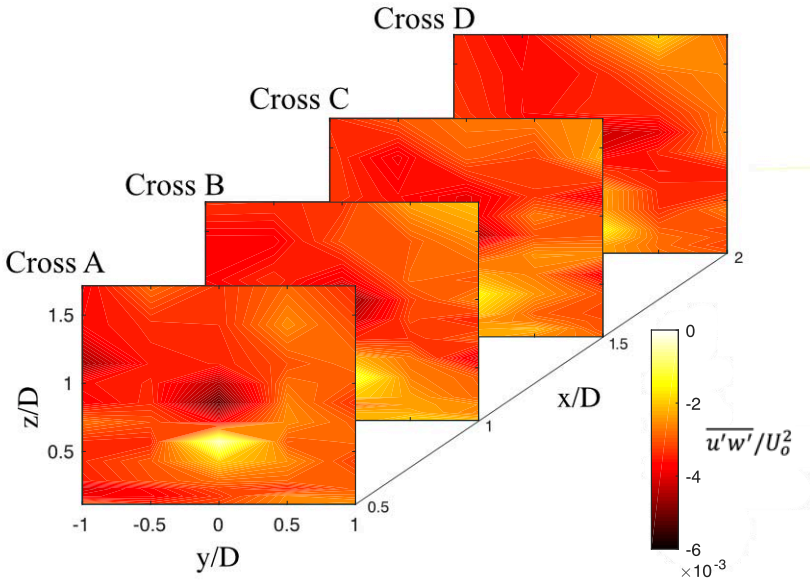

Figure 4.29: Reynolds stresses calculated for each cross section.

The Reynold stress behind the turbine is low in this case since the roughness of the inlet boundary layer is smaller, and the turbulent wake extension is also reduced,

which is consistent with the results obtained in the work of Barlas et al. (2016).

Figure 4.30 shows the energy distribution in the frequency domain, in terms of the power spectrum, for the P1 (a) and P4 (b) profiles in Section C, at rotor height $z/D = 0.86$. The spectral density decreases as we move away from the wind turbine, decreasing in the high-frequency region, as shown in both plots (a) and (b).

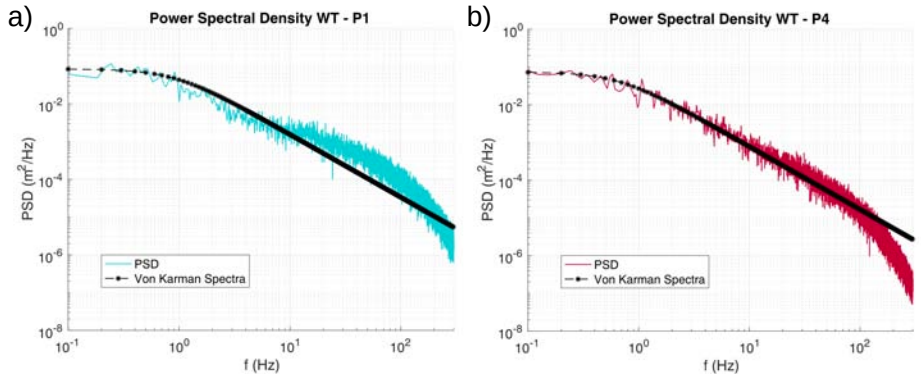

Figure 4.30: Power Spectral Density and Von Karman at rotor height for Profiles 1-4.

4.5.5 Wind turbine behind a hill over flat grassland. Configuration 4.

In configuration C4, the incident wind profile upwind the wind turbine shows lower values than in the previous case (C3), so the wind potential to be extracted will be smaller than the estimated in that area without obstacle presence, considering only roughness and wind potential characteristics. Figure 4.31 has been obtained from PIV data, consequently, results are directly comparable with Figures 4.23 and 4.25.

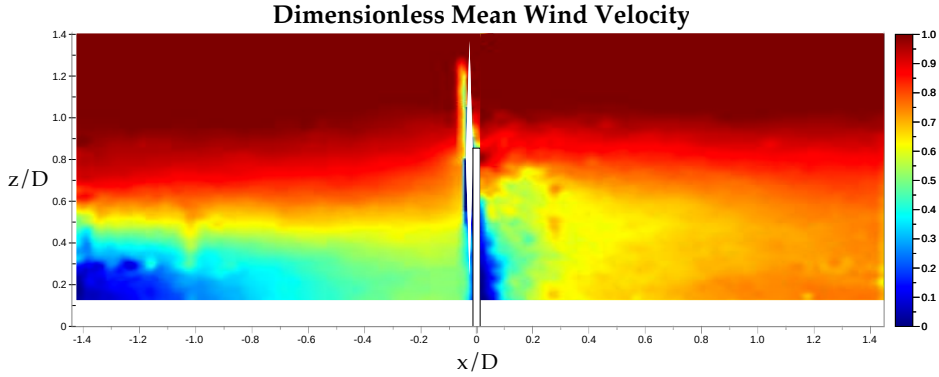

Figure 4.31: Dimensionless mean wind velocity upwind and downwind a wind turbine, located over flat grassland and behind a hill (C4).

The influence of the wind turbine itself overlaps with the influence of the hill. This results in a velocity decreasing, which still noticeable at a distance $x/D = 1.4$, which compared to Figure 4.25, would limit the spatial layout configuration of other wind turbines around it to avoid overlap between turbulent wakes, as shown in the study of Porté-Agel et al., 2020. From $z/D = 1.1$ in height, the velocity has reached stabilization again, with values equal or very close to the inflow in the input ABL.

4.5.6 Wind turbine on top of a hill over scrubland. Configuration 5.

Finally, for this configuration, measurements have been taken across five sections (Figure 4.11). Figures 4.32 and 4.33, correspond to Section C ($y = 0$), next to the wind turbine, since the changes due to turbine presence and blades movement are more significant at that location. In Figure 4.32, the ABL is represented by a continuous line marked with black triangles, so it can be seen how the first measured profiles, closer to the position of the hill and the wind turbine, are more disturbed with respect to the initial one. In the near wake, modifications produced by the wind turbine are added to those generated by the topography, in this case, the Hill1. Mainly, alterations due to wind turbine functioning are more noticeable at the height of $0.6 \leq z/D \leq 1.4$.

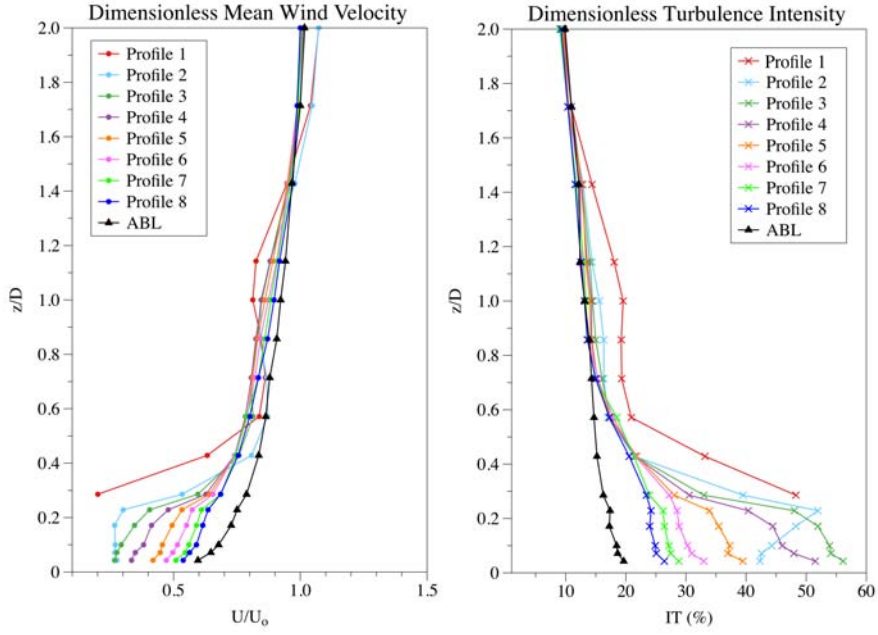

Figure 4.32: Vertical profiles of velocity and turbulence intensity measured streamwise the hill and the wind turbine.

At rotor height, the dimensionless wind speed exhibits values $U/U_o = 0.85$, while at the total height of the wind turbine (height up to the blades), $z/D = 1.78$, the dimensionless wind speed reaches values of approximately $U/U_o = 0.95$. Regarding the percentages of turbulence intensity variation, at rotor height, this variable suffers an increase of 18.34%, decreasing to 12% for the total height of the wind turbine. This value is coherent; it is expected that the highest turbulence is produced at this point, decreasing as we move in height positively or negatively. These values are not fully recovered until a height of $z/D = 1.8$ for mean velocity and $z/D = 2.2$ for turbulence intensity.

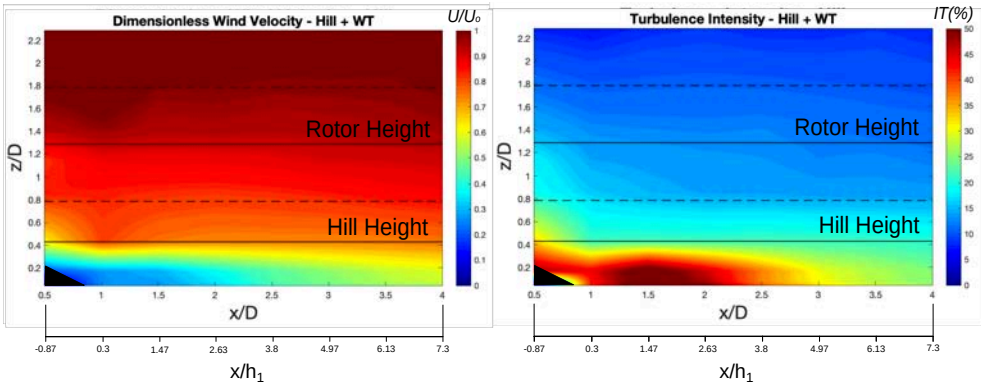

Figure 4.33: Dimensionless wind velocity and turbulence intensity for Section C. The dashed line shows the height to which the wind turbine blades reach. The black triangle shows the area where the hill is located, where there is no data, from which the measurements have been taken.

For all Figures 4.34, 4.35 and 4.36, for Cross A Section, the measurements have been taken just above the hill, so the lowest measurement in height at point $z/D = 0.28$. For this reason, the area below this position is shown in white color.

Figures 4.34, 4.35 and 4.36 show the streamwise flow evolution up to a distance of $x/D = 4$ for eight cross-sections of the dimensionless mean wind velocity (U/U_o), Turbulence Intensity (IT) and the Reynolds stress ($\overline{u'w'}/U_o^2$) at distances $x/D = 0.5, 1, 1.5, 2, 2.5, 3, 3.5, 4$, streamwise the model. For the three variables, the tendency to flow stabilization towards initial conditions can be observed. The largest effects are produced up to a distance of approximately $x/D = 3$, in particular for variables U and IT; increasing this distance up to x/D=4, for the Reynolds Stress $\overline{u'w'}$. In this study, total flow recovery is not reached because the far wake extends to a greater distance according to the work of Porté-Agel et al. (2020).

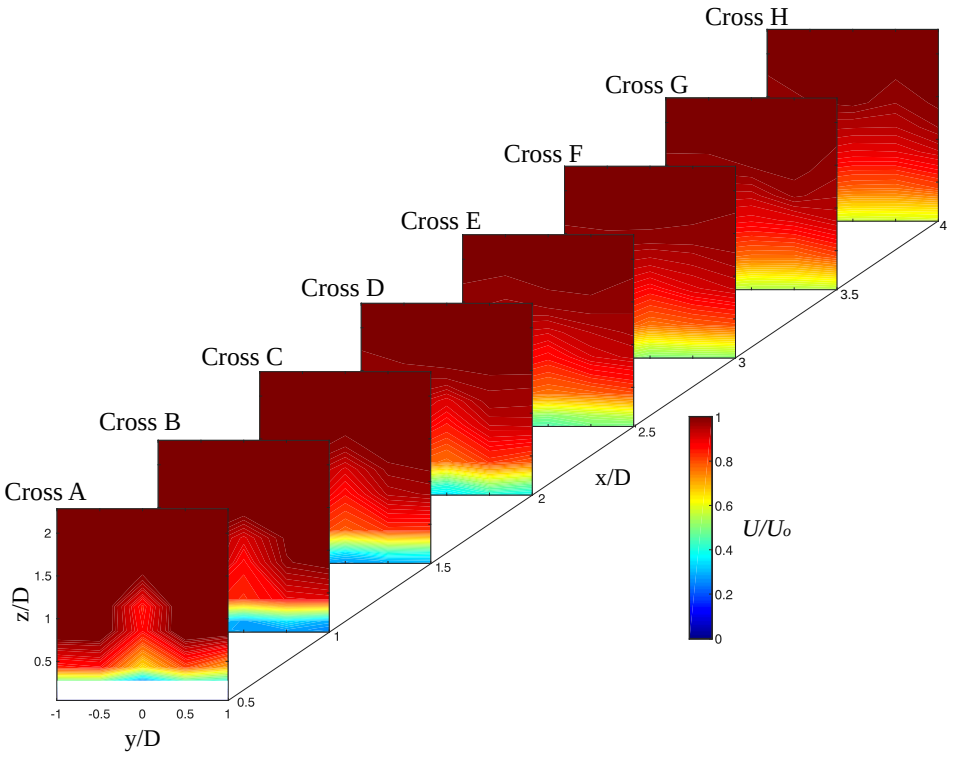

Figure 4.34: Dimensionless wind velocity for each crosswise section.

The wake is observed to grow laterally and vertically as it moves streamwise, and the value of the velocity component downstream increases with respect to Cross A (Figure 4.34). The most significant influence on the entire section is observed below a height of $z/D \leq 0.5$, and more concentrated between $-0.5 \leq y/D \leq 0.5$.

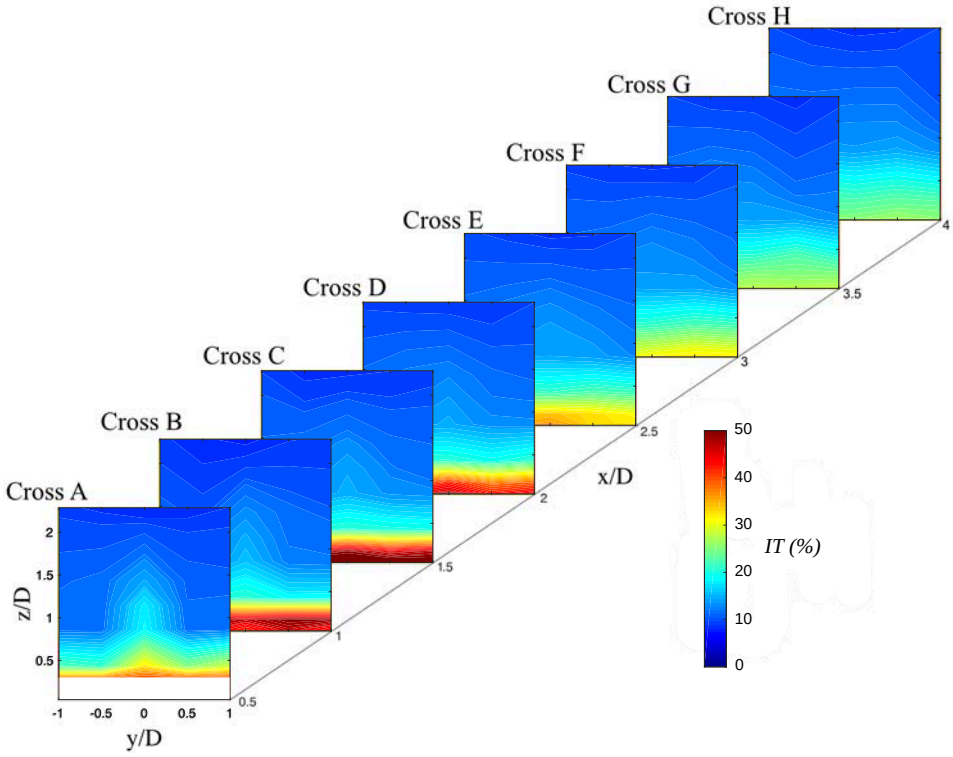

Figure 4.35: Dimensionless Turbulence Intensity for each crosswise section.

Figure 4.35 shows that the turbulence intensity not only increases but also is concentrated in the near wake for Cross A and Cross B, and this effect expands in all directions as we move downwind. The turbulence decreases in the upper part of the section; however, it remains high below a height of z/D=1, with values between $30\% \leq IT \leq 50\%$ in Cross B, C, and D, decreasing to values of $20\% \leq IT \leq 30\%$.

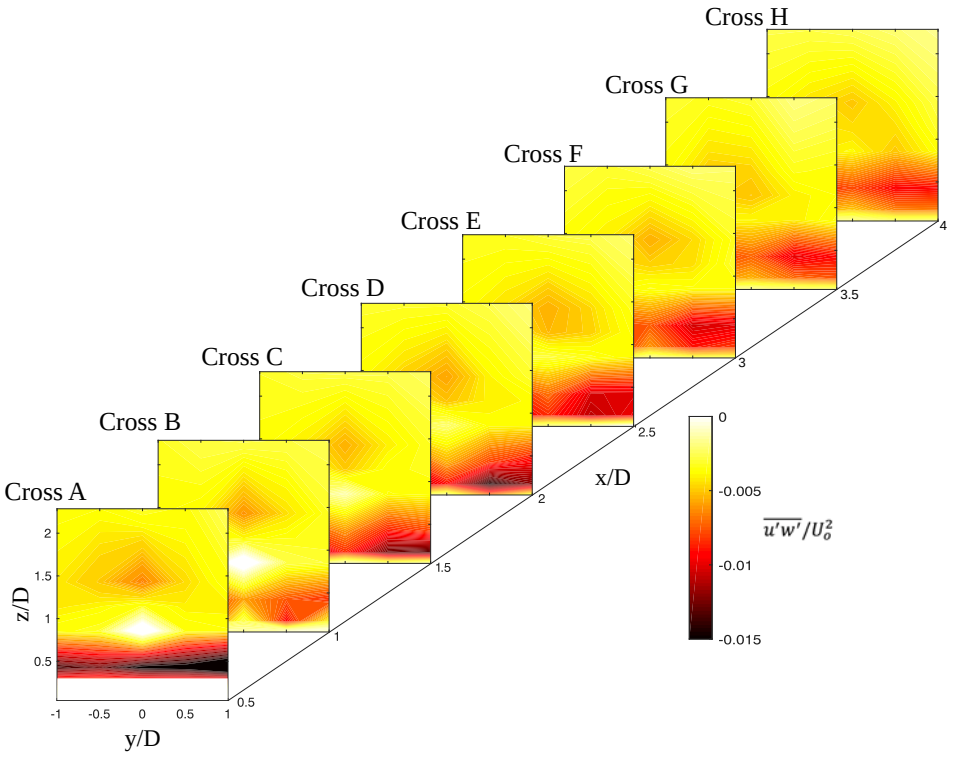

Figure 4.36: Reynolds stress calculated for each cross section.

Spatial distribution on the turbulent momentum flux, or Reynolds stress, (Figure 4.36), non-dimensionalized with respect to the reference velocity, shows the airflow entrainment from the outer to the central wake area. There is an evolution of the shear stress within the whole area, whose effect is noticeable, presenting values between $-0.01 \leq \overline{u'w'}/U_o^2 \leq -0.005$ below a height of $z/D = 0.8$. Except in the section at x/D=1, where reverse flow and vorticity are foreseeable.

The energy distribution in the frequency domain, in terms of the power spectrum, is shown in Figure 4.37 for the P1 (a) and P4 (b) profiles in Section C, at rotor height $z/D = 1.3$. As well as the classical Von Karman spectrum obtained for each configuration, the spectral density decreases as we move away from the wind turbine, decreasing in the high-frequency region, as can be seen by comparing both plots (a) and (b). Comparing the results of PSD behind a wind turbine, with and without hill (Figure 4.30), values are higher in the presence of hill (C5), especially for the high-frequencies domain.

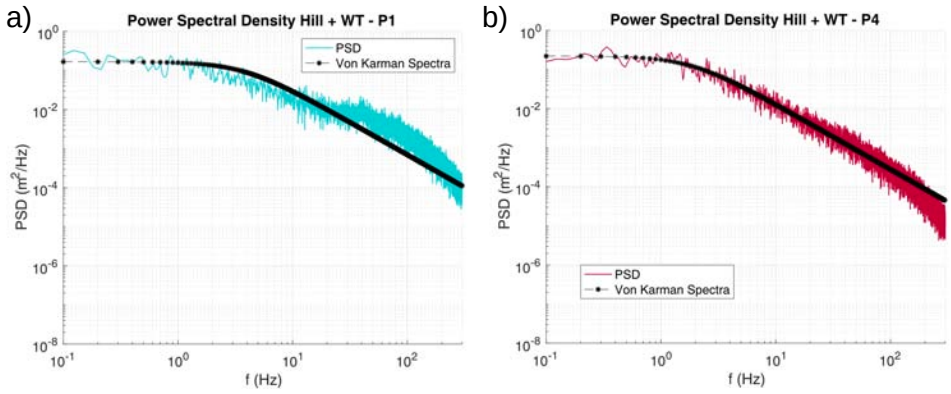

Figure 4.37: Power Spectral Density and Von Karman at rotor height for Profiles 1-4.

4.5.7 Comparison between scenarios

A direct comparison of the mean velocity and turbulence intensity in the wind field behind the analyzed configurations is performed. For this comparison, specific coordinates are selected for each case, as shown in the Figure 4.38 and in the Tables 4.2, 4.5.7, 4.4 and 4.5.

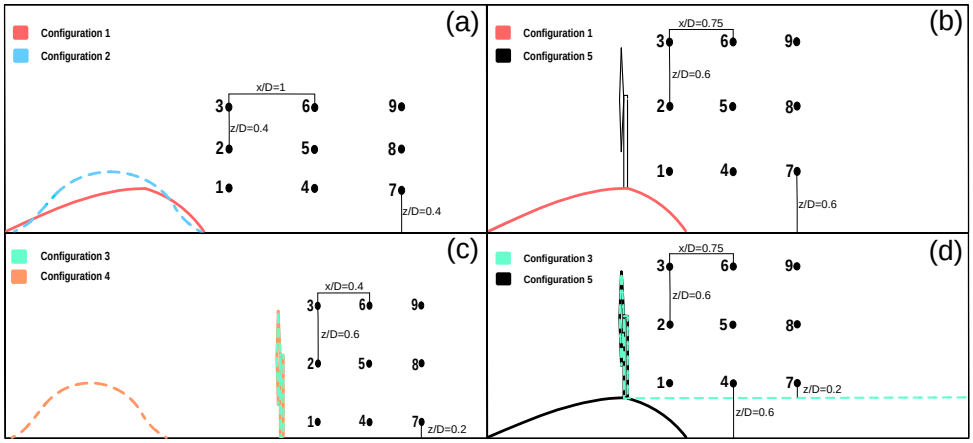

Figure 4.38: Spatial coordinates of the points selected for comparison between configurations being: (a) comparison between configuration 1 and 2, (b) comparison between configuration 1 and 5, (c) comparison between figure 3 and 4, and (d) comparison between figure 3 and 5.

Corresponding spatial points have been selected to make the comparison as accurate as possible. The coordinates have different values in some cases, as the measurement area differs in the respective configurations. The ratios included in each of the tables have been calculated such that:

$$R_{U_1} = \frac{U_{C1}}{U_{C2}}, \quad R_{U_2} = \frac{U_{C1}}{U_{C5}}, \quad R_{U_3} = \frac{U_{C3}}{U_{C4}}, \quad R_{U_4} = \frac{U_{C3}}{U_{C5}} \tag{4.15}$$

$$R_{IT_1} = \frac{IT_{C1}}{IT_{C2}}, \quad R_{IT_2} = \frac{IT_{C1}}{IT_{C5}}, \quad R_{IT_3} = \frac{IT_{C3}}{IT_{C4}}, \quad R_{IT_4} = \frac{IT_{C3}}{IT_{C5}} \tag{4.16}$$

where indices a, b, c and d refer to the four comparisons made between the different configurations.

Comparison A: Configuration 1 vs. Configuration 2

In this section, a direct comparison of the flow behavior around two types of hills with different shapes and heights is made, corresponding to configurations 1 and 2, whose points of comparison are shown in Figure 4.38(a).

In general, the velocity is higher for Configuration C1, a more heterogeneous hill, with a greater length, lower height, and gentler slope. However, more significant turbulence is observed in the C2 case, except for some points in the mid-far wake, at the height of $z/D = 1.2$. Some of the variations between the two configurations may be due in part to the type of instrumentation used, as detailed in Chapter 2 and Jiménez-Portaz et al. (2020b). Attending to Figure 4.23, it shows a flow behavior similar to the one obtained for a hill over scrubland (Figure 4.22). In this case, the influence of the topographic element is noticeable at a higher height because the hill height (h_2) is greater than the first hill analyzed (h_1).

As expected, at a distance $x/h_2 = 5.41$ (Figure 4.23), the influence of the hill on the wind flow is still noticeable. For an equivalent position, taking into account the distance with respect to the height of each hill, in the C1 configuration, the average velocity is 10% smaller than in the C2 configuration, i.e., the disturbance generated by the obstacle on the atmosphere is more significant (Figure 4.22). These results coincide with the work of Kamada et al. (2019) and Frenkiel (1962), proving that not only the height of the hill alters the airflow but also the shape and length of the obstacle.

			U/U_o		$IT(\%)$		Rates	
Point	x/D	z/D	C1	C2	C1	C2	R_{U_1}	R_{IT_1}
1	1	0.4	0.78	0.61	23.45	37	1.3	0.63
2	1	0.8	0.98	0.98	12.50	18	1	0.69
3	1	1.2	1.00	1.04	11.20	11.7	0.96	0.96
4	2	0.4	0.79	0.69	20.84	21	1.1	0.99
5	2	0.8	0.93	0.86	13.16	21	1.08	0.63
6	2	1.2	0.98	1.01	11.42	9	0.97	1.27
7	3	0.4	0.77	0.59	20.62	23	1.35	0.9
8	3	0.8	0.92	0.83	13	21	1.11	0.62
9	3	1.2	0.97	0.99	11.36	10	0.98	1.14
Mean value			0.9	0.84	15.28	19.08	1.09	0.87

Table 4.2: Comparison between Configuration 1 and 2

Comparison B: Configuration 1 vs. Configuration 5

In this case, the influence of the wind turbine located on top of a hill is analyzed, comparing with the measurements taken only with the hill, corresponding to configurations 1 and 5, whose points of comparison are shown in Figure 4.38(b). A higher value of velocity and lower turbulence intensity is observed in Configuration C1, which shows the influence of the wind turbine, especially in the area of influence of the wind turbine tower, coinciding with points 1, 4, and 7 in Figure 4.38(b). The values become similar in both configurations as we move away from the obstacles.

			U/U_o		$IT(\%)$		Rates	
Point	x/D	z/D	C1	C5	C1	C5	R_{U_2}	R_{IT_2}
1	0.5	0.6	0.95	0.73	14.4	28.5	1.3	0.5
2	0.5	1.2	1.03	0.86	11.26	17.6	1.05	0.64
3	0.5	1.8	1.02	1	9.8	12	1.02	0.82
4	1.25	0.6	0.92	0.8	14.57	19.9	1.15	0.73
5	1.25	1.2	0.99	0.9	11.25	14	1.1	0.8
6	1.25	1.8	1.01	0.99	9.7	11.4	1.02	0.85
7	2	0.6	0.88	0.77	15.33	19.12	1.14	0.8
8	2	1.2	0.98	0.89	11.4	13.3	1.1	0.86
9	2	1.8	1.01	0.98	9.5	11.2	1.03	0.85
Mean value			0.98	0.88	11.9	16.34	1.1	0.76

Table 4.3: Comparison between Configuration 1 and 5

To complete the spatial variation analysis of the airflow, four top-view sections (yx) are plotted at different heights: level 1 at $z/D = 0.1$, level 2 at $z/D = 0.43$,

level 3 at $z/D = 1.43$ and level 4 at $z/D = 2.3$. For each level, the comparison between the flow in the presence of the turbine and the flow with hill only is shown.

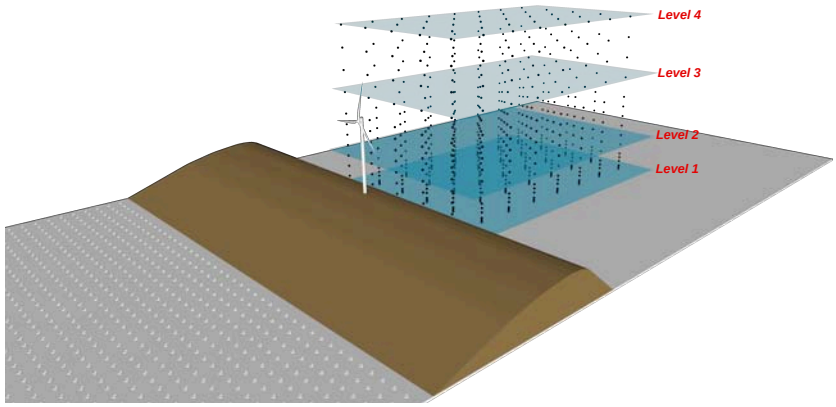

Figure 4.39: Height levels to compare results from measurements with and without wind turbine. Where levels height are: level 1 at $z/D = 0.1$, level 2 at $z/D = 0.43$, level 3 at $z/D = 1.43$ and level 4 at $z/D = 2.3$.

Figure 4.39 shows in blue color the four levels at which the variables of interest have been analyzed, the results of which are shown in Figures 4.40 and 4.41. At levels 1 and 2 (Figure 4.40), the wind velocity decreasing is higher in the case of the configuration with the presence of a turbine. With a velocity reduction of about 6% in such a case, compared to the wind field behind a single hill. At the level 3, the difference between the two configurations is even greater, mainly in the areas between $0.25 \leq y/D \leq 1$ and $-1 \leq y/D \leq -0.25$. Where the velocity reduction is around 9% higher in the case with a wind turbine. This behavior is to be expected, taking into account that this is the greatest influence of the rotating blades. For sufficiently high height, as shown in level 4, differences between both configurations (C1 and C5) are negligible, reaching equilibrium and recovering the shape of the ABL input.

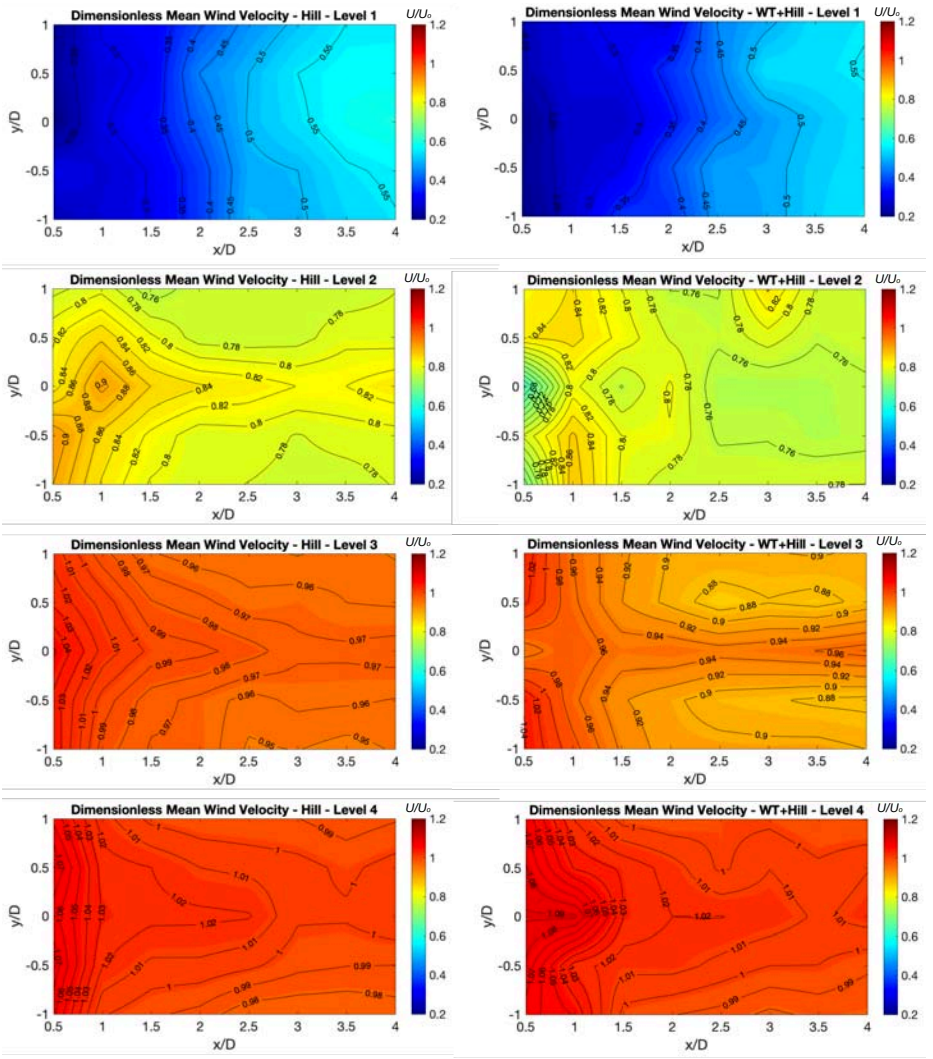

Figure 4.40: Four comparison sections of dimensionless mean velocity for the case of topography with hill (left) and with wind turbine (right). The top view is shown for each of the sections.

Turbulence generated is presented in Figure 4.41. For level 1, the turbulence intensity has values of approximately 5% higher, while this difference is more negligible for levels 2 and 3, ranging between 2-3% in the far wake but about 10% higher in the near wake. As in the mean velocity, the turbulence intensity is more homogeneous at level 4, with barely appreciable differences between both configurations.

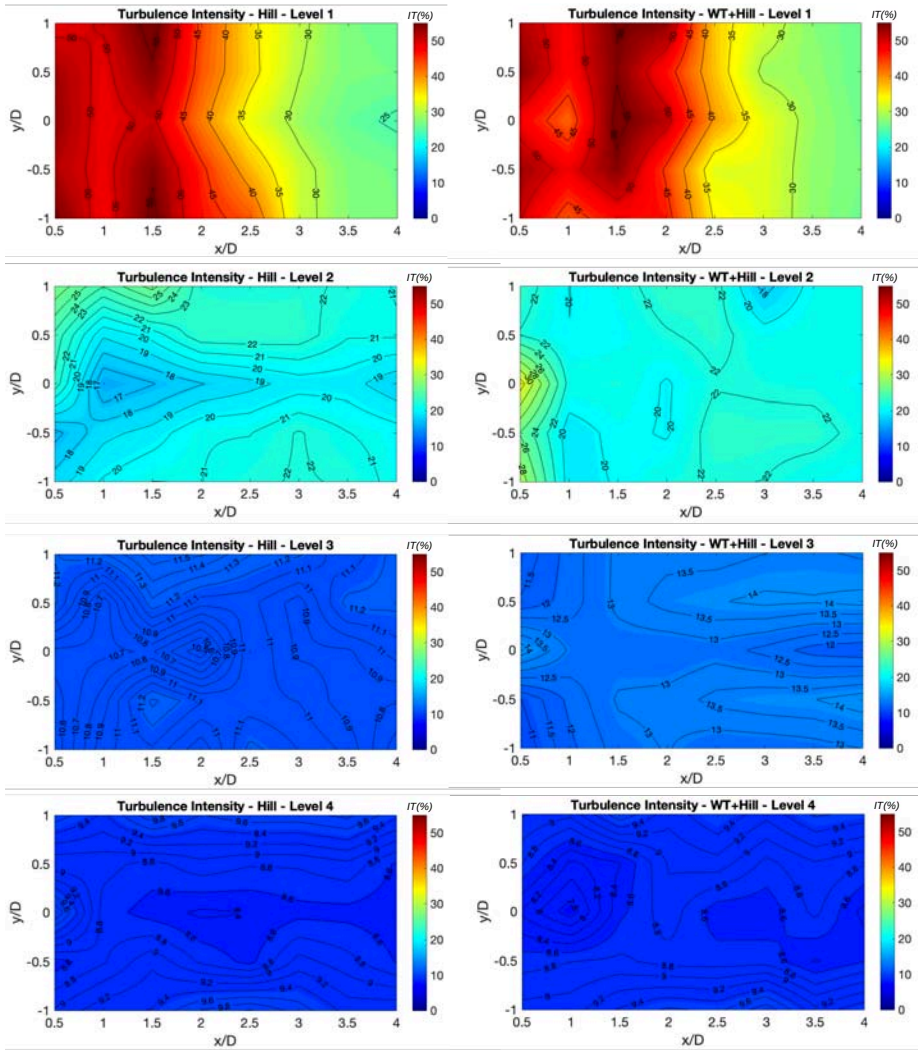

Figure 4.41: Four comparison sections of dimensionless turbulence intensity in % for the case of topography with hill (left) and with wind turbine (right). The top view is shown for each of the sections.

The differences discussed above are more readily visible in Figure 4.42, in which the variables of interest are shown for the different levels, but only the contour lines are represented, superimposing the values for each of the configurations in the same graph. The black lines correspond to the values measured with the wind turbine (C5), and the red lines (mean wind velocity) and green lines (turbulence intensity) to the values measured with only the presence of the hill (C1).

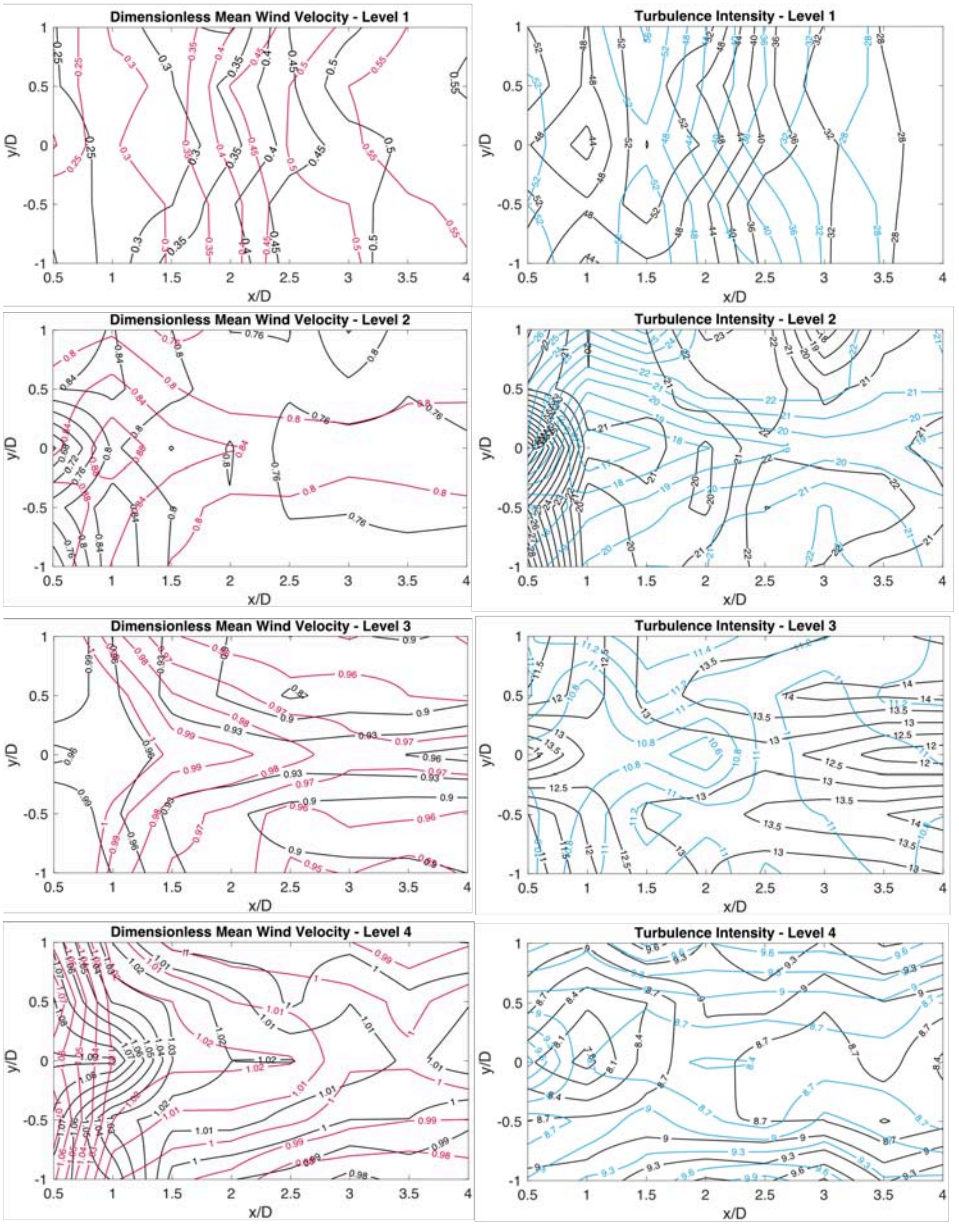

Figure 4.42: Four comparison sections of dimensionless mean wind velocity (right) and turbulence intensity in % (left) for the case of topography with hill and with wind turbine. The top view is shown for each of the sections. Black lines correspond to configuration C5 and the red lines (mean wind velocity) and blue lines (turbulence intensity) to configuration C1.

According to previous graphs, it can be proven that, despite the hill influence, the wind turbine also significantly impacts the lower layers. At a streamwise distance of $x/D = 2.5$, the hill influence decreases, being this effect more noticeable for the turbulence intensity variable. At a distance of approximately $x/D = 4$, the wind turbine influence decreases, equaling mean speed and turbulence values to those obtained only with the hill model.

Comparison C: Configuration 3 vs. Configuration 4

Finally, this section analyzes the influence of the presence of obstacles upwind a turbine and the differences in flow behavior with and without obstacles (Configurations 3 and 4), whose points of comparison are shown in Figure 4.38(c). The data compared in this section were taken with the same instrument (PIV) and in the same wind tunnel (CCWT).

The wind speed is more homogeneous in Configuration C3, and the turbulence intensity is up to 25% lower. The presence of an obstacle, such as a hill, decreases the inflow reaching the wind turbine and generates turbulent phenomena, so these inlet conditions will directly influence the wake behind the turbine. However, at points 3, 6, and 9 in Figure 4.38(c), the velocity is more homogeneous in the C4 configuration.

The alterations of the wind turbine itself overlap with the influence of the hill. This results in a velocity decreasing, which still noticeable at a distance $x/D = 1.4$, which compared to Figure 4.25, would limit the spatial layout configuration of other wind turbines around it to avoid overlap between turbulent wakes, as shown in the study of Porté-Agel et al. (2020).

			U/U_o		$IT(\%)$		Rates	
Point	x/D	z/D	C3	C4	C3	C4	R_{U_3}	R_{IT_3}
1	0.4	0.2	0.56	0.56	28	38	1	0.74
2	0.4	0.8	0.83	0.78	21	34	1.06	0.62
3	0.4	1.4	1.014	1.068	8.9	9.7	0.95	0.92
4	0.8	0.2	0.77	0.72	12	18	1.07	0.68
5	0.8	0.8	0.85	0.83	11	20	1.04	0.55
6	0.8	1.4	1.02	1.075	8.7	9.9	0.95	0.88
7	1.2	0.2	0.79	0.76	11	19	1.04	0.58
8	1.2	0.8	0.87	0.86	10	19	1.01	0.53
9	1.2	1.4	1.03	1.073	8.4	11	0.96	0.76
Mean value			0.86	0.86	13.2	19.8	1.01	0.7

Table 4.4: Comparison between Configuration 3 and 4

Comparison D: Configuration 3 vs. Configuration 5

Finally, the characteristics of the wake behind a wind turbine on flat ground are compared with the wake behind a wind turbine on top of a hill. The same wind turbine is located in two different topographies (Configuration 3 and 5), as described in the previous sections, whose points of comparison are shown in Figure 4.38(d). The data compared in this section were taken with the same instrument (HWA) and in the same wind tunnel (OCWT).

In this case, the wind speed is higher and more homogeneous in the C5 configuration; however, the turbulence intensity increases, except for some specific points within the wake (Table). It should be noted that the distance from the ground to the height of the rotor is different in both cases (the height from the ground for Configuration C3 is marked with a dashed line in the Figure), which will have a direct influence on the results since the input profile is different in each case. In the case of Configuration C3, the influence of the wind turbine tower is more noticeable than in the hillside location, whose impact is "masked" by the effect generated by the hill itself.

	C3		C5		U/U_o		$IT(\%)$		Rates	
Point	x/D	z/D	x/D	z/D	C3	C5	C3	C5	R_{U_4}	R_{IT_4}
1	0.5	0.2	0.5	0.6	0.68	0.73	20.81	28.5	0.93	0.73
2	0.5	0.8	0.5	1.2	0.75	0.86	18.93	17.6	0.87	1.08
3	0.5	1.4	0.5	1.8	0.94	1	11.35	12	0.94	0.95
4	1.25	0.2	1.25	0.6	0.72	0.8	17.22	19.9	0.9	0.87
5	1.25	0.8	1.25	1.2	0.84	0.9	14.65	14	0.93	1.05
6	1.25	1.4	1.25	1.8	0.96	0.99	11.14	11.4	0.97	0.98
7	2	0.2	2	0.6	0.73	0.77	15.28	19.12	0.95	0.8
8	2	0.8	2	1.2	0.86	0.89	13.5	13.3	0.97	1.01
9	2	1.4	2	1.8	0.95	0.98	11.21	11.2	0.97	1
Mean value					0.83	0.88	14.9	16.3	0.94	0.94

Table 4.5: Comparison between Configuration 3 and 5

4.5.8 Replication of tests in both tunnels

Figure 4.43 shows the theoretical and measured vertical profiles for mean wind speed, and turbulence intensity measured in the OCWT and CCWT for the configuration studied in Section 4.5.4. The left in Figure 4.43 shows the comparison of velocity profiles measured in both wind tunnels. Differences are almost non-exist; however, the right in Figure 4.43 shows an average increase of 2% in IT in the OCWT, conserving the vertical shape of the profile.

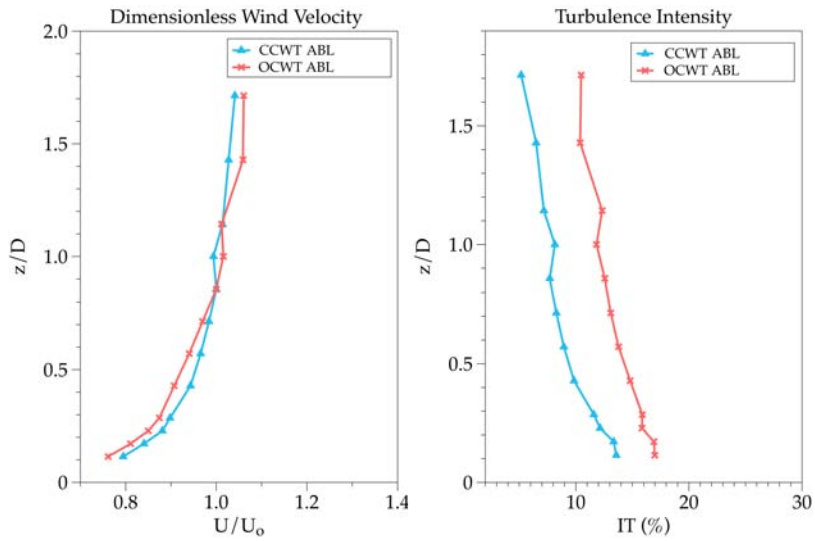

Figure 4.43: ABL simulation in both wind tunnels and comparison with the theoretical profile.

In Figure 4.44, dark colors mean a lower speed with respect to the reference value due to the presence and blades rotation of the wind turbine. The mean wind velocity is stabilized and homogenized earlier in the OCWT, both in height and downwind. While in the CCWT at a height $z/D = 1.6$, the flow has not yet wholly recovered.

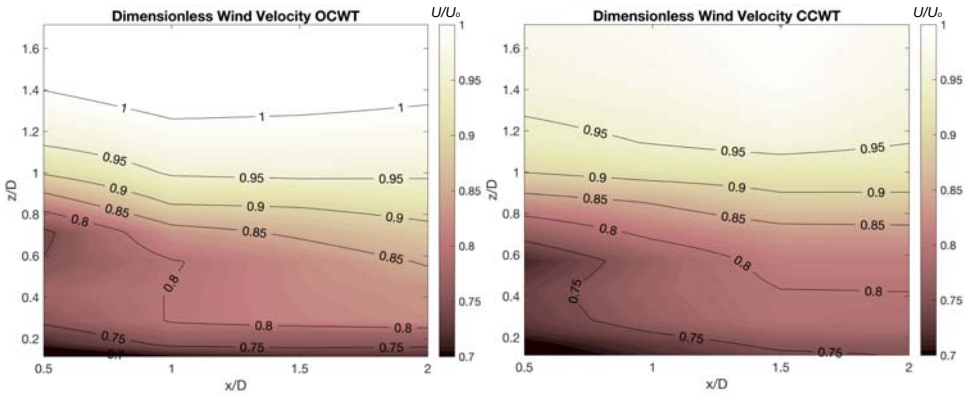

Figure 4.44: Dimensionless mean wind velocity downwind of the wind turbine in the OCWT (right) and the CCWT (left).

In Figure 4.45 the lighter colors are translated into a greater intensity of turbu-

lence. An increase in IT is noticed in the area next to the wind turbine, generated by its operation and size. For the OCWT, the IT is higher compared to the CCWT, especially as we move to leeward. According to the vertical inflow profiles, at the height of approximately $z/D = 1.3$, these differences are higher, reaching almost double in the case of the OCWT. In general, wind flow is less turbulent inside the CCWT, but the shape of the vertical profile is conserved in both tunnels. These results are in agreement with those obtained in Section 2.5.3, Chapter 2.

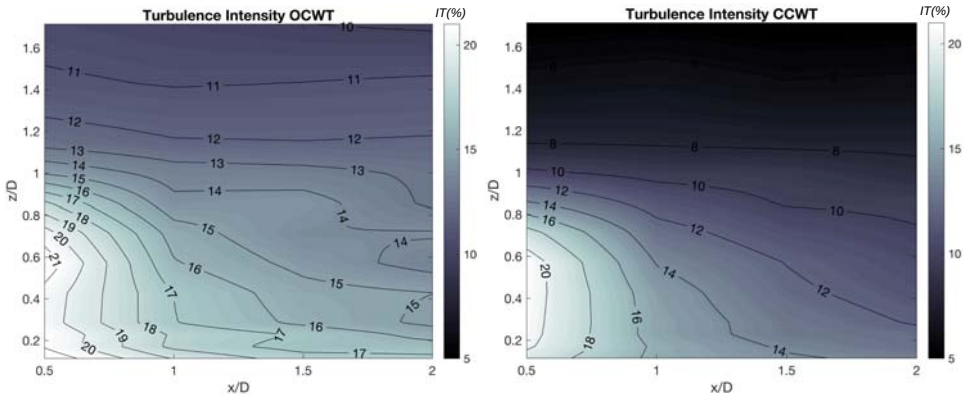

Figure 4.45: Dimensionless turbulence intensity in % downwind of the wind turbine in the OCWT (right) and the CCWT (left).

4.6 Conclusions and discussion

The results from this chapter show the influence of a wind turbine (located at the ABL under neutral atmospheric conditions) on the wind fields over hilly terrain, which are in agreement with similar research works. The Reynolds number established according to the work of Chamorro et al., 2012 is fulfilled, which guarantees that the airflow is fully turbulent and the flow around the model is mechanically similar to the prototype. These results could be extrapolated to reality, and the wake behind the wind turbine could be parameterized correctly.

In this chapter, measurements have been taken with two different types of instruments: Hot Wire Anemometry and Particle Image Velocimetry systems. With the first one, measurements have been obtained covering a large area behind the models and at different sections. On the other hand, the PIV has allowed us to obtain measurements in more detail, for a smaller area but with higher resolution and closeness to the models. As a result, the color-coding in the graphs obtained from PIV and HWA measurements is different, covering a higher range of velocities in PIV measurements. When using this instrument, the measurements have been

taken closer to the models so that the velocity reduction effects are more noticeable, and it is necessary to widen the range used for better visualization.

The results derived from the tests only in the presence of a hill demonstrate the critical role that topography has within the atmospheric boundary layer since it completely transforms the wind flow characteristics behind it, mainly in the areas close to the surface. Given the experimental results for the two types of hills studied (results of Sections 4.5.2 and 4.5.3), it is evident not only their influence on the wind field but also how the height, shape, and slope of the hill affect it, reducing the speed by 10% in the case of the hill with a longer length and gentler slope. To avoid the effect of the hill on the wind field, the distance between the hill and the wind turbine must be greater than seven times the height of the hill, depending on every case. These results are consistent with those obtained in works carried out only with a topography element (He et al., 2014), and in those that integrate a wind turbine (Medici, Davide and Alfredsson, PH, 2006).

According to the effects generated by the wind turbine, it is deduced that the turbulent wake generated presents similar characteristics with the same range of variation, even using different inflow reference velocities, with turbulence intensity values increasing by 18% at rotor height and mean wind speed decreasing by 16%. In the high-frequency domain, at rotor height, the wind turbine produces high turbulent energy, which, according to the work of Ali et al. (2019), could be modeled as an active turbulence generator, imposing new scales of energy dissipation within the turbulent wake. These spatial and temporal fluctuations must be taken into account when estimating the wind potential to be extracted at each site, as it can be overestimated because it has a direct effect on wind power extraction, and therefore, on the selection of the optimal site for each wind turbine within a wind farm (Frenkiel, 1962).

The wind field characterization performed in the presence of a wind turbine with allowed motion has a remarkable influence on the near wake. The mean velocity decrease and the increase of the turbulence intensity are more evident in the central wake area, where the wind turbine blades are in motion. It is observed that streamwise, the influence of the wind turbine slowly decreases; however it decreases faster with height. Even so, the wake stabilizes as it moves away, although to see the full effect, it would be necessary to study the full wake. The near and far wake is directly influenced by the presence of the turbine, its characteristics, and its size. However, the far wake is more influenced by the inflow, topography, and terrain characteristics.

The values of velocity and turbulent characteristics are slightly lower in flat grassland terrain without hills. This may be due not only to factors related to the interaction of the wind turbine with the environment but also to the environmental characteristics, the type of simulated boundary layer, or other external factors.

The replication of tests with the same setup and scaled models had not been done before, so that this work can serve as a reference for future tests and comparison and the study of wind farm management. Wind flow is less turbulent inside the closed-section wind tunnel, and the shape of the vertical profile is conserved in both tunnels. This difference may be due to specific characteristics of the open-section wind tunnel or the airflow recirculation around external objects. It is concluded that the facility's characteristics can affect the results; although it will not change the power estimated, it can overestimate the variables related to the turbulence intensity and the damage from wind over the wind turbine.

Part III

5. Environmental effects of wind farms

Current regulations of wind farms are focused on market interests and the design of infrastructures; however, the current Environmental Impact Studies in Andalusia lack specificity and adaptability to the type of project and its particularities. On this basis, the process of analysis and the methodology proposed should be used as a tool to develop evidence-based policies under conditions of uncertainty, including the system dynamics from an integral point of view. This chapter shows a methodological proposal of analysis based on the results of new own experimental tests, current legislation and regulations, and results from other authors. This method includes simulations of climatic spatial–temporal series and ecosystem cycles, considering the impacts during all phases of the project, based on selected indicators appropriate to Mediterranean drylands. Based on relevant bibliography, the proposed methodology highlights the importance of obtaining the project's total costs, including social and environmental costs.

5.1 Environmental Impact Study of wind farms

5.1.1 Problem statement

Andalusian and Spanish regulations and legislation are developed at different levels for the project management and evaluation of wind energy exploitations (Sequeira and Santos, 2018). Nevertheless, these regulations do not go into detail on the control of their environmental impact beyond what has been stated in the Environmental Impact Study (EIS) (Ley de 9 de julio, 7/2007; Ley de 9 de diciembre, 21/2013; Villarroya and Puig, 2010), echoed by the European Commission regarding the difficulties of monitoring the quality of impact studies (Sanz-Rubiales, 2010). These studies are carried out through an inventory of species, a description of the environment, and the use of stationary and global indicators. In addition, these studies offer lower ecological compensation that should be expected in the context of sustainability, lack of specificity and adaptability to the type of project, and the absence of obligatory procedures and applicable measures. Furthermore, in most cases, the measures to be carried out appear as proposals rather than obligatory conditions to be fulfilled and on which will depend, among others, the acceptance or rejection of the project (Villarroya and Puig, 2010).

Following previously mentioned, the objective of this section is to offer a methodological proposal for the EIS and some management recommendations applicable to onshore wind farms, based on the natural and dynamic behavior of the system. An analysis of current environmental impacts, legislation, and regulations has been carried out to develop this model through their mutual repercussion based on complementary information from experimental tests. A specific methodology is provided for each environmental component, indicators, determinants of alterations, and scales of spatial–temporal variation. The methodology and recommendations proposed to apply to wind farms located in Andalusia and other semi-arid regions and can be extrapolated to other areas.

5.1.2 Wind farms legislative framework

Intending to minimize the environmental impact of conventional energy exploitation, interest in renewable energies has increased. As a result, several environmental protection laws and plans have been adapted to promote clean energies and adapt consolidated legislation to environmental sustainability.

A fundamental part of any project is the legislation applicable to each of its phases and as a whole. This section includes some of the primary laws and regulations applicable to wind energy projects at the Regional, State, and European levels. Since their first publication, these laws have been modified but remain applicable and updated for April 2021.

International Law

- Directiva (UE) 2018/2001 del Parlamento Europeo y del Consejo, de 11 de diciembre de 2018, relativa al fomento del uso de energía procedente de fuentes renovables.
- Directiva 2014/52/UE del Parlamento Europeo y del Consejo, de 16 de abril de 2014, por la que se modifica la Directiva 2011/92/UE, relativa a la evaluación de las repercusiones de determinados proyectos públicos y privados sobre el medio ambiente.
- Europa 2050: una economía baja en carbono para 2050.
- Directiva (UE) 2015/996 de la Comisión, de 19 de mayo de 2015, por la que se establecen métodos comunes de evaluación del ruido en virtud de la Directiva 2002/49/CE del Parlamento Europeo y del Consejo.
- Directiva 92/43/CEE del Consejo, de 21 de mayo de 1992, relativa a la conservación de los hábitats naturales y de la fauna y flora silvestres.
- Directiva 2009/147/CE del Parlamento Europeo y del Consejo, de 30 de noviembre de 2009, relativa a la conservación de las aves silvestres.
- European Landscape Convention o Convenio de Florencia. Convenio Europeo del Paisaje.

National Law

- Orden IET/931/2015, de 20 de mayo, por la que se modifica la Orden ITC/1522/2007, de 24 de mayo, por la que se establece la regulación de la garantía del origen de la electricidad procedente de fuentes de energía renovables y de co-generación de alta eficiencia.
- Orden TED/314/2021, de 26 de marzo, por la que se aprueban adaptaciones de carácter técnico del documento "Planificación Energética. Plan de desarrollo de la red de transporte de energía eléctrica 2015-2020", aprobado por Acuerdo del Consejo de Ministros de 16 de octubre de 2015.
- Decreto-ley 16/2019, de 26 de noviembre, de medidas urgentes para la emergencia climática y el impulso a las energías renovables.
- Real Decreto 661/2007, de 25 de mayo, por el que se regula la actividad de producción de energía eléctrica en régimen especial.
- Ley 24/2013, de 26 de diciembre, del Sector Eléctrico.
- Real Decreto 297/2013, de 26 de abril, por el que se modifica el Decreto 584/1972, de 24 de febrero, de Servidumbres Aeronáuticas y por el que se modifica el Real Decreto 2591/1998, de 4 de diciembre, sobre la Ordenación de los Aeropuertos de Interés General y su Zona de Servicio, en ejecución de lo dispuesto por el artículo 166 de la Ley 13/1996, de 30 de diciembre, de Medidas Fiscales, Administrativas y del Orden Social.
- Ley 34/2007, de 15 de noviembre, de calidad del aire y protección de la atmósfera.

- Ley 22/2011, de 28 de julio, de residuos y suelos contaminados.
- Real Decreto 9/2005, de 14 de enero, por el que se establece la relación de actividades potencialmente contaminantes del suelo y los criterios y estándares para la declaración de suelos contaminados.
- Real Decreto 413/2014, de 6 de junio, por el que se regula la actividad de producción de energía eléctrica a partir de fuentes de energía renovables, cogeneración y residuos.
- Ley 37/2003, de 17 de noviembre, del Ruido.
- Decreto 1432/2008, de 29 de agosto, por el que se establecen medidas para la protección de la avifauna contra la colisión y electrocución en líneas eléctricas de alta tensión.
- Ley 21/2013, de 9 de diciembre, de evaluación ambiental.
- Real Decreto 183/2015, de 13 de marzo, por el que se modifica el Reglamento de desarrollo parcial de la Ley 26/2007, de 23 de octubre, de Responsabilidad Medioambiental, aprobado por el Real Decreto 2090/2008, de 22 de diciembre.
- Ley 6/2010, de 24 de marzo, de modificación del texto refundido de la Ley de Evaluación de Impacto Ambiental de proyectos, aprobado por el real Decreto Legislativo 1/2008, de 11 de enero.
- Ley 21/2015, de 20 de julio, por la que se modifica la Ley 43/2003, de 21 de noviembre, de Montes.
- Ley 10/2015, de 26 de mayo, para la salvaguardia del Patrimonio Cultural Inmaterial.
- Ley 33/2015, de 21 de septiembre, por la que se modifica la Ley 42/2007, de 13 de diciembre, del Patrimonio Natural y de la Biodiversidad.

Regional Law

- Ley 2/2007, de 27 de marzo, de fomento de las energías renovables y del ahorro y eficiencia energética de Andalucía.
- Ley 1/1994, de 11 de enero, de Ordenación del Territorio de la Comunidad Autónoma de Andalucía.
- Ley 7/2002, de 17 de diciembre, de Ordenación Urbanística.
- Ley 7/2007, de 9 de julio, de Gestión Integrada de la Calidad Ambiental.
- Decreto 239/2011, de 12 de julio, por el que se regula la calidad del medio ambiente atmosférico y se crea el Registro de Sistemas de Evaluación de la Calidad del Aire en Andalucía.
- Decreto 357/2010, de 3 de agosto, por el que se aprueba el Reglamento para la Protección de la Calidad del Cielo Nocturno frente a la contaminación lumínica y el establecimiento de medidas de ahorro y eficiencia energética.
- Decreto 6/2012, de 17 de enero, por el que se aprueba el Reglamento de Protección contra la Contaminación Acústica en Andalucía, y se modifica

el Decreto 357/2010, de 3 de agosto, por el que se aprueba el Reglamento para la Protección de la Calidad del Cielo Nocturno frente a la contaminación lumínica y el establecimiento de medidas de ahorro y eficiencia energética.
- Decreto 5/2012, de 17 de enero, por el que se regula la autorización ambiental integrada y se modifica el Decreto 356/2010, de 3 de agosto, por el que se regula la autorización ambiental unificada.
- Decreto 18/2015, de 27 de enero, por el que se aprueba el reglamento que regula el régimen aplicable a los suelos contaminados.
- Decreto 73/2012, de 22 de marzo, por el que se aprueba el Reglamento de Residuos de Andalucía.
- Ley 2/1989, de 18 de julio, por la que se aprueba el inventario de Espacios Naturales Protegidos de Andalucía y se establecen medidas adicionales para su protección.
- Ley 8/2003, de 28 de octubre, de la flora y la fauna silvestres.
- Decreto 178/2006, de 10 de octubre, por el que se establecen normas de protección de la avifauna para las instalaciones eléctricas de alta tensión.
- Decreto 23/2012, de 14 de febrero, por el que se regula la conservación y el uso sostenible de la flora y la fauna silvestres y sus hábitats.
- Estrategia del paisaje de Andalucía, 2012.
- Ley 14/2007, de 26 de noviembre, de Patrimonio Histórico de Andalucía.

5.1.3 Environmental implications of its operation

The atmospheric stability and daily variability significantly determine the wake development and the kinematic characteristics associated with the airflow. Consequently, the balances of mass, energy, and momentum change, producing alterations on the environmental components directly or indirectly related to these phenomena. The global components affected, the relationship between them, and the ecosystem changes are detailed in Figure 5.1.

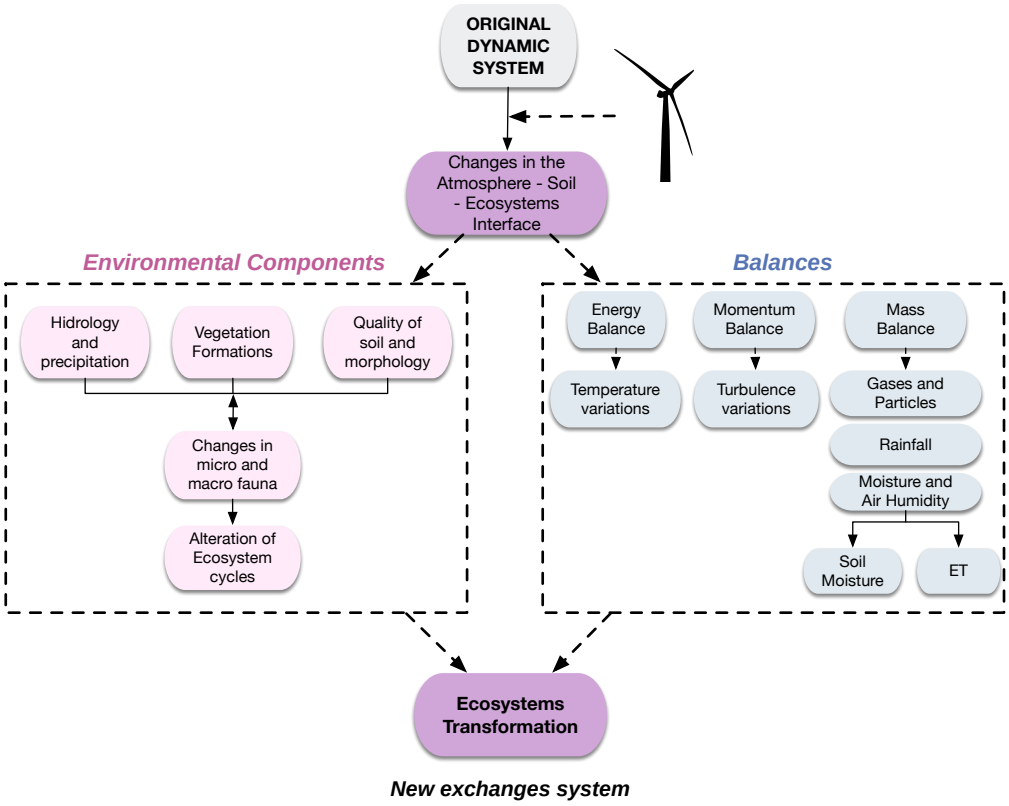

Figure 5.1: Environmental components affected, variables and indicators involved.

5.1.4 Proposed methodology

The sustainable generation of electrical energy through the transformation of kinetic energy from wind demands a reliable method of exploitation and decision-making. Therefore, it is necessary to analyze the project requirements based on evidence and under conditions of uncertainty (Carriger et al., 2016), enhancing the scientific-technical knowledge about the dynamic processes at the atmosphere-soil-ecosystem interface. Furthermore, to carry out a correct integrated study may be incorporated an operation protocol for those situations in which the resources cannot be exploited for some time; or permanently under certain climatic, environmental, and social conditions, including stress level thresholds of the environmental components (Samhouri et al., 2010).

Given the above considerations, this chapter proposes a methodology that integrates the balances, exchanges, and alterations on the ecosystem cycles, evaluated jointly with the environmental costs. The information and theoretical development

on which this work is based are sufficiently advanced, developed, and tested to implement the proposed methodology possible. Figure 5.2 schematically shows this methodology, which is summarized in the following steps:

1. Characterization of the environment. Once the project's objectives and requirements have been defined, a detailed description of the environment, the variables of interest, and the environmental descriptor susceptible to impact must be provided.
2. Definitions. It should be defined for each environmental descriptor: indicators and balances, methods of impact detection, scales of variations, and impact levels.
3. Simulation of atmospheric variables. Preliminary simulations are necessary to develop multi-criteria strategies to quantify and evaluate the impact of wind farms before their installation. The selection of the target scales of simulation for each descriptor is based on the minimum required spatial and time resolutions and the associated models. First of all, a wind time series simulation tool and time series reproduction models are needed to determine the initial dynamic state of the SBL (Solari and Losada, 2016). In addition, the required level of aggregation in the general context of the impact analysis should be assessed at this point.
4. Simulation of environmental variables. Firstly, changes of key hydrological variables are usually the significant drivers of impacts on other processes and ecosystems. From the generation of weather variable maps on the target time scales (by spatial interpolation schemes) to obtaining soil moisture and evapotranspiration rates, many available models simulate the water and energy balance on a distributed basis. Although the daily scale is adequate to perform such balance for most environmental applications, the choice of hydrological models that operate on an hourly basis is desired to identify potential tipping points in some processes that cannot be assessed on daily calculations (e.g., soil moisture below the permanent wilting point of plants). Moreover, models capable of simulating semi-arid and other water-controlled environments are needed (e.g., in mountain sites in southern Spain, (Gómez-Giráldez et al., 2019). As a representative example of such a model and it integrates both weather variables mapping in highly heterogeneous areas and a distributed water and energy balance based on physical processes (Polo et al., 2009), and it has been applied to many applications in Andalusia and other Mediterranean-type regions. Secondly, once the hydrological drivers are estimated on the target time horizon and the significant spatial scales, other environmental variables can be retrieved.
5. Verification of spatial–temporal evolution. Once the balances are determined, the variables of interest are simulated, and the simulations are integrated with the indicators for each of the selected descriptors, it is necessary to verify their

evolution at different spatial–temporal scales, following the approach found in other contexts such as coast evolution or maritime projects (López-Ruiz et al., 2018; ROM 1.1-18, 2018). After previous simulations, the process must be repeated, including the alterations on the SBL, evaluated through affection indicators and experimental tests (Jiménez-Portaz et al., 2016), and verify the 'new evolution' in spatial–temporal terms for each of the environmental descriptors.

6. Definition of multi-criteria strategies (Díaz Cuevas et al., 2017; García-Morales et al., 2015). Based on the simulations with and without wind turbines, it is necessary to define a series of multi-criteria strategies, including the periods of exploitation, operation, conditioned operation, and operational shutdown of the wind farm or part of the wind turbines. As a result, the project's sustainability must be achieved, with a pre-established environmental monitoring plan to confirm that none of the environmental descriptors exceeds its threshold value.
7. Definition of an environmental monitoring plan. A monitoring plan is required to control and predict possible impacts and react in advance or with an immediate response to the occurrence of the impact.
8. Total costs. The total costs of the project should be analyzed, including the environmental costs. It is recommended to use a methodology similar to the one outlined in ROM 1.1-18 (2018) and Wu et al. (2019), the calculation of which is not presented in this thesis.
9. End of useful life. At the end of the useful life of a wind energy project, it will be decided whether to: (i) dismantle the wind farm, including an environmental restoration plan; (ii) extend the useful life of the wind farm. A new global study of the system is then required, in which the changes concerning the initial conditions are considered, and the whole process described in the previous steps must be repeated.

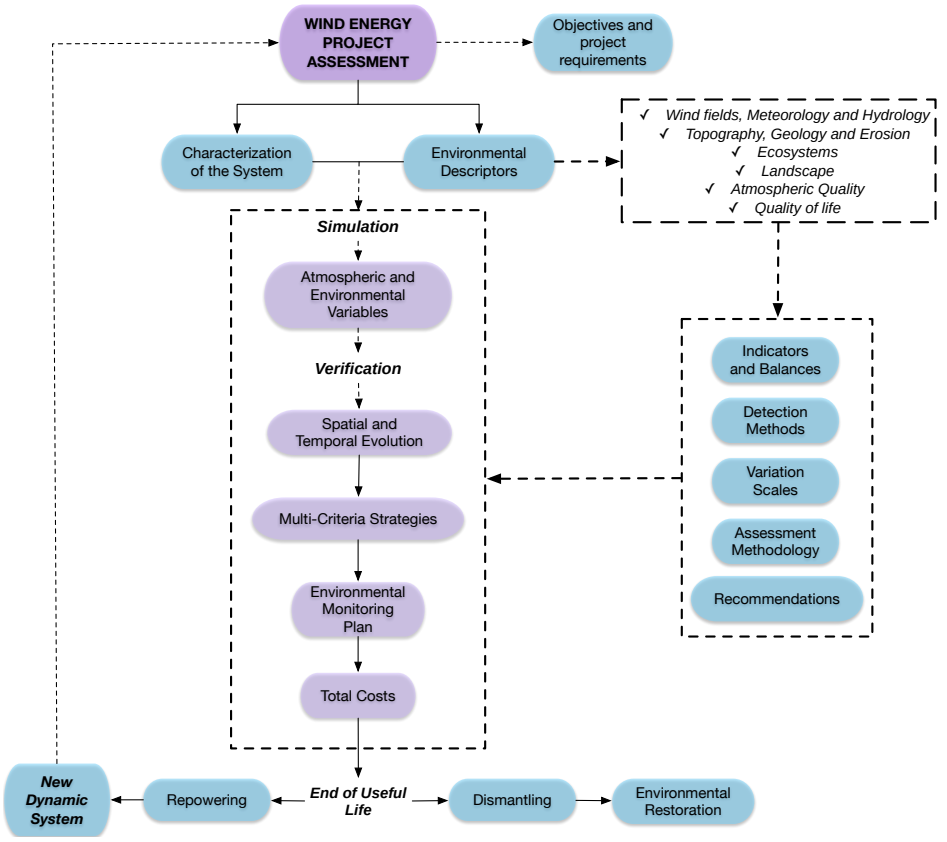

Figure 5.2: Flow chart of the methodology to follow in the management and environmental study of a wind energy project.

5.2 Environmental facts, indicators and recommendations

Environmental descriptors and elements involved in the mutual interaction between wind turbines and surface boundary layer are required to conduct an appropriate simulation. That information encompasses descriptors relative to wind fields, topography, soil science, geology and erosion, meteorology and hydrological system, ecosystem and ecological niche, atmospheric quality, noise pollution, landscape, waste, and quality of life. The proposed indicators involved in this paper are described hereunder, concerning dynamic monitoring, affectation mechanism, and management recommendations. The application and calculation method for each indicator is detailed in the works cited in the text. Indeed, the proposed impact indicators allow the quantification of changes in balances during the simulation. However, it has to be highlighted that these indicators are not stationary and have to be analyzed following spatial and temporal variation scales previously identified.

5.2.1 Wind fields, meteorology and hydrological system

Description and Affectation Mechanism

The wake generated by a wind turbine is affected by changes in kinematics variables and works as a sink of kinetic energy, which effect is intensified by the overlap between wakes (Porté-Agel et al., 2020) and the cumulative effect of having another windfarm nearby. As a result, it produces a deceleration of velocity and an increase in turbulence intensity. The turbulence fluctuations in the wake are defined by the wind turbine elevation above ground, the layout of the infrastructures, the initial wind flow, the soil roughness, the topography, and the meteorology.

Turbulence phenomena in the ABL modify moisture, temperature, wind shear gradients, convection, advection, and conduction patterns. Numerical tests show that wind farms produce impacts over the meteorology; and the land surface fluxes of momentum and scalars as the temperature, the heat, and the moisture (Roy, 2011). In addition, these variables drive and are modified by the water cycle, changing the rainfall distribution (Fiedler and Bukovsky, 2011) and the local, regional and global climate (Miller and Keith, 2018; Redfern et al., 2019; Wang and Prinn, 2017) over areas about 18-23 km downwind (Roy, 2011).

Depending on the wind farm layout and the upstream wake interaction, it has been proven that: (1) in staggered wind farms, the temperature near the wind farm increases and decreases with height, and the relative humidity (RH) near the surface is reduced; (2) by contrast, in aligned wind farms the surface heat fluxes are reduced downwind and increased upwind; in this case, the RH variation is lower than in the previous case (Haywood et al., 2020; Zhang et al., 2013). Annually, time variations in the Mediterranean climate are higher during the rainy season. On a daily scale, changes are more substantial at early morning hours, when the ABL is stable, stratified, and with high vertical gradients (Stull, 2016). Changes during the night in the near-surface temperature induced by wind farms are more pronounced in the Stable Boundary Layer (Roy and Traiteur, 2010).

Assessment Methodology

To evaluate the mutual interaction between wind field and the processes at the SBL scale, baseline indicators are selected for wind speed, turbulence, meteorological and hydrological processes. The mean wind speed Um and the turbulence intensity IT are proposed as baseline indicators for the wind field. They are appropriate to characterize the wind flow (Porté-Agel et al., 2020; Yang et al., 2020) using data from wind tunnel experimental tests, measurements with anemometers in situ, weather stations, LiDAR systems (Light Detection And Ranging) (Banta et al., 2015; Zhan et al., 2020) or TLS (Tethered Lifting System), and also carrying out theoretical estimations (Jiménez-Portaz et al., 2016; Porté-Agel et al., 2020). In

addition, the potential evapotranspiration is the baseline indicator for the impact over the meteorology and the hydrological system. This overall indicator comprises some others system variables, and it is quantifiable from temperature and precipitation.

Daily scale, wind gusts are stronger in the daylight hours, and wind shear is higher at night–time. The turbulent wakes recover faster during the day than during the night due to the higher turbulence intensity present at daytime (Porté-Agel et al., 2020). At a seasonal level, Mediterranean areas show slower wind speed values that increase during winter periods. Wind flow fluctuations are essential to obtain quantitative and qualitative information regarding balances and exchange alterations and defining how severely the environment is affected (Chapter 1).

Recommendations

Wind farm layout optimization and the appropriate location selection are the main steps to minimize the impacts. The proper selection of the location reduces the effects generated inside the turbulent wake and the intersection between different wakes. Turbulence decreases thankful to the previous measure, and it mitigates the mixture in the vertical temperature, momentum, and heat transport profiles (Zhang et al., 2013), and transforms the hydrological patterns, among others (Figure 5.1). Operational stop can be required during higher affection periods if these are not simultaneous with the highest energy demand periods. In extreme cases, the possibility of removing some specific infrastructures should be evaluated.

5.2.2 Topography, geology, soil and erosion

Description and Affectation Mechanism

According to Segalini (2017), the location of wind turbines over hilly terrain results in a faster recovery of the turbulent wake to the initial state. Terrain type, soil cover, and topography set the conditions for the governing factors of the project, namely: power extraction, wind profiles, and turbulence intensity. Direct and indirect changes on these components, such as geotechnical, topographic, and soil cover elimination, need to be studied in detail. Most of them produced during construction and dismantling phases, altering soil characteristics and eventually polluting surface waters.

From the standpoint of the alteration patterns, the scale of spatial transformation corresponds to those areas strongly modified by the intrusion. At the same time, the main temporal change is essentially tied to dry seasons since compaction effects increase the potential erosion, the fragmentation (Toy et al., 2002), and the torrential rain runoff.

Assessment Methodology

The baseline indicators to assess topography, geology, and soil are proposed according to the Soil Compaction Index (SCI) –which is possible to calculate depending on the machinery type- and the Erosion Rate (Rücknagel et al., 2015). After that, it is possible to evaluate soil structural changes and ecological alterations, especially those related to microflora and microfauna loss. In addition, the soil pollution factor can be quantified to assess the general condition and the soil evolution trend. Finally, it can be measured through soil sample analysis and laboratory measurements.

Recommendations

The control and mitigation measures should be the least intrusive. The areas of interest and the areas with high erosion probability should be protected first before any action over terrain. Ecological sensitive areas should also be marked with beacons. The study of rainfall patterns is recommended to prevent working activities during periods with a higher probability of intense rainfall.

The use of existing trails and the design of new roads adapted to the terrain might help reduce the intrusion through diggings and waterway destruction. It is even possible to prevent overflow and erosion processes by reducing the width of the roads and adding ditches and drains. Other methods to decrease erosion are hill slope flattening, construction of barriers, bundles, biological cover or natural fibers (Mendoza, 2011), micro-relief generation, and terrain chemical stabilization in some cases, when no risk of soil pollution is ensured. Pile topsoil on mounds can reduce the loss of moisture and general properties. This material can be used to restore affected areas, following this procedure along the project lifetime and after its dismantling.

Appropriate waste management is essential during the project's lifetime and after it. Stocking areas must be delimited inside the wind farm, reusing sterile products generated as construction material and piling vegetation waste on mounds. Finally, machinery cleaning inside the wind farm should be avoided, and all waste generated must be recycled when possible; otherwise, it should be relocated to authorized dumpsites.

5.2.3 Ecosystems and ecological niche

The meteorology and the hydrological system set the limit and define the morphology, the water availability, and the type of vegetation and fauna. Fauna and flora diversity can be affected during all project phases and mainly during construction and dismantling.

Plant species

Description and Affectation Mechanism

Besides intrinsic value, the vegetation modulates the landscape, takes part in gases and moisture exchanges, and determines soil type. Therefore, vegetation removal supposes increased soil erosion risk and direct and indirect impacts over other elements. Furthermore, knowing the vegetation cover characteristics before and after the exploitation, it is possible to evaluate its spatial–temporal evolution. Hence, it is essential to identify vegetation series, coverage, average plant height, and special conservation status.

The life cycle of vegetation can be related to wind flow through seed dispersal and evaporation rate, both modified by turbulence and velocity changes. Most plant species have anemochorus dispersion, being needed a seed dispersion model according to wind profiles (Beckman et al., 2020; Nathan et al., 2011). Seasonal and year–over–year variations depend on the plant's life cycle, so a comparison with a control area is necessary to evaluate the plant's evolution produced by changes associated with wind energy exploitation.

The land surface temperature changes due to the influence of turbulence on evapotranspiration and the decrease of soil and plant moisture levels. This is a fundamental aspect in dry climate zones, just as in the case of Andalusia.

Assessment Methodology

The fractional vegetation cover, f_c, which describes a vertical projection of the areal proportion of a landscape occupied by green vegetation, is proposed as the indicator. Indeed, the impact level on vegetative coverage can be assessed according to f_c variation. Remote sensing techniques are helpful to quantify the f_c index, (Gao et al., 2020), employing the calculation of the NDVI index (Normalized Difference Vegetation Index) and applying a linear relation between NDVI and f_c. The NDVI itself can also be used to monitor other hydrological states of the soil, difficult to track on a long-term basis in large areas, and it is a beneficial and cost-effective data source in ecological studies of vegetation even in mountain sites (Gómez-Giráldez et al., 2014).

Recommendations

The measures proposed in this case are divided into two types. On the one hand, plant protection measures, and on the other hand, restoration treatment. It is appropriate to demarcate areas where special species exist, limit access to external staff, avoid trenches near trees, and carry out silviculture treatments over the existing vegetation.

The vegetation removal is recommended only when necessary, and historical

specimens should be transplanted to other places (if it is impossible, preserve it in–situ). Plant shrub species are indicated to be sown around wind turbines, alongside edible and soil protective species when possible, avoiding the use of invasive species and controlling their appearance.

Fauna

Description and Affectation Mechanism

Birds and bats have been selected as representative species of this affection (Sánchez-Zapata et al., 2016), which should be studied at a population level, inventoried, and cataloged according to the special conservation status. Collisions, flight patterns and displacement disturbances, barrier effect, and habitat loss are the most common alterations on birds and bats.

Certain bird species could be affected more than others; therefore, it is required to analyze specific cases, identify zones potentially suitable for siting wind farms, and reduce the impact on sensitive periods. More affected species in the South of Europe are Golden Eagle, Egyptian vulture, Vulture, and Dupont's Lark, among others (Atienza et al., 2012). Concerning bats, most recorded cases belong to sedentary species.

Wind turbines attract bats (Laranjeiro et al., 2018). Thus, it is necessary to obtain information about refuges, breeding colonies, and feeding sites. The bats' population should be studied through sound recording, infrared cameras, acoustic and activity detectors to select an appropriate location with a limited population to facilitate the monitoring process (Obrist and Boesch, 2018).

Temporal variations are defined by life and reproductive cycles for each species and the local and global atmospheric conditions. To spatial variations, flight patterns and migration routes should be known because of the higher impact over these areas.

Assessment Methodology

The proposed baseline indicators for fauna are flight patterns display and their variations, habitat loss, collision risk, and electrocutions, which can be calculated using the methods proposed by Johnson et al. (2016) and Vifard et al. (2020). Time-lapse images around wind farms (Yoshihashi et al., 2017), high-resolution data, radar technology, and GPS ease the evaluation of the spatial movement of birds and their modifications based on wind changes (Safi et al., 2013). Birds can detect wind turbines and modulate their flight patterns. However, to skirt wind farms, birds need to spend more energy, decreasing their survival (Atienza et al., 2012). Habitat loss might be evaluated through bird-watching, with or without GPS/GSM transmitters, and monitoring their location.

Collisions are a direct cause of death, being one of the most noticeable and measurable effects. Ground searches are recommended to find bird corpses byline or concentric transects, covering an area at least 10 % bigger than the rotor diameter (Atienza et al., 2012). The ideal indicator for bird's fact is the fatality rate proposed by SEO/BirdLife. For bats, the process of detection is similar, using parallel bands from 50 to 60 meters of width; the suggested indicator is the number rate of fatalities corrected for wind turbine and area per year (Sánchez-Navarro et al., 2019). Other alternative methods can be used, as the age-structured stochastic density-dependent matrix model proposed by Schippers et al. (2020).

Recommendations

As in the previous case, measures are divided into protective and restorative or countervailing. The most important one is the appropriate location selection. The wind farms must be set almost 10 km away from Special Protection Areas and avoiding the ecologic barrier.

Works must be planned out of breeding periods, and bird species should be inventoried, and long-term monitored. High-risk periods and high mortality hours require energy production standstill and removal of some infrastructures in extreme cases. Some more recommendations are: increasing blade visibility and a suitable type of illumination, avoiding flashes and white lights, minimizing the birds and bats attraction, and cleaning carrion from surroundings.

Low-speed wind turbines reduce bird's mortality; however, it produces an opposite effect over bats populations. Variable velocity wind turbines capable of adapting their rotation speed depending on the period is an alternative. Systems like DTBird (May et al., 2012) can be used to control wind turbine operation when an individual is detected, and ultrasound emission can be helpful for bats.

Hazard mapping and vulnerability

The definition of spatial areas susceptible to alterations can be a helpful way to create hazard maps, according to exchange processes between the Earth System and the ecosystems, species vulnerability, and so on, making also feasible to identify areas with a higher risk of affection. In the case of fauna, following the methodology published by Atienza et al. (2012), it is possible to obtain the vulnerability from a specific location depending on the species abundance and its sensitivity, understanding the vulnerability as the population risk of being altered by an external factor. Limitations arising from the special conservation status of the species must be taken into account. It is recommended to apply species distribution models like the one proposed by Laranjeiro et al. (2018).

5.2.4 Noise pollution

Description and Affectation Mechanism

Noise pollution is directly related to impact overpopulation, being increased by stronger winds. There are two categories of wind turbine noise: mechanical noise and aeroacoustic or aerodynamic noise (McCunney et al., 2014). It is possible to estimate the noise propagation, knowing the initial sound level in the field of study and the topographic and meteorological conditions (Shen et al., 2019).

According to Sedaghatizadeh et al. (2017), the interaction between sound waves and vortex in the wind turbine wake increases the sound perception in the area influenced by the turbulent wake, behaving as a sound driver in the flow direction. The spatial variation is related to wind speed and direction, the distance from the wind turbine, and the temperature (Cotté, 2019; Keith et al., 2019). The main alteration is observed daily, although it is noticed that noise levels are higher during construction and dismantling periods due to the machinery operations.

Assessment Methodology

Generally, as is advised in the current regulation, the acoustic rate is the most suitable indicator. Taking into account prevailing winds, acoustic power level, reference noise level, measurements indoor and outdoor dwellings, and data acquisition quality of specific emitters (Keith et al., 2019). Moreover, models of noise generation coupled with propagation models turn out to be a tool to simulate wind turbines noise (Zhu et al., 2018); thus, a source model is necessary to calculate sound pressure level upwind (Cotté, 2019). Appropriate equipment must be used to avoid distortions by external factors such as the air humidity (Keith et al., 2019).

Recommendations

It is necessary to analyze noise pollution (indoor and outdoor dwellings) based on noise propagation variations according to gradients and balance modifications; to prevent high sound levels near populated areas. Noise maps are recommended to select the optimum location. Daily noise alterations should also be considered to prevent the underestimation of decibels generated.

The enhancement in blade design, and the wind turbine placement upwind, induce a decrease in the aerodynamic noise. As for the mechanical noise, the machinery conditions have to be inspected during the construction and dismantling periods and carry out maintenance operations of the nacelle. In exceptional cases, it is possible to install guard panels at the expense of landscape quality.

5.2.5 Landscape

Description and Affectation Mechanism

Wind farms are usually located in places with high biodiversity value and bring a substantial change in the landscape's character, in which the visual quality is decisive. This impact could be classified into daytime impact due to the number of wind turbines and nighttime impact resulting from position lights. Moreover, changes in geomorphology and vegetation suppose a visual impact, depending on the area and the global damage level (Banta et al., 2015).

Assessment Methodology

In Andalusia, all wind turbine areas have been digitalized, which is of interest for the management of these installations, obtaining fundamental indicators as the density of wind turbines per km^2, between others (Díaz-Cuevas and Domínguez-Bravo, 2015). So, it has been proven that multi-criteria techniques, including GIS, are suitable tools to identify suitable areas for wind farm installation.

The "Guía de integración paisajística de parques eólicos en Andalucía", (Ghislanzoni et al., 2014), provides appropriate indicators for this environmental descriptor and the "Sistema de Visibilidad de Andalucía (SVA)" (Cáceres et al., 2014), comes up with a general method to evaluate the landscape impact. The visual impacts can be classified, according to the previous references, into two categories: annulment and intrusion.

Complementary, other methodologies could be helpful, as the one proposed by Sklenicka and Zouhar (2018), through the use of landscape indexes, as a fundamental tool for the decision-making process, or the work of Lizcano et al. (2017), which uses virtual reality and 3D models to illustrate the visual effect generated by a wind farm project.

Recommendations

The measures regarding the landscape impact are widely linked to field operations. Slope stabilizing using native plants and avoidance of extensive dig are recommended. The materials have to be similar in appearance to the bare ground to avoid color contrasts. Natural screens and the use of rock oxidizers are helpful.

Wind turbine installation in predominant skylines should be avoided, neutral finish, white or grey matt color, and in exceptional cases, removal of some infrastructures could be necessary. The SVA proposes the selection of areas depending on the following models: intervisibility, minimize the skyline value, visual projection, level of intrusion, among others (Cáceres et al., 2014; Ghislanzoni et al., 2014).

5.2.6 Atmospheric quality

Description and Affectation Mechanism

The quality of the atmosphere in the surrounding of the wind farm is determined by indicators of atmospheric pollutants, gas exchanges, dusty wind, suspended particles, and light pollution. An appropriate evaluation of this environmental descriptor can be achieved by knowing in advance its quality through the above indicators and the influence of balances and exchanges over the pollutants dispersion and the direction of transportation (Bui and Lu, 2019). A suitable approach can be achieved with the analysis of wind flow changes and meteorological conditions, and with the study of the system before and after its setting.

During the construction and dismantling phases, a bigger quantity of pollutants is emitted, prevailing dust particles due to machinery operations. These effects are amplified during dry seasons and over areas with a high erosion rate.

Light pollution can be softened accounting for the light signaling normative and respecting aeronautical limitations. It is necessary to minimize and monitor the suspended dust and the pollutants particles: the machinery should be checked regularly, using alternative fuels and slowing down, cleaning wheels, and using tarpaulins. Finally, periodical irrigations over roads and work areas must be done and in the most extreme cases, carry out a soil chemical stabilization.

5.2.7 Quality of life and cultural heritage

Description and Affectation Mechanism

The quality of life is difficult to quantify. Health affections, residents' perception of surroundings (Vlami et al., 2020), annoyances associated with wind farm and socioeconomic changes, are some intercurrent variables in the 'Quality of life' concept (Katsaprakakis, 2012). Most studies analyze prolonged exposure to wind turbines, especially sound, but there are few references to clinically apparent health effects (Freiberg et al., 2019).

Assessment Methodology

Some indicators targeted on an accurate estimation of life quality are noise level, shadow flicker presence, infrasound, electromagnetic radiation, and visual quality index. There might be other evolving yet subjective facts, strongly dependent on population issues such as general opinions, economic benefits, epidemiology problems, among others (Freiberg et al., 2019).

Recommendations

Active involvement of population and native inhabitants, labor market, and tourism promotion are recommended, and other activities like cropping of otherwise barren land, shepherding, improvement in the local population acceptance, among others. Some other activities are proposed, including hiking, notice boards, interpretation centers, workshops, and dissemination conferences.

Appropriate guidelines on visual impacts and noise pollution should be carried out. It is difficult to decrease the shadow flicker impact, but it is possible to avoid its action over residential areas optimizing the wind farm layout. In exceptional cases, it could be considered the use of protective screens, especially at night.

5.3 Example of application

This section includes a basic example of the application of the proposed methodology. This example focuses on the first part of the proposed methodology, referring to the characterization of the environment, definition of environmental components and indicators, simulations of atmospheric variables, and simulations of environmental variables.

As a first step, a characterization of the environment is made, defining the topography, surface roughness, wind velocity, and type of infrastructure to be installed. In this example, a single wind turbine is simulated in a standard location of an Andalusian wind farm in a silvopastoral system with low vegetation cover, specifically in the area of Cádiz described in Chapter 4. Mean wind velocity and turbulence intensity have been selected as descriptors for this case study.

5.3.1 Simulation of atmospherics variables and temporal evolution

The changes due to the mean wind velocity modified by the operation of the wind turbine itself, assuming constants for the rest of the variables, are analyzed. To accomplish this, some rates of variations for the mean speed and the turbulence intensity are obtained from experimental data, from tests carried out in a boundary layer wind tunnel, described in Chapter 4.

Figure 5.3 shows a sketch of the points where measurements have been taken and the selected points (NW, MW, and FW) (Porté-Agel et al., 2020) for subsequent data comparison (before and after the wind farm installation).

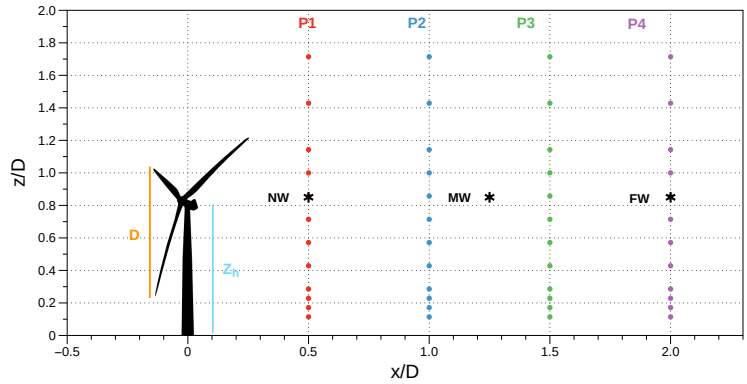

Figure 5.3: Sketch of measurements taken on 4 profiles (P1, P2, P3 and P4). Where: i) D (105 m) is the diameter of the circumference drawn by the wind turbine blades; ii) z_h (90 m) is the hub axis height; iii) NW (Near Wake), MW (Medium Wake) and FW (Far Wake), are the points chosen for the comparison of values with and without wind turbine.

The vertical profiles of mean wind velocity and turbulence intensity downwind (P1-P4), for the central section just behind the wind turbine, and the reference profile of the simulated ABL are represented according to the characteristics of the selected study area (Figures 5.4 and 5.5). The figures show the shape of the wind turbine as a reference for comparing results based on the dimensions of the model.

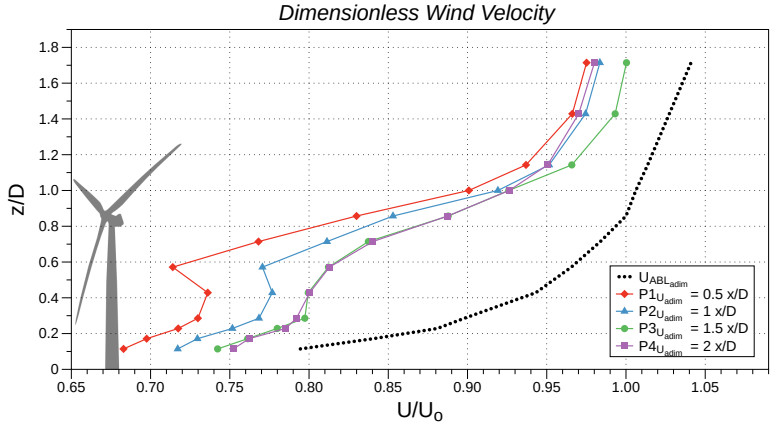

Figure 5.4: Dimensionless mean wind velocity vertical profiles. Dimensioned the reference velocity measured at a height equal to D (105 m).

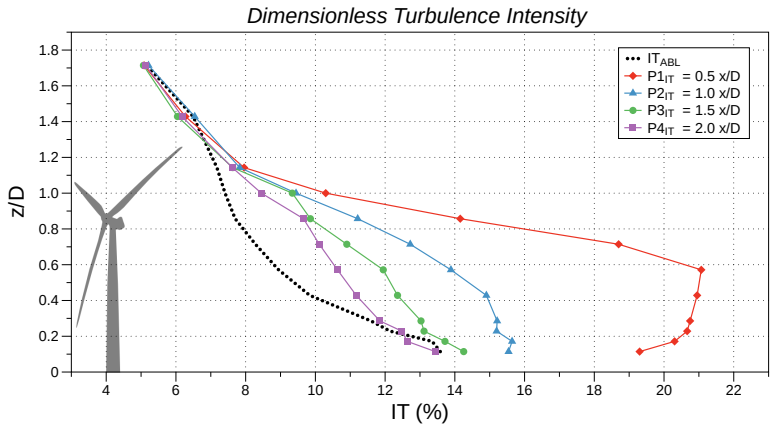

Figure 5.5: Turbulence intensity vertical profiles.

Each ratio is defined as the value from the start-up of the wind turbine (subindex *wt*), divided by the input value (subindex *ABL*). The downwind variation ratios are represented in the whole area measured in the wind tunnel (R_U and R_{IT}):

$$R_U = U_{wt}/U_{ABL} \quad R_{IT} = IT_{wt}/IT_{ABL} \tag{5.1}$$

The following Table 5.1 shows the values for Profile 1 (P1 Figure 5.3), the closest to the wind turbine. Values of R_U lower than unity mean that the velocity is lower behind the wind turbine, and values of R_{IT} higher than unity mean that turbulence intensity is higher behind the wind turbine, except for points 11 and 12.

Point	z/D	x/D	U_{ABL}	U_{WT}	R_U	IT_{ABL}	IT_{WT}	R_{IT}
1	0.1143	0.5	0.852	0.732	0.86	1.358	19.300	1.42
2	0.1714	0.5	0.901	0.748	0.83	1.335	20.303	1.52
3	0.2286	0.5	0.945	0.769	0.81	1.215	20.664	1.70
4	0.2857	0.5	0.963	0.783	0.81	1.159	20.748	1.79
5	0.4286	0.5	1.011	0.789	0.78	9.839	20.950	2.13
6	0.5714	0.5	1.035	0.766	0.74	8.945	21.069	2.36
7	0.7143	0.5	1.055	0.824	0.78	8.280	18.698	2.26
8	0.8571	0.5	1.072	0.890	0.83	7.699	14.155	1.84
9	1	0.5	1.066	0.966	0.91	8.149	10.297	1.26
10	1.1429	0.5	1.087	1.005	0.92	7.176	7.956	1.11
11	1.4286	0.5	1.102	1.036	0.94	6.494	6.272	0.97
12	1.7143	0.5	1.116	1.046	0.94	5.167	5.088	0.98

Table 5.1: Dimensionless wind velocity and turbulence intensity values, and ratios calculated for the first measured vertical profile.

Figures 5.6 and 5.7 show the mean velocity and turbulence intensity ratios over the entire measured area of interest. On the other hand, figure 5.8 shows the initial time series and those modified for each of the three points for mean wind speed.

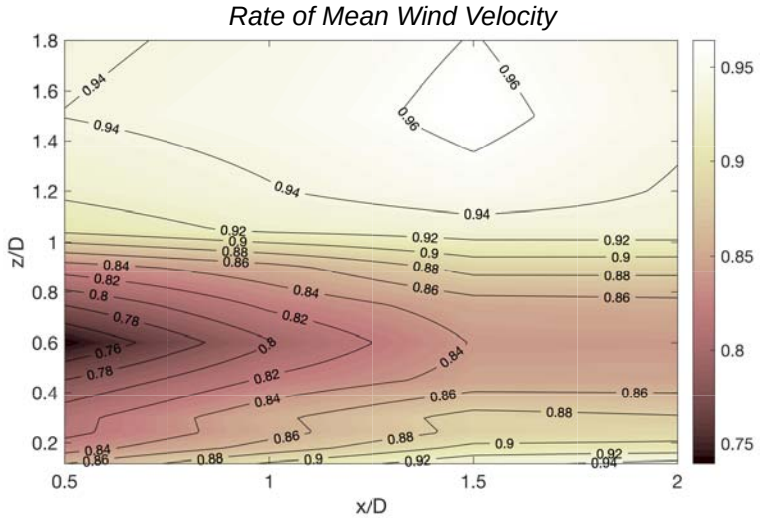

Figure 5.6: Ratio of variation of mean wind velocity with respect to the initial velocity in the ABL.

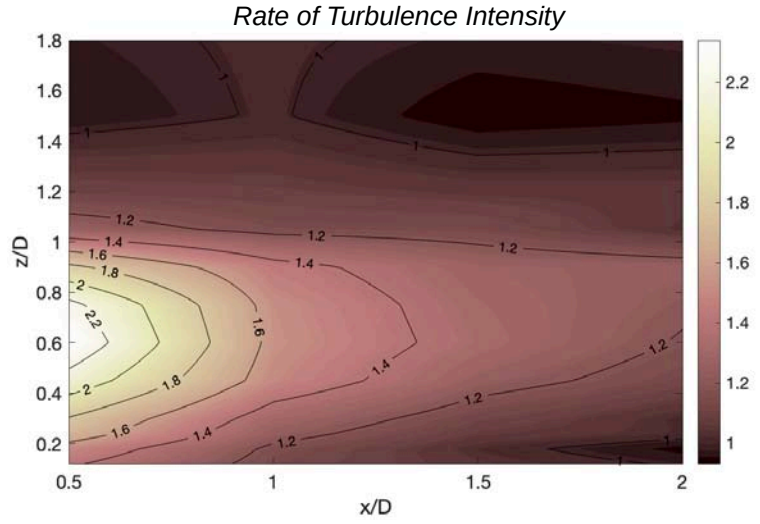

Figure 5.7: Ratio of variation of turbulence intensity with respect to the initial turbulence in the ABL.

Once the area of study has been selected, the necessary spatial dataset is downloaded from the *ERA-Interim reanalysis database* of the Copernicus Marine and Environmental Monitoring Service. Wind velocity time series are obtained for one month, November of 2015, in this case. The mean variation rates in the selected points (NW, MW, and FW) are applied to the time series, as Figure 5.8 shows.

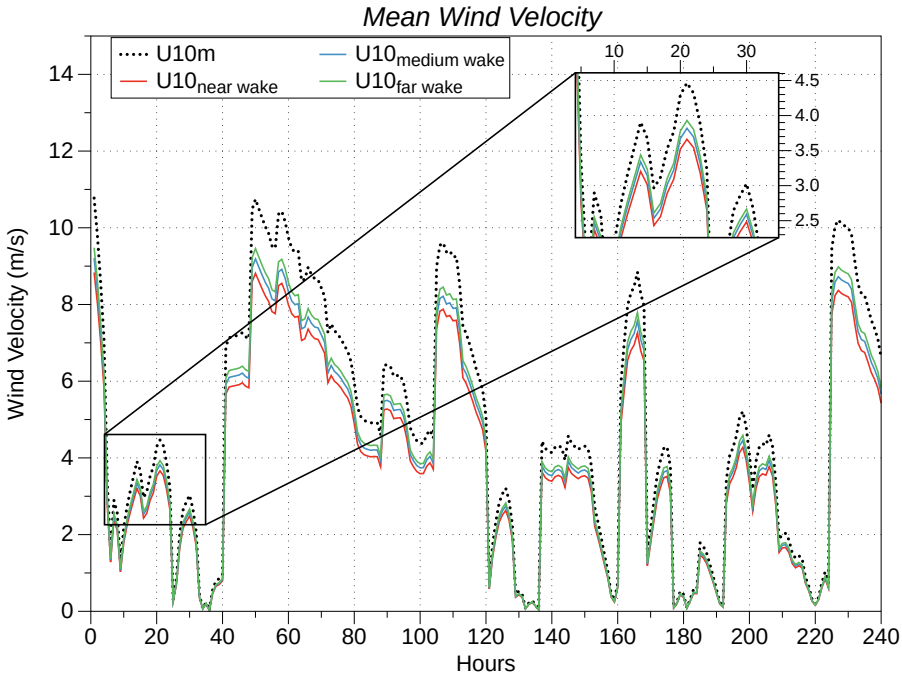

Figure 5.8: Initial time series and those modified (after wind turbine installation) for each of the three points (NW,MW,FW) for mean wind velocity.

After obtaining the above results and the other environmental variables that are part of the system, multi-criteria strategies must be defined for the specific site, together with a monitoring plan, the calculation of total costs, including social and environmental costs, and a plan for restoration or repowering after the end of the useful life of the park or wind turbine in question.

5.4 Conclusions and discussion

Wind farms can modify the exchange and interaction processes between the Atmosphere and the Earth's surface. There are direct and indirect links between mass, energy, and momentum balances and the alterations produced over the environmental components, the power loss, and the fatigue loads in wind turbines.

At present, regulations and policies applied to wind energy focus on the market's interests and the design innovation of infrastructures to promote wind farm development. However, there is no specific law for a more acceptable regulation of the environmental management of these wind farms to avoid impacts and adapt them to the environmental system dynamics. Moreover, current Environmental Impact Studies analyze the environmental components in a stationary way, without analyzing the interaction between them and the influence of balances between atmosphere-soil-ecosystems.

In this thesis, an improved methodology is proposed, based on the results of experimental tests and on relevant literature and results of other authors, which includes simulations of climatic spatial and temporal series, ecosystem cycles, and exploitation periods taking into account the exchange processes and integrating indicators of the spatial and temporal evolution of the system.

The indicators selected are appropriate for Mediterranean drylands, so, in applying this methodology to areas with different biotopes, new indicators should be selected and identified to better define the behavior and constraints of native elements and their ecosystems.

Traditional measures might not be enough in most cases and should be adapted to monitoring programs and the system evolution. Some recommendations are suggested to avoid or mitigate the alterations during all project phases. The methodology proposed to recommend obtaining the project's total costs, taking into account the environmental costs. Through these recommendations, optimization might be expected regarding the sustainability of the project.

Finally, the repowering of wind farms is considered as the priority action for the already installed wind farms, analyzing different scenarios to optimize the energy extraction (Santos-Alamillos et al., 2017). In this case, the complete analysis showed before should be repeated, following the methodology proposed in Figure 5.2. A new EIS and the definition of new management strategies are mandatory in this case.

Reviewing the level of detail in which the affected components are studied in current Andalusian EISs, it can be observed that the analysis carried out is qualitative and shows a lack of specificity in the selection of indicators and methodologies. Comparing the level of detail for each component with the indicators proposed, the following diagram is obtained (Figure 5.9, adapted from Uffe Elbaek Model (Krogerus and Tschäppeler, 2012)). This model assigns scores from 1 to 10 to each ax, which, in this case, refers to the descriptors studied to analyze the environmental impact of wind farms. In general, the methodology proposed in this work covers the different axes more entirely than the current environmental impact studies. The process of analysis and the proposed methodology should be used as tools to develop evidence-based policies under conditions of uncertainty, including the

system dynamics from a comprehensive point of view.

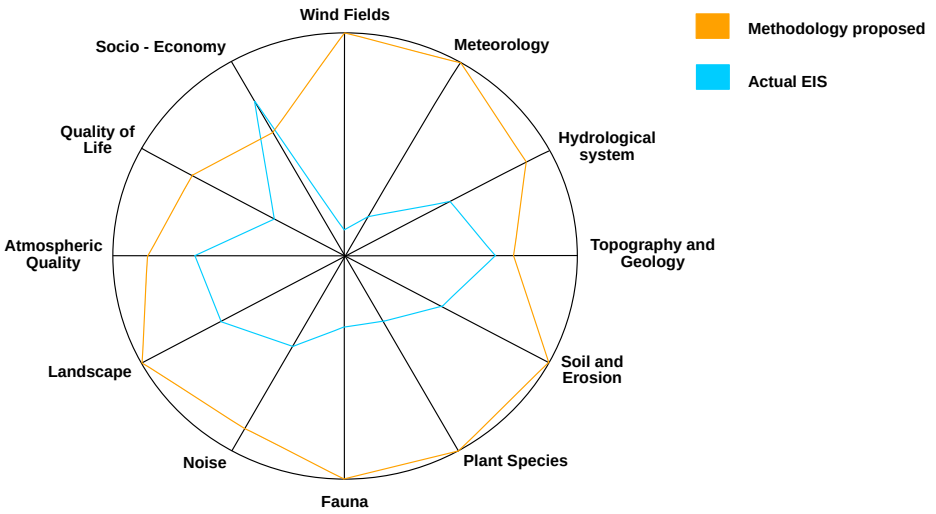

Figure 5.9: Qualitative comparison between the study of the affected components in the proposed work and the current EISs.

The example shown in this chapter attempts to show a first approximation of the proposed methodology. It is a primary case, which serves to graphically observe how, through the application of some preliminary ratios, it is possible to see the effect that a wind turbine generates on fundamental mechanical variables.

The present research may be used as a reference method for future studies. A more detailed description of the guidelines can also be found in the recommendations document published by Jiménez-Portaz et al., 2017.

IV Part IV

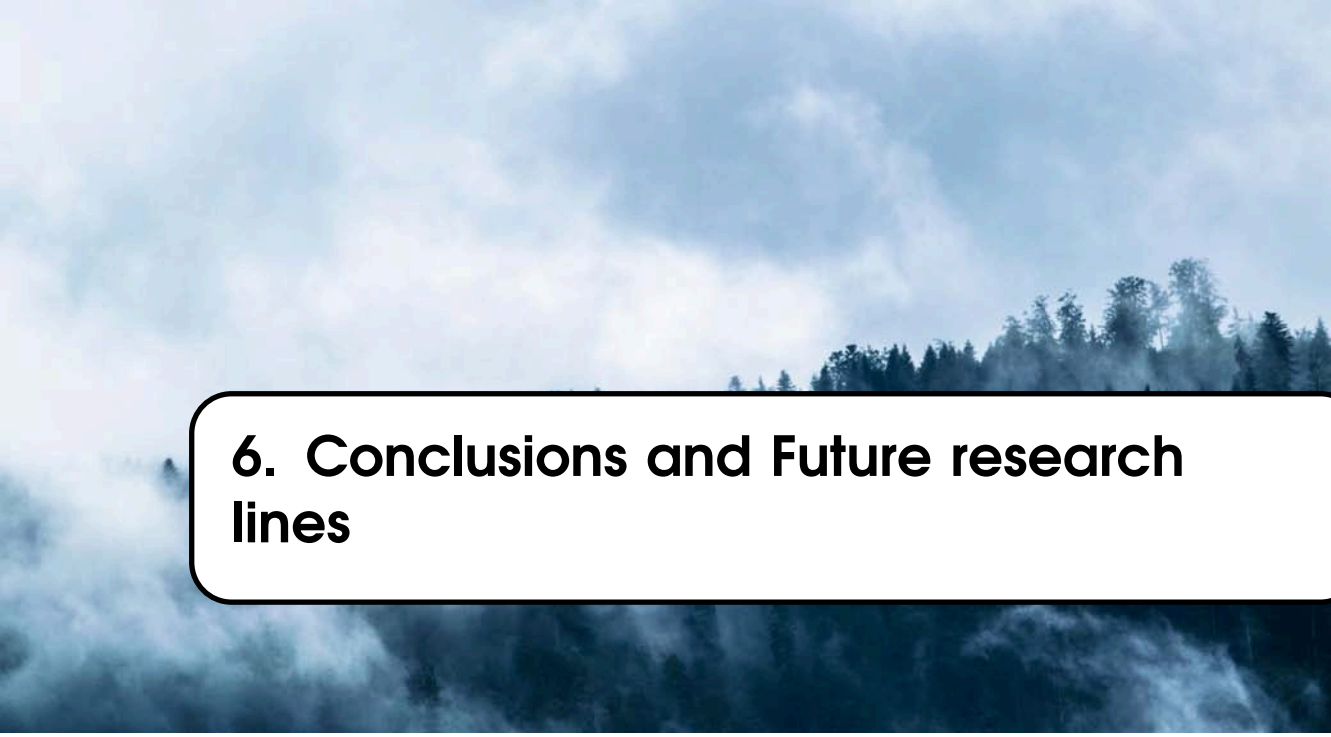

6. Conclusions and Future research lines

6.1 General and specific conclusions

This thesis analyzes the interaction between the atmospheric boundary layer and natural and man-made exploitation systems, such as wind farms and olive groves in Andalusia. Firstly, detailed experiments have been carried out in two different wind tunnels with and without models, comparing the results from different configurations and obtaining complete knowledge about the processes and changes produced in every case. The Andalusian olive grove is located in flatlands and hills, terraces near the mountain tops. Depending on its location, its impact on the landscape, hydrology, erosion, and the amount of pollen in suspension that can later reach the populations, will become more critical. On the other hand, the effects of roughness generated by different obstacles and canopies, as we have seen for the models tested, will directly affect the wind potential to be extracted in adjacent wind farms or implanted next to the olive grove itself (Floors et al., 2018).

Thus, a new management model requires a global understanding of the system, analyzing its elements, how they interact, and modifying the surrounding environments.

In response to the questions posed initially, the main conclusions of this work are obtained:

Q1. How does the airflow behave inside the wind tunnel? Can a boundary layer wind tunnel, conventionally used in aerodynamics and structural testing, be used in environmental studies?

An overview of the tunnel performance has been obtained from the measurement taken in the tunnel entrance and test section. The analysis regards the mean and turbulent characteristics of the flow, and it includes details about the turbulence production, the Reynolds stress, the vertical velocity skewness, the vorticity, and finally, the spectral properties. Lack of symmetry in the tunnel behavior is observed, which could be addressed to the positioning of the tunnel in the hosting room and the asymmetrical airflow recirculation. This analysis represents a fundamental knowledge to better schedule tests and better interpret future activity results. The current characteristics of the tunnel, and the modifications proposed in Chapter 2, demonstrate that it is a suitable tool for environmental studies and scale simulations.

Q2. What are the characteristics of wind flow and turbulence in the different sections of an empty wind tunnel?

There is flow retardation and turbulence enhancement in areas adjacent to the wall; however, the wind field is relatively homogeneous at a distance large enough from the sidewalls. Comparing results from experiments in the OCWT from the IISTA with experiments in the CCWT from CET, it has been shown that mean flow is more homogeneous in the OCWT, but the turbulence intensity is higher across the board. On the other hand, similar values of Reynolds number suggest that both tunnels are mechanically similar.

Q3. Can an ecosystem itself affect the flow around it and other environmental components? Can it even affect the development of the ecosystem itself?

The development of an ecosystem influences micrometeorology and is involved in the interaction between the surface and the atmosphere. The plantation arrangements, as traditional or intensive olive groves, play a fundamental role in the ecosystem processes; they reduce velocity, modify the turbulence, and affect the microclimate. However, at the same time, it is essential to ensure the airflow through the agroecosystem, which depends on the spatial characteristics and the individual trees. Depending on its location, its impact on the landscape, hydrology, erosion, and the amount of pollen in suspension that can later reach the populations, will become more critical.

Q4. How to study and manage an agroforest system according to its land-use management or farming system?

Management of current and new agroecosystems has become a challenge for managers and decision-makers because of the new intensive farming models in the last decade. In addition, climate change, together with the increase in allergies

associated with olive pollen and the ecosystem's long-term improvement and preservation, has generated a social problem that needs to be analyzed in-depth. In this way, a direct correlation can be made between the type of exploitation carried out in natural ecosystems, such as the olive grove, with aerodynamic parameters. In this case, variables such as the Reynolds number and the aerodynamic diameter allow us to understand how the system works and how to manage it. So, being aware of the ecosystem's behavior as a whole, we can predict its response by modifying any of the parameters studied in this work.

Q5. How do wind farms interact with the atmospheric boundary layer? What does this interaction depend on?

Wind farms directly affect the location in which they are placed, due not only to the presence of the wind turbine but also to the rotation of its blades. This fact generates a turbulent wake behind it, characterized by altering the airflow, decreasing the wind velocity, and increasing the turbulence characteristics. The wake development and evolution will depend on the wind turbine location, size, and proximity to other obstacles or wind turbines. Generally, at the rotor height, a wind speed decrease of 15%, while looking at turbulence increases the intensity of 18% for the inflow measurements. These percentages vary slightly depending on whether the wind turbine is located on flat terrain or top of a hill.

The comparison made with different obstacles, in different sections and height levels shows the overall hill influence; it is evident not only their influence on the wind field but also how the height, shape, and slope of the hill affect it, reducing the speed by 10% in the case of the hill with a longer length and gentler slope. To avoid the effect of the hill on the wind field, the distance between it and the wind turbine must be greater than seven times the height of the hill but also depending on the hill shape, length, and slope. So, obstacles will be decisive in developing the turbulent wake and the wind potential to be extracted from a given area.

Q6. How can we study the disturbances generated by a wind farm and minimize their impact?

Traditional measures might not be enough in most cases and should be adapted to monitoring programs and the system dynamics evolution. Based on a comprehensive and detailed analysis of the leading environmental effects of wind energy fields, an integrative methodology is provided, improved, and adapted to the dynamic nature of the environment. It includes procedures, indicators, and tools necessary to assess the impact and manage the system more sustainably.

This type of analysis has been applied to wind farms in Andalusia but can be extrapolated to other regions and types of wind farms, identifying new indicators and defining the behavior and constraints of native ecosystems.

The process of analysis and the proposed methodology should be used as tools

to develop evidence-based policies under conditions of uncertainty, including the system dynamics from a comprehensive point of view.

Q7. Can the management strategies of the systems studied be adapted to sustainability criteria?

By understanding the system's behavior as a whole, it is possible to adopt strategies of analysis and management based on scientific knowledge for both natural and artificial exploitations. These strategies try to adapt traditional techniques and new technologies to the dynamics of the system, including aerodynamic and environmental variables, different spatio–temporal scales, and studying every case in a particular way according to its particularities.

6.2 Future research lines

This thesis's conclusions and main results allow suggesting the following future research lines to complement and complete the experimental tests carried out and develop, apply, and improve the management methodologies proposed. For all these reasons, the following future research lines are proposed:

- Optimize and improve the performance of the wind tunnel to achieve a more homogeneous flow and, thus, minimizing the alterations derived from the room in which the tunnel is located. On the other hand, the aim is to extend the use and applications, transforming the current tunnel, purely mechanical, into a climatic tunnel, introducing heating elements to test temperature variables.
- As a future research line, the aim is to produce and program an integrated model that includes all the factors involved in the wind energy project, validated through experimental and in-situ data. This comprehensive model should include the following approaches: i) technical, ii) social, iii) environmental, and iv) financial and economic, in addition to optimization achieving of wind farms based on previous work.
- Extend the study of the interaction between the olive grove and the atmosphere, including analyzing other environmental variables, models to understand the processes evolution, and comparing the different systems. Future work is proposed to extend the tests carried out, including other models, layout configurations, and vegetation coverages. In addition to incorporate a few of the fundamental environmental variables, such as temperature or humidity changes. Based on these tests, we plan to develop models and relationships between different environmental variables, including:
  - Pollen dispersion
  - Evapotranspiration variation
  - Variations and alterations at tree level and at plantation scale
  - Dispersion of pathogens

  - Soil erosion
- Compare and correlate the experimental results with the field measurements in situ to obtain a global vision, extrapolate the results to the field, and improve the model to be obtained.
- In addition, it is opened the possibility of recommendations development that, based on the dynamics of the system and previous studies, will allow to optimize the management of the ecosystem, improve its production, diminish environmental affections, and improve sanitary conditions, reducing the amount of pollen in suspension that arrives at the population centers.
- Extend the methodology proposed for olive groves to other agricultural and forest ecosystems of high importance, such as pine forests or pasture systems. These are affected by climatic pressure, management, diseases and pests, forest fires, among many others.

Nomenclature

Roman symbols

$\overline{u'v'}$	Shear stress
$\overline{u'w'}$	Reynolds stress
$\overline{U}$	Mean wind velocity
A	Hill width
a	Height of the tunnel
A_o	Total area of the section
B	Overall agro-forest width
b	Width of the tunnel
C_w	Crosswise corridor width
CAV	Curl Angular Velocity
D	Rotor diameter

D_h	Aerodynamic diameter of the wind tunnel
D_m	Aerodynamic diameter
D_p	Aerodynamic diameter of the plantation
D_r	Aerodynamic diameter of the tree row
D_t	Aerodynamic diameter of the tree unit
D_{hill}	Aerodynamic diameter of the hill
D_{hwt}	Aerodynamic diameter on top of a hill
D_{ref}	Hydraulic Diameter
D_{wt}	Aerodynamic diameter of the wind turbine over flat terrain
E	Geometric scale
e_l	Streamwise distance between trees
Ef	Turbine efficiency
ET	Evapotranspiration
f	Frequency
h	Hill height
h_t	Tree height
H_{obs}	Obstacle total height
H_{wt}	Wind turbine total height
IT	Turbulence Intensity
ITc	Turbulence Intensity comparison
L	Hill length (Chapter 4)
L	Overall agro-forest length (Chapter 3)
L_s	Distance between hill and wind turbine
L_u	Longitudinal length scale
m	Air mass
n	Frequency

P	Production term
P_w	Theoretical power
PSD	Power Spectral Density
R	Turbine-blade radius
r_I	Ratio between the turbulence intensities
r_r	Aerodynamic row radius
R_U	Ratio between mean velocities
r_U	Ratio between the mean wind velocities
R_{IT}	Ratio between the turbulence intensities
Re	Reynolds number
Re_p	Reynolds number for plantation
Re_r	Reynolds number for tree row
Re_t	Reynolds number for each tree
Re_x	Reynolds number in the x direction
Re_{hill}	Reynolds number for the hill over flat terrain
Re_{hwt}	Reynolds number for the wind turbine on top of a hill
Re_{ref}	Reynolds number of reference
Re_{wt2}	Reynolds number for the wind turbine over flat terrain and behind a hill
Re_{wt}	Reynolds number for the wind turbine over flat terrain
S_u	Espectral density function of u
S_w	Skewness
t	Time
t_r	Tree crown radius
TKE	Turbulent Kinetic Energy
U	Mean wind velocity
u	Instantaneous wind velocity

u'	Gust velocity
u_*	Friction velocity
u_*^2	Kinematic momentum flux
U_l	Instantaneous wind velocity
U_o	Input/reference wind velocity
Uc	Mean velocity comparison
w	Vertical component of the velocity vector
WTW	Wind Tunnel Width
x	Streamwise distance
z	Height
z_b	Thickness of the boundary layer
z_h	Wind turbine tower height
z_o	Aerodynamic surface roughness length

Greek symbols

δ	Boundary layer thickness
λ	Scale ratio
μ	Air dynamic viscosity
μ_a	Air dynamic viscosity
ν_a	Air kinematic viscosity
ρ	Air density
ρ_a	Air density
σ	Standard deviation
σ^2	Variance
τ	Stress
φ_U	Variation rate for U

φ_{IT} Variation rate for IT

φ_{TKE} Variation rate for TKE

Constants

C Constant for smooth-walled flows

g Gravitational acceleration

Je Jensen number

k Von Karman constant

Acronyms

ABL Atmospheric Boundary Layer

$BLWT$ Boundary Layer Wind Tunnel

$CCWT$ Closed Circuit Wind Tunnel

CET Centre of Excellence Telč

CFD Computational Fluid Dynamics

FFT Fast Fourier Transform

GPS Global Positioning System

GSM Global System for Mobile

HWA Hot Wire Anemometer

$IISTA$ Andalusian Institute for Earth System Research

$ITAM$ Institute of Theoretical and Applied Mechanics

$NDVI$ Normalized Difference Vegetation Index

$OCWT$ Open Circuit Wind Tunnel

PIV Particle Velocimetry Image

SBL Surface Boundary Layer

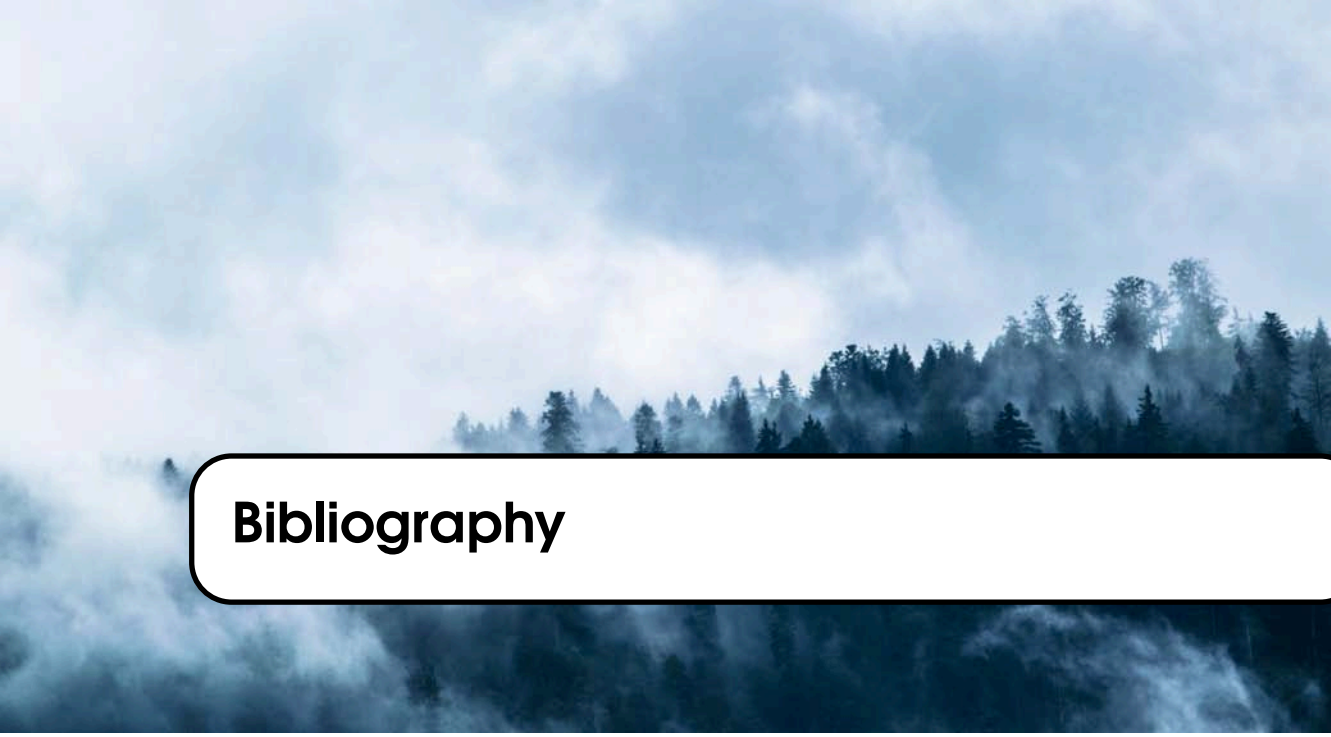

Bibliography

Books

AEE (2020). *Anuario Eólico 2020. Toda la información del sector en el año 2019*. AEE - Asociación Empresarial Eólica (cited on pages 112, 113).

Atienza, J. C., Fierro, I. M., Infante, O., Valls, J., and Domínguez, J. (2012). *Directrices para la evaluación del impacto de los parques eólicos en aves y murciélagos*. Volume 1 (cited on pages 176, 177).

Barlow, J. B., Rae, W. H., and Pope, A. (1999). *Low-speed wind tunnel testing*. John Wiley & Sons (cited on pages 50, 51).

Ghislanzoni, M., Dacal, M. R., and Clavero, F. C. (2014). *Guía de integración paisajística de parques eólicos en Andalucía*. Consejería de Medio Ambiente y Ordenación del Territorio. Junta de Andalucía, page 291 (cited on pages 113, 179).

Gómez, J. A. (2009). *Sostenibilidad de la producción de olivar en Andalucía* (cited on page 82).

Guzmán-Álvarez, J. R., Gómez, J. A., and Rallo, L. (2009). *El olivar en Andalucía: lecciones para el futuro de un cultivo milenario*, pages 7–19 (cited on page 82).

Jiménez-Portaz, M., Losada, M. A., Polo, M. J., Donázar, J. A., and Ibáñez, C. (2017). *Recomendaciones para la Evaluación Ambiental de Parques Eólicos en*

Andalucía. Consejería de Economía, Innovación, Ciencia y Empleo.Junta de Andalucía, page 94 (cited on page 187).

Kaimal, J. C. and Finnigan, J. J. (1994). *Atmospheric boundary layer flows: their structure and measurement*. Oxford university press (cited on page 52).

Krogerus, M. and Tschäppeler, R. (2012). *The decision book: 50 models for strategic thinking*. WW Norton & Company (cited on page 186).

Ley de 9 de julio (7/2007). *Gestión Integrada de la Calidad Ambiental*. Comunidad Autónoma de Andalucía (cited on page 164).

Ley de 9 de diciembre (21/2013). *De evaluación ambiental*. Jefatura del Estado (cited on page 164).

Longo, S. (2011). *Analisi Dimensionale e Modellistica Fisica: Principi e applicazioni alle scienze ingegneristiche*. Springer Science and Business Media (cited on page 85).

— (2021). *Dimensional Analysis and Physical Modelling*. Springer (cited on page 105).

Nieuwstadt, F. T., Westerweel, J., and Boersma, B. J. (2016). *Turbulence: introduction to theory and applications of turbulent flows*. Springer (cited on page 62).

ROM 1.1-18 (2018). *ROM 1.1. Recomendaciones para el Proyecto de Construcción de Diques de Abrigo*. Puertos del Estado (cited on page 170).

Schlichting, H. and Gersten, K. (2016). *Boundary-layer theory*. Springer (cited on pages 61, 64).

Simiu, E. and Yeo, D. (2019). *Wind effects on structures: Modern structural design for wind*. John Wiley & Sons (cited on page 50).

Solari, G. (2019). *Wind Science and Engineering Origins, Developments, Fundamentals and Advancements*. en. Cham: Springer (cited on page 105).

Stull, R. (2016). *Practical Meteorology: an algebra based survey of atmospheric science*. BC Campus, page 12 (cited on pages 40, 61, 114, 115, 172).

Toy, T. J., Foster, G. R., and Renard, K. G. (2002). *Soil erosion: processes, prediction, measurement, and control*. John Wiley & Sons (cited on page 173).

Uruba, V. (2012). *Turbulence Handbook for Experimental Fluid Mechanics Professionals*. Skovlunde: Dantec Dynamic (cited on page 62).

Whiteman, C. D. (2000). *Mountain meteorology: fundamentals and applications*. Oxford University Press (cited on page 37).

Articles

Albrecht, A. T., Jung, C., and Schindler, D. (2019). "Improving empirical storm damage models by coupling with high-resolution gust speed data". In: *Agricultural and forest meteorology* 268, pages 23–31 (cited on page 83).

Ali, N., Hamilton, N., Calaf, M., and Cal, R. B. (2019). "Turbulence kinetic energy budget and conditional sampling of momentum, scalar, and intermittency fluxes

in thermally stratified wind farms". In: *Journal of Turbulence* 20.1, pages 32–63 (cited on page 158).

Aly, A. M. and Gol-Zaroudi, H. (2017). "Atmospheric boundary layer simulation in a new open-jet facility at LSU: CFD and experimental investigations". In: *Measurement: Journal of the International Measurement Confederation* 110, pages 121–133 (cited on page 51).

Arnqvist, J., Segalini, A., Dellwik, E., and Bergström, H. (2015). "Wind Statistics from a Forested Landscape". en. In: *Boundary-Layer Meteorology* 156.1, pages 53–71 (cited on page 83).

Banta, R. M., Pichugina, Y. L., Brewer, W. A., Lundquist, J. K., Kelley, N. D., Sandberg, S. P., II, R. J. A., Hardesty, R. M., and Weickmann, A. M. (2015). "3D Volumetric Analysis of Wind Turbine Wake Properties in the Atmosphere Using High-Resolution Doppler Lidar". In: *Journal of Atmospheric and Oceanic Technology* 32.5, pages 904–914 (cited on pages 172, 179).

Barlas, E., Buckingham, S., and Beeck, J. van (2016). "Roughness effects on wind-turbine wake dynamics in a boundary-layer wind tunnel". In: *Boundary-Layer Meteorology* 158.1, pages 27–42 (cited on page 141).

Baudena, M., D'Andrea, F., and Provenzale, A. (2008). "A model for soil-vegetation-atmosphere interactions in water-limited ecosystems". In: *Water Resources Research* 44.12 (cited on page 41).

Beckman, N. G., Aslan, C. E., Rogers, H. S., Kogan, O., Bronstein, J. L., Bullock, J. M., Hartig, F., HilleRisLambers, J., Zhou, Y., Zurell, D., Brodie, J. F., Bruna, E. M., Cantrell, R. S., Decker, R. R., Efiom, E., Fricke, E. C., Gurski, K., Hastings, A., Johnson, J. S., Loiselle, B. A., Miriti, M. N., Neubert, M. G., Pejchar, L., Poulsen, J. R., Pufal, G., Razafindratsima, O. H., Sandor, M. E., Shea, K., Schreiber, S., Schupp, E. W., Snell, R. S., Strickland, C., and Zambrano, J. (2020). "Advancing an interdisciplinary framework to study seed dispersal ecology". en. In: *AoB PLANTS* 12.2. Publisher: Oxford Academic (cited on page 175).

Belcher, S. E., Harman, I. N., and Finnigan, J. J. (2012). "The Wind in the Willows: Flows in Forest Canopies in Complex Terrain". en. In: *Annual Review of Fluid Mechanics* 44.1, pages 479–504 (cited on page 82).

Brunet, Y. (2020). "Turbulent Flow in Plant Canopies: Historical Perspective and Overview". en. In: *Boundary-Layer Meteorology* 177.2-3, pages 315–364 (cited on pages 82, 83).

Cáceres, F., Romero, D., Guerrero, J. J., Ghislanzoni, M., Giménez de Azcárate, F., and Moreira, J. M. (2014). "Parametrización numérica de las relaciones visuales del territorio: el Sistema de Visibilidad de Andalucía. REDIAM". In: (cited on page 179).

Carlier, J. and Stanislas, M. (2005). "Experimental study of eddy structures in a turbulent boundary layer using particle image velocimetry". In: *Journal of Fluid Mechanics* 535, page 143 (cited on page 73).

Carriger, J. F., Barron, M. G., and Newman, M. C. (2016). "Bayesian Networks Improve Causal Environmental Assessments for Evidence-Based Policy". In: *Environmental science & technology* 50.24, pages 13195–13205 (cited on page 168).

Cattafesta, L., Bahr, C., and Mathew, J. (2010). "Fundamentals of wind-tunnel design". In: *Encyclopedia of Aerospace Engineering* (cited on page 79).

Chamorro, L. P. and Porté-Agel, F. (2009). "A wind-tunnel investigation of wind-turbine wakes: boundary-layer turbulence effects". In: *Boundary-layer meteorology* 132.1, pages 129–149 (cited on page 116).

Chamorro, L. P., Arndt, R., and Sotiropoulos, F. (2012). "Reynolds number dependence of turbulence statistics in the wake of wind turbines". In: *Wind Energy* 15.5, pages 733–742 (cited on pages 61, 126, 157).

Chamizo, S., Serrano-Ortiz, P., López-Ballesteros, A., Sánchez-Cañete, E. P., Vicente-Vicente, J. L., and Kowalski, A. S. (2017). "Net ecosystem CO2 exchange in an irrigated olive orchard of SE Spain: Influence of weed cover". In: *Agriculture, Ecosystems & Environment* 239, pages 51–64 (cited on pages 82, 84).

Champagne, F., Harris, V., and Corrsin, S. (1970). "Experiments on nearly homogeneous turbulent shear flow". In: *Journal of Fluid Mechanics* 41.1, pages 81–139 (cited on pages 69, 70).

Cheng, X. X., Dong, J., Peng, Y., Zhao, L., and Ge, Y. J. (2017). "Full-Scale / Model Test Comparisons to Validate the Traditional ABL Wind Tunnel Simulation Technique : A Literature Review". In: *Preprint* (cited on page 51).

Cheng, H., Liu, C., and Kang, L. (2020). "Experimental study on the effect of plant spacing, number of rows and arrangement on the airflow field of forest belt in a wind tunnel". In: *Journal of Arid Environments* 178, page 104169 (cited on pages 83, 94).

Cleugh, H. (1998). "Effects of windbreaks on airflow, microclimates and crop yields". In: *Agroforestry systems* 41.1, pages 55–84 (cited on pages 83, 109).

Cotté, B. (2019). "Extended source models for wind turbine noise propagation". In: *The Journal of the Acoustical Society of America* 145.3. Publisher: Acoustical Society of America, pages 1363–1371 (cited on page 178).

Coudou, N., Buckingham, S., and Beeck, J. van (2017). "Experimental study on the wind-turbine wake meandering inside a scale model wind farm placed in an atmospheric-boundary-layer wind tunnel". In: 854, page 012008 (cited on page 50).

Cuesta Cañas, J. A. et al. (2008). "Comportamiento aerodinámico de un dispositivo ahuyenta aves y estudio de campos de viento sobre topografía compleja". In: (cited on page 56).

Cuevas, P., Biberacher, M., Domínguez-Bravo, J., and Schardinger, I. (2018). "Developing a wind energy potential map on a regional scale using GIS and multi-criteria decision methods: the case of Cadiz (south of Spain)". en. In: *Clean Tech-*

nologies and Environmental Policy 20.6, pages 1167–1183 (cited on pages 112, 116).

Dellwik, E., Laan, M. P. van der, Angelou, N., Mann, J., and Sogachev, A. (2019). "Observed and modeled near-wake flow behind a solitary tree". In: *Agricultural and Forest Meteorology* 265, pages 78–87 (cited on page 83).

Díaz Cuevas, M. d. P., Pita López, M. F., Fernández Tabales, A., and Limones Rodríguez, N. (2017). "Energía eólica y territorio en Andalucía: diseño y aplicación de un modelo de potencialidad para la implantación de parques eólicos". In: *Universidad de Alicante. Instituto Interuniversitario de Geografía* (cited on page 170).

Dupont, S., Brunet, Y., and Jarosz, N. (2006). "Eulerian modelling of pollen dispersal over heterogeneous vegetation canopies". en. In: *Agricultural and Forest Meteorology* 141.2-4, pages 82–104 (cited on pages 82, 108).

Dupont, S., Défossez, P., Bonnefond, J.-M., Irvine, M. R., and Garrigou, D. (2018). "How stand tree motion impacts wind dynamics during windstorms". In: *Agricultural and Forest Meteorology* 262, pages 42–58 (cited on page 83).

ESDU, I. (2001). "Characteristics of Atmospheric Turbulence Near the Ground—Part II: Single Point Data for Strong Winds (Neutral Atmosphere)". In: *Engineering Sciences Data Unit, IHS Inc., London, UK, Report No. ESDU* 85020 (cited on page 52).

Fiedler, B. and Bukovsky, M. (2011). "The effect of a giant wind farm on precipitation in a regional climate model". In: *Environmental Research Letters* 6.4, page 045101 (cited on page 172).

Floors, R., Enevoldsen, P., Davis, N., Arnqvist, J., and Dellwik, E. (2018). "From lidar scans to roughness maps for wind resource modelling in forested areas". en. In: page 18 (cited on page 191).

Florescu, A., Barabas, S., and Dobrescu, T. (2019). "Research on Increasing the Performance of Wind Power Plants for Sustainable Development". en. In: *Sustainability* 11.5. Number: 5 Publisher: Multidisciplinary Digital Publishing Institute, page 1266 (cited on page 112).

Freiberg, A., Schefter, C., Girbig, M., Murta, V. C., and Seidler, A. (2019). "Health effects of wind turbines on humans in residential settings: Results of a scoping review". en. In: *Environmental Research* 169, pages 446–463. (Visited on 09/07/2020) (cited on page 180).

Frenkiel, J. (1962). "Wind profiles over hills (in relation to wind-power utilization)". In: *Quarterly Journal of the Royal Meteorological Society* 88.376, pages 156–169 (cited on pages 148, 158).

Gao, L., Wang, X., Johnson, B. A., Tian, Q., Wang, Y., Verrelst, J., Mu, X., and Gu, X. (2020). "Remote sensing algorithms for estimation of fractional vegetation cover using pure vegetation index values: A review". en. In: *ISPRS Journal of Photogrammetry and Remote Sensing* 159, pages 364–377 (cited on page 175).

García-Morales, R. M., Baquerizo, A., and Losada, M. Á. (2015). "Port management and multiple-criteria decision making under uncertainty". English. In: *Ocean Engineering* 104, pages 31–39 (cited on page 170).

Gardiner, B., Achim, A., Nicoll, B., and Ruel, J.-C. (2019). "Understanding the interactions between wind and trees: an introduction to the IUFRO 8th Wind and Trees Conference". In: *Forestry: An International Journal of Forest Research* 92.4, pages 375–380 (cited on page 83).

Giometto, M., Christen, A., Egli, P., Schmid, M., Tooke, R., Coops, N., and Parlange, M. (2017). "Effects of trees on mean wind, turbulence and momentum exchange within and above a real urban environment". en. In: *Advances in Water Resources* 106, pages 154–168 (cited on page 83).

Gómez-Giráldez, P. J., Aguilar, C., and Polo, M. J. (2014). "Natural vegetation covers as indicators of the soil water content in a semiarid mountainous watershed". In: *Ecological indicators* 46, pages 524–535 (cited on page 175).

Gómez-Zotano, J., Alcántara-Manzanares, J., Olmedo-Cobo, J. A., and Martínez-Ibarra, E. (2015). "La sistematización del clima mediterráneo: identificación, clasificación y caracterización climática de Andalucía (España)". In: *Revista de Geografía Norte Grande* 61, pages 161–180 (cited on page 37).

Gómez-Giráldez, P. J., Aguilar, C., Caño, A. B., García-Moreno, A., and González-Dugo, M. P. (2019). "Remote sensing estimation of net primary production as monitoring indicator of holm oak savanna management". In: *Ecological Indicators* 106, page 105526 (cited on page 169).

Gromke, C. (2018). "Wind tunnel model of the forest and its Reynolds number sensitivity". In: *Journal of Wind Engineering and Industrial Aerodynamics* 175, pages 53–64 (cited on pages 50, 83).

Haghighi, E. and Kirchner, J. (2016). "A process-based evapotranspiration model incorporating coupled soil water-atmospheric controls". In: *EGU General Assembly 2016, held 17-22 April, 2016 in Vienna Austria* 18 (cited on page 41).

Hao, Y., Kopp, G. A., Wu, C.-H., and Gillmeier, S. (2020). "A wind tunnel study of the aerodynamic characteristics of a scaled, aeroelastic, model tree". In: *Journal of Wind Engineering and Industrial Aerodynamics* 197, page 104088 (cited on page 50).

Haywood, J. S., Sescu, A., and Adkins, K. A. (2020). "Large eddy simulation study of the humidity variation in the shadow of a large wind farm". en. In: *Wind Energy* 23.2, pages 423–431 (cited on page 172).

He, Y., Chan, P., and Li, Q. (2014). "Standardization of raw wind speed data under complex terrain conditions: A data-driven scheme". In: *Journal of Wind Engineering and Industrial Aerodynamics* 131, pages 12–30 (cited on pages 116, 158).

Hesp, P. A., Dong, Y., Cheng, H., and Booth, J. L. (2019). "Wind flow and sedimentation in artificial vegetation: Field and wind tunnel experiments". en. In: *Geomorphology* 337, pages 165–182 (cited on page 83).

Hogan, R. J., Grant, A. L., Illingworth, A. J., Pearson, G. N., and O'Connor, E. J. (2009). "Vertical velocity variance and skewness in clear and cloud-topped boundary layers as revealed by Doppler lidar". In: *Quarterly Journal of the Royal Meteorological Society: A journal of the atmospheric sciences, applied meteorology and physical oceanography* 135.640, pages 635–643 (cited on pages 71, 89, 103).

Hong, Y., Kim, D., and Im, S. (2016). "Assessing the vegetation canopy influences on wind flow using wind tunnel experiments with artificial plants". In: *Journal of Earth System Science* 125.3, pages 499–506 (cited on page 83).

Iglesias, A., Garrote, L., Flores, F., and Moneo, M. (2007). "Challenges to manage the risk of water scarcity and climate change in the Mediterranean". In: *Water Resources Management* 21.5, pages 775–788 (cited on page 38).

Jeong, S.-H. and Lee, S.-H. (2020). "Effects of windbreak Forest according to tree species and planting methods based on wind tunnel experiments". In: *Forest Science and Technology* 16.4, pages 188–194 (cited on page 83).

Jiménez-Portaz, M., Bello-Millán, F., Folgueras, P., Clavero, M., and Losada, M. (2016). "Wind flow around a wind turbine system over hilly terrain and its environmental effects: wind tunnel tests". In: *ICREPQ* (cited on pages 56, 115, 170, 172).

Jiménez-Portaz, M., Clavero, M., and Losada, M. (2019). "Experimental Analysis of Wind Interaction with Olive Grove and the Atmospheric Surface Boundary Layer". In: *European Journal of Sustainable Development* 8.5, pages 180–180 (cited on page 56).

Jiménez-Portaz, M., Chiapponi, L., Clavero, M., and Losada, M. A. (2020a). "Air flow quality analysis of an open-circuit boundary layer wind tunnel and comparison with a closed-circuit wind tunnel". In: *Physics of Fluids* 32.12, page 125120 (cited on pages 84, 94, 105).

Jiménez-Portaz, M., Del-Rosal-Salido, J., Clavero, M., Pospisil, S., and Ortega, M. (2020b). "Hot Wire Anemometry and Particle Image Velocimetry techniques comparison for wind tunnel measurements". In: *Abstract book: IAHR Europe Congress*, page 852 (cited on page 148).

Jiménez-Portaz, M., Clavero, M., and Losada, M. Á. (2021). "A New Methodology for Assessing the Interaction between the Mediterranean Olive Agro-Forest and the Atmospheric Surface Boundary Layer". In: *Atmosphere* 12.6, page 658 (cited on page 108).

Johnson, D. H., Loss, S. R., Smallwood, K. S., and Erickson, W. P. (2016). "Avian fatalities at wind energy facilities in North America: a comparison of recent approaches". In: *Human–Wildlife Interactions* 10.1, page 3 (cited on page 176).

Kamada, Y., Maeda, T., Yamada, K., et al. (2019). "Wind tunnel experimental investigation of flow field around two-dimensional single hill models". In: *Renewable Energy* 136, pages 1107–1118 (cited on page 148).

Kamimura, K., Gardiner, B., Dupont, S., and Finnigan, J. (2019). "Agent-based modelling of wind damage processes and patterns in forests". In: *Agricultural and forest meteorology* 268, pages 279–288 (cited on page 83).

Katsaprakakis, D. A. (2012). "A review of the environmental and human impacts from wind parks. A case study for the Prefecture of Lasithi, Crete". In: *Renewable and Sustainable Energy Reviews* 16.5, pages 2850–2863 (cited on page 180).

Keith, S. E., Michaud, D. S., Feder, K. P., Soukhovtsev, V., Voicescu, S. A., Denning, A. R., Tsang, J., Broner, N., and Richarz, W. G. (2019). "Wind turbine audibility calculations inside dwellings". In: *The Journal of the Acoustical Society of America* 145.4. Publisher: Acoustical Society of America, pages 2435–2444 (cited on page 178).

Kozmar, H. and Laschka, B. (2019). "Wind-tunnel modeling of wind loads on structures using truncated vortex generators". In: *Journal of Fluids and Structures* 87, pages 334–353 (cited on page 65).

Kuznetsov, S., Ribičić, M., Pospíšil, S., Plut, M., Trush, A., and Kozmar, H. (2017). "Flow and turbulence control in a boundary layer wind tunnel using passive hardware devices". In: *Experimental Techniques* 41.6, pages 643–661 (cited on page 74).

Laranjeiro, T., May, R., and Verones, F. (2018). "Impacts of onshore wind energy production on birds and bats: recommendations for future life cycle impact assessment developments". en. In: *The International Journal of Life Cycle Assessment* 23.10, pages 2007–2023 (cited on pages 176, 177).

Lindman, Å. and Söderholm, P. (2016). "Wind energy and green economy in Europe: Measuring policy-induced innovation using patent data". In: *Applied energy* 179, pages 1351–1359 (cited on page 112).

Lionello, P., Özsoy, E., Planton, S., and Zanchetta, G. (2017). "Climate Variability and Change in the Mediterranean Region". en. In: *Global and Planetary Change* 151, pages 1–3 (cited on page 37).

Liu, C., Zheng, Z., Cheng, H., and Zou, X. (2018). "Airflow around single and multiple plants". In: *Agricultural and Forest Meteorology* 252, pages 27–38 (cited on page 83).

López-Ruiz, A., Bergillos, R. J., Lira-Loarca, A., and Ortega-Sánchez, M. (2018). "A methodology for the long-term simulation and uncertainty analysis of the operational lifetime performance of wave energy converter arrays". In: *Energy* 153, pages 126–135 (cited on page 170).

Manickathan, L., Defraeye, T., Allegrini, J., Derome, D., and Carmeliet, J. (2018). "Comparative study of flow field and drag coefficient of model and small natural trees in a wind tunnel". In: *Urban Forestry & Urban Greening* 35, pages 230–239 (cited on page 92).

Martín Rodríguez, P., Martín Rodríguez, E., Loredo-Souza, A., and Camano Schettini, E. B. (2014). "Utilización de anemómetro de hilo caliente a temperatura

constante para mediciones de velocidad de aire en túnel de viento". In: *Ingeniería Electrónica, Automática y Comunicaciones* 35.1, pages 78–92 (cited on page 53).

Mattuella, J. M. L., Loredo-Souza, A., Oliveira, M. G. K., and Petry, A. P. (2016). "Wind tunnel experimental analysis of a complex terrain micrositing". In: *Renewable and Sustainable Energy Reviews* 54, pages 110–119 (cited on page 51).

May, R., Hamre, Ø., Vang, R., and Nygård, T. (2012). "Evaluation of the DTBird video-system at the Smøla wind-power plant". In: *Detection capabilities for capturing near-turbine avian behaviour. NINA Report* 910, page 27 (cited on page 177).

McCunney, R. J., Mundt, K. A., Colby, W. D., Dobie, R., Kaliski, K., and Blais, M. (2014). "Wind turbines and health: A critical review of the scientific literature". In: *Journal of Occupational and Environmental Medicine* 56.11, e108–e130 (cited on page 178).

Medici, Davide and Alfredsson, PH (2006). "Measurements on a wind turbine wake: 3D effects and bluff body vortex shedding". In: *Wind Energy* 9.3, pages 219–236 (cited on page 158).

Mendoza, C. D. (2011). "Alternatives for erosion control by using conventional coverage, non-conventional coverage and revegetation". In: *Revista Ingenieria E Investigacion* 31.3, pages 80–90 (cited on page 174).

Miller, L. M. and Keith, D. W. (2018). "Climatic Impacts of Wind Power". en. In: *Joule* 2.12, pages 2618–2632 (cited on page 172).

Montaldo, N., Curreli, M., Corona, R., and Oren, R. (2020). "Fixed and variable components of evapotranspiration in a Mediterranean wild-olive - grass landscape mosaic". en. In: *Agricultural and Forest Meteorology* 280, page 107769 (cited on pages 104, 108).

Moon, M., Li, D., Liao, W., Rigden, A. J., and Friedl, M. A. (2020). "Modification of surface energy balance during springtime: The relative importance of biophysical and meteorological changes". In: *Agricultural and Forest Meteorology* 284, page 107905 (cited on pages 83, 105).

Nathan, R., Katul, G. G., and Bohrer, G. (2011). "Mechanistic models of seed dispersal by wind". In: *Theoretical Ecology* (cited on page 175).

Nemitz, E., Loubet, B., Lehmann, B. E., Cellier, P., Neftel, A., Jones, S. K., Hensen, A., Ihly, B., Tarakanov, S. V., and Sutton, M. A. (2009). "Turbulence characteristics in grassland canopies and implications for tracer transport". en. In: page 19 (cited on page 83).

Obrist, M. and Boesch, R. (2018). "BatScope manages acoustic recordings, analyses calls, and classifies bat species automatically". In: *CJZ Virtual Special Issues* 01.03. Publisher: NRC Research Press, pages 939–954 (cited on page 176).

Om Ariara Guhan, C., Arthanareeswaran, G., Varadarajan, K., and Krishnan, S. (2016). "Numerical optimization of flow uniformity inside an under body-oval

substrate to improve emissions of IC engines". In: *Journal of Computational Design and Engineering* 3.3, pages 198–214 (cited on page 77).

Orlandi, F., Rojo, J., Picornell, A., Oteros, J., Pérez-Badia, R., and Fornaciari, M. (2020). "Impact of Climate Change on Olive Crop Production in Italy". en. In: *Atmosphere* 11.6, page 595 (cited on page 82).

Paço, T. A., Pôças, I., Cunha, M., Silvestre, J. C., Santos, F. L., Paredes, P., and Pereira, L. S. (2014). "Evapotranspiration and crop coefficients for a super intensive olive orchard. An application of SIMDualKc and METRIC models using ground and satellite observations". In: *Journal of Hydrology* 519, pages 2067–2080 (cited on page 108).

Pan, X., Wang, Z., Gao, Y., Zhang, Z., Meng, Z., Dang, X., Lu, L., and Chen, J. (2020). "Windbreak and airflow performance of different synthetic shrub designs based on wind tunnel experiments". In: *Plos one* 15.12, e0244213 (cited on pages 107, 109).

Podhrázská, J., Kučera, J., Doubrava, D., and Doležal, P. (2021). "Functions of Windbreaks in the Landscape Ecological Network and Methods of Their Evaluation". In: *Forests* 12.1, page 67 (cited on pages 107, 109).

Poëtte, C., Gardiner, B., Dupont, S., Harman, I., Böhm, M., Finnigan, J., Hughes, D., and Brunet, Y. (2017). "The Impact of Landscape Fragmentation on Atmospheric Flow: A Wind-Tunnel Study". en. In: *Boundary-Layer Meteorology* 163.3, pages 393–421 (cited on pages 82, 83).

Polo, M., Herrero, J., Aguilar, C., Millares, A., Moñino, A., Nieto, S., and Losada, M. (2009). "WiMMed, a distributed physically-based watershed model (I): Description and validation". In: *Environmental Hydraulics: Theoretical, Experimental & Computational Solutions*, pages 225–228 (cited on page 169).

Porté-Agel, F., Bastankhah, M., and Shamsoddin, S. (2020). "Wind-Turbine and Wind-Farm Flows: A Review". en. In: *Boundary-Layer Meteorology* 174.1, pages 1–59 (cited on pages 115–117, 142, 143, 154, 172, 173, 181).

Quill, R., Sharples, J. J., and Sidhu, L. A. (2020). "A Statistical Approach to Understanding Canopy Winds over Complex Terrain". en. In: *Environmental Modeling & Assessment* 25.2, pages 231–250 (cited on pages 82, 108).

Ramli, N. I., Ali, M. I., Saad, M. S. H., and Majid, T. (2009). "Estimation of the roughness length (zo) in Malaysia using satellite image". In: *Wind Engineering* (cited on page 53).

Redfern, S., Olson, J. B., Lundquist, J. K., and Clack, C. T. M. (2019). "Incorporation of the Rotor-Equivalent Wind Speed into the Weather Research and Forecasting Model's Wind Farm Parameterization". en. In: *Monthly Weather Review* 147.3. Publisher: American Meteorological Society, pages 1029–1046 (cited on page 172).

Rodríguez Folgueras, P. et al. (2012). "Caracterización del campo de vientos a sotavento de un aerogenerador marino. Influencia de la inclinación del rotor sobre el afloramiento de aguas profundas". In: (cited on page 56).

Roy, S. B. and Traiteur, J. J. (2010). "Impacts of wind farms on surface air temperatures". In: *Proceedings of the National Academy of Sciences* 107.42, pages 17899–17904 (cited on page 172).

Roy, S. B. (2011). "Simulating impacts of wind farms on local hydrometeorology". In: *Journal of Wind Engineering and Industrial Aerodynamics* 99.4, pages 491–498 (cited on page 172).

Rücknagel, J., Hofmann, B., Deumelandt, P., Reinicke, F., Bauhardt, J., Hülsbergen, K.-J., and Christen, O. (2015). "Indicator based assessment of the soil compaction risk at arable sites using the model REPRO". In: *Ecological Indicators* 52, pages 341–352 (cited on page 174).

Safi, K., Kranstauber, B., Weinzierl, R., Griffin, L., Rees, E. C., Cabot, D., Cruz, S., Proaño, C., Takekawa, J. Y., Newman, S. H., Waldenström, J., Bengtsson, D., Kays, R., Wikelski, M., and Bohrer, G. (2013). "Flying with the wind: scale dependency of speed and direction measurements in modelling wind support in avian flight". In: *Movement Ecology* 1.1, page 4 (cited on page 176).

Samhouri, J. F., Levin, P. S., and Ainsworth, C. H. (2010). "Identifying thresholds for ecosystem-based management". In: *PLoS ONE* 5.1, e8907 (cited on page 168).

Santos-Alamillos, F., Thomaidis, N. S., Usaola-García, J., Ruiz-Arias, J., and Pozo-Vázquez, D. (2017). "Exploring the mean-variance portfolio optimization approach for planning wind repowering actions in Spain". In: *Renewable Energy* 106, pages 335–342 (cited on page 186).

Sánchez-Navarro, S., Rydell, J., and Ibáñez, C. (2019). "Bat fatalities at wind-farms in the lowland Mediterranean of southern Spain". In: *Acta Chiropterologica* 21.2, pages 349–358 (cited on page 177).

Sanz-Rubiales, I. (2010). "Los Efectos Ambientales Acumulativos de los Parques Eolicos. Su Evaluacion Articulos Doctrinales: Derecho Administrativo". eng. In: *Revista Juridica de Castilla y Leon* 21, pages 185–216 (cited on page 164).

Schindler, D. and Mohr, M. (2019). "No resonant response of Scots pine trees to wind excitation". In: *Agricultural and forest meteorology* 265, pages 227–244 (cited on page 83).

Schippers, P., Buij, R., Schotman, A., Verboom, J., Jeugd, H. v. d., and Jongejans, E. (2020). "Mortality limits used in wind energy impact assessment underestimate impacts of wind farms on bird populations". en. In: *Ecology and Evolution* 10.13, pages 6274–6287 (cited on page 177).

Sedaghatizadeh, N., Arjomandi, M., Cazzolato, B., and Kelso, R. (2017). "Wind farm noises: Mechanisms and evidence for their dependency on wind direction". In: *Renewable Energy* 109, pages 311–322 (cited on page 178).

Segalini, A., Fransson, J. H. M., and Alfredsson, P. H. (2013). "Scaling Laws in Canopy Flows: A Wind-Tunnel Analysis". en. In: page 15 (cited on pages 83, 102).

Segalini, A. (2017). "Linearized simulation of flow over wind farms and complex terrains". In: *Philosophical Transactions of the Royal Society A: Mathematical, Physical and Engineering Sciences* 375.2091. Publisher: Royal Society (cited on page 173).

Sequeira, T. N. and Santos, M. S. (2018). "Renewable energy and politics: A systematic review and new evidence". en. In: *Journal of Cleaner Production* 192, pages 553–568 (cited on page 164).

Shen, W. Z., Zhu, W. J., Barlas, E., and Li, Y. (2019). "Advanced flow and noise simulation method for wind farm assessment in complex terrain". en. In: *Renewable Energy* 143, pages 1812–1825 (cited on page 178).

Sklenicka, P. and Zouhar, J. (2018). "Predicting the visual impact of onshore wind farms via landscape indices: A method for objectivizing planning and decision processes". en. In: *Applied Energy* 209, pages 445–454 (cited on page 179).

Solari, S. and Losada, M. (2016). "Simulation of non-stationary wind speed and direction time series". In: *Journal of Wind Engineering and Industrial Aerodynamics* 149, pages 48–58 (cited on page 169).

Sonin, A. A. (2001). "The physical basis of dimensional analysis". In: *Department of Mechanical Engineering, MIT, Cambridge, MA*, pages 1–57 (cited on page 85).

Takahashi, K. (2018). "Incorporating a tensor in the effective viscosity model of turbulence and the Reynolds stress". In: *AIMS Mathematics* 3.4, page 554 (cited on page 69).

Theodorsen, T. (1952). "Mechanisms of turbulence". In: *Proceedings of the Midwestern Conference on Fluid Mechanics* (cited on pages 60, 73).

Tian, Y., Yang, Q., Yang, N., Li, B., and Chen, B. (2011). "Statistical spectrum model of wind velocity at Beijing Meteorological Tower". In: *Science China Technological Sciences* 54.11, page 2869 (cited on page 66).

Varshney, K. and Poddar, K. (2011). "Experiments on integral length scale control in atmospheric boundary layer wind tunnel". In: *Theoretical and applied climatology* 106.1-2, pages 127–137 (cited on page 51).

Vifard, S., Skidmore, A. K., Naimi, B., Venus, V., Muñoz, A. R., and Toxopeus, A. G. (2020). "Identifying Birds' Collision Risk with Wind Turbines Using a Multidimensional Utilization Distribution Method". In: *Wildlife Society Bulletin* 44.1, pages 191–199 (cited on page 176).

Villarroya, A. and Puig, J. (2010). "Ecological compensation and Environmental Impact Assessment in Spain". In: *Environmental Impact Assessment Review* 30.6, pages 357–362 (cited on page 164).

Viola, F., Caracciolo, D., Pumo, D., and Noto, L. V. (2013). "Olive yield and future climate forcings". In: *Procedia Environmental Sciences* 19, pages 132–138 (cited on page 104).

Vlami, V., Danek, J., Zogaris, S., Gallou, E., Kokkoris, I. P., Kehayias, G., and Dimopoulos, P. (2020). "Residents' Views on Landscape and Ecosystem Services

during a Wind Farm Proposal in an Island Protected Area". In: *Sustainability* 12.6, page 2442 (cited on page 180).

Voutsinas, S., Glekas, J., and Zervos, A. (1992). "Investigation of the effect of the initial velocity profile on the wake development of a wind turbine". In: *Journal of Wind Engineering and Industrial Aerodynamics* 39.1-3, pages 293–301 (cited on page 125).

Wang, C. and Prinn, R. (2017). "Potential climatic impacts and reliability of very large-scale wind farms". In: *Climate Change and the Future of Sustainability*, page 23 (cited on page 172).

Wei, X., Dupont, E., Gilbert, E., Musson-Genon, L., and Carissimo, B. (2016). "Experimental and Numerical Study of Wind and Turbulence in a Near-Field Dispersion Campaign at an Inhomogeneous Site". en. In: *Boundary-Layer Meteorology* 160.3, pages 475–499 (cited on page 83).

Westerweel, J., Elsinga, G. E., and Adrian, R. J. (2013). "Particle image velocimetry for complex and turbulent flows". In: *Annual Review of Fluid Mechanics* 45, pages 409–436 (cited on page 53).

Wieringa, Jon (1992). "Updating the Davenport roughness classification". In: *Journal of Wind Engineering and Industrial Aerodynamics* 41.1, pages 357–368 (cited on pages 52, 132).

Wu, J., Wang, H., Wang, W., and Zhang, Q. (2019). "Performance evaluation for sustainability of wind energy project using improved multi-criteria decision-making method". In: *Journal of Modern Power Systems and Clean Energy* 7.5, pages 1165–1176 (cited on page 170).

Xie, X., Cao, L., and Huang, H. (2018). "Thickened boundary layer theory for air film drag reduction on a van body surface". In: *AIP Advances* 8.5, page 055129 (cited on page 63).

Yang, X., Foti, D., Kelley, C., Maniaci, D., and Sotiropoulos, F. (2020). "Wake Statistics of Different-Scale Wind Turbines under Turbulent Boundary Layer Inflow". en. In: *Energies* 13.11. Number: 11 Publisher: Multidisciplinary Digital Publishing Institute, page 3004 (cited on pages 115, 172).

Yoshihashi, R., Kawakami, R., Iida, M., and Naemura, T. (2017). "Bird detection and species classification with time-lapse images around a wind farm: Dataset construction and evaluation". en. In: *Wind Energy* 20.12, pages 1983–1995 (cited on page 176).

Zhang, Q., Zeng, J., and Yao, T. (2012). "Interaction of aerodynamic roughness length and windflow conditions and its parameterization over vegetation surface". In: *Chinese science bulletin* 57.13, pages 1559–1567 (cited on page 87).

Zhang, W., Markfort, C. D., and Porté-Agel, F. (2013). "Experimental study of the impact of large-scale wind farms on land-atmosphere exchanges". In: *Environmental Research Letters* 8.1, page 15002 (cited on pages 172, 173).

Zhan, L., Letizia, S., and Iungo, G. V. (2020). "LiDAR measurements for an onshore wind farm: Wake variability for different incoming wind speeds and atmospheric stability regimes". In: *Wind Energy* 23.3, pages 501–527 (cited on page 172).

Zhu, W. J., Shen, W. Z., Barlas, E., Bertagnolio, F., and Sørensen, J. N. (2018). "Wind turbine noise generation and propagation modeling at DTU Wind Energy: A review". In: *Renewable and Sustainable Energy Reviews* 88, pages 133–150 (cited on page 178).